UNIVERSITY OF OKLAHOMA

GRADUATE COLLEGE

PLASMONIC PROPERTIES AND ENHANCED FLUORESCENCE OF GOLD AND DYE-DOPED SILICA NANOPARTICLE AGGREGATES

A DISSERTATION

SUBMITTED TO THE GRADUATE FACULTY

in partial fulfillment of the requirements for the

Degree of

DOCTOR OF PHILOSOPHY

By

NATHANIEL SCOTT GREEN
Norman, Oklahoma
2013

PLASMONIC PROPERTIES AND ENHANCED FLUORESCENCE OF GOLD AND DYE-DOPED SILICA NANOPARTICLE AGGREGATES

A DISSERTATION APPROVED FOR THE
DEPARTMENT OF CHEMISTRY AND BIOCHEMISTRY

BY

_____
Dr. Ronald L. Halterman, Chair

_____
Dr. Robert H. Cichewicz

_____
Dr. Daniel T. Glatzhofer

_____
Dr. Wai Tak Yip

_____
Dr. Edgar A. O'Rear III

This work, dedicated to my parents Scott Allen and Deanne Marie Green,

is the culmination of their endless love and support

Acknowledgements

This work would not have been possible without the vision and guidance of my advisor Dr. Ronald Halterman. I am sincerely grateful for all of the science, mentorship, friendship, and coffee.

I am grateful to the entire Department of Chemistry and Biochemistry. Specifically I would like to thank my committee members: Dr. Robert Cichewicz, Dr. Glatzhofer, Dr. Ivan Yip, and Dr. Edgar O'Rear III. The committee has kept me honest, accountable, and focused to become the scientist I am today. I would also like to thank Dr. George Richter-Addo and Dr. Mark Morvant for their leadership over the years.

I would like to thank my sister-at-arms, Dr. Vy Trinh, for her friendship through the beginning and end of this journey. My special thanks to all of my lab mates, past and present: Shawna Ellis, Dr. Shekar Mekala, Dr. Kalani Gunawardana, Dr. Anuradha Singh, Saravanan Ramasamy, Justin Garrett, and the many undergraduate researchers. I am grateful to so many friends that are not listed here.

I would also like to thank my incredible family for their love and support especially my mom, dad and Lora, Memo and Granddad and other family members. Thank you to my big brother Dr. Brandon Green for being my role model, my travel companion, and my best friend.

Most importantly I would like to thank my beautiful fiancée, Jordan Chapman, for her wisdom, patience, and love throughout this process. She has kept me grounded and focused on what is truly important in life. Because of her I know that I am the luckiest.

Table of Contents

List of Tables

List of Figures

Abstract

The development of metal-enhanced fluorescence has prompted a great interest in augmenting the photophysical properties of fluorescent molecules with noble metal nanostructures. Our research efforts, outlined in this dissertation, focus on augmenting properties of fluorophores by conjugation with gold nanostructures. The project goals are split into two separate efforts; *the enhancement in brightness of fluorophores* and *long distance non-radiative energy transfer between fluorophores*. We believe that interacting dye-doped silica nanoparticles with gold nanoparticles can facilitate both of these phenomena.

Our primary research interest is focused on optimizing brightness, as this goal should open a path to studying the second goal of non-radiative energy transfer. The two major challenges to this are constructing suitable nanomaterials and functionalizing them to promote plasmonically active complexes.

The synthesis of dye-doped layered silica nanoparticles allows for control over the discrete location of the dye and a substrate that can be surface functionalized. Controlling the exact location of the dye is important to create a silica spacer, which promotes productive interactions with metal nanostructures. Furthermore, the synthesis of silica nanoparticles allows for various fluorophores to be studied in similar environments (removing solvent and other chemo-sensitive issues).

Functionalizing the surface of silica nanoparticles allows control over the degree of silica and gold nanoparticle aggregation in solution. Heteroaggregation in solution is useful for producing well-aggregated clusters of many gold around a single silica

nanoparticle. The dye-doped surface functionalized silica nanoparticles can than be mixed efficiently with gold nanomaterials.

Aggregating multiple gold nanospheres around a single dye-doped silica nanoparticle can dramatically increase the fluorescent brightness of the sample via metal-enhanced fluorescence due to increase plasmonic scattering. Our aim is to promote heteroaggregation with functionalized silica nanoparticles while minimizing homoaggregation of silica-silica or gold-gold species. Reproducible production of multiple gold nanospheres about a dye-doped silica nanoparticle should lead to dramatic fluorescence brightness enhancements in solution.

Gold nanorods can potentially be used to establish radiationless energy transfer between hetero dye-doped silica nanoparticles via gold nanorod plasmon mediated FRET by aggregating two different dye-doped silica nanoparticles preferentially at opposite ends of the nanorod. End-cap binding is accomplished by tuning the strength of gold binding ligands that functionalize the surface of the silica nanoparticles. The gold nanorod can then theoretically serve as a waveguide by employing the longitudinal plasmon as a non-radiative energy transfer agent between the two different fluorophores, giving rise to a new ultrafast signaling paradigm. Heteroaggregation of dye-doped silica nanoparticles and gold nanorods can be potentially employed to as nano waveguides.

Construction and aggregation of functionalized silica and gold nano-materials provides an opportunity to advance the field of fluorescence. The synthesis of gold nano-particles allows control over their size and shape, which give rise to useful optical and electronic properties. Silica nanoparticles provide a framework allowing control

over a requisite distance for increasing beneficial and deceasing non-radiative dye-metal interactions as well fluorophore protection. Our aim is to take advantage of fine-tuned synthetic control of functionalized nanomaterials to realize the great potential of solution based metal-enhanced fluorescence for future applications.

Chapter I: Introduction

This chapter describes our efforts to develop a robust metal-enhanced fluorescence system by aggregating gold nanoparticles with dye-doped silica nanoparticles as well as establish long-range FRET-like radiationless energy transfer across a gold nanorod. Metal plasmonic interactions are dependent of the spectral properties of the fluorophore and distance from the surface of the metal.[1] Silica nanoparticles were chosen as scaffolding to host the appropriate conditions due their ease of synthesis,[2] efficient and variable methods for incorporating fluorophores,[3] and well-studied robustness in a variety of chemical environments.[4] Furthermore the silica surface can be functionalized to promote silica-gold aggregation while limiting the amount of silica-silica and gold-gold aggregates. Dye-doped silica- gold aggregation is important due to enhanced fluorescence that occurs when multiple gold nanoparticles are brought within close proximity of one another[5] and the fluorophores.[6] Finally, silica nanoparticles can also be aggregated with gold nanorods to establish radiationless energy transfer between hetero dye-doped silica nanoparticles via gold nanorod plasmon mediated FRET.

1.1.1 Principles of fluorescence and FRET

Fluorescence spectroscopy is sensitive technique that plays an important role in biochemical labeling, detection, and in solar cells. The process can be generally described as the radiative release of energy from an excited state of a molecule.[1] Figure 1.1 shows a tris(bipyridine)ruthenium(II) chloride (Rubpy) under ambient light and when the same molecule is exposed to a UV lamp (360 nm wavelength).

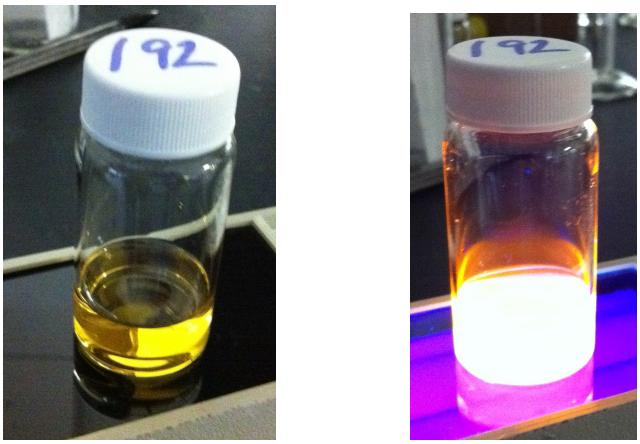

Figure 1.1. Aqueous solution of Rubpy before and after (left and right) exposure to 360 nm irradiation (from this work).

In the case of photo-fluorescence, the emitted light generally has less energy than the incident radiation, known as the Stokes' shift.[1] The distinct energy of excitation light versus emission energy is an important feature in fluorescence spectroscopy, as one energetic process can be studied independent of the other (Figure 1.2).[1] In which the absorption is of shorter wavelength (higher energy) than the emission (lower wavelength, lower energy). The ratio of emitted light to absorbed photons is given by the fluorescence quantum yield. The more efficient the fluorophore is at absorbing and emitting light, the higher the quantum yield.

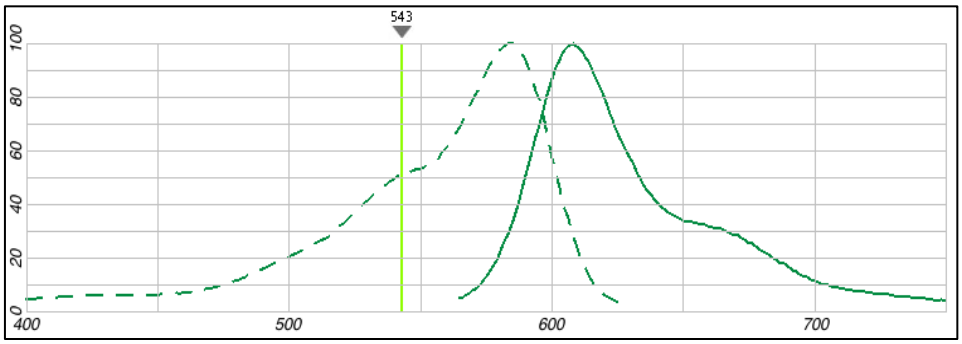

Figure 1.2. Dotted line absorbance, solid line emission spectra (from Invitrogen)

In addition to returning to the ground state through emission the excited fluorophore can energetically decay non-radiatively. One process be which this decay can occur is known as Förster resonance energy transfer (FRET).[3a] FRET efficiency (E) is distance dependent, as energy is transferred via two interacting dipoles according to equation (1).

$$E = \frac{1}{1 + \left(r/R_0\right)^6} \qquad (1)$$

Here, r is the distance between the acceptor and donor pair and R_0 is the Förster distance at which energy transfer is 50%.[1] Energy transfer efficiency is also dependent on the spectral overlap, the matching of donor emission and acceptor absorption, of the FRET pair (Figure 1.3).[7] Significant overlap between the donor emission and the acceptor absorption (shaded in red) provides efficient dipole oscillation interaction between the two species.[7] Our dye-doped silica and gold nanoparticle aggregates requires energy exchange between excited state fluorophores and neighboring metal species through a similar energy transfer process.

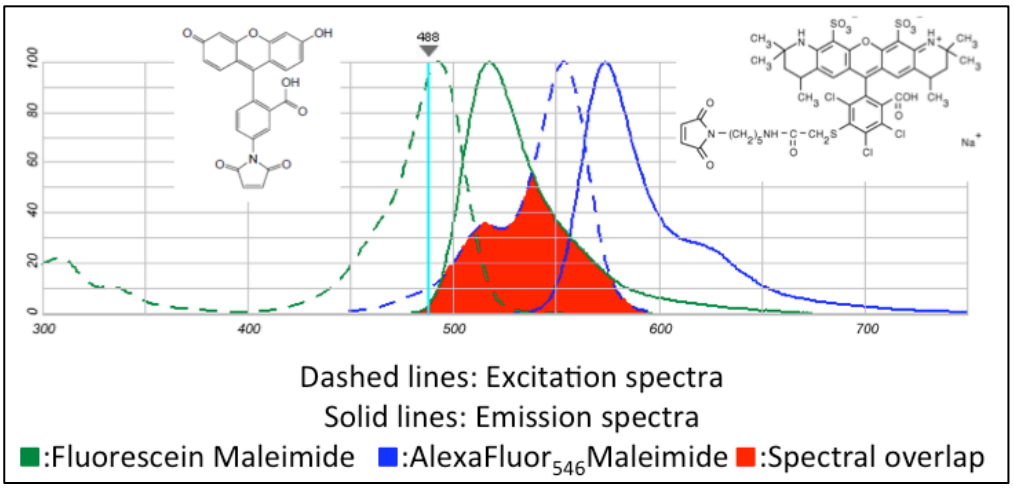

Figure 1.3. FRET-pair absorbance/emission overlap between donor (fluorescein maleimide) and acceptor (alexafluor$_{546}$ maleimide). (Image from Dr. Vy Trinh, modified from Invitrogen).

Quality overlap of the donor emission with the acceptor excitation leads to an efficient transfer of energy between the FRET pair.

FRET has recently enjoyed a surge in applications from fluorescence spectroscopy to biological imaging.[8] However, this process, as previously described, is highly distance dependent. We aim to eliminate the need to bring the fluorophores in close proximity, nm range, by employing a gold nanorod as a plasmonic waveguide[9] to facilitate long range, mm range, FRET-like non-radiative energy transfer (discussed further in chapter V).

1.1.2 Plasmonically active gold nanostructures

Our approach will be to utilize gold nanoparticle plasmon interactions with fluorophore-doped silica nanoparticles to produce metal-enhanced fluorescence. Gold nanostructures are desirable for their unique optical and electronic properties as well as

their fine-tune controllable synthesis.[10] The 'bottom-up' synthetic approach to metallic nanostructures affords many possible shapes and sizes.[11] We are interested in gold nanospheres and nanorods for dye-doped silica nanoparticle aggregation, as the fine-tuned synthetic control of these gold materials allows for control over the plasmon excitation energy band.[10b] Specifically we aim to take advantage of the single plasmonic resonance mode of gold nanospheres and one of the two modes afforded by the anisotropic nanorod structure.

Metal nanostructures display very different photophysical properties from their bulk metal counterparts due to the tight packing of electron density within a very small structure.[12] Interaction between an appropriately sized metal nanoparticle and visible light creates an oscillation in the soft electronic cloud surrounding the nanostructure (referred to as a plasmon resonance) (Figure 1.4).[5] The plasmon excitation can be measured by visible and near IR optical absorption, which is useful for determining overlap with fluorescent dyes.

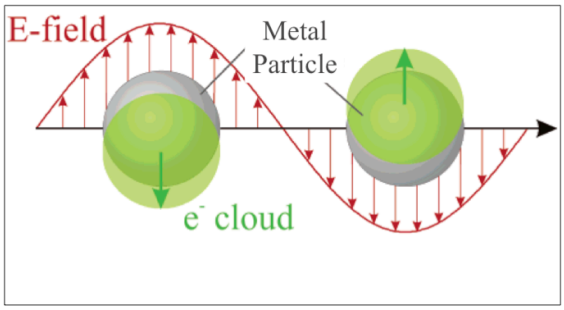

Figure 1.4. Cartoon representation of a metal nanoparticle and electromagnetic radiation interacting to create an oscillation in the electric field about the nanoparticle (plasmon resonance).

The plasmon resonance of gold nanospheres similarly occurs in gold nanorods except that two different modes, along the long axis (longitudinal) and the short axis (transverse), exists for gold nanorods.[11] Figure 1.5 shows the result of altering the aspect ratio, the relative length and width of a nanorod, on the absorbance of the transverse and longitudinal resonance modes of gold nanorods. Increasing the aspect ratio results in a significant red-shifting of the longitudinal plasmon band while the transverse mode is not generally effected.[13]

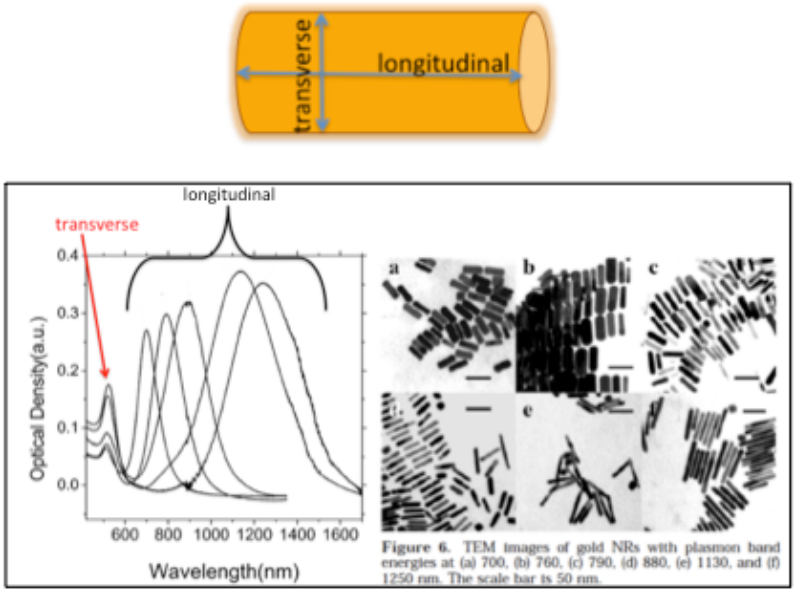

Figure 1.5. Cartoon schematic and experimental data displaying the two absorbance modes of gold nanorods (transverse and longitudinal) (Cartoon schematic from this work, experimental data from Kioobakht et al).

We aim to take advantage of this fine-tuned control over photophysical properties by preparing high quality gold nanospheres and rods for applications in dye-doped silica nanoparticle aggregation in which we will vary the absorbance and

emission overlap of each species to determine the optimal conditions for energy transfer in and out of the plasmon.

This work requires precise control over the size and shape of the gold nanoparticles. Fortunately prior reaction conditions have been established to grow these materials in exact and reproducible procedures. The key to these procedures is the relative amount of reductant and capping agent present during the growth of gold nanomaterials.

Gold nanospheres and rods are synthetically accessible via micelle-mediated Au(IV) reduction. The procedures for growing nanoparticles of various metals and shapes is well established in literature.[13] One notable difference in the preparation of spheres versus rods is the use of surfactant. Gold nanospheres are grown in citrate solution while rods are grown in a mixture of cetyltrimethylammonium bromide (CTAB) and silver nitrate.[14] This allows for a fine-tuned control over the size and shape of gold nanoparticles and thus control over their unique optical and electrical properties. (Figure 1.5).

1.1.3 Metal-enhanced fluorescence

Visible light is absorbed and scattered by the soft electronic cloud surrounding gold nanoparticles (the surface plasmon resonance). This energy exchange allows for a beneficial interaction with fluorophores known as metal enhanced fluorescence (MEF).[15] This phenomenon, extensively studied by Lakowicz et al.[1], is the result of non-radiative energy transfer between a fluorophore and a metal similar to FRET.[6] Many questions remain regarding the parameters to establish optimal MEF but what is

clear is the dependence on distance between the metal surface and the fluorophore.[15] Gold nanoparticles strongly absorb and scatter light in roughly the same spectral regions leading to decreased fluorescent signal from absorption while scattering has been shown to dramatically increase brightness.[16] This phenomenon is further enhanced if the gold nanoparticles are close enough to one another to couple plasmonic resonances. In this case increased excitation events and additional radiative pathways are provided by interacting the fluorophore with the metal plasmon.[17] Figure 1.6 displays the excitation events, both standard excitation and those extra pathways from being proximal to a metal nanoparticle (on the left), and emission pathways, again, both standard emission and pathways afforded by the metal (on the right).

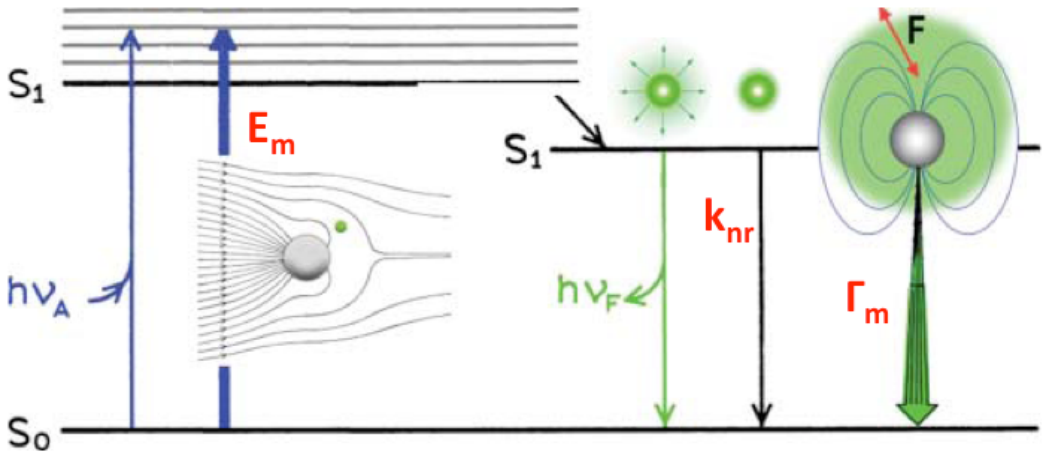

Figure 1.6. Jablonski diagram of a fluorophore placed near the surface of a metal nanoparticle (Image from Lakowicz et al).[17]

It could therefore be advantageous to construct small-diameter nanomaterial aggregates with fixed fluorophore distances as a means to achieve maximum enhancement. Dye-doped silica nanoparticles may provide an excellent platform to control this distance while still allowing for coupled plasmon interactions.

1.1.4 Dye-doped silica nanoparticles as MEF promoting scaffolds

To achieve solution-phase MEF we must both bring GNP onto a scaffold and to bring suitable fluorophores into the scaffold. Dye-doped silica nanoparticles are well suited to meet both requirements for metal nanoparticle aggregation as they provide a necessary barrier between the fluorophore and gold, protect the dye from environmental factors, and provide a means for facile surface coating that can bind multiple GNPs.

Various preparations such as the Stöber process[4], microemulsions[3b, 18], and layered silica[2] produce silica nanoparticles of different sizes and morphologies. The layered process is particularly useful for making small, uniform, and monodisperse particles. The fluorophores are incorporated into the silca nanopartilces by layering dye ontop of small silica cores followed by an additional shell growth.[2] Both the core and shell growth are facilitated by the condensation of tetraethylorthosilicate (TEOS). The shell growth (or layered) preparation is best suited for metal nanoparticle aggregation because the outer layer separates the dye from gold and protects the fluorophore from environmental factors such as oxidative stress and photobleaching.[19] Additionally, silica nanoparticles can be coated in various functional groups (e.g. amines, thiols, carboxylic acids).[3a] Surface coating of silica nanoparticles allows the exploration of several aggregation motifs; however characterization of these small aggregates requires special imaging methods and instrumentation.

1.1.5 Transmission electron microscopy imaging

In order to confirm the degree of aggregation we require suitable measurements that can differentiate between independent and aggregated materials. One excellent method for this measurement is transmission electron microscopy, although some

information can be gained from optical measurements as well (discussed in chapter III). TEM employs an electron beam to produce sample photographs. This imaging process accelerates a beam of electrons through a small sample where they are decelerated or deflected. An image is produced by the shadow cast from the material. An electron beam, unlike visible light, has a small enough wavelength (de Broglie wavelength) for nanomaterials to be easily resolved (as compared to being diffraction limited in a light microscope). The ability for material to stop an electron depends on its density, size, and the energy of the accelerated electrons. de Broglie previously established that the wavelength and momentum of an electron are inversely proportional. This relationship unfortunately dictates that contrast decreases as resolution increases; this presents a challenge for obtaining clear images of very small silica nanoparticles that lack electron stopping power.

1.2 Conclusion

Gold and silica nanomaterial aggregates present an opportunity to take advantage of beneficial plasmonic interactions with fluorophores while diminishing quenching pathways by engineering the silica nanoparticles with discrete dye locations. This system potentially allows for a new fundamental signaling motif that is more efficient, smaller, and less restrictive than previous methods. Challenges exist in determining the optimal spectral overlap, dye-metal distance, and aggregation conditions that will lead to large fluorescent brightness enhancements.

Hetero-fluorophore dye doped silica nanoparticle/ gold nanoparticle aggregates extend the possibility of long-range non-radiative energy transfer. This process is envisioned to be similar to Förster resonance energy transfer (FRET) with gold plasmon

resonances mediating the transfer thus diminishing the need for small inter-fluorophore distances.[3a] The distance between the fluorophores can be even further extended by the use of silica end decorated gold nanorods[20] via a plasmonic waveguide.[9] However, this phenomenon has not yet been reported and many challenges including, assessing the ability to place energy into and get it back out of the longitudinal plasmon between fluorophores, aggregating dye-doped silica nanoparticles particularly at the end caps of the rods, and determining the correct overlap of the FRET pairs and the gold longitudinal plasmon.

1.3 Research Focus

This dissertation describes our efforts to develop a robust metal-enhanced fluorescence system by aggregating gold nanoparticles with dye-doped silica nanoparticles as well as establish long-range FRET-like radiationless energy transfer across a gold nanorod. Therefore, the first section discusses the production, through TEOS condensation, and analysis via TEM, of high quality layered dye-doped silica nanoparticles. Next, we discuss our efforts to surface functionalize these dye-doped silica nanoparticles with ligands that preferentially bind to gold substrates as well as techniques for characterizing, through qualitative assays and aggregation data from optical spectra, the quality of the surface functionalization. The last two sections then focus on the application of our functionalized dye-doped silica nanoparticles with gold nanoparticles. The first of these sections discusses our efforts to create a metal-enhanced fluorescence (MEF) system by aggregating dye-doped silica nanoparticles with gold nanospheres, trying to promote heteroaggregation while diminish homoaggregation, as well as the various instrumental methods and techniques used to

characterize these aggregates, such as TEM imaging for morphology and optical spectra for photophysical changes. Finally we discuss our development of a plasmonic waveguide by aggregation of gold nanorods with dye-doped silica nanoparticles and the particular challenges with establishing a correct FRET pair and orientation of hetero dye system.

1.4 References

1. Lakowicz, J. R., *Principles of Fluorescent Spectroscopy*. 2nd ed.; Springer: 1999; p 725.

2. Hartlen, K.; Athanasopoulos, A.; Kitaev, V., Facile Preparation of Highly Monodisperse Small Silica Spheres (15 to >200 nm) Suitable for Colloidal Templating and Formation of Ordered Arrays. *Langmuir* **2008,** *24*, 1714-1720.

3. (a) Wang, L.; Tan, W., Multicolor FRET Silica Nanoparticles by Single Wavelength Excitation. *Nano Lett.* **2006,** *6* (1), 84-88; (b) Ma, D.; Kell, A. J.; Tan, S.; Jakubek, Z. J.; Simard, B., Photophysical Properties of Dye-Doped Silica Nanoparticles Bearing Different Types of Dye-Silica Interactions. *J. Phys. Chem. C* **2009,** *113*, 15974-15981.

4. Flachsbart, H.; Stober, W., Preparation of Radioactively Labeled Monodisperese Silica Spheres of Colloidal Size. *J. Colloid Interface Sci.* **1969,** *30* (4), 568-573.

5. Kelly, L. E.; Coronado, E.; Zhao, L. L.; Schatz, G. C., The Optical Properties of Metal Nanoparticles: The Influence of Size, Shape, and Dielectric Environment. *J. Phys. Chem. B* **2003,** *107*, 668-677.

6. Lakowicz, J. R., Radiative Decay Engineering 5: Metal-Enhanced Fluorescence and Plasmon Emission. *Anal. Biochem.* **2005,** *337*, 171-194.

7. Albani, J. R., *Forster Resonance Energy Transfer*. Blackwell Publishing Ltd.: Oxford, UK, 2008.

8. Jares-Erijman, E. A.; Jovin, T. M., FRET imaging. *NAture Biotech.* **2003,** *21* (11), 1387-1395.

9. Maier, S. A.; Kik, P. G.; Atwater, H. A.; Meltzer, S.; Harel, E.; Koel, B. E.; Requicha, A. A. G., Local Detection of Electromagnetic Energy Transport Below the Diffraction Limit in Metal Nanoparticle Plasmon Waveguides. *Nature Mater.* **2003,** *2*, 229-233.

10. (a) Frens, G., Controlled Nucleation for the Regulation of the Particle Size in Monodisperse Gold Suspensions. *Nature Phys. Sci.* **1973,** *241* (105), 20-22; (b) Gou, L.; Murphy, C. J., Fine-Tuning the Shape of Gold Nanorods. *Chem. Mater.* **2005,** *17*, 3668-3672.

11. Kioobakht, B.; El-Sayed, M. A., Preparation of Growth Mechanism of Gold Nanorods (NRs) Using Seed-Mediated Growth Method. *Chem. Mater.* **2003,** *15*, 1957-1962.

12. Halas, N. J., Plasmonics: An Emerging Field Fostered by Nano Letters. *Nano lett.* **2012,** *10*, 3816-3822.

13. Burda, C.; Chen, X.; Narayanan, R.; El-Sayed, M. A., Chemistry and Properties of Nanocrystals of Different Shapes. *Chem. Rev.* **2005,** *105*, 1025-1102.

14. Sau, T. K.; Murphy, C. J., Seeded High Yield Synthesis of Short Au Nanords in Aqueous Solution. *Langmuir* **2004,** *20*, 6414-6420.

15. Geddes, C. D.; Lakowicz, J. R., Metal-Enhanced Fluorescence. *J. Fluor.* **2002,** *12* (2), 121-130.

16. Lazarides, A. A.; Schatz, G. C., DNA-Linked Metal Nanosphere Materials: Structural Basis for the Optical Properties. *J. Phys. Chem. B* **2000,** *104*, 460-467.

17. Lakowicz, J. R.; Ray, K.; Chowdhury, M.; Szmacinski, H.; Fu, Y.; Zhang, J.; Nowaczyk, K., Plasmon-controlled Fluorescence: A New Paradigm in Fluorescence Spectroscopy. *Analyst* **2008,** *133*, 1308-1346.

18. Kumar, R.; Roy, I.; Ohulchanskyy, T. Y.; Goswami, L. N.; Bonoiu, A. C.; Bergey, E. J.; Tramposch, K. M.; Maitra, A.; Prasad, P. N., Covalenty Dye-linked, Surface-controlled, and Bioconjugated Organically Modified Silica Nanoparticles as Targeted Probes for Optical Imaging. *ACS Nano* **2008,** *2* (3), 449-456.

19. Santra, S.; Zhang, P.; Wang, K.; Tapec, R.; Tan, W., Conjugation of Biomolecules with Luminphore-Doped Silica Nanoparticles for Photostable Biomarkers *Anal. Chem.* **2001,** *73* (4988-4993).

20. Joseph, S. S. T.; Ipe, B. I.; Pramod, P.; Thomas, G. K., Gold Nanorods to Nanochains: Mechanistic Investigations on Their Longitudinal Assembly Using alpha,omega-Alkanedithiols and Interplasmon Coupling. *J. Phys. Chem. B* **2006,** *110*, 150-157.

Chapter II: Dye incorporation and synthetic control of silica nanoparticles

2.1 Chapter Overview

This chapter discusses the need for and our efforts to integrate organic fluorophores into structurally engineered silica nanoparticles for applications in gold nanostructure aggregate systems. The dye-metal interaction is highly dependent on photophysical and spatial properties of each species.[1] Silica nanoparticles were chosen as scaffolding to host the appropriate conditions due their ease of synthesis,[2] efficient and variable methods for incorporating fluorophores,[3] and well-studied robustness in a variety of chemical environments.[4]

Metal enhanced fluorescence is dependent of the spectral properties of the fluorophore and distance from the surface of the metal.[5] To this end, it is vital to be able to incorporate many different dyes into similar silica substrates in order to properly investigate the potential of the gold/silica aggregate system. However, different fluorophores lead to various experimental issues such as solubility, altered spectral properties in different environments, and fluorescence quenching.[6] Two of the main motifs for incorporating fluorophores into the silica matrix are covalent attachment[7] or through non-covalent physisorbtion.[2] This chapter discusses many different dyes in regards to their spectral properties, incorporation into silica, and potential uses in metal aggregate systems.

Multiple preparations have been reported for the synthesis of uniform monodisperse silica nanoparticles in a variety of conditions. These range from the

standard bearer Stöber preparation[4] in ethanol to microemulsions[8] and aqueous/organic biphasic growth systems.[9] These systems provide an array of conditions amenable to variations in nanoparticle size, shape, and incorporated dye. This chapter will outline the benefits and problems associated with several different silica nanoparticle preparations in relation to optimizing the gold/ dye-doped silica interaction (Figure 2.1).

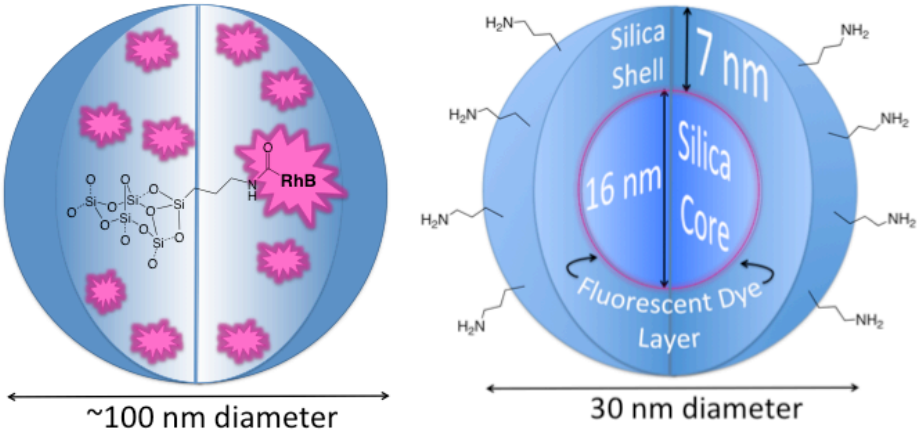

Figure 2.7. Cartoon schematic of fluorophore incorporation techniques in dye-doped silica nanoparticles (not to scale). (left) Random distribution throughout SiNP (right) discrete layered SiNP (from this work).

2.2 Introduction

Dye-doped silica nanoparticles are attractive scaffolds to facilitate fluorophore metal interactions due to the ability to fine-tune their size and shape[10], the various preparations under a variety of conditions[11], the tolerance of internal and external functionalization[12], and the constant protective environment they provide for a wide variety of dyes.[13] Silica is well known and studied for its chemical inertness and high

degree of functionality. For these reasons the synthesis, functionalization, and applications of dye-doped silica nanoparticles (SiNP) are the primary focus of this dissertation.

Silica nanoparticles serve two major functions in our aggregation model: first, create a physical barrier between the dye and the surface of the metal and second, promote the aggregation of the two species in solution. This chapter focuses on the spatial barrier created by comparing preparations and motifs for silica nanoparticle formation, as the topic of aggregation is the subject of chapter III.

The metal and dye proximity is important because the spatial relationship determines if the sample is quenched via oscillation dampening or no interaction is present when too close or far, respectively.[14] Previous experiments and recent literature[15] emphasize the vital role proximity plays in MEF. Liu et al have demonstrated an impressive size variation experiment in which a dye-bound polymer was elongated and contracted on a silver nanoparticle via temperature variation (Figure 2.2)[15].

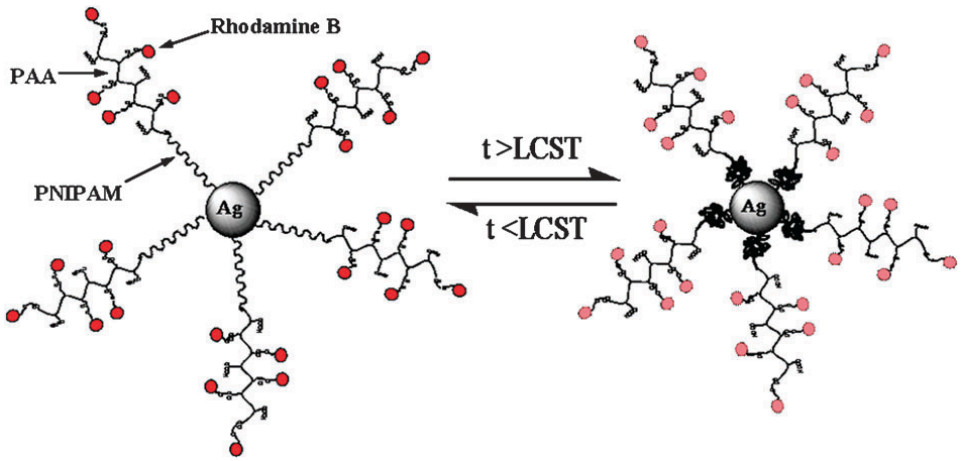

Figure 2.8. Diagram of thermoresponsive polymer-dye tethered to silver nanoparticles LCST= Lower critical solution temperature. PNIPAM= thermoresponsive polymer. PAA= Poly acrylic acid (binding RhB in bundles). (Image from Liu et al)[15]

Enhancement was observed when the polymer expanded approximately 30 nm from the metal while emission essentially fell to zero when the polymer contracted, bringing the fluorophores close to the surface of the metal (Figure 2.3).

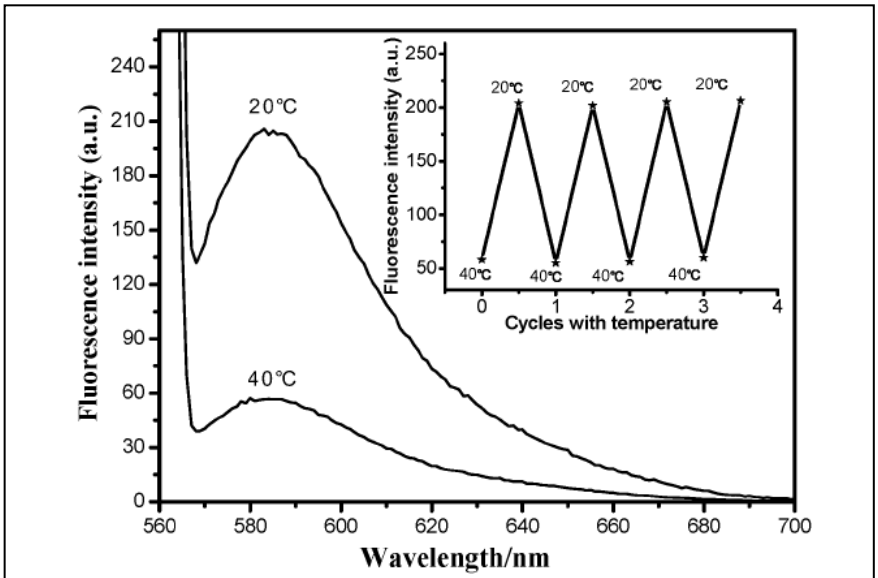

Fig. 3 Fluorescent emission spectra of the rhodamine B modified AgNPs (DP = 300) at 20 and 40 °C in an aqueous medium. The inset shows switchable fluorescence behavior upon temperature cycling.

Figure 2.9. On-off enhancement demonstrated by temperature variation. DP= degree of polymerization of the surface of the silver nanoparticles. (Image from Liu et al.)[15]

2.2.1 Comparison of silica nanoparticle preparations

Our aim is to synthesize silica nanoparticles with discrete localized areas where a fluorophore can be incorporated while still controlling size, shape, and monodispersity in a reproducible manner. Silica nanoparticles are formed by the condensation of a siloxane precursor under two general motifs: in solution nucleation and microemulsions.[16] These preparations take place under a variety of conditions that are well suited for controlling size, monodispersity, solubility, and complex architecture.

The Stöber preparation is perhaps the best established and most widely used method for growing silica nanoparticles.[4] Here, tetraethylorthosilicate (TEOS) is hydrolyzed in ethanol by catalytic amounts of ammonium hydroxide to producing silic

acid which then condenses with TEOS to produce silica nucleation sites.[17] The small nucleation sites continue to grow in the presence of more TEOS and ammonium hydroxide (Figure 2.4).

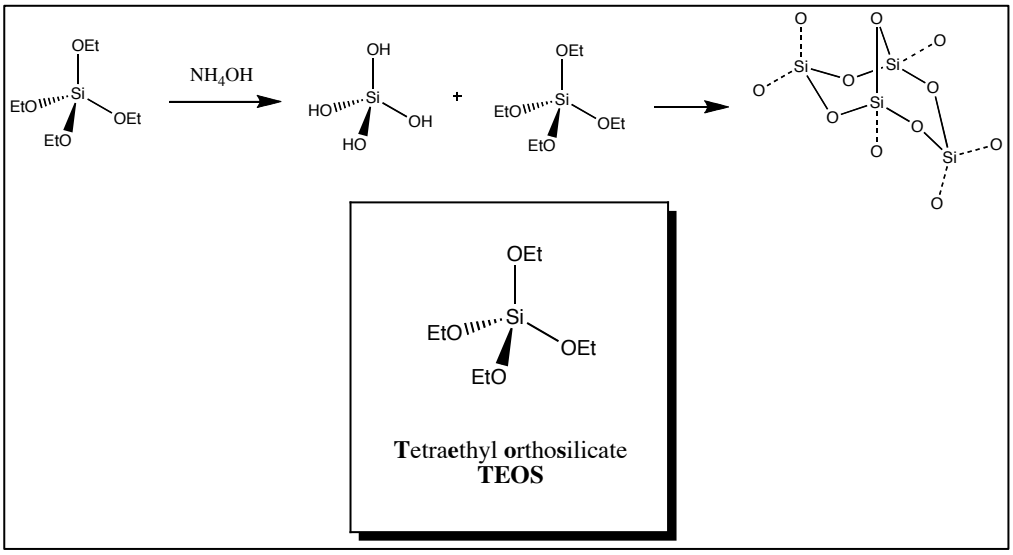

Figure 2.10. Hydrolysis and and condenstaion of TEOS and silic acid. (figure from this work).

The Stöber preparation can produce uniform spheres in the nanometer to micrometer range (although it is best suited for near micrometer range) and can also be used to effectively produce core shell structures with silica coatings.[18] The silica particle size is controlled by varying the amount of siloxane precursor as well as the reaction time and solvent.[19] Furthermore, this preparation is amenable to inclusion of a wide range of dyes via covalent siloxane handles *vida infra*.[3a]

The major drawbacks to the Stöber preparation are the lack of control over dye location and the general lack of uniformity with smaller, sub micron, diameter particles. Despite these drawbacks the Stöber preparation was the first, and still is one of the most

widely used, methods to produce silica nanospheres. Microemulsions were then developed to address the concern of well-order particles at smaller diameters.[16]

Microemulsions overcome the size limitation of the Stöber preparation by taking advantage of small, thermodynamically stable, micro-reaction environments created by mixing a surfactant with an organic solvent and water. These microemulsions can be performed as oil droplets in an aqueous environment (standard 'o/w' microemulsion)[20] or as aqueous droplets in an oil environment (reverse 'w/o' microemulsion).[8] The use of standard versus reverse microemulsion is dependent on the solubility of the desired fluorophore to incorporate into the silica. The diameter of the nanoparticles is mainly determined by the size of the micelles, determined by the ratio of water to surfactant used to grow them.[8] Microemulsions are commonly used to prepare silica nanospheres in the nanometer range (Figure 2.5).[21]

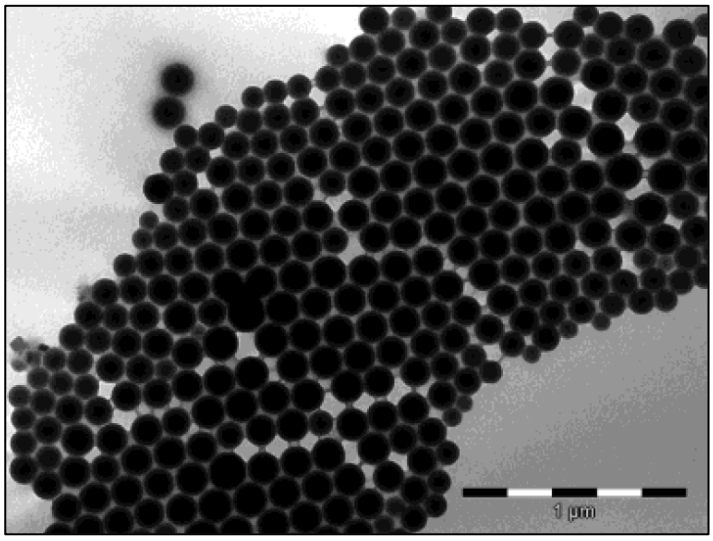

Figure 2.11. Sub-micrometer silica nanoparticles formed by a reverse emulsion process.[8]

Dyes can be incorporated into silica nanoparticles by analogous methods used in the Stöber preparation. As previously discussed these doping methods can be performed via covalent linkage or physisorption onto the silica matrix.[22] However, this process still suffers from lack of precise control over the physical location of the fluorophore (Figure 2.6).

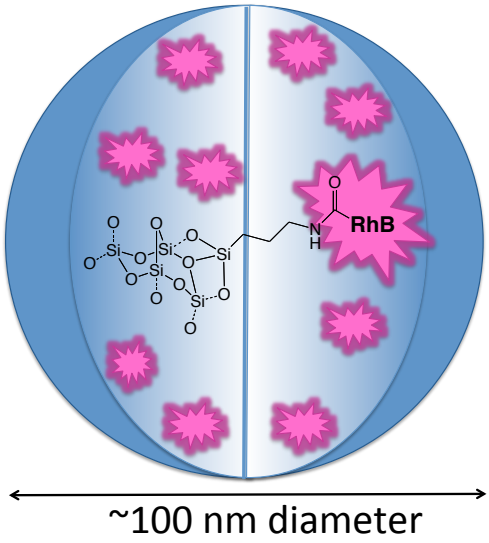

Figure 2.12. Cartoon schematic of random covalent dye incorporation throughout a silica nanoparticle formed in both by either the Stöber or microemulsion preparations (from this work).

Lack of spatial control over the dye within the silica matrix then leads to lack of control over the plasmonic interaction. The layered silica motif is employed to address both the size of silica nanoparticles as well as the selectively placing the dye in a particular location within the matrix.

Layered silica nanoparticles overcome the obstacles of size control and dye placement by slowly growing an outer shell of silica around a small dye-doped core.

The small diameter is achieved through two key modifications to the condensation of TEOS. First, basic amino acid are used in place of catalytic amounts of ammonium hydroxide.[23] Davis et al postulate that lysine associates with the electron dense silic acid to better facilitate nucleation of the growing silica particles thus allowing smaller, more uniform spheres to grow.[23] The use of basic amino acids as a catalyst was shown to grow small diameter silica nanospheres at unprecedented uniformity (Figure 2.7).[9]

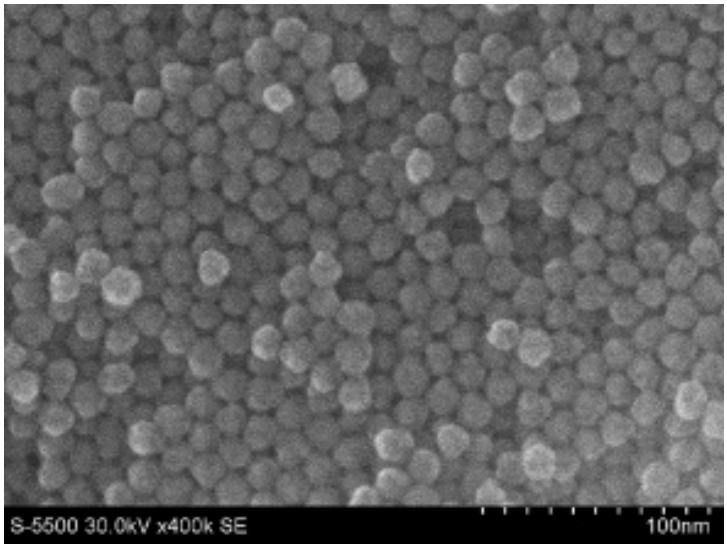

Figure 2.13. High resolution scanning electron microscopy (HRSEM) image of small diameter silica nanospheres grown with catalytic arginine. (Image from Yokoi et al)[9]

The second modification is the use of an aqueous/ organic biphasic system to achieve a slow delivery of the monomer dissolved in a top organic layer suspended over an aqueous layer containing the catalytic amino acid.[2] The siloxane is only hydrolyzed upon contact at the organic aqueous interface thus keeping the concentration of reactive monomer low during the growth process. Hartlen et al have shown this process can be iteratively to grow additional silica layers to produce particles from 15 to 200 nm in diameter.[2] Furthermore, this method allows for dyes to be incorporated specifically

between layers of the growing particle to create a constant fixed distance between all of the fluorophores and the surface of the sphere (Figure 2.8).

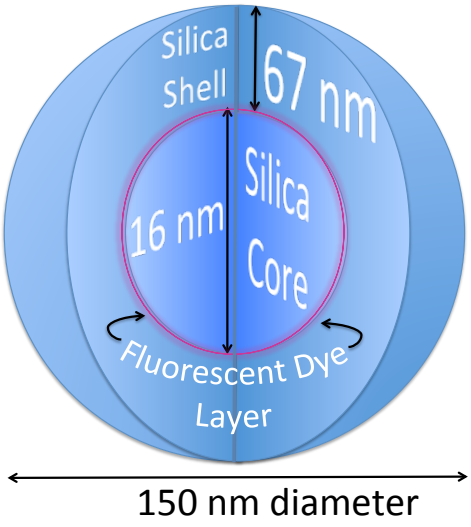

Figure 2.14. Cartoon schematic of a layered dye-doped silica nanoparticle. (from this work)

Silica nanospheres can be synthesized under a variety of conditions to produce a wide range of diameters and include many different dyes. This control allows for fine-tuned control over the environment of the dye and the physical space between the fluorophore and the surface of the silica. Once the silica framework is in place one must take into consideration how the nature of immobilizing the dyes within a particle.

2.2.2 Dye incorporation techniques

Our aim is to incorporate fluorophores into the matrix of silica nanoparticles to ensure that they are held a fixed distance from the surface of aggregated gold nanoparticles and that no dye leaches from the particles while maintaining their native

photophysical properties. The incorporation of fluorophores into the silica matrix is an important consideration for the efficacy of a metal-enhanced nanoparticle aggregate system. The dye must remain securely bound within the sphere while ensuring that the spectral properties are not negatively affected. Dye can either be covalently linked to the silica framework or physisorbed onto its surface and be trapped between layers.

Fluorophores can be covalently attached to silica through siloxane tethers that can be condensed into the sphere during nanoparticle growth.[24] Covalent attachment is most commonly accomplished through amide coupling with 3-aminopropyltriethoxy silane (APTES)[3a] but has been shown via thiol[24] and dextran[3b] linkages from commercially available or easily synthesized fluorophore derivatives (Figure 2.9).

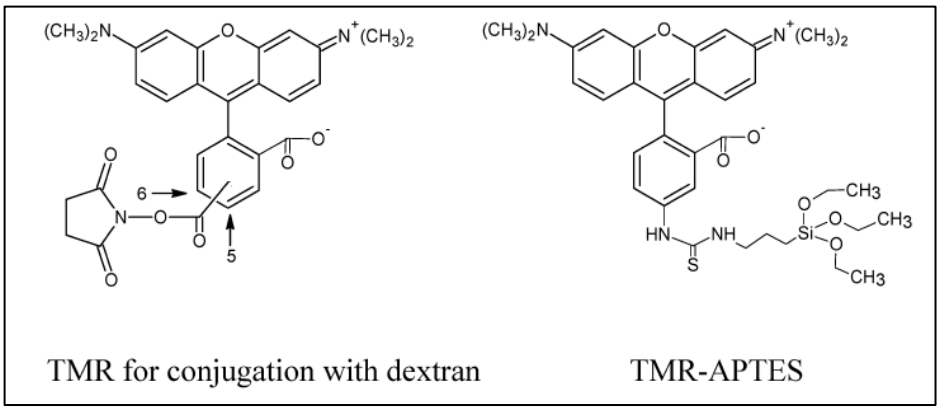

Figure 2.15. Modified fluorophores with tethers for covalent attachment to silica. (taken from Ma et al)[3b]

These methods ensure that molecules remain firmly attached to the silica matrix even in mesoporous particles.[11] However, these motifs are only available for fluorophores bearing moieties that can form covalent linkages under mild conditions that will not affect the fluorescence of the dye. Dyes lacking such functionality may be incorporated

in the silica matrix by being trapped in layers onto which fluorophores have been absorbed.

Fluorophores may be physisorbed, through attractive electrostatic intermolecular forces, onto the surface of silica nanospheres where they can be secured by being enveloped in additional silica layers.[2] However, this process requires that the incorporated dye exhibit at least a partial positive charge as the silica matrix is electron dense.[16] Hartlen et al have shown, and this work has verified, that no dye leaches from layered silica nanoparticle, where the dye is completely enveloped by silica, despite the weaker strength of electrostatic interactions compared to covalent linkages.[2]

The solubility and reactivity of the dye and the architecture of the nanoparticle determines which technique is most appropriate.[25] Connectivity is an important consideration for the inclusion of fluorophores into silica as a through study of dye-doped silica nanoparticle MEF aggregates necessarily must include the study of a library of dyes with many different spectral properties.

2.2.3 Incorporating multiple dyes into silica nanoparticles to create a diverse spectral library

Our experimental design requires that a number of dyes with various absorbance and emission bands are incorporated into silica nanoparticles in order to investigate the fluorophore-gold plasmon interaction. The inclusion of multiple dyes into silica nanoparticle/ gold nanoparticle aggregates is attractive, as this would provide a wide range of photophysical experiments in order to fully investigate the interaction between the fluorophore and the plasmon. Wang et al presented an excellent case of utilizing

multiple dyes within a single nanoparticle to allow for FRET to occur within a single sphere.[3a] These particles were then color tunable by varying the amounts of donor or acceptor dyes present in the silica, which led to variable emission of the FRET pair donors and acceptors (Figure 2.10).

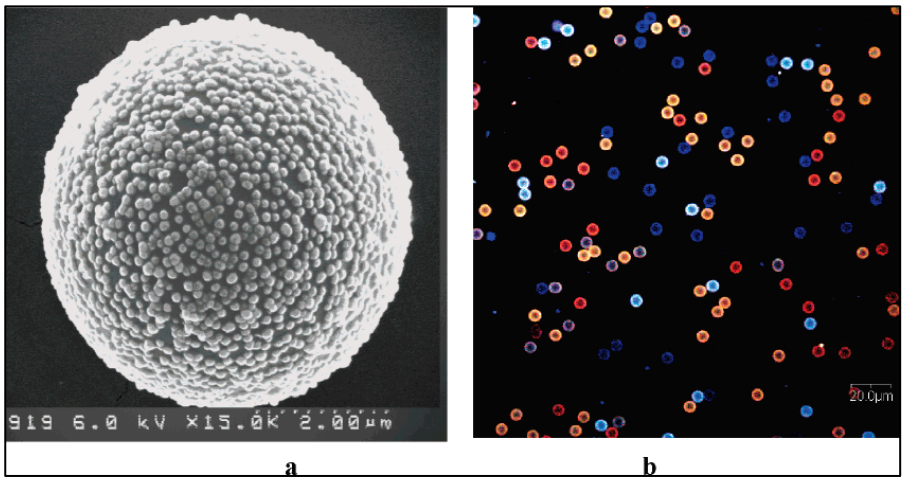

Figure 2.16. Multiple FRET-paired dyes doped into single silica nanospheres. a) silicananoparticles attached to a larger latex microsphere. b) confocal image of different microsphere-nanosphere complexes excited under a 488 nm Argon-ion laser. (Image from Wang et al).[3a]

The optimal relationship between the excitation energy of the metal plasmon and the absorbance/ emission of the fluorophore is still poorly understood.[1] Therefore, it is appropriate to investigate dyes that absorb and emit below[3b], above[26], and with[27] the plasmonic resonance band of the desired metal nanoparticle (Figure 2.11). Rubpy is shown to absorb light below the wavelength of GNPs but emit at a higher wavelength than the spheres. The absorbance and emission bands of rhodamine B both overlap with gold nanorods and spheres. PyCy5 absorbs and emits light at significantly higher

wavelengths than gold nanospheres. The absorption spectrum of gold nanorods is generally at longer wavelength that GNP (and is the focus of chapter IV).

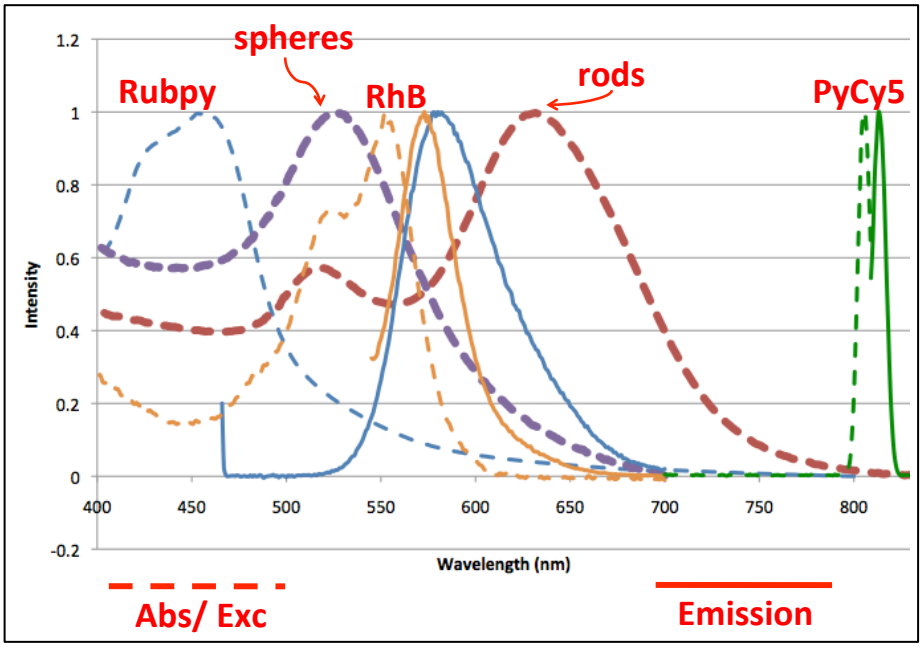

Figure 2.17. Normalized absorbance and emission spectra for tris(bipyridine)ruthenium(II) chloride (Rubpy), gold nanospheres, rhodamine B (RhB), gold nanorods, and 1,1'-diethyl-2,2'-dicarbocyanine iodide (PyCy5). (from this work).

The variety of absorbance and emission bands of different fluorophores allows for the investigation of spectral overlap effect with metal nanostructures.

Dye-doped silica nanoparticles are attractive targets for applications in MEF aggregate systems as they are obtainable with fine-tuned control over size, tolerate covalent linkages or provide an electron rich substrate for physisorption, accepting of multiple dyes to be included within the silica framework. We hypothesize that controlling the location and identity of a fluorophore within a uniform silica nanoparticle will fix the distance between the surface of gold nanostructures in

nanoparticle aggregates, which will lead to desirable plasmonic overlap to produce metal enhanced fluorescence and plasmonic waveguides.

2.3 Results and Discussion

We prepared silica nanoparticles by the Stöber preparation,[19] microemulsions,[8] and a layered preparation,[2] that were doped with a series of dyes ranging from blue absorbing (Rubpy) to near-IR (NIR) absorbing (Cy5) under covalent and non-covalent conditions in order to investigate their ensemble applications in gold nanostructure aggregates. Dye-doped silica nanospheres were characterized by UV-visible absorption, fluorometry, dynamic light scattering (DLS), and transmission electron microscopy (TEM) imaging to identify spectral and morphological features. Our hypothesis is that producing high-quality silica nanospheres with a discrete location for dye incorporation will create a path towards successfully creating in-solution metal enhanced fluorescence and plasmonic mediated energy transfer via gold nanostructure aggregation.

2.3.1 Dye-doped silica nanoparticles prepared by the Stöber preparation

The Stöber preparation was first attempted due to its wide-spread application and ease of synthesis,[17] but this process failed to produce uniform small diameter silica nanoparticles. Moreover, dyes are randomly distributed throughout the silica nanoparticles in the doping process, which does not provide the precise spatial control that is needed for gold nanoparticle aggregation. However, the Stöber preparation provided the first example of dye-doped silica nanoparticles in our group[28] and much has been gained in the pursuit of perfecting this approach.

The Stöber preparation yielded silica nanoparticles that were large, lacked morphological uniformity, and had a propensity to form large homo-aggregates. Figure 2.12 shows a TEM image of one preparation where co-condensation of rhodamine B-APTES conjugate Stöber preparation in ethanol was examined.

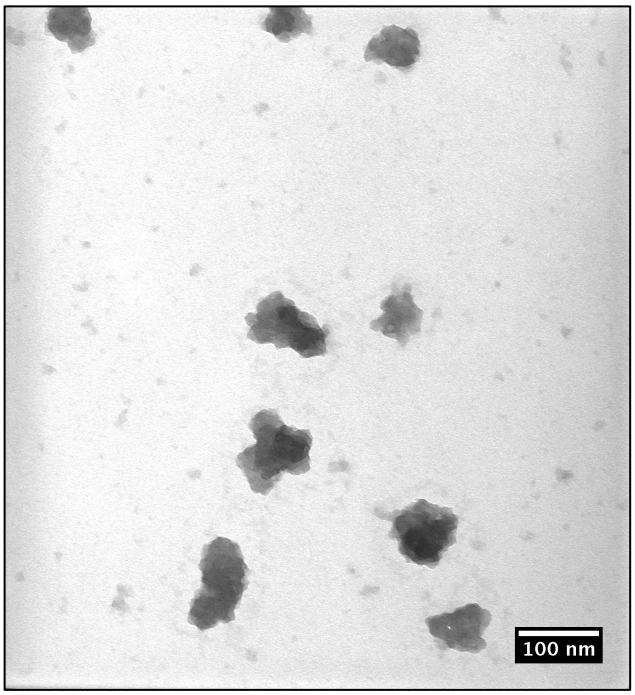

Figure 2.18. TEM image of RhB-APTES conjugate-doped silica nanoparticles produced by the Stöber preparation.

The silica clusters produced by the Stöber preparation in Figure 2.12 are not desirable due to their lack of uniformity, which would place the fluorophores at random distances to gold nanoparticles upon aggregation. Furthermore, silica-silica aggregation masked important dye-doped silica surface area that was needed to be in contact with the gold surface. This aggregation is visible in TEM images (Figure 2.12) but also in dynamic light scattering experiments (Figure 2.13). Dynamic light scattering

experiments were used to determine the hydrodynamic diameter, compared to the physical diameter of dry, drop-coated sample in TEM imaging, based on the physical size of the particles and aggregates that may form in solution. The effective diameter found across five separate scans indicates that there is a large discrepancy in the size of the particulate mater, raging from 125.7 nm in diameter to 24615.1 nm (± 4869.9 nm). The extremely wide size distribution indicates the formation of large aggregates in solution. Complexes with diameters in the tens of microns would not be seen in the TEM images as such aggregates can readily dissociate as they are drop coated onto the surface of a dry copper grid although there is additional TEM evidence of smaller aggregate formation.

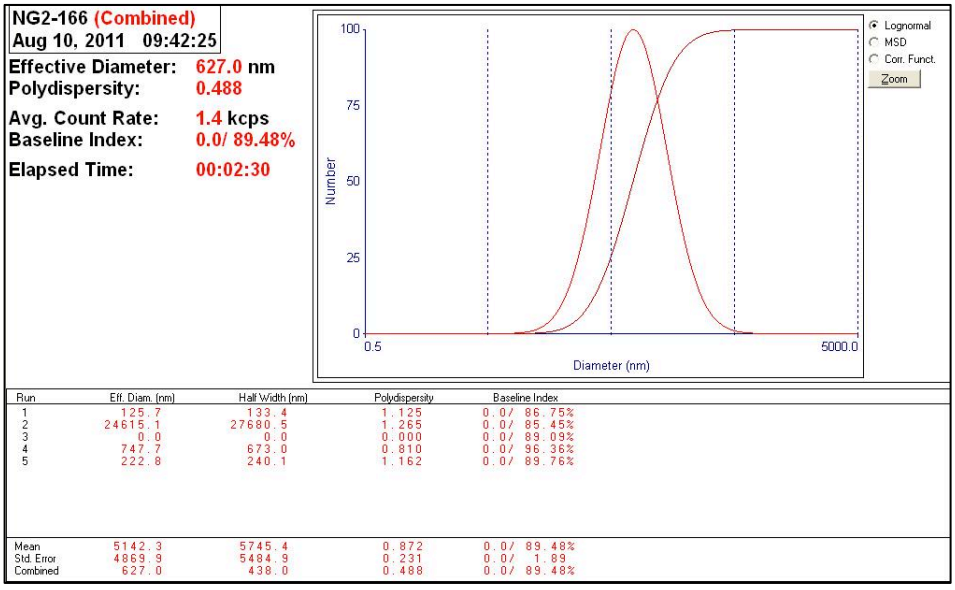

Figure 2.19. DLS analysis of RhB-APTES conjugate-doped SiNP prepared by the Stöber method.

The formation of aggregates is easily envisioned given the general lack of uniformity and poor development of individual silica nanoparticles. We concluded that,

despite early successes in our group, the Stöber preparation was not a viable method for producing small-diameter, uniform, dye-doped silica nanoparticles. We next looked to employing the reverse emulsion processes for the development of dye-doped silica nanoparticles.

2.3.2 Silica nanoparticle emulsions preparations (reverse and standard)

In order to overcome the lack of control over size and shape of the silica nanoparticles produced in the Stöber preparation we looked to employ microemulsion methods. Our hypothesis was that emulsion preparations would grant access to small-diameter well-formed particles that could be reproducibly utilized in gold aggregate systems to produce metal enhanced fluorescence and the development of plasmonic waveguides. The reverse emulsion preparation, water dispersed into oil (w/o), is the most common emulsion preparation of small diameter silica nanoparticles[16] and was thus our first attempt.

We attempted reverse microemulsion preparations in order to investigate the use of a water suspension in oil to produce small-diameter silica nanoparticles within micro aqueous reaction vessel. The emulsion is thermodynamically stable due to the presence of surfactant and co-surfactant molecules added to the suspension. Therefore, altering the relative amounts of surfactant or water to the oil medium can be used to alter the overall size of the microsphere in the emulsion.[8]

Figure 2.14 shows a TEM image of particles, using the previously established reaction conditions,[8] which employ the surfactant Igepal® CA-520 to produce silica nanoparticles with diameters of 14 nm. The silica nanoparticles produced in reverse

emulsion method using Igepal® CA-520 were more spheroidal than particles from the Stöber preparation but this method similarly did not produce small-diameter spheres that heavily aggregated on the TEM grid.

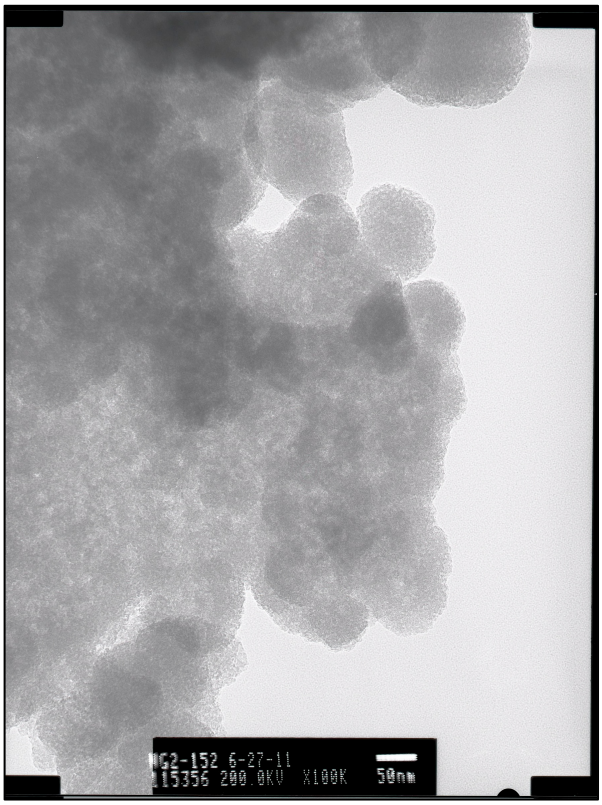

Figure 2.20. TEM image of silica nanoparticles produced via the reverse emulsion (w/o) process with Igepal® CA-520 surfactant.

UV-vis absorption data further supports the formation of large silica aggregates from the reverse emulsion process using Igepal® CA-520 (Figure 2.15). The absorbance spectrum shows significant light scattering occurring beginning at 530 nm until 400 nm, which indicates large particles present in solution. These particles indiscriminately reflect light of all wavelengths due to their average diameters being

larger than the wavelength of incident light, thus giving the appearance of very large absorption at those wavelengths.[29]

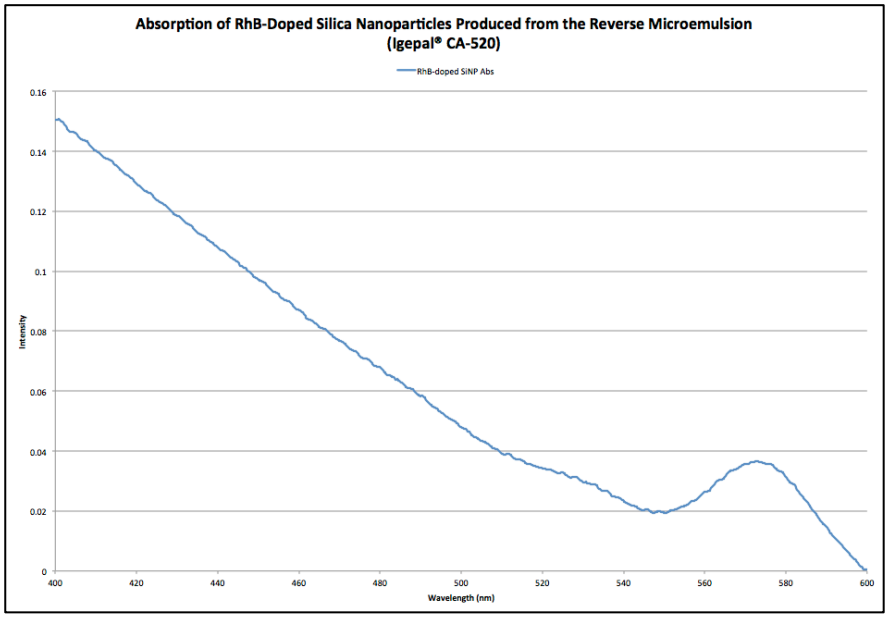

Figure 2.21. Absorption spectrum of rhodamine B-doped silica nanoparticles produced in a reverse emulsion preparation using Igepal® CA-520.

Similar microemulsion preparations have been attempted using Triton X-100 surfactant[22] in our lab that similarly resulted in large silica aggregates. While the desired small-diameter particles were not observed we were able to form more spheroidal morphologies with the reverse emulsion compared to the Stöber preparation. Therefore, we chose to attempt a standard microemulsion to investigate if switching the role of water and oil in the mixture would yield small-diameter silica nanoparticles.

In order to grow smaller and more uniform silica nanoparticles we attempted a standard emulsion preparation.[21b] Here, a microemulsion of oil droplets dispersed in an aqueous medium (o/w), was created by the addition of the surfactant Tween-80 and

dimethylsulfoxide (DMSO) to an excess of water to produce a cloudy solution that became transparent upon stirring. Rhodamine B was doped into the growing particles via co-condensation through the siloxane conjugate APTES precursor, similar to the Stöber preparation. The size of these dye-doped silica particles were controlled by vary the ratio of surfactant, water, and silica precursor as discussed with the reverse emulsion process. Figure 2.16 shows a TEM of these dye-doped silica nanoparticles produced by the standard emulsion process.

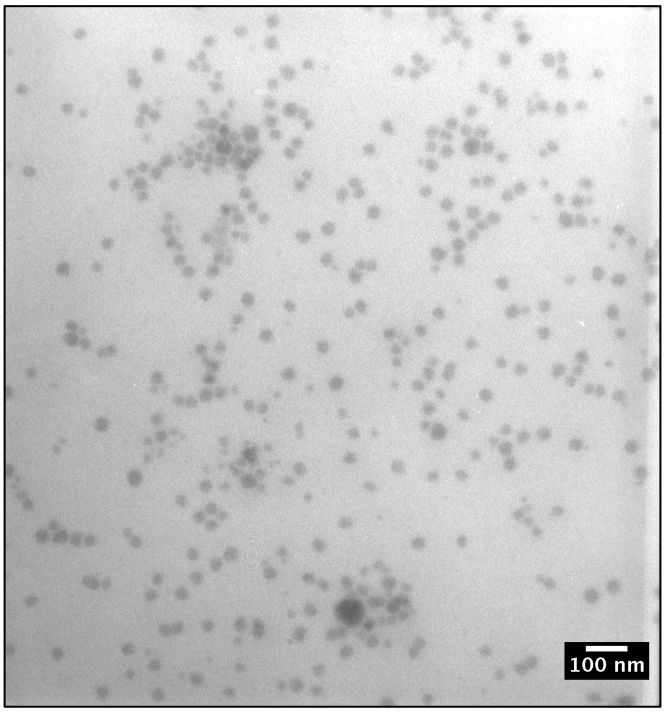

Figure 2.22. TEM image of rhodamine B-doped silica nanoparticles prepared by the standard microemulsion process.

Dye-doped silica nanoparticles formed in this standard emulsion preparation had an average diameter of 30 nm with a variation of ± 6 nm. Furthermore they show excellent spherical uniformity and there is little-to-no aggregation present. Absorbance

measurements, shown in Figure 2.17, support the lack of aggregation in the system. The absorbance spectrum confirms small particle diameter and lack of aggregation, as there is no significant scattering curve visible in the lower wavelengths (< 500 nm).

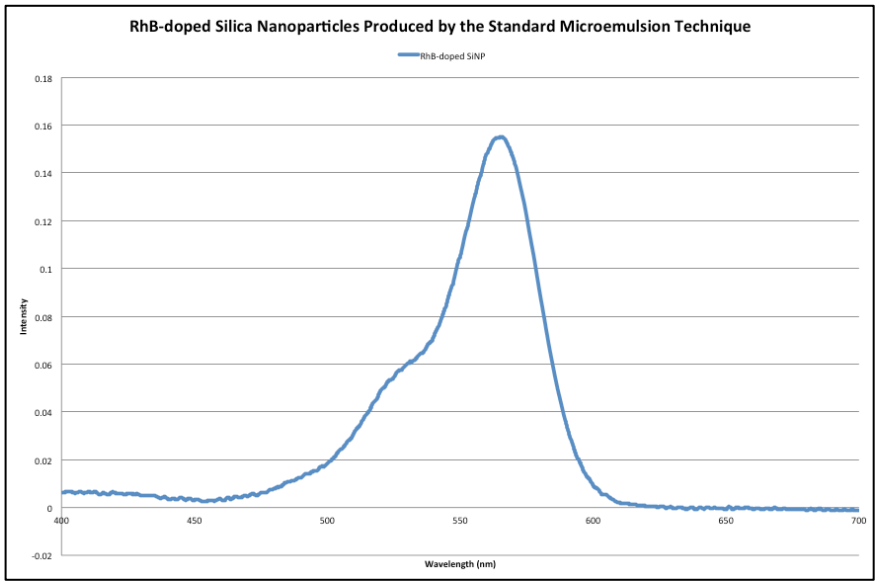

Figure 2.23. Absorbance spectrum of rhodamine B-doped silica nanoparticles that were produced using the standard microemulsion preparation. No low wavelength scattering present.

The lack of scattering is in stark contrast with the absorption spectrum of the reverse emulsion preparation seen in Figure 2.15.

Silica nanoparticles produced by the standard emulsion prep are too small to clean by conventional centrifugation so membrane dialysis and centrifugation were utilized to remove excess reagents.[20] The entire contents of the microemulsion was added to a micro-porous cellulose membrane tube with a molecular weight cutoff (MWCO) of 12-14 kD and dialyzed against water. Pores in the cellulose membrane were large enough to allow unreacted ammonium hydroxide, co-surfactant butanol

molecules, and un-reacted RhB-APTES conjugate through but were small enough to keep the 30 nm diameter particles within the tube. However, Kumar et al[20] claim that micelles, formed by the surfactant Tween-80, were too close in size to the silica nanoparticles to be separated by mild diffusion along a concentration gradient. Thus, a centrifuge membrane was used to lyse the micelles, via centrifugal force, into the reservoir of the tube. Figure 2.18 shows a picture of the centrifuge membrane assembly.

Figure 2.24. Nanosep centrifugal device prior to be centrifuged. The red band is a label for the MWCO (30 kD)

Initial attempts of separating the Tween-80 micelles from silica nanospheres were performed with 30 kD pores that were generously donated from the West lab. During TEM sample preparation stickiness of the grids was noted and the TEM images would not properly resolve as the nanoparticles were surrounded by micellular layers due to increasing the thickness of the sample (see Figure 2.16). Thus, the smaller MWCO filter may not have allowed for all of the micelles to separate.New100 kD

(MWCO) filters were obtained in or group and should help remove excess amount of surfactant from the silica nanoparticles.

Reverse and standard microemulsions can be utilized to overcome some of the challenges seen in the Stöber preparation. The standard emulsion is especially well-suited to produce small diameter, < 50 nm, silica nanoparticles with relatively good monodispersity and no homo-aggregation. However, these methods still do not address the issue of creating a discrete location for the dye within the silica matrix, which can theoretically lead to undesirable quenching effects if a random distribution of the dye are too close to the surface of the gold nanoparticles. Dye location issues are than finally addressed by employing the layered silica nanoparticle preparation.

2.3.3 Layered silica nanoparticles

We investigated the formation of dye-doped silica nanoparticles by physirobing dye onto small silica cores and securing them in place by growing additional silica around the dye-core complex. Layered silica nanoparticles were prepared via multiple sequential base catalyzed TEOS condensations in an aqueous/organic biphasic system.[2] The size of the particles was found to be dependent on the identity and amount of base, the amount of TEOS, and duration of reaction.[9] Reacting arginine under previously established reaction conditions[2] produced small monodisperse core silica particles 16 nm in diameter (Figure 2.19). Fluorophores of interest were then physisorbed onto the surface of the silica cores. Then additional TEOS condensation, analogous to the core-shell synthesis, produced layered particles. The size of the outer shell was varied by limiting the amount of precursor TEOS in the system. Figure 2.19 shows an example of the architecture of the SiNPs as well as TEMs of the cores and shelled products.

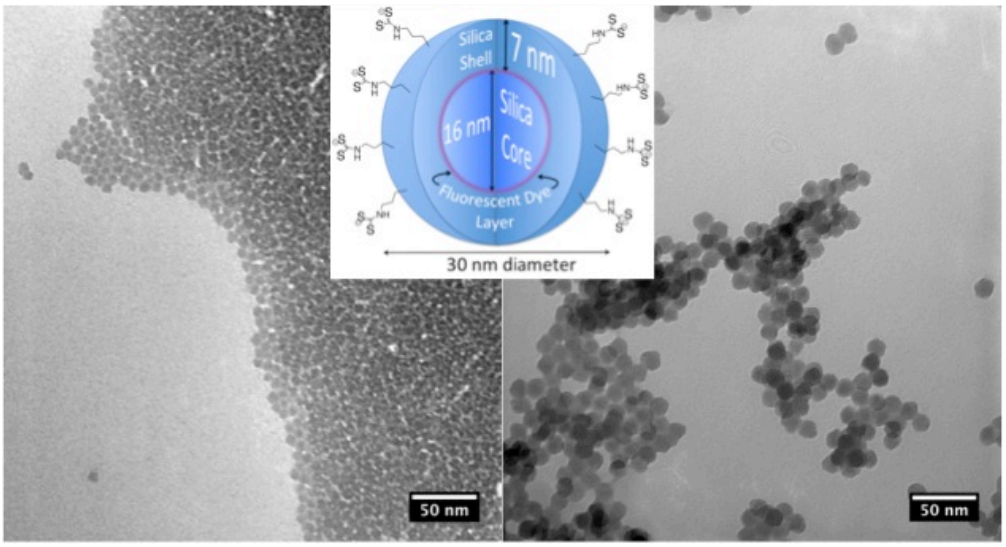

Figure 2.19. TEM image of silica nanoparticles before (left) and after (right) dye physisorbtion and shell re-growth. (center) Cartoon representation of dye-doped particles. (from this work)

The layered preparation has proven to be the most useful preparation of small diameter particles with excellent uniformity (Figure 2.20). In this figure we note the consistently uniform small diameter morphology especially in the magnified image shown in Figure 2.21.

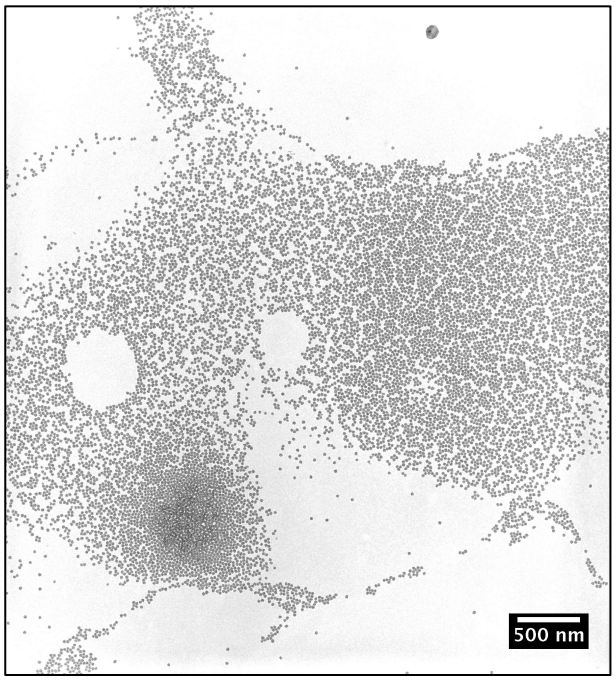

Figure 2.20. NG2-235.TEM image of a small diameter core-doped silica nanoparticles. (from this work).

Figure 2.21 shows a magnified TEM image to emphasize the relatively well-formed surface of the silica nanoparticles produced via the layered preparation. The layered preparation clearly appears to be the best option for preparing uniform, small diameter, dye-doped silica nanoparticles.

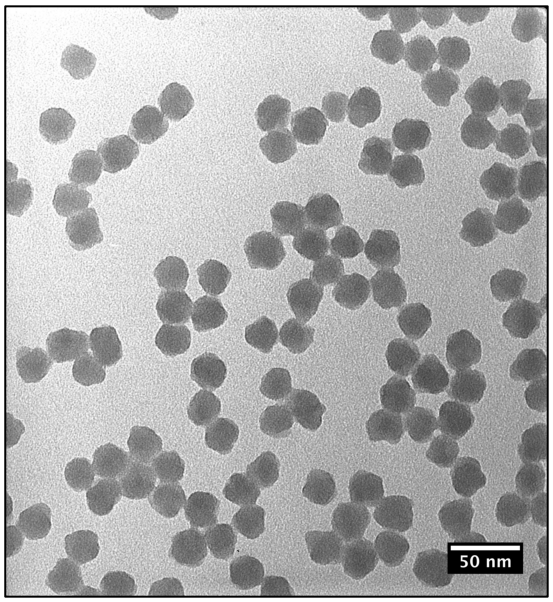

Figure 2.21. Magnified TEM image of small diameter (average ~24 nm) core-doped layered silica nanoparticles. (from this work).

TEM images show excellent monodispersity and clean transformation of TEOS precursor. Magnified images do show some morphological variation within the small diameter particles but this could also be due to interactions with the imaging instrument. Very thin regions of silica can be thermally sensitive to the interaction with the electron beam used to image the material. This especially can occur at high magnification and at the interface of two nanoparticles (Figure 2.21 above showing apparently fused nanoparticles). Morphing of the outer surface is not seen as readily with larger silica nanoparticles produced by the layered preparation *vida infra*. The dye-doped silica nanoparticles must then be cleaned via membrane dialysis, as the particles are too small to cleanly centrifuge down into a pellet similar to the microemulsion preparation described above.

Membrane dialysis was found to be useful for cleaning small diameter silica nanoparticles and could be used to determine the amount of dye that was incorporated into the silica. The process takes advantage of a concentration gradient established by adding a concentrated sample into a semi-permeable membrane bag and allowing water to replace small molecules in the sample while larger species are unable to cross the membrane. Small amounts of arginine and any unreacted dye must be removed from the reaction mixture before the sensitive nanomaterials were carried on to surface functionalization reactions (see chapter III). Moreover, the amount of dye incorporated into the silica could be determined by carefully monitoring the amount of fluorophore leached into the aqueous supernatant (Figure 2.22). Dialysis was allowed to proceed for several hours in a sealed system before changing out the water. Monitoring aliquots of each supernatant allowed for the calculation of leached dye via Beer's law (see experimental section for concentration calculations). The supernatant was continually changed until no signal was observed via UV-Vis, indicating no more free dye was present in solution. The difference between the amount of dye originally added during the preparation and the amount calculated from the supernatant gave the amount of dye present in solution.

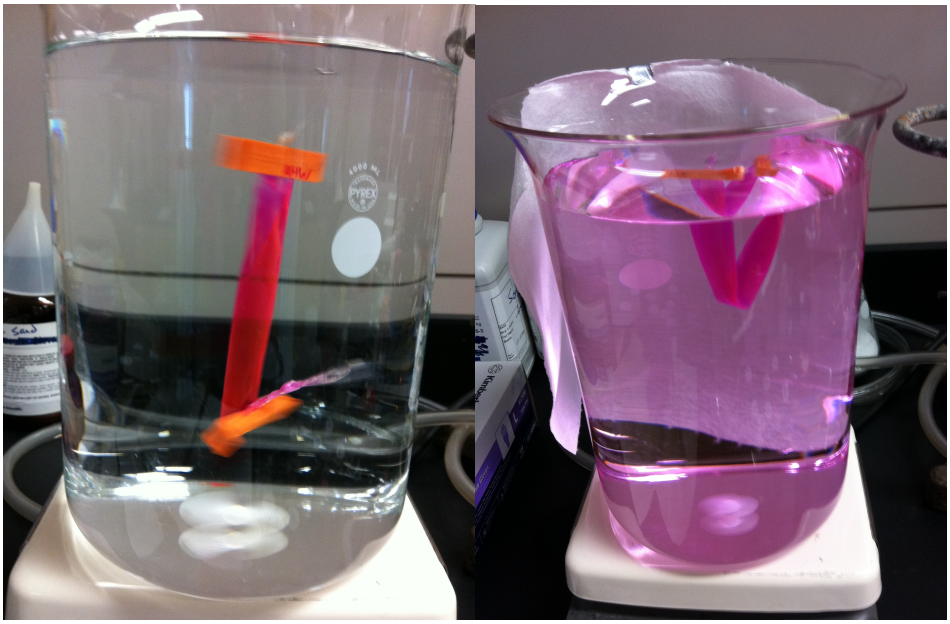

Figure 2.22. (Left) Initial dialysis setup using cellulose membrane with a molecular weight cut-off (MWCO) of 12-14 kD. (Right) After 12 hr wash (1 water change)

The layered preparation showed excellent dye incorporation (e.g. 95% incorporation for the addition of ~3 mg of dye to a standard core preparation, see experimental section for calculations). Knowledge of the amount of incorporate dye is important due to the possibility of destructive dye-dye aggregation that can lead to quenching.[6]

Forming multiple layers of dye on a silica nanoparticle could be counterproductive to producing enhancement as these layers could produce pi-pi stacks of dye, which may enable emission quenching. The number of layers of rhodamine B present in a single nanosphere were calculated based on the average diameter of the silica cores and the amount of dye incorporated into the silica (see experimental section

for calculation details). One layer of dye was calculated to be present per 16 nm diameter core (given 95% incorporation of rhodamine B and assumed facial stacking of a model measured area, see experimental section 2.5.6). This is reasonably supported by analysis of the preparation. The dye was reversibly physisorbed onto the surface of the silica spheres. While pi-pi stacking is energetically favorable, the stronger attractive force is electrostatic between the partially negative surface of the silica and the positive surface of the rhodamine B. Dissociation of dye-dye interactions is then much larger than the dissociation of the dye silica complex, especially in the ever decreasing free-dye concentration environment of the dialysis setup. Thus, dialysis provides an important tool for determining the amount of dye and cleaning small diameter silica nanoparticles that are tool small to clean via centrifugation. However, similar experiments are more easily accomplished with larger silica nanospheres that have enough mass to effectively form a pellet via centrifugation.

Large-diameter silica nanoparticles can also be produced via the layered preparation. The over-all larger diameter is a consequence of adding a greater amount of TEOS (compared to the small-diameter preparation) in the shell growth stage (Figure 2.23). The layering process can be employed to effectively grow the outer shell in small incremental steps for fine size control within the range of tens of nanometers.

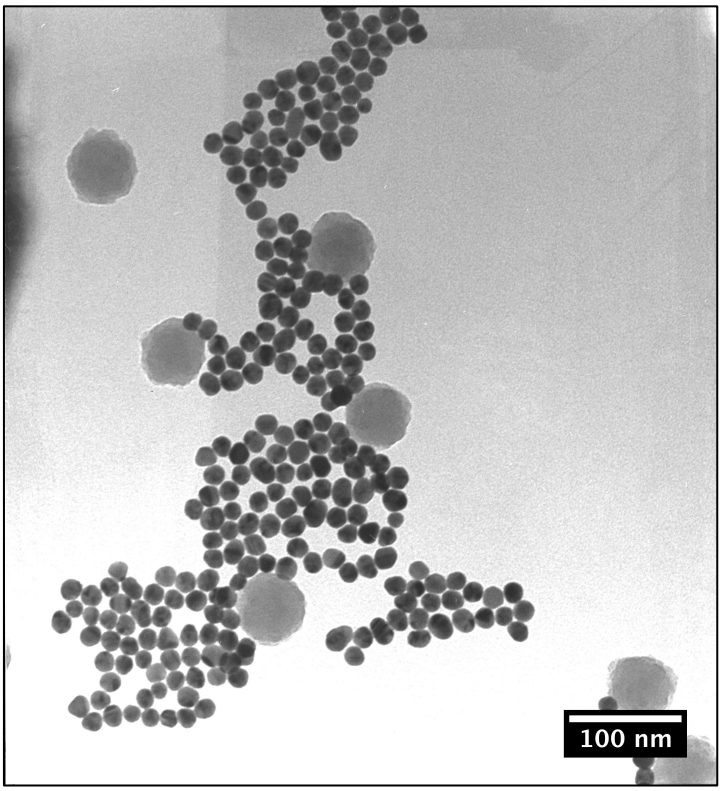

Figure 2.23. TEM of silica nanoparticles grown by the layered preparation (d~ 60 nm) with citrate-capped GNP for size reference.

The silica nanoparticles produced were roughly 60 nm in diameter with excellent spherical uniformity. Figure 2.24 shows silica nanoparticles that have been grown to an average diameter of 150 nm from those shown in Figure 2.23. Further increased TEOS addition provided particles with average diameters of approximately 150 nm with similar excellent uniformity.

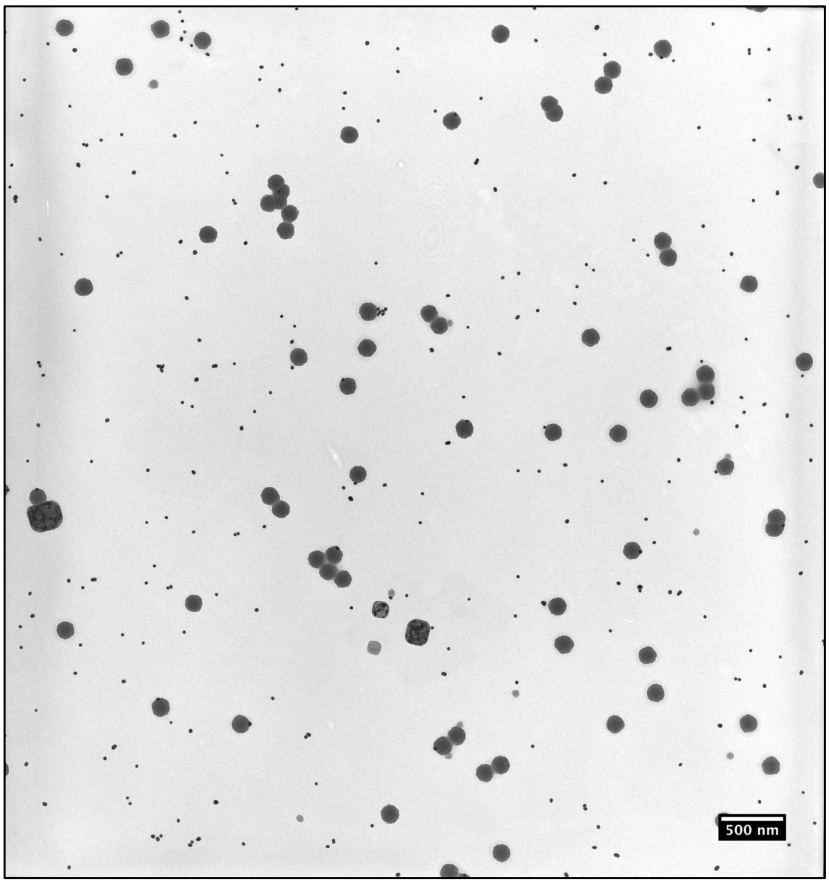

Figure 2.24. TEM image of uncoated large-diameter silica nanospheres (average diameter ~150 nm) produced by the layered preparation (GNP added for size reference).

The silica shell growth, catalyzed by additional amounts of TEOS and arginine, produces excellent uniformity at all size ranges. Figure 2.25 is a magnified image of the same sample shown in Figure 2.24 to display the relatively uniformly smooth surface that is developed in the layered process.

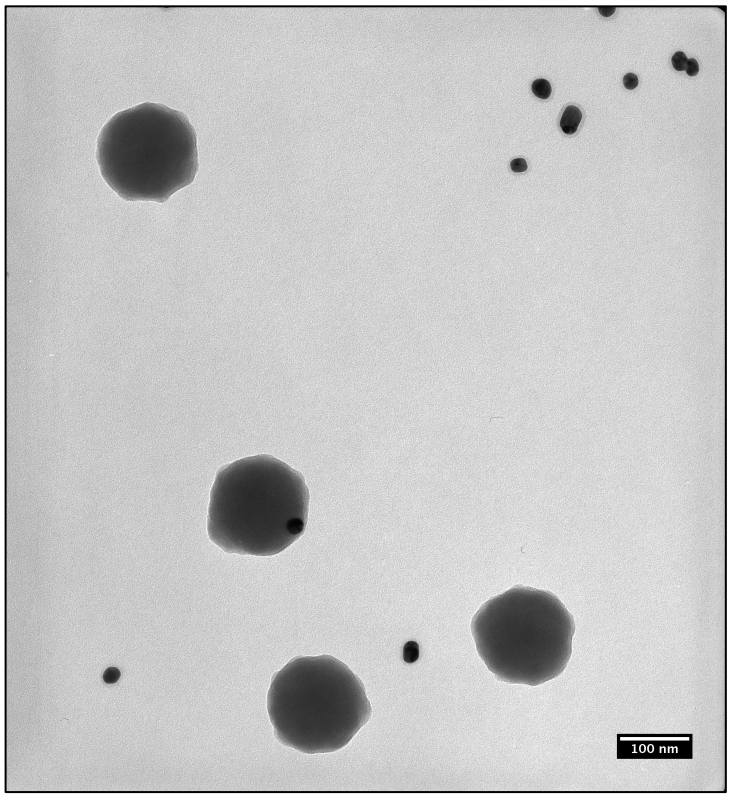

Figure 2.25. Magnified TEM image of uncoated large-diameter silica nanospheres (average diameter ~150 nm) produced by the layered preparation (GNP added for size reference).

Scanning electron microscopy (SEM) images further support the formation of monodisperse spherical silica nanoparticles (Figure 2.26). These topographical images are useful for further investigating the three-dimensional stacking that can occur with pure SiNP samples in ways that are not possible with two-dimensional TEM images.

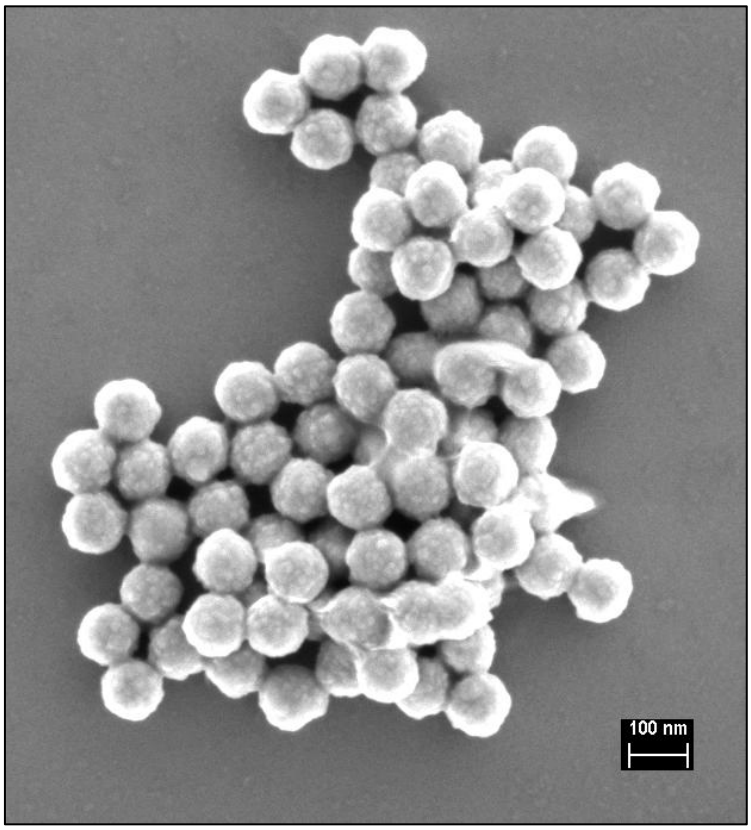

Figure 2.26. Scanning electron microscopy (SEM) of large diameter silica nanoparticles produced by the layered preparation.

The layered preparation is similarly successful at preparing large diameter particles with excellent monodispersity. This preparation eliminates the need for membrane dialysis as the larger particles can more simply be cleaned via centrifugation. Moreover, the added size control allows for a larger spacer to be put in place between the surface of the gold and the dye.

In summary, we investigated forming dye-doped silica nanoparticles by a layered approach whereby the incorporated fluorophore would be located in a discrete layer around the silica core. The preparation was successful at producing well-formed small-diameter particles with size variations from 30-150 nm grown in our lab.

Furthermore, dyes were readily incorporated to the layered spheres (95% in one case), as confirmed by absorption measurements of dialysis supernatant. The concentration of incorporated dye and silica nanoparticles allowed us to calculate that one layer rhodamine B was formed within a single sphere. The ability to fine-tune the size, discretely control the location of dye, and relative ease of dye incorporation make the layered SiNP preparation ideal for producing dye-doped silica and gold nanoparticle aggregates to produce metal enhanced fluorescence and plasmonic mediated energy transfer.

2.3.4 Fluorophore Incorporation and Selection Considerations

In order to probe the differences between covalently linking or simply absorbing various dyes into the silica framework of a nanoparticle we investigated tethering the siloxane precursor (APTES) as well as physisorbing the fluorophores into silica nanoparticles. We investigated six different fluorophores from commercially available rhodamine B, Rubpy, Texas Red, PiCy3, and PyCy5 as well as synthetically obtained BODIPY (Figure 2.27). The fluorophores were incorporated into silica nanospheres based on their solubility and ability to covalently attach (RhB and BODIPY) or incorporate by ionic attraction (TexasRed, Rubpy, PiCy3, and PyCy5). A large library of dye-dope silica nanoparticles is important for probing the best spectral overlap with metal nanoparticles.

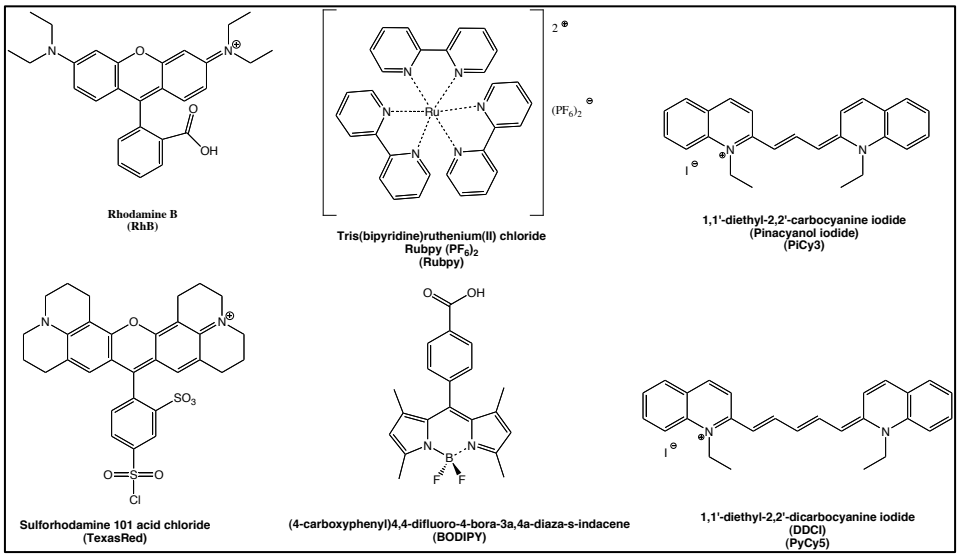

Figure 2.27. A sample of fluorophores that were doped into silica nanoparticles.

Our goal was to determine if particular fluorophores could be matched with our established preparation of silica nanoparticles.

2.3.5 Covalent silica-fluorophore linkages

We investigated covalently linking two fluorophores (RhB and BODIPY) to the silica matrix in order to investigate the effect this bond would have on the absorbance/ emission of the species. Successful dye incorporation into the SiNPs was monitored by absorption, emission, and excitation spectroscopy as well as TEM imaging. Dye leaching was monitored by analysis of supernatant emission spectra over the course of several weeks. As discussed below, no leaching was observed over this time frame.

We attached the siloxane precursor (3-aminopropyl)triethoxysilane (APTES) to dyes, such as rhodmaine B and BODIPY (Figure 2.27), to covalently add a tether that could be condensed into the silica framework. APTES conjugation to organic

fluorophores was accomplished through previously established amide coupling chemistry (Figure 2.28).[3a]

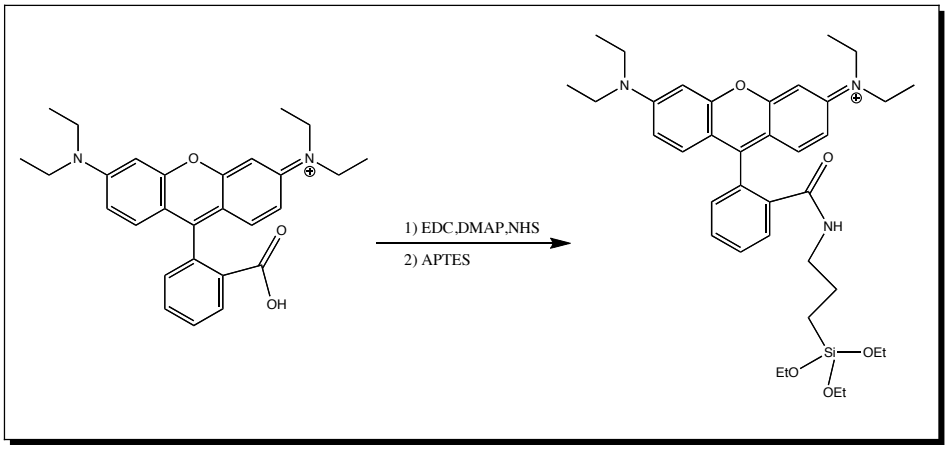

Figure 2.28. Amide coupling reaction of rhodamine B with APTES via EDC/NHS activation.

In order to form an amide bond between the RhB and APTES the carboxylic acid of the dye must first be activated. Carboxylic activation occurs by reacting the dye with 1-ethyl-3-(3-dimethylaminopropyl)carbodiimide (EDC) followed by nucleophilic acyl substitution with N-hydroxysuccinimide (NHS) to form the activated NHS ester. The dye-NHS ester is then readily substituted by APTES to form the dye-siloxane conjugate (Figure 2.29). The dye-NHS ester was carried on without purificaiton or characterization due to the hydrolysis sensitive APTES hanldle.

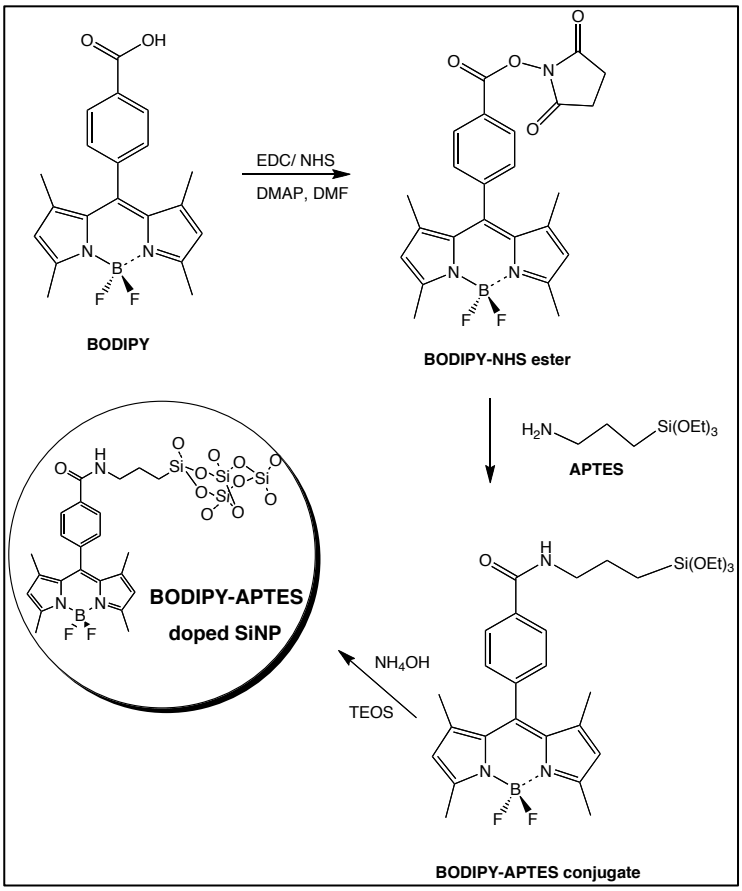

Figure 2.29. Formation of a BODIPY APTES tether via EDC activation for incorporation into silica nanoparticles.

APTES conjugation and covalent incorporation into silica nanoparticles is readily accomplished with any dyes bearing a carboxylic acid such as rhodamine B, Texas Red, and BODIPY. The rhodamine derivatives (Texas Red and rhodamine B) are commercially available while BODIPY was synthesized by our group (see experimental section 2.5.8).

Fluorophore carboxylic activation as found to be completely reversible without jeopardizing the integrity of the dye. BODIPY-NHS ester was readily saponified back to the free carboxylic acid, which could then be incorporated into silica via

physisorbtion (Figure 2.30). The saponification reaction was followed by TLC (measured against pure BODIPY), which showed one discrete molecule in reaction spot. BODIPY re-incorporation into SiNPs was monitored by comparing the original NHS BODIPY and layered BODIPY emission spectra, which did not vary significantly indicating no significant BODIPY damage occurred.

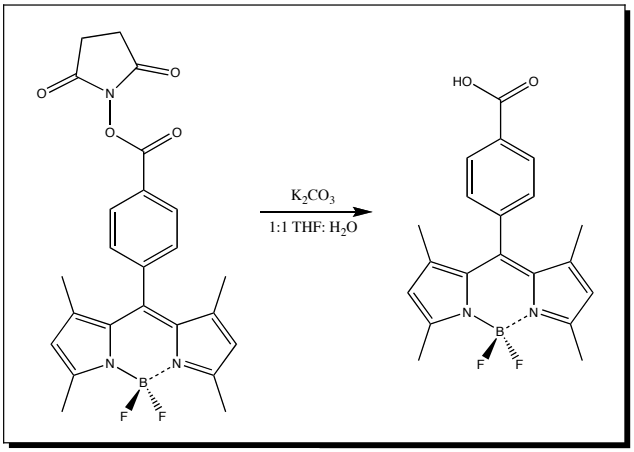

Figure 2.30. Recycling of free carboxylic acid BODIPY from NHS-ester activated species via potassium carbonate catalyzed saponification. (from this work).

The saponification reaction proceeded cleanly to yield the free carboxylic acid BODIPY (Figure 2.30), as verified by spotting against a pure BODIPY TLC spot, that was then incorporated into silica nanoparticles via the layered preparation described above. Figure 2.31 shows a picture of BODIPY at ground state, excited, and incorporated into a silica nanoparticle during dialysis.

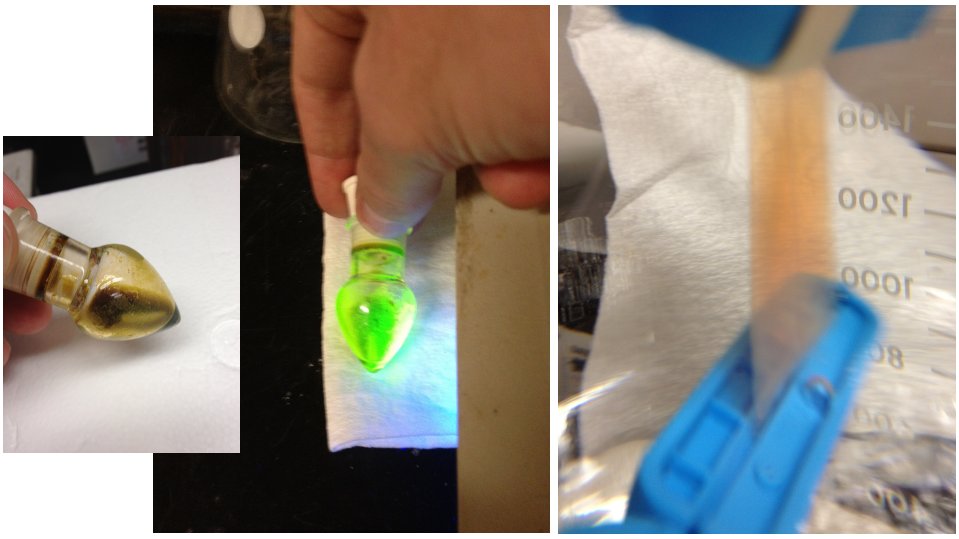

Figure 2.31. (Left to right) BODIPY in ground state in solution, excited by UV lamp in solution, and ground state while physisorbed into layered silica nanoparticles.

The images give a visual overview to support BODIPY's tolerance to covalent modification, as the dye is clearly still able to be fluoresce post saponification. We expect that significant damage of the dye during covalent modification would result in no observable emission of the dye.

APTES conjugation is robust and reversible application for fluorophores bearing carboxylic acids but it is important to consider the effects covalent attachment has on the fluorophore absorbance and emission.

It is important that the absorption and emission properties of fluorophores are not significantly altered during incorporation into silica nanoparticles. Degradation or alterations in absorbance and emission of an incorporated fluorophore may result in poor plasmon overlap, which may lead to decreased metal-enhanced fluorescence.

We initially studied rhodamine B for changes in absorbance spectra in covalently and non-covalently attached silica nanoparticle incorporation. Figure 2.32 shows a moderate red shifting (10 nm) of RhB that has been bound to APTES compared to that which has been physisorbed onto the surface.

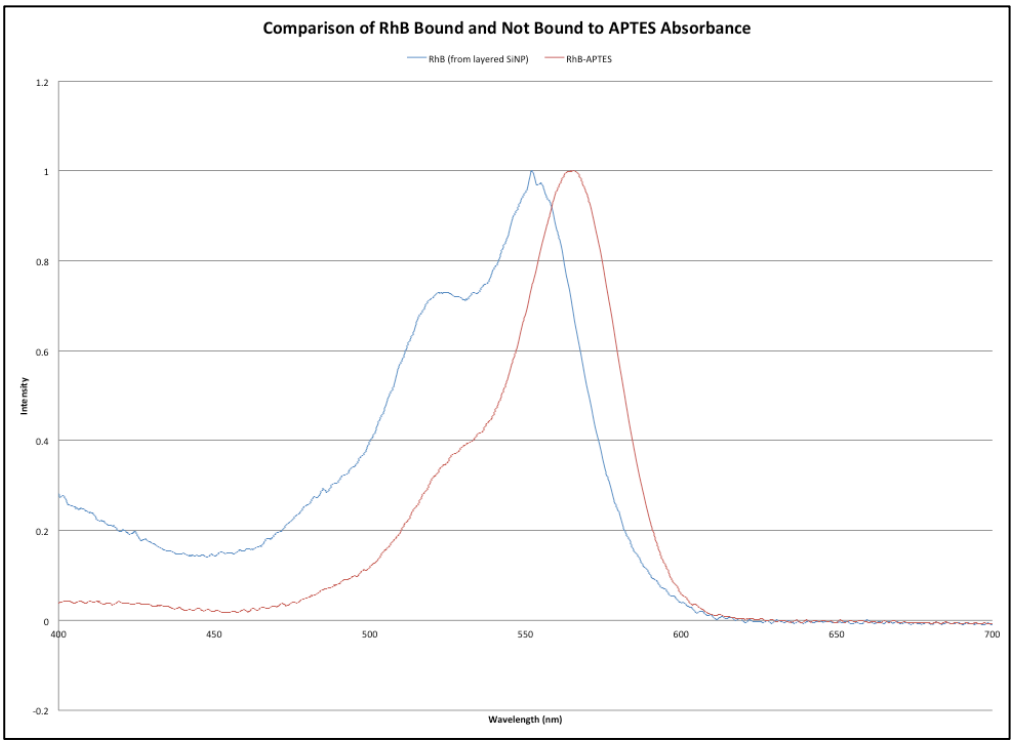

Figure 2.32. Normalized absorbance comparison of rhodamine B covalently bound to APTES (red line) and RhB from a layered SiNP preparation (blue line).

The small 10 nm red shift was deemed not significant enough to impede the investigation of rhodamine B with gold nanoparticles. These absorbance spectra indicate that little fluorophore perturbation occurred outside of the increased electron donation via induction. Thus, covalent incorporation appeared to be a viable method for securing rhodamine B to silica nanoparticles without significantly augmenting its spectral properties. Rubpy-doped SiNPs are discussed in chapter IV regarding

aggregation with GNPs. TexasRed and PiCy3 doped SiNPs are discussed in chapter V as a potential FRET pair for the formation of a nanowaveguide.

We investigated covalently linking fluorophores to the silica matrix to investigate the effect this bond would have on the absorbance/ emission of the species and to investigate how attachment effected dye leaching. Dyes were cleanly incorporated into silica nanoparticles via covalent attachment through APTES amide linkage with little perturbation of their absorbance profiles. Furthermore, APTES functionalization was shown to be reversible, which indicates the integrity of the dye is not compromised during linkage. However, this APTES conjugation only applies to fluorophores bearing carboxylic acid moieties. Dyes lacking this functionality can often be incorporated into silica nanoparticles via enveloping physisorbed dye within layers of silica.

2.4 Chapter Summary

This chapter discussed the need for and our efforts to integrate organic fluorophores into structurally engineered silica nanoparticles for applications in gold nanostructure aggregate systems in order to facilitate metal enhanced fluorescence. Silica nanoparticles are well-suited to incorporate dye molecules in order to appropriately position the fluorophores away from the surface of the metal, which is a key factor to establishing metal enhanced fluorescence.[14] As highlighted below, we found the layered silica nanoparticles preparation best accomplishes dye-incorporation for MEF systems, incorporating a wide range of dyes into silica nanoparticles did not significantly alter their photophysical properties, and covalent attachment is not always

required for dye incorporation but does not damage the fluorescent brightness of the fluorophore if needed.

Many preparations exist for synthesizing silica nanoparticles based on the condenstation of siloxane monomers (Figure 2.4). These silica nanoparticle preparations produce a number of different sizes and morphologies of SiNPs.

The Stöber preparation produced particles in the nanometer to micrometer range (although it is best suited for near micrometer range) and could also be used to effectively produce core shell structures with silica coatings. However, this preparation was found to produce irregular and large diameter particles that would not be useful for metal aggregate systems (Figure 2.12).

The use of microemulsions overcame the size limitation of the Stöber preparation by taking advantage of small, thermodynamically stable, micro-reaction environments created by mixing a surfactant with an organic solvent and water. The size of the particles was controlled by the ratio of surfactant, oil, and water. Microemulsion preparations were successful at preparing small diameter silica nanoparticles but the dye would, as was the case of the Stöber preparation, randomly distribute throughout the silica particle (Figure 2.6).

Layered silica nanoparticles overcome the obstacles of size control and dye placement by slowly growing an outer shell of silica around a small dye-doped core. The layered preparation has been shown to produce SiNPs from 15 to 200 nm by iteratively growing additional silica layers around a small inner core.[2] This process was especially attractive due to the discrete control over dye location within the silica matrix

(Figure 2.8). Layered silica nanoparticles were produced in our lab with excellent uniformity and monodispersity and represent an exciting frontier for investigating the interaction of dye-doped silica and metal nanoparticles. (Figure 2.19)

Inclusion of multiple dyes into silica nanoparticle/ gold nanoparticle aggregates was pursued as this method provided a wide-range of photophysical overlaps in order to fully investigate the interaction between the fluorophore and the plasmon. We investigated a number of dyes from blue absorbing (Rubpy) to near-IR (NIR) absorbing (Cy5) (Figure 2.27) to establish a wide range of absorption and emission bands. Solubility was found to mainly determine the ability to incorporate a dye into silica nanoparticles. Rhodamine B was found to incorporate 95% of initial dye loading by dialysis supernatant absorption analysis (experimental section 2.5.5), which represented one layer of RhB formed around each sphere (experimental section 2.5.6). A large library of dye-dope silica nanoparticles is important for probing the best spectral overlap with metal nanoparticles and is obtainable via physisorption and covalent incorporation of dye.

We investigated covalently linking fluorophores to the silica matrix in order to investigate the effect this bond would have on the absorbance/ emission of the species. Covalent attachment was readily accomplished with dyes that contained carboxylic acid moieties via NHS-activated APTES substitution (Figure 2.29). Covalent attachment showed minimal perturbation of the fluorophore absorbance (Figure 2.32). Furthermore, the reactive moiety was cleanly removed to produce the free acid fluorophore intact (Figure 2.31). Covalent attachment, while not necessary for every preparation of dye

doped silica nanoparticles, is a viable method for incorporating fluorophores bearing carboxylic acid moieties into silica matrices.

Dye-doped silica nanoparticles were investigated for their application in nanoparticle aggregates. The particles were studied according to preparation of silica, incorporation of various dyes, and the methods used to secure the fluorophores to the particles. We found that layered dye-doped silica nanoparticles have the greatest potential to achieve necessary parameters to achieve metal enhanced fluorescence by aggregation with gold nanoparticles.

2.5 Experimental and Methods

2.5.1 Stöber Preparation[17]

A 20 mL screw-top scintillation vial was cleaned by subsequent washes with 1M HCl, Millipore water (17.8 MΩ), 1M NaOH, and finally Millipore water (17.8 MΩ) again before the reagents were added. The freshly cleaned scintillation vial was charged with ethanol (absolute, 10 mL) ammonium hydroxide (300 μL, 29% w/w), and rhodamine B-APTES conjugate (experimental section 2.5.7) (30 mg, 0.04 mmol) and a small magnetic stir bar. The solution was stirred until the dye appeared homogenous in solution. Tetraethylorthosilicate (TEOS) (50 μL, 0.002 mmol) was then added all at once. The solution was stirred at room temperature in the dark for 5 h to produce a cloudy pink solution. The entire reaction flask was partitioned into several 1.5 mL pop-cap centrifuge tubes, which were then spun at 15,000 rpm for 10 min, which produced a bright pink pellet at the bottom of each tube. The supernatant of each tube was removed and the remaining contents were all collected into one 1.5 mL pop-cap centrifuge tube. This material was suspended in water (17.8 MΩ, 1.5 mL) via sonication before being

centrifuged down again. This process was repeated for a total of 3x water washes and additionally 3X with ethanol (absolute, 1.5 mL) each time spinning at 15,000 rpm for 10 min. The material was re-suspended in 1 mL of water before being applied to aggregation experiments.

2.5.2 Reverse Microemulsion Silica Nanoparticle Preparation[8]

Igepal®CA-520 (0.437 g) was dissolved in heptane (10 mL) in a clean 20 mL scintillation vial. Rubpy (90 μL, 0.1 M) and TEOS (0.1 mL), and ammonium hydroxide (60 μL, 29.6% w/w) were subsequently added before the mixture was stirred at room temperature for 24 h. The emulsion was broken by adding ethanol (3 mL), before the particles were washed twice with ethanol (1.5 mL) and once with water (1.5 mL) as described in section 2.5.1 to provide a bright orange suspension.

2.5.3 Standard Microemulsion Silica Nanoparticle Preparation[21b]

APTES RhB precursor (experimental section 2.5.7) (0.1g, 0.2 mmol) was triturated with a ethyl acetate/ hexanes (50/50) mixture after the solvent was removed in vacuo. The resulting solid was desiccated overnight in the reaction flask before a small portion of the triturated dye (~10 mg) was dissolved in dimethylsulfoxide (DMSO) (4 mL). The emulsion was then prepared in a separate clean 20 mL scintillation vial by adding Tween-80 (0.2 g), 1-butanol (0.3 mL), DMSO (0.1 mL), water (17.8 MΩ, 10 mL), and a magnetic stir bar. The emulsion was vigorously stirred before the previously prepared APTES-RhB in DMSO mixture (0.1 mL) was added. Next, vinyltriethoxysilane (VTES) (0.1 mL, 0.47 mmol) was stirred into the emulsion for 1 h before ammonium hydroxide (29% w/w, 10 μL) and mercaptopropyltrimethoxysilane (MPTMS) (10 μL, 0.5 μmol) were added and the mixture was stirred overnight at room

temperature. The particles were cleaned via cellulose membrane dialysis (MWCO= 12-14 kDa) as described in section 2.5.4. Next, the particles were spun down through a centrifuge membrane filter (30 kD pore size, Pall Corp. Omega Nanosep Centrifuge Membrane Filter) for 30 min at 14,000 rpm. The SiNP were collected as dark pink powder in the top of filter (retentate), which were easily re-suspended in DI water (0.5 mL, the capacity of the filter) before being carried on to further experiments.

2.5.4 Layered silica preparation[2]

Core SiNP preparation: L-arginine (9.1 mg, 0.052 mmol) was dissolved in water (6.9 mL) in a clean 20 mL scintillation vial with a small magnetic stir bar. Cyclohexane (0.45 mL) was then added to form a biphasic (aqueous/organic) system that was heated in an oil bath to 60 °C. Tetraethylorthosilicate (TESO) (0.55 mL, 2.5 mmol) was added carefully to the top organic layer before the vial was tightly re-capped and placed back in the oil bath. The mixture was slowly stirred, attempting to minimize disturbance of the top organic layer. The vial was heated at 60 °C for 24 h before the small diameter (13-15 nm) silica nanoparticles were removed from the aqueous layer. These particles were isolated by removing the colloidal aqueous suspension to give a transparent liquid, which was carried on without any further purification.

Dye physisorbption and shell growth: SiNP cores (1 mL) were mixed with the selected dye (specific examples below) overnight at room temperature via mechanical inversion to allow the dye molecules to physisorb onto the hydroxy coated surface of the SiNP. The SiNP/dye solution was then added to a 20 mL scintillation vial with water (3.6 mL) and a small magnetic stir bar. Cyclohexane (0.5 mL) was then added before the biphasic

mixture was heated to 60 °C. TEOS (0.352 mL,, 1.57 mmol) was added. The mixture was stirred at this temperature for 24 h to give a bright pink suspension.

Dialysis: The entire aqueous portion of the SiNP preparation, post shell growth, was added to a 5-6 inch strip of cellulose dialysis tubing (MWCO 12-14 kDA, Spectrum Labs) after it had been soaked in water for 15 min and sealed from one end with a dialysis clamp. Any excess air was removed from the dialysis tubing before a second clamp was added to the top, leaving roughly 20% of negative space, an evacuated area for water to fill, in the bag to allow for water influx. A small strip of Styrofoam was then added to the top clamp in order to float the dialysis tube. This assembly was then placed in a 4 L beaker filled with 2 L of milipore water and a magnetic stir bar. The water was replaced after an initial 4 h and again after 12 h to ensure there was never a significant concentration of dye in the dialysis water. The clamp was removed and the freshly cleaned particles were diluted with water to 10 mL in a volumetric flask to account for variations in the amount of water that entered the membrane in each preparation to produce a transparent pink solution.

Silica shell re-growth: A 20 mL scintillation vial was charged with layered RhB-doped core SiNP (1 mL, 16 nm diameter), water (3.6 mL), and a magnetic stir bar. To this, L-arginine (1.07 mg) was added. Cyclohexane (0.5 mL) was added to create a top organic layer. The vial was heated to ~60 °C before TEOS (0.4 mL) was added carefully to the top layer. The vial was then tightly capped and slowly stirred, to minimize perturbation of the top layer as much as possible, at 60 °C for 30 h. This resulted in a cloudy pink solution. The suspension was cleaned via centrifugation three times, spinning at 15,000 rpm for 10 minutes, replacing the supernatant with milipore water (1.5 mL, 17.8 MΩ)

each time to give a light pink suspension. TEM confirmed the resulting clean particles had an average diameter of 60 nm.

2.5.5 Calculation of rhodamine B incorporation into silica nanoparticles.

Aliquots of aqueous supernatant were measured for absorbance to calculate the total amount of dye that had not been incorporated into the particles. The aliquots were taken from sealed dialysis chambers to ensure accurate concentration readings. These samples were compared to a standard dilution series of known dye concentration to determine incorporated concentration. The process was as follows:

A series of ten-fold dilutions were made of a 43.42 μM aqueous solution of rhodamine B. The absorbance of each sample was measured and plotted versus concentration to produce a line represented by equation 1.

$$y = 0.9703x + 0.0028 \qquad (1)$$

The line was then fit through the origin as no absorbance should be expected from no dye present giving equation 2.

$$y = 0.963x \qquad (2)$$

The first aliquot of dialysis supernatant showed an absorbance of 0.077 (at λ_{max}= 554.4) thus giving a concentration of:

$$x = \frac{0.077}{0.963} = 0.079\ \mu M$$

The dialysis was carried out in 3 L of milipore water (accurately measured via graduated cylinder) thus giving the total number of mols from the first dialysis:

$$0.079\ \frac{\mu\ \text{mols}}{L} \times 3\ L = 0.237\ \mu\text{mols} = \ 2.37\times10^{-7}\ mols\ of\ RhB$$

The second dialysis gave an absorbance of 0.005 after three additional days giving a concentration of:

$$x = \frac{0.005}{0.963} = 0.0052\ \mu\text{M} \times 3\ L = 0.0156\ \mu\text{mols} = 1.56\times10^{-8}\ mols\ of\ RhB$$

Thus, the total amount of rhodamine B collected from the dialysis supernatant is:

$$2.37\times10^{-7} + 1.56\times10^{-8} = \mathbf{2.53\times10^{-7}}\ total\ mols\ of\ RhB\ from\ dialysis$$

Given that 2.36 mg of rhodamine B was initially doped into the layered particles and that the molecular weight of RhB is 443.56 g/mol, the starting molar concentration was:

$$2.36\ mg\ Rhb = \frac{0.00236\ g\ RhB}{443.56\ {}^{g}/_{mol}} = \mathbf{5.34\times10^{-6}}\ mols\ of\ RhB\ intially\ added$$

Thus the percent recovery is given by:

$$\frac{2.53\times10^{-7}\ total\ mols\ of\ RhB\ from\ dialysis}{5.34\times10^{-6}\ mols\ of\ RhB\ intially\ added} \times 100 = 4.73\ \%\ recovery$$

Therefore the percentage dye incorporated is: **95.58 % dye incorporation.**

2.5.6 Calculation of number of layers of rhodamine B per layered silica nanoparticle.

The numbers of layers of rhodamine B within each layered silica nanoparticles were calculated using the dye incorporation and dry weight data from the experiment mentioned above. First, the number of silica nanoparticle cores were calculated. Next, the number of rhodamine dye molecules necessary to create one layer (assumed

simplified close packing model) was calculated. Finally, the number of possible layers in the system (determined from the % incorporation previously mentioned above) were divided by the number of particles to give the total number of layers of rhodamine B in each layered silica nanoparticle.

The number of silica nanoparticles in the system were calculated based on the spherical mass equation 3.

$$m = dv = \frac{4}{3}\pi r^3 d \qquad (3)$$

Given the density of amorphous silica is 2.2 g/cm^3, a 16 nm diameter silica nanoparticle core has a mass of:

$$m = \frac{4}{3}\pi(8\times10^{-7}cm)^3\times 2.2\,{}^{g}/_{cm^3} = 4.7\times10^{-18}\,{}^{g}/_{SiNP\ core}$$

Assuming 100% conversion of TEOS ($Si(OEt)_4$, mw=208.33 g/mol) to silic acid ($Si(OH)_4$, mw=92.08 g/mol) and thus 100% conversion into silica nanoparticles the addition of 0.520 g of TEOS gives:

$$\frac{0.52\ g\ TEOS}{208.33\ {}^{g}/_{mol}} = 2.5\times10^{-3} mols\ of\ TEOS = \frac{1\ mol\ of\ SiO_4}{1\ mol\ of\ TEOS} = \frac{92.08\ g\ of\ SiO_4}{1\ mol\ SiO_4}$$

$$= 0.2302\ g\ of\ SiO_4\ initially\ added$$

Therefore:

$$\frac{0.2303\ g\ of\ SiO_4\ added}{4.7\times10^{-18}\ {}^{g}/_{SiNP\ core}} = 4.89\times10^{16}\ SiNP\ cores\ produced$$

Only 1 mL of the initial 6.9 mL of total preparation volume is coated in RhB at a time giving:

$$\frac{4.89\times10^{16}\ SiNP\ cores}{6.9\ mL\ total\ vol} = \mathbf{7.08\times10^{15}\ SiNP\ cores/mL}$$

The approximate area of a single rhodamine B molecule was determined by molecular modeling assuming a simplified rectangular boundary about the frozen structure (Figure X).

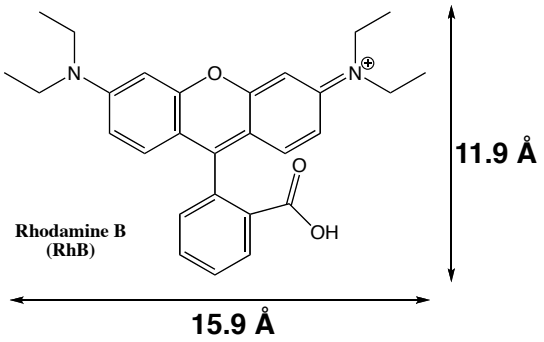

Figure 2.25. Schematic of RhB dimensions as determined by molecular modeling

Thus the simplified area is given as:

$$Area\ of\ rhodamine\ B = h\times w = 11.9\ \text{Å} \times 15.9\ \text{Å} = 189.2\ \text{Å}^2$$

The area of a 16 nm diameter nanosphere core is given by:

$$Core\ nanosphere\ area = 4\pi r^2 = 4\pi\left(80\text{Å}\right)^2 = 80424.7\ \text{Å}^2$$

Thus the number of rhodamine B molecules needed to form one monolayer across the surface area of a core nanospheres is:

$$\frac{80424.7\ \text{Å}^2}{189.2\ \text{Å}^2} = 425\ rhodamine\ B\ molcules\ in\ one\ layer$$

Finally, given that 95% dye is incorporated into the SiNP (previously established, see above) then:

$$5.34\times10^{-6}\ mols\ of\ RhB \times 95\%\ incorporation$$

$$= 5.07\times10^{-6}\ mols\ RhB\ absorbed\ onto\ silica \times 6.02\times10^{23}\ RhB\ molecule/_{mol}$$

$$= 3.01\times10^{18}\ RhB\ molecules$$

Therefore:

$$\frac{3.01\times10^{18}\ RhB\ molecules}{425\ rhodamine\ B\ molcules\ in\ one\ layer} = 7\times10^{15}\ possible\ layers\ of\ RhB$$

Giving a final number of layers of rhodamine B dye per single layered silica nanoparticle from 1 mL of stock core preparation as:

$$\frac{7\times10^{15}\ possible\ layers\ of\ RhB}{7.08\times10^{15}\ SiNP\ cores/_{mL}} = 0.98\ \approx \mathbf{1}\ \boldsymbol{RhB\ layer/_{SiNP\ core}}$$

2.5.7 RhB Amide coupling and SiNP incorporation (Stöber preparation)[3a]

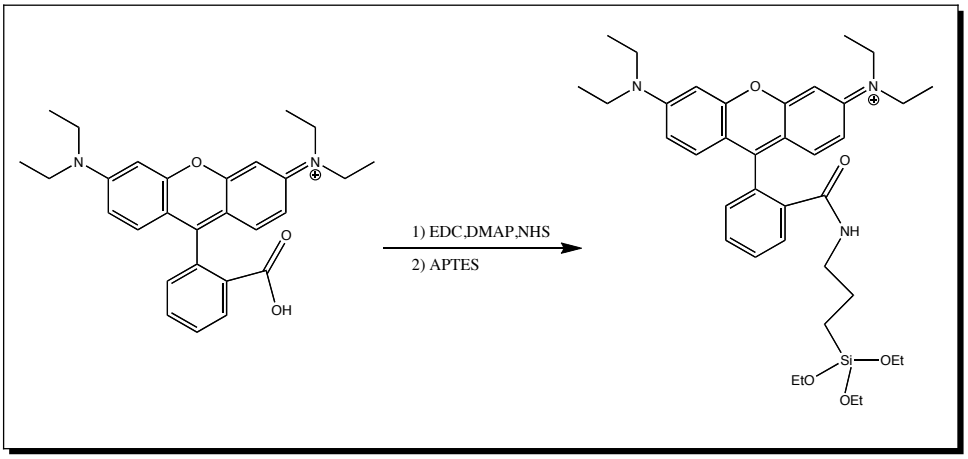

Rhodamine B (RhB) (0.1 g, 0.2 mmol), 1-ethyl-3-(3-dimethylaminopropyl)carbodiimide (EDAC) (0.08 g, 0.4 mmol), N-hydroxysuccinimide (NHS) (0.05 g, 0.4 mmol), and 4-dimethylaminopyridine (DMAP) (0.005 g, 0.04 mmol) were stirred together in DMF (5 mL) under N_2 for 4 h before 3-aminopropyltriethoxysilane (APTES) (0.08 g, 0.04 mmol) was added dropwise. The mixture was stirred overnight. The RhB-siloxane precursor (1.0 mL) was then added to a solution of ethanol (16.75 mL, 95%) and ammonium hydroxide (1.28 mL, 29% w/w) in a new glass vial that was then stirred for 4 h at room temperature. Tetraethylorthosilicate (TEOS) (0.71 mL, 3.2 mmol) was then slowly added before the solution was stirred overnight to give a dark pink solution.

2.5.8 BODIPY synthesis[30]

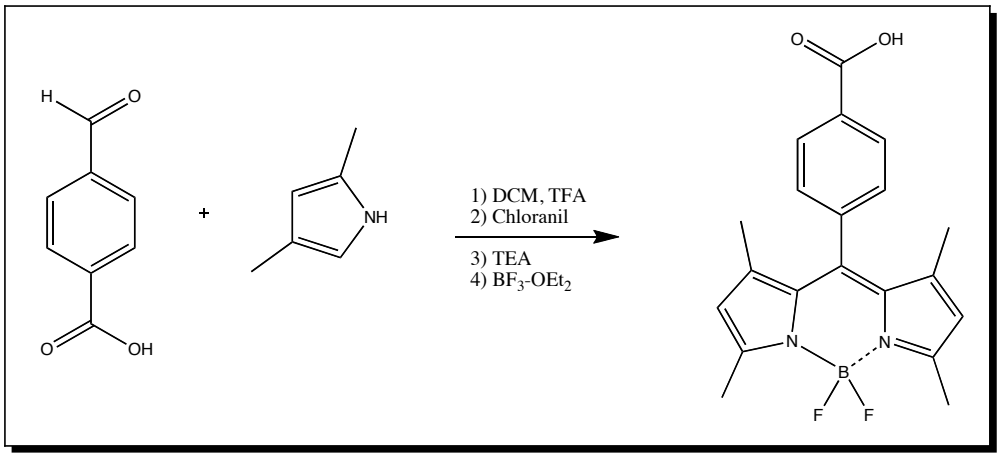

4-Formylbenzoic acid (0.2 g, 1.3 mmol), 2,4-dimethylpyrrole (0.2g, 2.6 mmol), and TFA (2 drops) were stirred together in DCM (25 mL) at room temperature overnight. Chloranil (0.2 g, 0.91 mmol), triethylamine (TEA) (1.5 mL) were added after 30 minutes, and BF3•OEt_2 (1.5 mL) after 2.5 h. The reaction mixture was pumped down and extracted with diethyl ether several times and dried over sodium sulfate. The resulting dark purple solid (fluorescent green in solution) was then purified via column chromatography (1:1 petroleum ether: ethylacetate). ^{1}H NMR (300 MHz, $CDCl_3$): δ 8.25 (d, 2H, J = 8 Hz), 7.45 (d, 2H, J = 8 Hz), 5.99 (s, 2H), 2.05 (s, 12H).

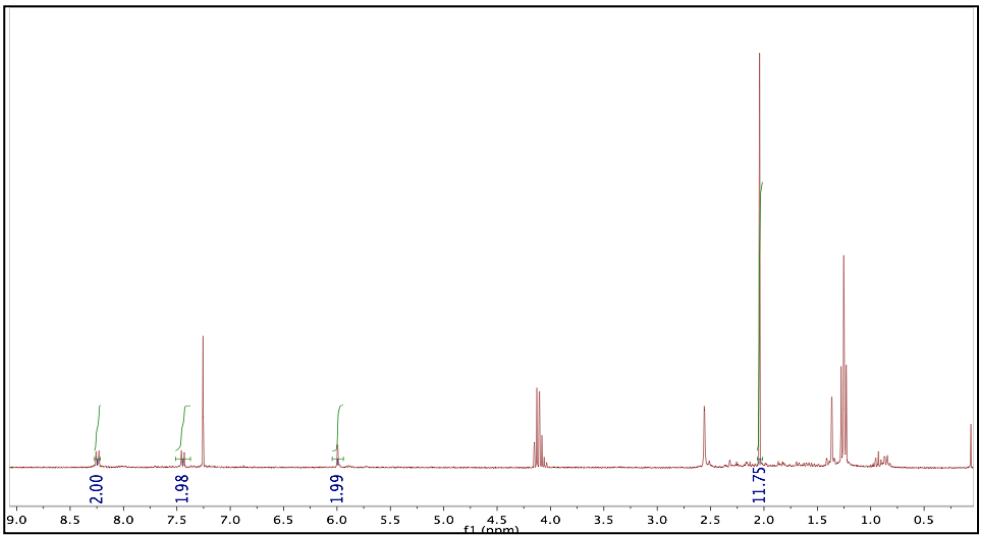

Figure 2.33. BODIPY ^{1}H NMR.

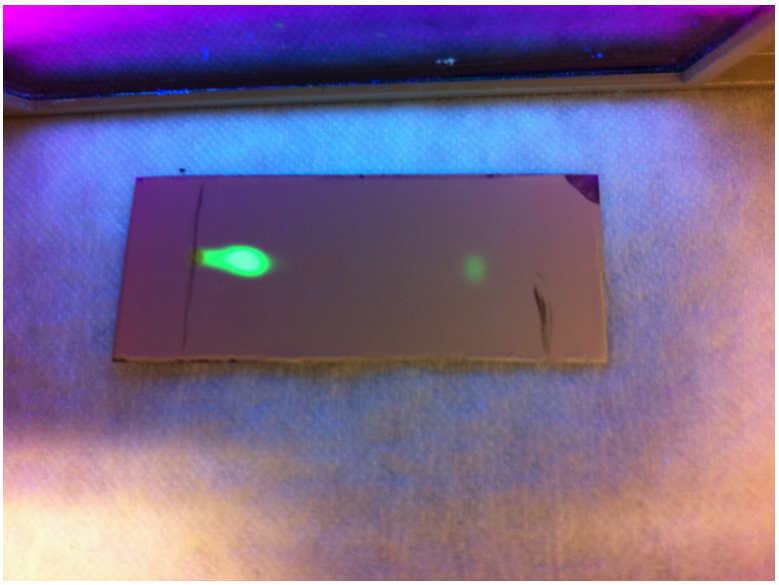

Figure 2.34. BODIPY TLC (1:1 pet ether: ethyl acetate).

2.5.9 BODIPY-APTES precursor and SiNP incorporation

4-Carboxyphenyl BODIPY (0.37 g, 1.0 mmol), 1-ethyl-3-(3-dimethylaminopropyl)carbodiimide (EDAC) (0.38 g, 2.0 mmol), N-hydroxysuccinimide (NHS) (0.23 g, 2.0 mmol), and 4-dimethylaminopyridine (DMAP) (0.02 g, 0.2 mmol)

were stirred together in DMF (25 mL) overnight at room temperature. The air and water sensitive siloxane was directly incorporated into silica without any further purification or analysis. An aliquot of the reaction mixture (1.5 mL) was removed and added to a solution of ethanol (16.75 mL, 95%) and ammonium hydroxide (1.28 mL, 29% w/w) in a new glass vial that was then stirred for 4 h at room temp. Tetraethylorthosilicate (TEOS) (0.71 mL, 3.2 mmol) was then slowly added before the solution was stirred overnight.

2.5.10 Saponification of BODIP-NHS ester

Dark brown purple solid BODIPY-NHS ester was dissolved in 1:1 THF:water (5 mL) followed by the addition of potassium carbonate (~21 mg). The solution was heated to 50 °C overnight in a sealed vessel under magnetic stirring. The resulting green fluorescent material was extracted first with ether (a poor choice for BODIPY) then DCM. The aqueous portion was acidified with a few mL of 1 M HCl allowing for BODIPY carboxylate protonation. TLC analysis showed very clean product conversion with the DCM extraction (R_f = ~0.1 for 1:1 ethyl acetate : petroleum ether).

2.6 References

1. Lakowicz, J. R.; Ray, K.; Chowdhury, M.; Szmacinski, H.; Fu, Y.; Zhang, J.; Nowaczyk, K., Plasmon-controlled Fluorescence: A New Paradigm in Fluorescence Spectroscopy. *Analyst* **2008,** *133*, 1308-1346.

2. Hartlen, K.; Athanasopoulos, A.; Kitaev, V., Facile Preparation of Highly Monodisperse Small Silica Spheres (15 to >200 nm) Suitable for Colloidal Templating and Formation of Ordered Arrays. *Langmuir* **2008,** *24*, 1714-1720.

3. (a) Wang, L.; Tan, W., Multicolor FRET Silica Nanoparticles by Single Wavelength Excitation. *Nano Lett.* **2006,** *6* (1), 84-88; (b) Ma, D.; Kell, A. J.; Tan, S.; Jakubek, Z. J.; Simard, B., Photophysical Properties of Dye-Doped Silica Nanoparticles Bearing Different Types of Dye-Silica Interactions. *J. Phys. Chem. C* **2009,** *113*, 15974-15981.

4. Flachsbart, H.; Stober, W., Preparation of Radioactively Labeled Monodisperese Silica Spheres of Colloidal Size. *J. Colloid Interface Sci.* **1969,** *30* (4), 568-573.

5. Lakowicz, J. R., *Principles of Fluorescent Spectroscopy*. 2nd ed.; Springer: 1999; p 725.

6. Halterman, R. L.; Moore, J. L.; Yip, W. T., Cucurbit[7]uril Disrupts Aggregate Formation Between Rhodamine B Dyes Covalently Attached to Glass Substrates. *J. Fluoresc.* **2011,** *21*, 1467-1478.

7. Xu, J.; Liang, J.; Li, J.; Yang, W., Multicolor Dye-Doped Silica Nanoparticles Independent of FRET. *Langmuir* **2010,** *26* (20), 15722-15725.

8. Bagwe, R. P.; Yang, C.; Hilliard, L. R.; Tan, W., Optimization of Dye-Doped Silica Nanoparticles Prepared Using a Reverse Microemulsion Method. *Langmuir* **2004,** *20*, 8336-8342.

9. Yokoi, T.; Sakamoto, Y.; Terasaki, O.; Kubota, Y.; Okubo, T.; Tatsumi, T., Periodic Arrangement of Silica Nanospheres Assisted by Amino Acids. *J. Am. Chem. Soc.* **2006,** *128*, 13664-13665.

10. Nguyen, Q. X.; Belgard, G. T.; Taylor, J. J.; Murthy, V. S.; Halas, N. J.; Wong, M. S., Water-Phase Synthesis of Cationic Silica/Polyamine Nanoparticles. *Chem. Mater.*

2012, *24*, 1426-1433.

11. Trewyn, B. G.; Slowing, I. I.; Giri, S.; Chen, H.-T.; Lin, V. S.-Y., Synthesis and Functionalization of a Mesoporous Silica Nanoparticle Based on the Sol-Gel Process and Applicaitons in Controlled Release. *Acc. Chem. Res.* **2007,** *40*, 846-853.

12. Qhobosheane, M.; Santra, S.; Zhang, P.; Tan, W., Biochemically functionalized silica nanoparticles. *Analyst* **2001,** *126*, 1274-1278.

13. Alberto, G.; Miletto, I.; Viscardi, G.; Caputo, G.; Latterini, L.; Coluccia, S.; Martra, G., Hybrid Cyanine-Silia Nanoparticles: Homogeneous Photoemission Behavior of Entrapped Fluorophores and Consequent High Brightness Enhancement. *J. Phys. Chem. C* **2009,** *113*, 21048-21053.

14. Geddes, C. D.; Lakowicz, J. R., Metal-Enhanced Fluorescence. *J. Fluor.* **2002,** *12* (2), 121-130.

15. Liu, J.; Li, A.; Tang, J.; Wang, R.; Kong, N.; Davis, T. P., Thermoresponsive Silver/polymer Nanohybrids with Switchable Metal Enhanced Fluorescence. *Chem. Commun.* **2012,** *48*, 4680-4682.

16. Liang, S.; John, C. L.; Xu, S.; Chen, J.; Jin, Y.; Yuan, Q.; Tan, W.; Zhao, J. X., *Silica-Based Nanoparticles: Design and Properties*. Springer-Verlag: Berlin, 2010; Vol. 2010.

17. Yao, G.; Wu, Y.; Schiavone, D. L.; Wang, L.; Tan, W., *Particulate Systems in Nano- and Biotechnologies*. CRC Press: 2008.

18. (a) Graf, C.; Vossen, D. L. J.; Imhof, A.; van Blaaderen, A., A General Method to Coat Colloidal Particles with Silica. *Langmuir* **2003,** *19*, 6693-6700; (b) Durgun, G.; Ocakoglu, K.; Ozcelik, S., Systematic Tuning of Hydrodynamic Diameter of Uniformed Fluorescent Silica Nanoparticles. *J. Phys. Chem. C* **2011**.

19. Stober, W.; Fink, A.; Bohn, E., Controlled Growth of Monodisperse Silica Spheres in the Micron Size Range. *J. Colloid Interface Sci.* **1968,** *26*, 62-69.

20. Kumar, R.; Roy, I.; Ohulchanskyy, T. Y.; Goswami, L. N.; Bonoiu, A. C.; Bergey, E. J.; Tramposch, K. M.; Maitra, A.; Prasad, P. N., Covalenty Dye-linked, Surface-controlled, and Bioconjugated Organically Modified Silica Nanoparticles as Targeted Probes for Optical Imaging. *ACS Nano* **2008,** *2* (3), 449-456.

21. (a) Carpenter, A. W.; Slomberg, D. L.; Rao, K. S.; Schoenfisch, M. H., Influence of Scaffold Size on Bactericidal Activity of Nitric Oxide-Releasing Silica Nanoparticles. *ACS Nano* **2011,** *5* (9), 7235-7244; (b) Roy, I.; Ohulchanskyy, T. Y.; Pudavar, H., E.; Bergey, E. J.; Oseroff, A. R.; Morgan, J.; Dougherty, T. J.; Prasad, P. N., Ceramic-Based Nanoparticles Entrapping Water-Insoluble Photosensitizing Anticancer Drugs: A Novel Drug-Carrier System for Photodynamic Therapy. *J. Am. Chem. Soc.* **2003,** *125* (26), 7860-7865.

22. Jin, Y.; Lohstreter, S.; Pierce, D. T.; Parisien, J.; Wu, M.; Hall, C. I.; Zhao, J. X., Silica Nanoparticles with Continuously Tunable Sizes: Synthesis and Size Effects on Cellular Imaging. *Chem. Mater.* **2008,** *20*, 4411-4419.

23. Davis, T. M.; Snyder, M. A.; Krohn, J. E.; Tsapatsis, M., Nanoparticles in Lysine-Silica Sols. *Chem. Mater.* **2006,** *18*, 5814-5816.

24. Cohen, B.; Martin, C.; Iyer, S. K.; Wiesner, U.; Douhal, A., Single Dye Molecule Behavior in Fluorescent Core-Shell Silica Nanoparticles. *Chem. Mater.* **2012,** *24*, 361-372.

25. Ma, D.; Tan, S.; Jakubek, Z. J.; Simard, B., On the Structural Stability of Dye-Doped Silica Nanoparticles. *Proc. 7th IEEE* **2007**, 651-655.

26. Buschmann, V.; Weston, K. D.; Sauer, M., Spectroscopic Study and Evaluation of Red-Absorbing Fluorescent Dyes. *Bioconj. Chem.* **2003,** *14*, 195-204.

27. Blackledge, C. W.; Tabarin, T.; Masson, E.; Forster, R. J.; Keyes, T. E., Silica nanoparticles containing a rhodamine dye and multiple gold nanorods. *J. Nanopart. Res.* **2011,** *13*, 4659-4672.

28. Gunawardana, K. B. Study of Metal-Enhanced Fluorescence of Dye Doped Silica Nanoparticles. University of Oklahoma, Norman, 2012.

29. Martens, H.; Nielsen, J. P.; Engelsen, S. B., Light Scattering and Light Absorbance Separated by Extended Multiplicative Signal Correction. Application to Near-Infrared Transmission Analysis of Powder Mixtures. *Anal. Chem.* **2003,** *75*, 394-404.

30. Loudet, A.; Burgess, K., BODIPY Dyes and Their Derivatives: Syntheses and Spectroscopic Properties. *Chemical Reviews* **2007,** *107* (11), 4891-4932.

Chapter III: Surface modification of dye-doped silica and gold nanoparticles

3.1 Chapter Overview

This chapter describes our efforts to functionalize the surface of dye-doped silica and gold nanoparticles to promote hetero-aggregation[1] in order to achieve metal enhanced fluorescence (Figure 3.1).

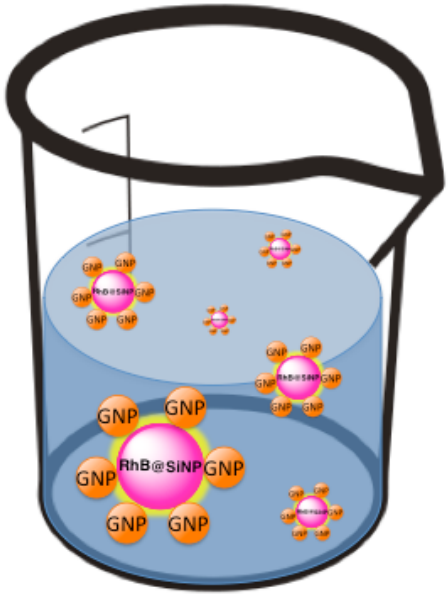

Figure 3.26. Dye-silica nanoparticles (RhB@SiNP) surface functionalized to aggregate gold nanoparticles (GNP) in solution. (Image from this work).

As shown in Figure 3.1, our primary aim is to develop a silica surface functionalization that promotes silica gold aggregation while limiting the amount of silica-silica and gold-gold aggregates. Dye-doped silica- gold aggregation is important due to enhanced fluorescence that occurs when multiple gold nanoparticles are brought within close proximity of one another[2] and the fluorophores.[3] This chapter describes our attempts to

alter the surface of dye-doped silica nanoparticles with electron dense ligands (amine, thiol, and dithiocarbamate (DTC)) in ethanolic and aqueous suspensions to promote desired silica-gold hetero-aggregation to produce metal enhanced fluorescence in solution.

3.2 Introduction

Gold nanoparticle binding to silica based on coordination and electrostatic interactions have been well studied over the last decade.[4] Adjusting the electron density and charge of the ligands on gold or silica and the solvent system can alter aggregation of these species.[4b, 5] Therefore, our aim is to selectively bind multiple gold nanoparticles around a single functionalized silica particle in solution using a ligand on silica which promotes gold-silica aggregation while minimizing the amount of silica-silica aggregation.

In order to maximize attachments to the silica surface it often must be cleaned. Piranha solution (a mixture of concentrated sulfuric acid and hydrogen peroxide) is frequently used to remove any oxidized organic material of solid silica substrates to produce exposed hydroxyl groups along the surface.[6] This technique has been shown to be an extremely dangerous explosion hazard[7] but, if used correctly, may provide a method to efficiently prepare the surface of silica nanoparticles for the addition of reactive ligands to promote the binding of gold nanoparticles.

Electrostatic binding of dye-doped silica and gold nanoparticles was previously attempted by Gunawardana and Halterman.[4c] They postulated that coating silica nanoparticles in amines would give positively charged surfaces that could interact with

negatively charged surfaces of gold that has been covered in carboxylic acids at the same neutral pH (Figure 3.2).

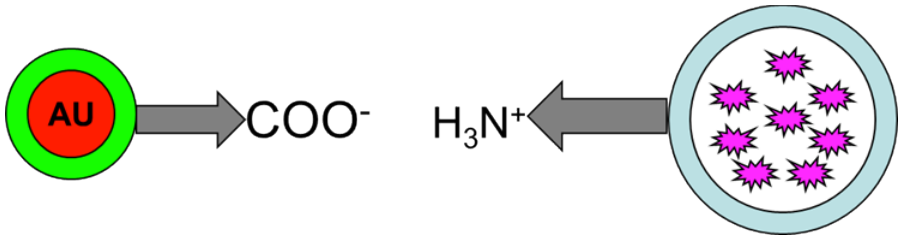

Figure 3.27. Salt bridge formation of amine coated silica nanoparticles and carboxylic acid coated gold nanoparticles (image from Ganawardana and Halterman)[4c]

Electrostatic binding provides a strong interaction between both particles but this process lacks fine-tune control over the binding interaction and can be disrupted by competing inorganic counter ions in the medium (Figure 3.3).[4c]

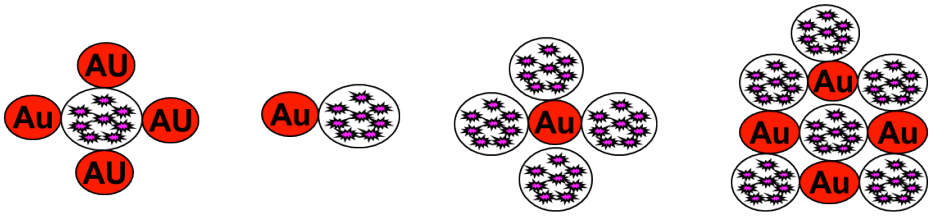

Figure 3.28. Different heteroaggregates that can be formed aggregation via electrostatic interactions. (Image from Gunawardana and Halterman)[4c]

The desired heteroaggregation of multiple gold nanoparticles around a single dye-dope silica nanoparticle which theoretically leads to the greatest enhancement (discussed in more detail in chapter IV) is difficult to achieve by electrostatic binding.[2] Thus, a more precise method for promoting aggregation was pursued where the degree of aggregation between the two nanoparticle could be achieved.

Gold is well-known to form strong bonds with primary amines and thiols.[4a, 8] In 1933, Weiser postulated that these electron dense ligands bound tightly to a gold (I) coating that surrounded the outside of gold nanoparticles prepared by the citrate reduction in water (Figure 3.4).[9] In this figure we see that colloidal gold nanoparticles consists of a Au^0 core with Au(I) shell surrounding the outside. The thin layer of Au(I) is responsible for GNPs high affinity for electron rich ligands.[9]

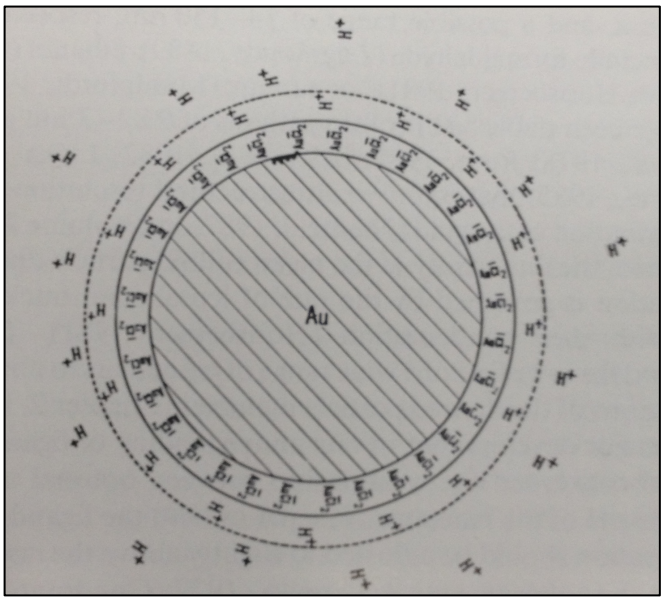

Figure 3.29. Diagram of the composition of a colloidal gold nanoparticle in solution. (Image from Weiser).[9]

Amines remain to be the most commonly used ligands for gold nanoparticle binding due to their ease of installation, chemical stability, and generally strong biding constants.[10] Amine coatings are desirable due to their ease of incorporating aminopropyltriethoxysilane (APTES)[11] or 2-aminoethanethiol hydrochloride (AET) onto various substrates. Yong et al[8b] have previously reported effectively aggregating citrate-capped gold nanospheres around AET-coated polystyrene nanospheres (Figure

X). In these systems gold was postulated to attach to the nanobeads due to the electron density imparted by the lone pairs of electrons nitrogens of the ligands.[8b]

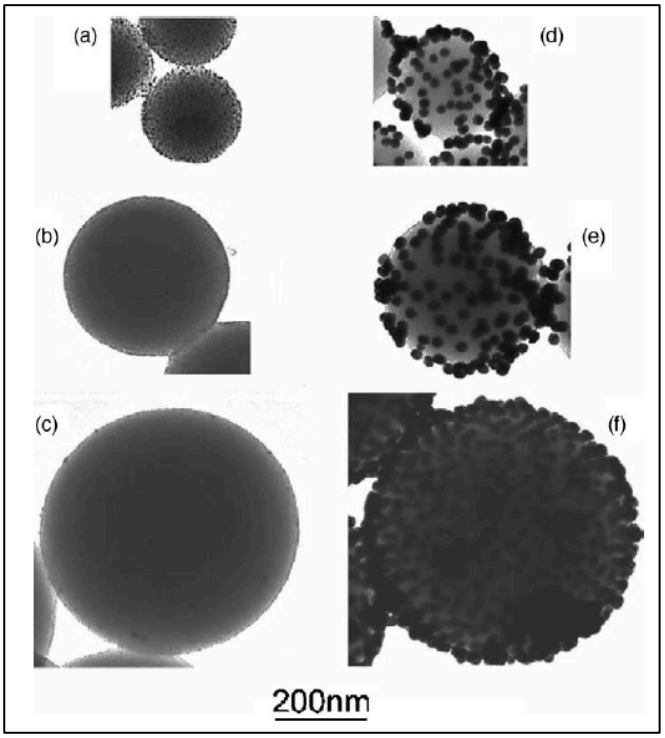

Figure 3.30. TEM images of 188, 296, and 543 nm amine-coated polystyrene spheres mixed with (a-c) THPC-gold and (d-f) 12 nm citrate gold nanoparticles.[8b]

Similar systems have been reported for silica nanospheres with clusters of gold nanoparticles.[4b] These well-established procedures provide an excellent means to bind gold and dye-doped silica nanoparticles together but they fail to address concerns about the impact of the chemical environment, as amine ligands are sensitive to pH changes.[4a]

Amine ligands also benefit from a facile detection method that can be used to monitor the quality of silica surface functionalization. Zeta potential measurements are a useful tool for determining the stability of a colloidal system made up of charged particles.[12] The zeta potential for a charged colloidal solution can be determined by

measuring a particle's electrophoretic movement, or movement through solution, when placed in a potential gradient field (Figure 3.6).[13]

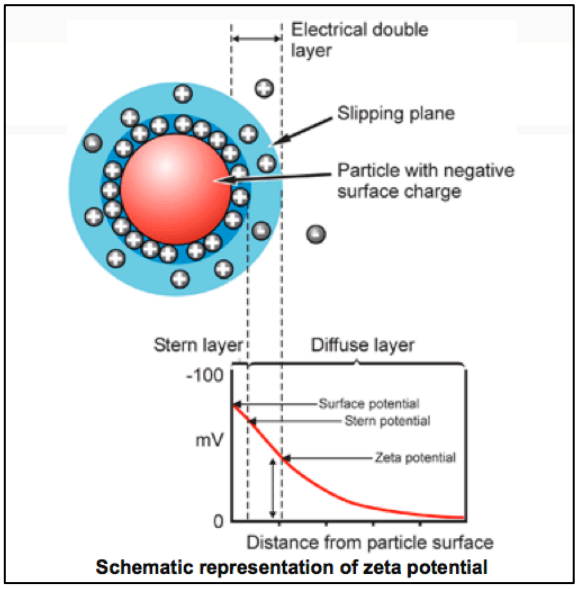

Figure 3.31. Schemetic representation of a the zeta potential of a charged particle. (Image from Malvern Instruments Ltd)[13]

Large zeta potentials (generally greater than ±30 mV)[12] are indicative of large differences in charge between the surface of the suspended particles and the solution, which give rise to stable suspensions of particles that do not easily homo-aggregate.[14] It is important to note that the sign of the zeta potential does not always necessarily reflect the charge of the surface of the particle but rather the relative magnitude of a surface-solution charge difference.[13] Zeta potential measurements are useful in determining changes on the surface of silica nanoparticles as well as the stability of the resulting suspension.

The ninhydrin assay is a facile method for qualitatively determining the presence of primary amines in an unknown sample.[15] This technique is commonly used

to detect the presence of free amino acids during DNA synthesis reaction as the primary amine moiety reacts with ninhydrin to produce a dark blue purple Schiff base (Figure 3.7).[16]

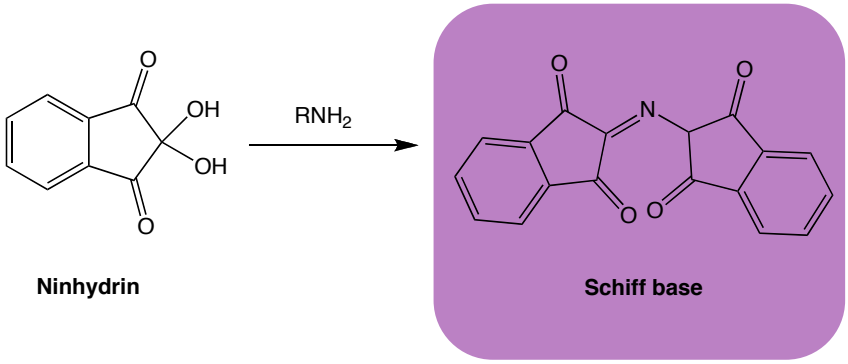

Figure 3.32. Reaction of ninhydrin with a primary amine to form a colored Schiff base.[16] (image from this work).

The ninhydrin assay can be employed to detect amines on the surface of silica nanoparticles by spotting an aliquot of nanoparticle suspension onto a TLC plate before developing with an ethanolic solution of ninhydrin.[15b] Amines are easily detected by the development of blue-purple spots on the plate. The ninhydrin assay is a useful tool for qualitatively assessing the presence of amines in an unknown sample.

Thiol ligands are also commonly used to bind gold nanoparticles to solid supports.[17] These ligands are advantageous over amine ligands in that they are less sensitive to pH changes compared to amines.[18] However, thiols are sensitive to oxidative coupling to form disulfide bonds leading to large undesirable aggregates of coated material (Figure 3.8).[17b]

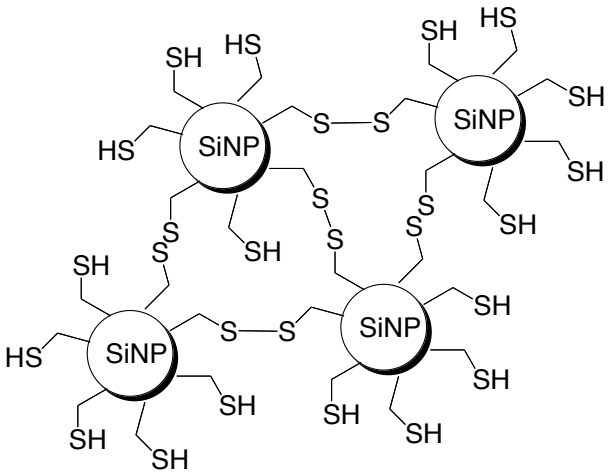

Figure 3.33. Homoaggregation of thiol coated SiNP via formation of disulfide bonds (from this work).

This problem can be avoided by creating aggregates in non-oxidizing environments (i.e. nitrogen atmosphere) but this limitation would complicate future applications of dye-dope silica nanoparticle and gold nanoparticle aggregates. Therefore, a more robust and universally applicable ligand was developed with the formation of the dithiocarbamate (DTC) ligand.

Dithiocarbamate (DTC) ligands are advantageous over previous thiol and amine systems because they bear a full negative charge that theoretically helps to minimize silica-silica aggregation via electrostatic repulsion. Wei et al developed methodology to connect terminal amine ligands to gold via the spontaneous formation of DTC at the surface of the gold (Figure 3.9)[19]

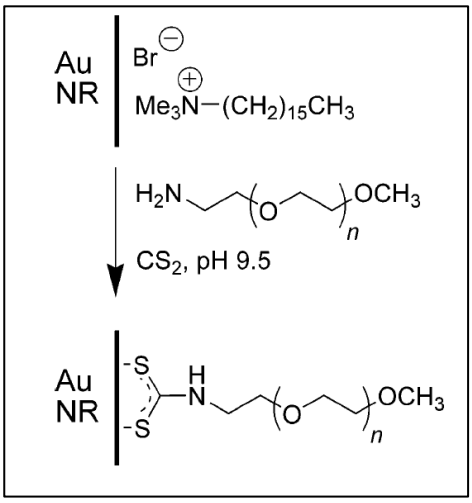

Figure 3.34. DTC formation on the surface of gold nanorods (AuNR). (Image from Huff et al)[20]

However, this method is best performed in ethanolic environments that are not suitable for citrate-capped gold.[10] Longer-chain thiol ether cappings are required to stabilize gold in ethanolic solutions.[4c] Aqueous citrate-capped gold nanoparticles are very sensitive to aggregation if the dielectric constant of the medium changes or the concentration of citrate is too low. The *in situ* development of DTC was then shown to be very effective displacing the strongly binding thiol polyether coatings (Figure 3.10).[17b]

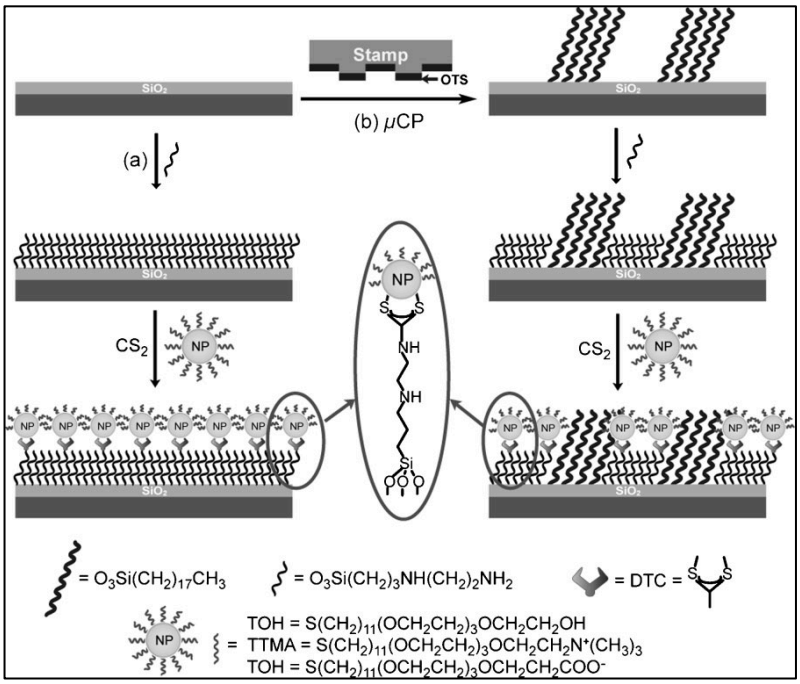

Figure 3.35. Long chain DTC ligands binding to gold nanoparticles on a template substrate. (Image from Parl et al)[17b]

The outer surface of silica nanoparticles can be modified to house useful functional groups that allow formation of aggregates with gold nanoparticles. The primary amine of APTES can then be converted into dithiocarbamate (DTC) see figure 3.11) which effectively binds to gold.[17b]

Silica nanoparticles can be surfaced functionalized to promote aggregation with gold nanoparticles via electrostatic or bonding forces. Chemical bonds are a more attractive method as the degree of aggregation can be more easily controlled to bind multiple gold particles around few silica species. Our hypothesis is that multiple gold nanoparticles can be promoted to bind to a single dye-doped silica nanoparticle by carefully selecting the surface functionality of the silica.

3.3 Results and Discussion

Silica nanoparticles were surface functionalized with thiols, amines, and dithiocarbamate (DTC) ligands through condensation of appropriate siloxane precursors onto synthetically attainable dye-doped silica to determine the optimal coating conditions for gold nanospheres aggregation. The effects of surface cleaning by piranha solution were also investigated with regards to the efficiency of ligand incorporation and effects on particle stability.

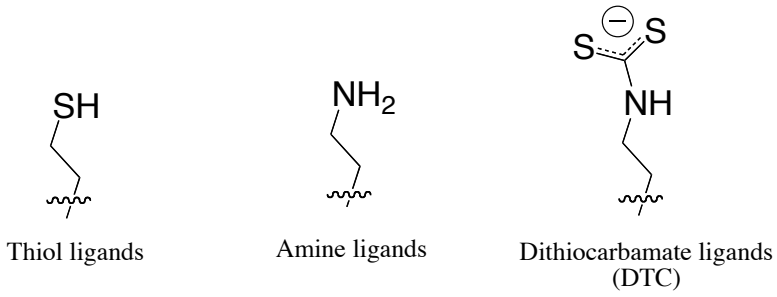

Figure 3.36. Range of gold binding ligands that can be functionalized onto silica nanoparticles. (from this work).

Aggregation and silica nanoparticle morphology was monitored via gold plasmon shifts in absorbance spectra and transmission electron microscope (TEM) imaging while surface functionality was studied by ninhydrin assay, IR, and zeta potential.

3.3.1 Effect of piranha cleaning dye-doped silica nanoparticles

Piranha cleaning was studied for it efficacy in preparing dye-doped silica nanoparticles for surface functionalization with small molecule siloxanes. Our aim was to determine if the benefit of creating a more reactive silica surface, and thus produce a better functionalized particle, outweighed the risk of destroying the nanospheres outright. Piranha cleaning was attempted prior to amine coating so that the particles

could be studied for amine incorporation via ninhydrin assay before the particles were characterized for morphological changes via TEM imaging.

Silica nanoparticles were briefly mixed with piranha solution (70% con H_2SO_4 / 30% H_2O_2) for approximately five seconds before they were diluted with deionized water in an effort to limit that amount of time the concentrated solution reacted with the silica. These particles were washed thoroughly before being coated with amine and washed (*vida infra*) before being spotted onto silica plates. Two samples were piranha cleaned and two were not; one sample of each of these was amine coated (Table 3.1).

Sample i.d.	**Piranha Cleaned?**	**Amine addition?**
A	yes	yes
B	yes	no
C	no	Yes
D	no	No

Table 3.1. Preparation of silica nanoparticles to study effect of piranha cleaning on amine incorporation.

Cleaned particles, concentrated in water post reactions, were then compared to their supernatant solutions that were obtained from the centrifugation washes by ninhydrin analysis on silica TLC plates (Figure 3.12). The development of a dark blue/purple spot signifies the presence of amines even at very low concentrations.[15c]

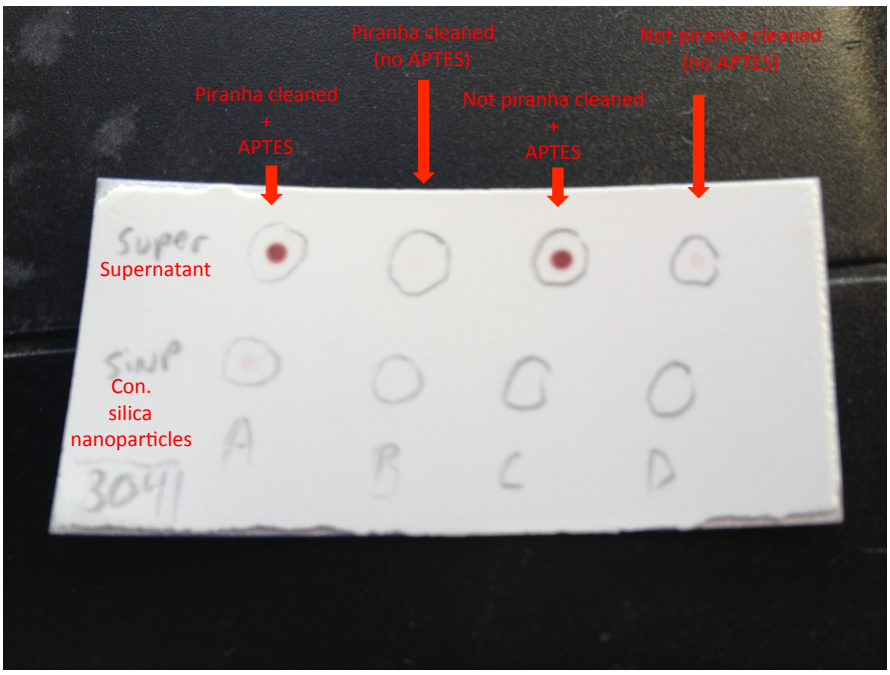

Figure 3.37. Ninhydrin assay of silica nanoparticles that have been treated (or not) with piranha solution and amine coating.

The TLC ninhydrin assay suggests that only silica nanoparticles that were piranha cleaned were successfully amine coated as 'sample A' is the sample that developed a spot. (Note: that the faint spot seen in the supernatant of 'sample D' is a contamination carry over from the concentrated previous 'supernatant C' as all of the supernatant spots were made at one time). This supports the hypothesis that piranha cleaning will activate the surface of silica nanoparticles to better incorporate amine functionality in order to optimize gold nanoparticle aggregation.

Silica nanoparticles that were and were not treated with piranha solution and APTES condensation were mixed with gold nanoparticles and measured over time by UV-Vis absorption (Figure 3.13). The absorbance was compared at 523 nm for each sample as this local maxima did not shift during GNP aggregation.

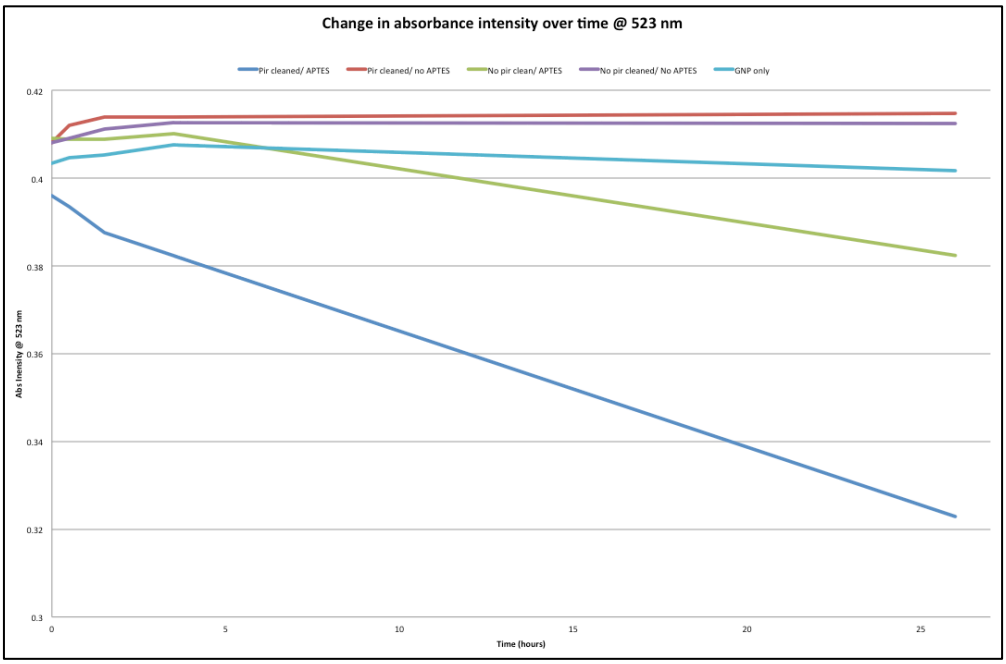

Figure 3.38. Absorbance spectra of silica nanoparticles treated (and not treated) with piranha solution and APTES before being mixed with citrate capped gold nanospheres.

The gold plasmon resonance decreases as free gold in solution is aggregated with silica nanoparticles. The absorption spectra confirm that silica nanoparticles that were pre-cleaned with piranha solution before being treated with APTES (sample A, blue line) aggregated gold at a faster rate than particles that were simply treated with amine (sample C, green line). TEM imaging was then performed to determine the effect piranha solution had on the morphology of the silica nanoparticles.

Figure 3.14 shows a TEM image of silica nanoparticles that were pre-cleaned with piranha solution before being amine coated and mixed with gold nanoparticles (sample A from table 3.1).

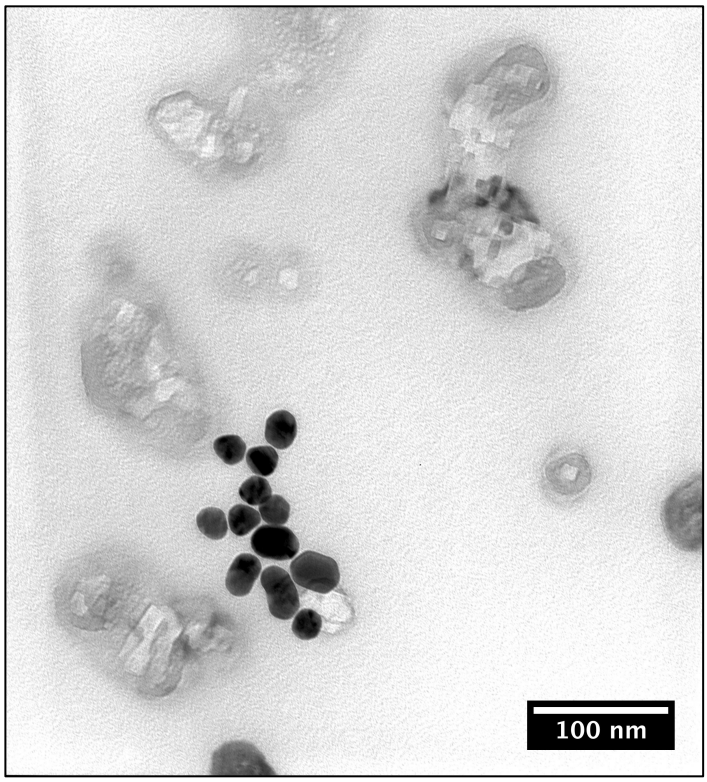

Figure 3.39. TEM image of amine-coated silica nanoparticles (light grey) treated with piranha solution mixed with citrate-capped gold nanoparticles (black material).

The TEM image shows significant damage to the silica after piranha cleaning. The light and dark splotches suggest that areas of the spheres have been dissolved leaving behind a jagged skeleton of the nanospheres. Note that the gold nanoparticles were added after piranha cleaning and are thus unaffected by its use in the preparation of this mixture. The image from Figure 3.14 is in stark contrast with particles that were not treated with piranha solution (Figure 3.15). Silica particles that were simply coated in amine without piranha cleaning did not show any sign of degradation by TEM imaging. In fact, excellent silica-gold aggregation was observed (discussed in greater detail in chapter IV).

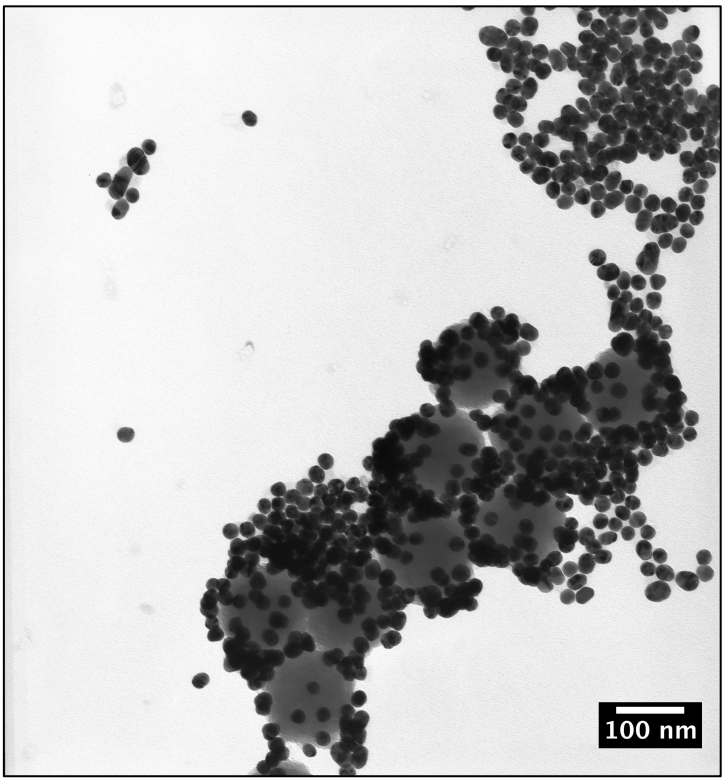

Figure 3.40. TEM image of amine-coated silica nanoparticles that have not been pre-cleaned with piranha solution mixed with citrate-capped gold nanoparticles.

The images in Figures 3.14 and 3.15 are significant because they emphasize how caution should be used when investigating gold aggregation about silica nanoparticles. The effect of amine and thiol coating will be discussed in later sections of this chapter but it clear from these studies that piranha cleaning is not an effective method for preparing a reactive surface on dye-dope silica nanoparticles.

3.3.2 Investigation of amine coating on silica-gold nanoparticle aggregation

In order to promote aggregation between dye-doped silica nanoparticles and gold nanospheres we investigated the effect of coating the silica surface with amines.

The optimal method of coating silica nanoparticles with amines was determined by comparing different protocols for installing (3-aminopropyl)triethoxysilane (APTES) by acid catalyzed hydrolysis, refluxing in toluene, and co-condensation with tetraethylorthosilicate (TEOS). The successful installation of amines was investigated by ninhydrin assay, zeta potential, IR, and gold nanoparticle binding studies.

The most common method for installing amines onto silica substrates is the acid catalyzed hydrolysis of APTES (Figure 3.16).[11] Here, APTES is mixed with small amounts of glacial acetic acid in aqueous or ethanolic suspensions of dye-doped silica nanoparticles. The acid promotes a condensation reaction between the free hydroxyl groups on the surface of the silica particles and the siloxane moieties of APTES.

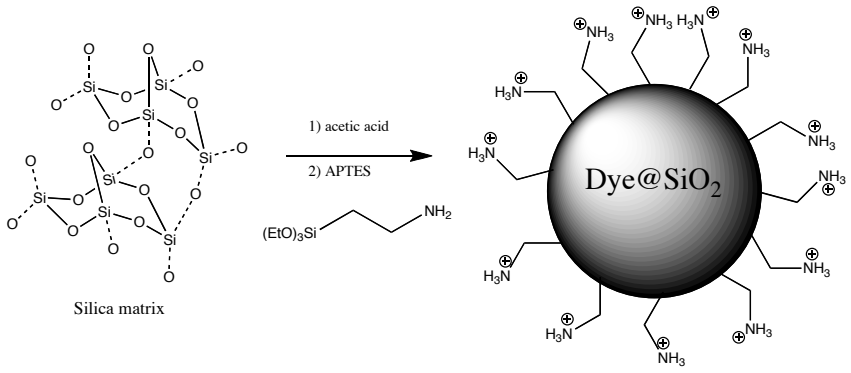

Figure 3.41. Synthetic scheme of condensing APTES onto the surface of silica nanoparticles.

This process is especially useful for nanoparticle application as very mild conditions does not threaten the structural integrity of the silica (Figure 3.17).

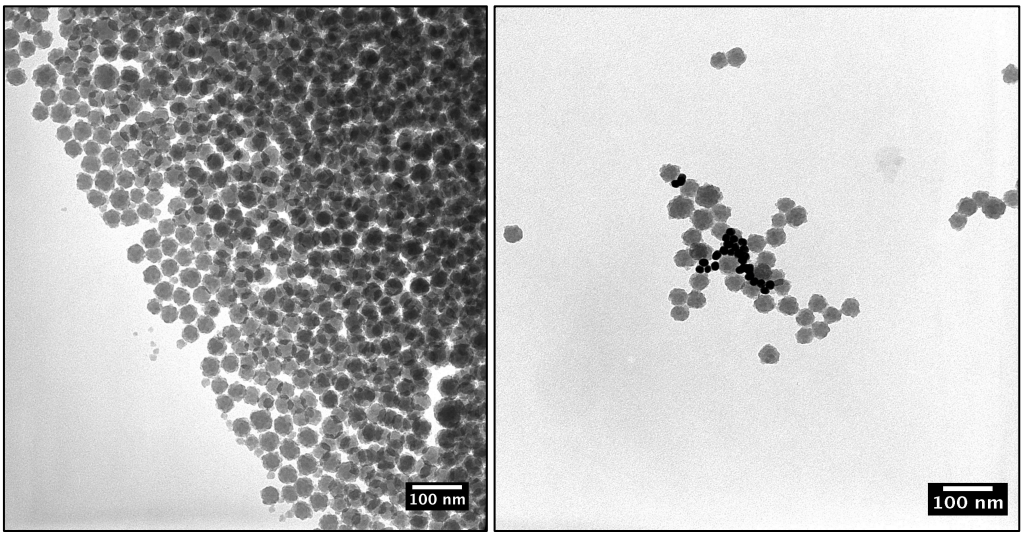

Figure 3.42. TEM images of layered dye-doped silica nanoparticles before (left) and after (right) APTES coating catalyzed by glacial acetic acid. Gold nanoparticles were added to the sample on the right (dark black material).

Figure X shows no significant changes in the morphology of the silica post APTES coating in glacial acetic acid. This acid stability is important given the previous results of complete destruction of the silica framework by piranha cleaning (Figure 3.14). However, TEM imaging does not allow us to investigate the presence of amines on the surface of the silica nanoparticles. The ninhydrin assay is a convenient method for detecting amine surface functionality.

The ninhydrin assay indicated that ethanol is a superior solvent for both the condensation reaction media and for removing unreacted APTES molecules. Spots were taken from subsequent supernatant washes of two samples that were run under identical conditions except for solvent (Figure 3.18).

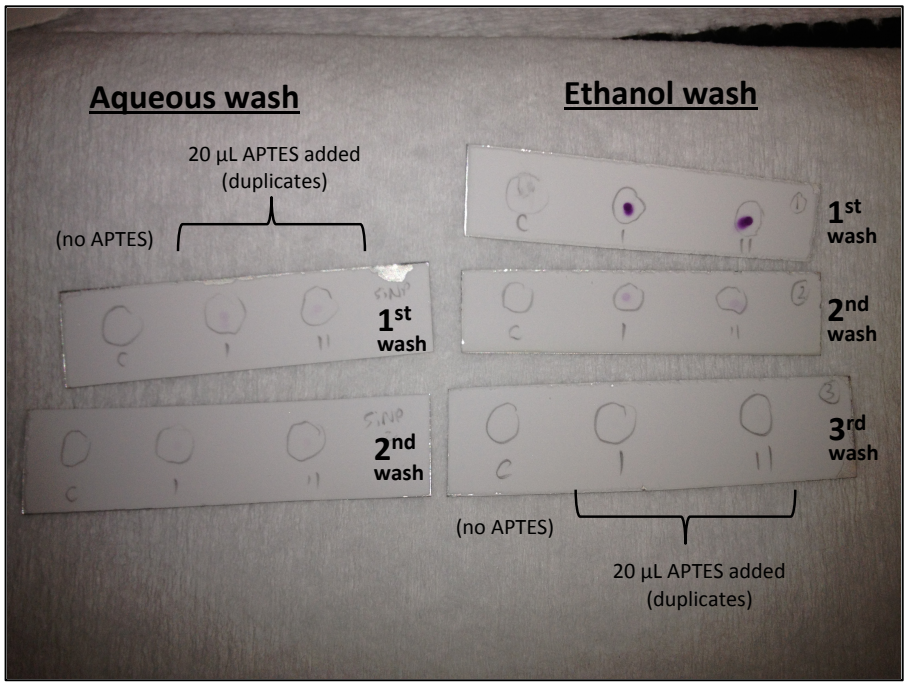

Figure 3.43. Comparative ninhydrin study of APTES coating and washing in water vs. ethanol. Spots are taken from supernatant liquid after centrifugation from reacting in their respective solvents.

Silica nanoparticles that were reacted with APTES in water showed very little APTES present in the supernatant of the first wash compared to the ethanol counter part indicating that more amine was present in solution in the ethanol preparation. Furthermore, the decrease in intensity of the amine spot over subsequent washes was much less dramatic in water, which indicates that less excess amine is being removed from the supernatant with each wash. These results are rationalized by the poor solubility of APTES and relatively good solubility of the hydrolyzed silic acid derivative in aqueous solutions. Thus, the interaction between APTES and free hydroxyl groups on the surface of the silica nanoparticles is poor in aqueous solutions which leads to poor coating and slow removal of the small amount of dissolved APTES.

We have found ethanol to a superior solvent over water for the surface functionalization of silica nanoparticles.

Amine functionality on silica nanoparticles is also evident by changes in the absorbance spectra of gold nanoparticles upon aggregation in solution (Figure 3.19). A significant shoulder and gradual red-shift is seen in the absorbance spectra that indicates an increasingly larger amount of gold nanoparticle aggregation.

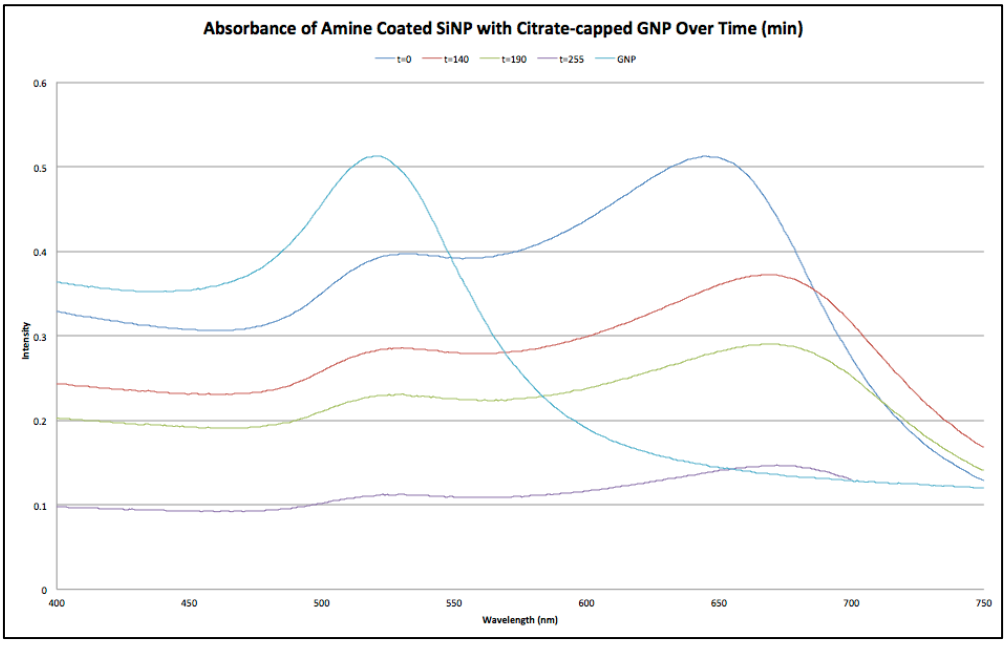

Figure 3.44. Absorbance spectra of citrate-capped gold nanoparticles aggregated with amine coated silica nanoparticles over time.

These spectra are in stark contrast with silica nanoparticles that have not been functionalized with amines (Figure 3.14, section 3.3.1). Thus, amine ligands show great promise as gold binding ligands in solution. However, these ligands do not consistently produce similar aggregates within identical systems. We speculate that the amine interactions are complicated by subtle changes in pH when introduced to citrate capped-

gold nanoparticles. Therefore, we continued to search for more robust ligands that produced similar aggregation across many samples. Amine ligands are attractive targets for promoting silica and gold nanoparticle aggregation but struggle to produce consistent results.

3.3.3 Investigation of thiol coating on silica-gold nanoparticle aggregation

We investigated thiol coatings of dye-doped silica nanoparticles in order to reproducibly aggregate gold nanoparticles (Figure 3.20). Thiol coating was accomplished by acid catalyzed condensation of (3-mercaptopropyl)trimethoxysilane (MPTMS) onto the surface of silica nanoparticles by the same procedure APTES was used during amine coating.

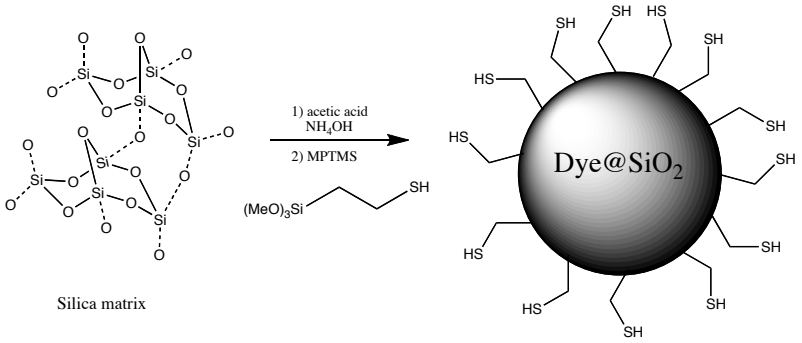

Figure 3.45. Reaction scheme for functionalizing the surface of silica nanoparitcles with thiol groups.

The thiol-coated nanoparticles were then characterized by zeta potential analysis to determine if there was any effect of changing the surface functionality from the hydroxy-coated silica (Figure 3.21). The zeta potential of thiol coated silica nanoparticles in an un-buffered aqueous solution was found to be 42.8 mV, which

indicates a stable colloidal suspension (generally, zeta potentials above 30 mV are considered stable).[14]

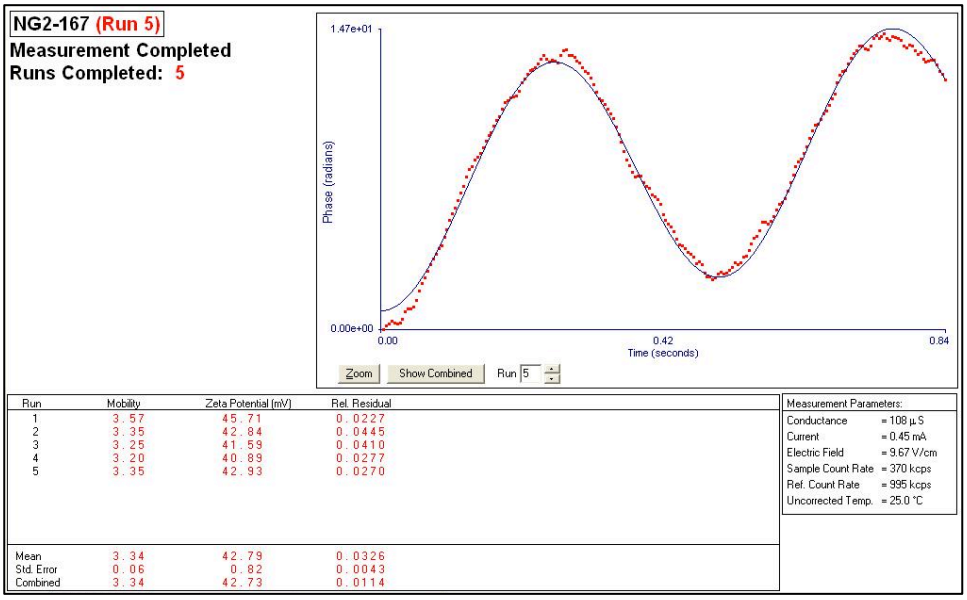

Figure 3.46. Zeta potential analysis, calculated from a dynamic light scattering (DLS) experiment, of thiol coated silica nanoparticles.

Thus, this data indicates that silica nanoparticles coated in thiol are relatively stable when compared to the un-coated, free hydroxy silica (Figure 3.22). Un-coated silica nanoparticles were found to have a zeta potential of 18.8 in a un-buffered aqueous solution. This decrease in colloidal stability supports the formation of a more negatively charged surface area of particles that have been coated in thiol.

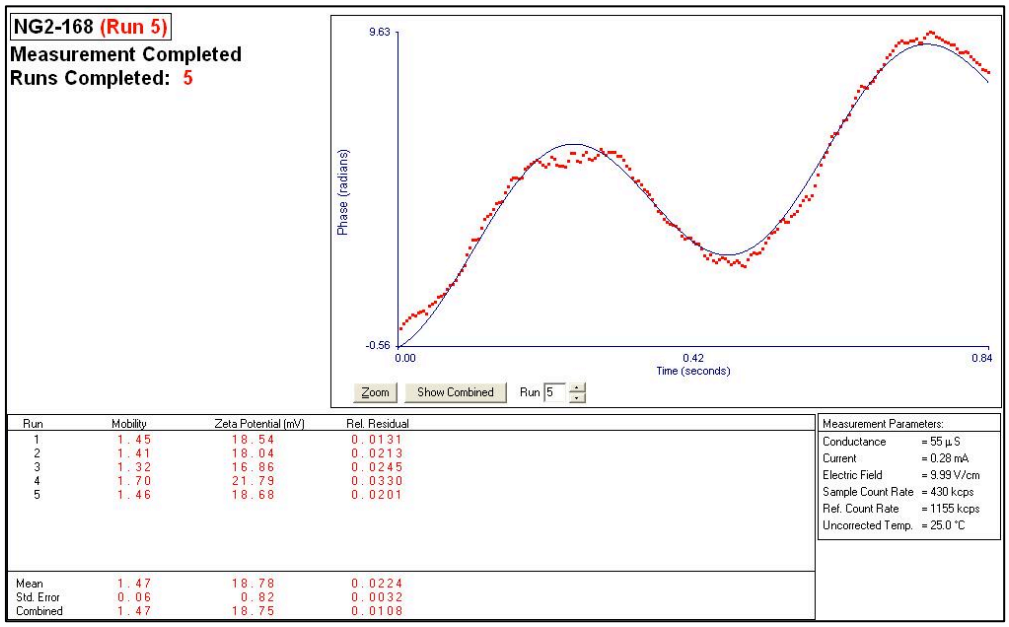

Figure 3.47. Zeta potential analysis, calculated from a dynamic light scattering (DLS) experiment, of un-coated silica nanoparticles.

However, caution should be used in the analysis of this data as the particles coated in this experiment were from early preparations and were thus not well formed (Figure 3.23). The silica does not appear to show an particle formation but instead displays an amorphous gel-like substance.

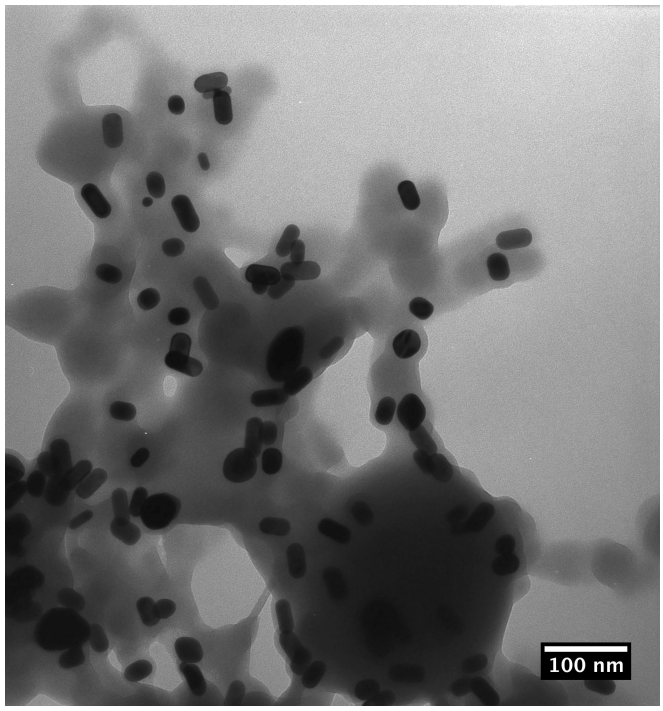

Figure 3.48. TEM image of thiol coated silica nanoparticles mixed with CTAB coated gold nanorods.

While these particles are not well formed they do show a high affinity for the surface of gold nanorods, with a large number of rods becoming completely encompassed within the silica framework. However, TEM imaging of layered dye-doped silica nanoparticles suggest that the surface of the dye-doped silica nanoparticles is not compromised during thiol coating (Figure 3.24). The before and after TEM images show well-formed silica nanoparticles.

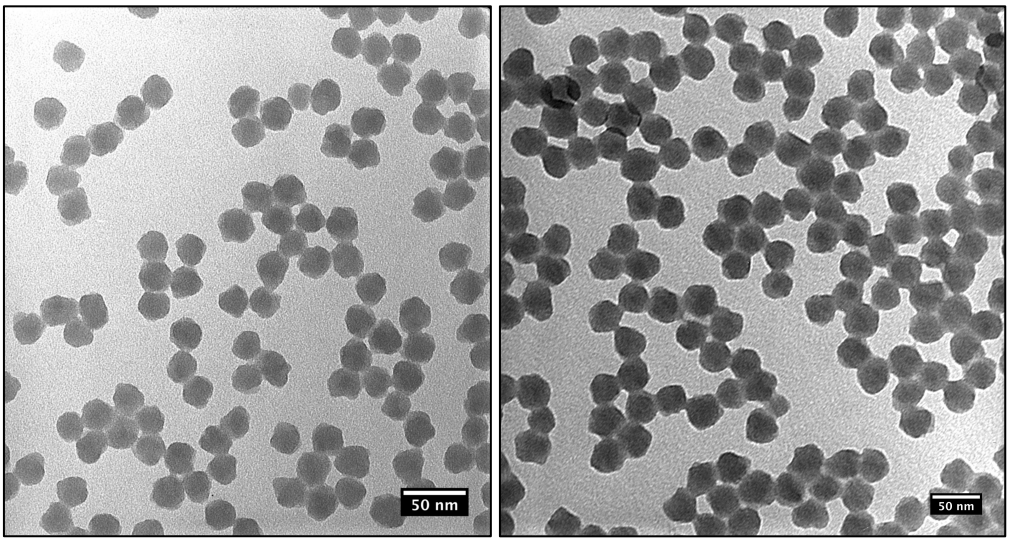

Figure 3.49. TEM images of layered dye-doped silica nanoparticles before (left) and after (right) thiol coating.

Thiol coating is a possibly productive pathway towards achieving dye-doped silica- gold nanoparticle aggregates. The thiol group does not appear to be as sensitive to environmental changes as amine coatings but they present a possible issue of homo-aggregation via disulfide bonds. Thus, we investigated dithiocarbamate as a potential silica coating moiety to promote desired gold-silica aggregation.

3.3.4 Investigation of dithiocarbamate (DTC) coating to promote silica-gold **nanoparticle aggregation**

Dithiocarbamate (DTC) ligands were applied to dye-doped silica nanoparticles to provide a strong binding interaction with gold, similar to amines, while simultaneous decreasing the amount of silica-silica aggregation, often seen with thiols, due to electrostatic surface charge repulsion. Furthermore, DTC ligands are attractive because

the process takes advantage of amine chemistry already present on the surface of the silica (Figure 3.25).

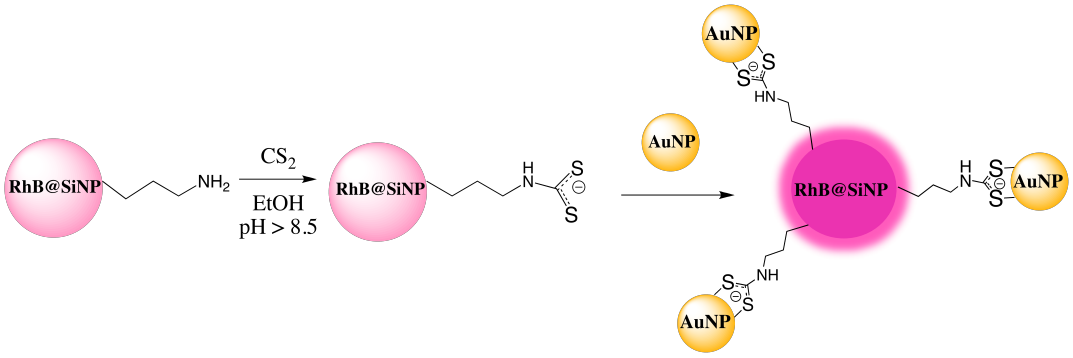

Figure 3.50. Cartoon schematic of amine-coated dye-doped silica nanoparticles conversion to dithiocarbamate (DTC) ligands before aggregation with gold nanoparticles. (Image from Gunawardana, Green, and Halterman).[4c]

The DTC ligand is formed by a nucleophilic attack of the surface amine groups onto carbon disulfide (CS_2) in basic conditions to give a resonance stabilized anionic bi-dentate binding unit.[17b] Typically, DTC conversion, performed in ethanol, would follow amine coating with APTES giving a propyl chain length distance from the surface of the silica nanoparticle. We found that DTC capped particles bound too rapidly to citrate-capped molecules, causing the gold to instantly form dark black flakes in solution, which indicated complete gold gold aggregation had occurred. Thus, it is necessary to mix DTC coated silica-nanoparticles in ethanolic solutions of the more stable ($CH_3O(CH_2CH_2O)_2C_{10}H_{20}SH$) (ether-capped) gold nanoparticles. These ligands were synthesized by Anuradha Singh in the Halterman lab.[21]

No useful aggregation was produced by a short chain DTC ligand coated on the surface of dye-doped silica nanoparticles when mixed with ether-capped gold nanoparticles.

The longer, more stable, ether-capped gold nanoparticles are theoretically difficult to displace with short chain DTC ligands on silica nanoparticles (Figure 3.26)

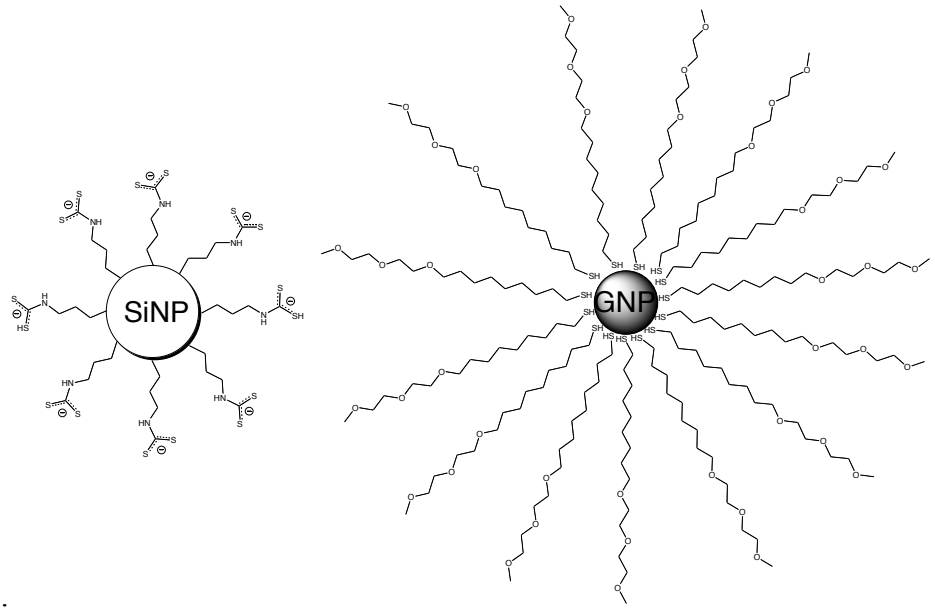

.

Figure 3.51. Cartoon schematic of potential binding issues related to a short DTC ligand coated silica nanoparticles (SiNP) mixed with long-chain ether capped gold nanoparticles (GNP) (image from this work).

We speculate that difficulties in promoting silica-gold aggregates arise from the inability of the shorter DTC ligand on the surface of the silica to interdigitate with the long chain ether surrounding the gold nanoparticles. Thus, the ether displacement is slow as the rate of DTC attachment is hindered by a kinetically disfavored approach. For this reason we studied the effects of attaching a longer chain DTC ligand to silica to overcome distance restrictions of the shorter ligands.

3.3.5 Synthesis and application of tetraethylene glycol derivative coating for silica-gold nanoparticle aggregation

We investigated applying a synthetic long chain tetraethylene glycol (TEG) siloxane derivative with superficial gold binding moieties in order to achieve improved aggregation with ether-capped gold nanoparticles through ligand interdigitation. The long-chain silica tether consisted of a modified TEG skeleton with a propyl siloxane precursor attached to one end with an amine or DTC moiety at the other. This allowed the tether to be covalently attached to the silica and have the gold attractive moiety extend further away from the silica nanoparticle surface (Figure 3.27).

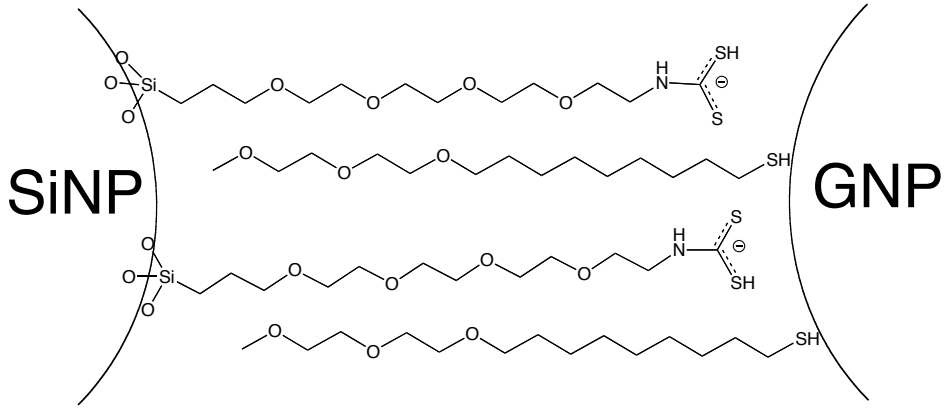

Figure 3.52. Cartoon schematic of a synthetic long-chain DTC silica nanoparticle (SiNP) tether interdigitating with the long-chain ether capping of a gold nanoparticle (GNP) (from this work).

We predict that increasing the length of the silica tether will allow silica and gold nanoparticles to aggregate more effectively as the silica bound DTC moiety can more easily reach the surface of the gold compared to the shorter propyl chains described in section 3.3.4.

The longer silica tether is synthetically accessible by modification of the tetraethylene glycol (TEG) skeleton (Figure 3.28).

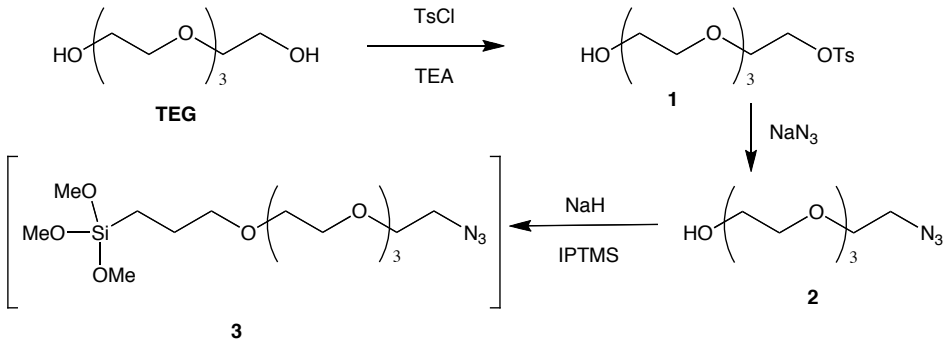

Figure 3.53. Synthetic scheme to produce the siloxane precursor **3**.

Monotosylation of the tetraethylene glycol (TEG) gave monotosyl-TEG **1** in a statistical mixture that was readily purified by column chromatography. Next, the tosyl group was substituted with sodium azide (NaN_3) to produce azide-TEG **2**, which was carried on without further purification. Siloxane precursor **3** was produced by nucleophilic substitution of (3-iodopropyl)trimethoxysilane (IPTMS) with the alkoxide of azide-TEG **2**. Siloxane **3** undergoes hydrolysis in air and water and was thus carried on crude to be condensed onto the surface of layered-dye doped silica nanoparticles immediately following production. Figure 3.29 shows the synthetic scheme for attaching the TEG tether to layered dye-doped silica nanoparticles and the transformations resulting in the production of superficial DTC ligands. These compounds were characterized by ^{1}H NMR. Most notably in the ^{1}H NMR spectrum we observed shifting in the methylene group closest to the tosyl (and later azide) that shift from 3.7 to 4.2 ppm.

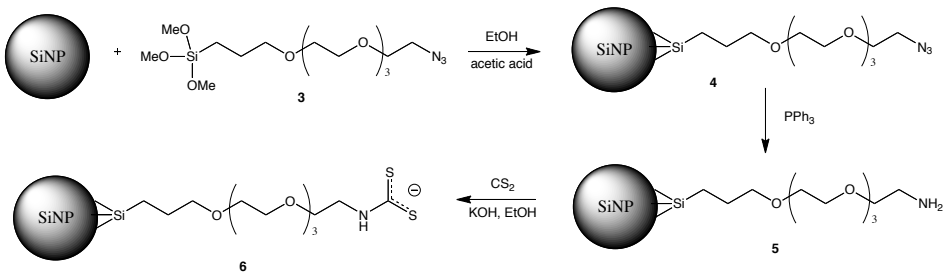

Figure 3.54. Synthetic scheme of TEG-SiNP attachment and subsequent SiNP surface chemistry to produce DTC ligands.

Azide-TEG **3** was condensed onto the surface of dye-doped layered silica nanoparticles by acid catalysis in ethanol to give azide-SiNP **4**. The azide moiety was then converted into an amine via the Staudinger reaction to produce **5**. The amine coating was confirmed by ninhydrin assay (Figure 3.30) before being transformed into DTC-SiNP **6**. Quantitative analysis is difficult at this point as the number of nanoparticles is unknown and the amount of amines present relative to the overall size of a silica nanoparticle creates too much noise for most standard detection methods (i.e. NMR and even qualitative IR).

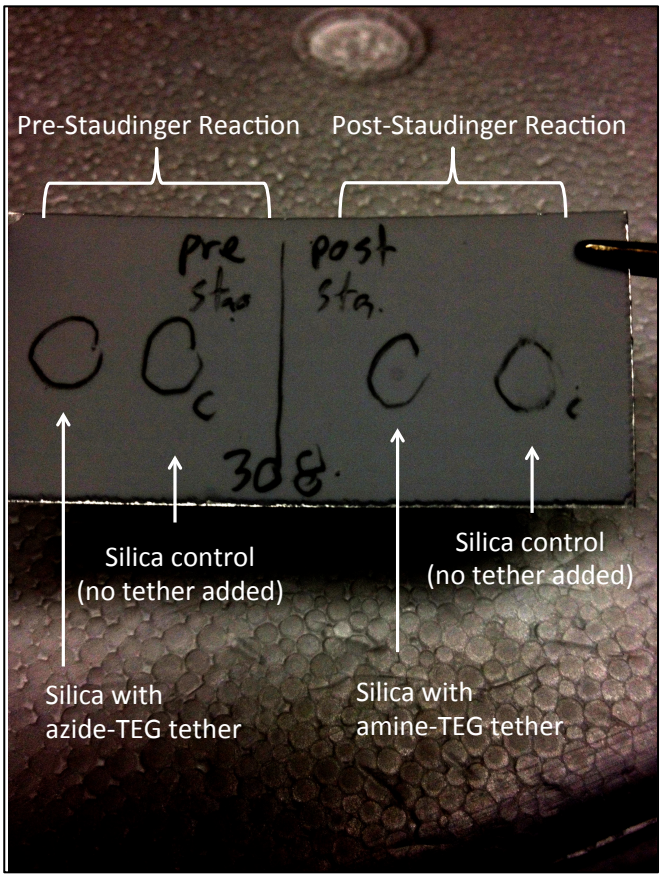

Figure 3.55. Picture of a ninhydrin assay (on a silica TLC plate) of azide-TEG SiNP **4** and amine-TEG SiNP **5** after the Staudinger reaction. The entire images contrast has been altered to emphasis the presence of amine seen in the amine-TEG tether spot.

The development of the faint blue-purple spot seen in the 'silica with amine-TEG tether' spot is indicative of a successful attachment of the long chain tether to the dye-doped SiNP. The particles were washed multiple times with water and ethanol, which decreases the likelihood that the amine signal may come from residual tether in solution. A portion of the amine-coated sample was then converted into DTC ligands before mixing the ligands, amine and DTC, separately with ether-capped GNP and were monitored for changes in the gold plasmon absorbance (Figure 3.31).

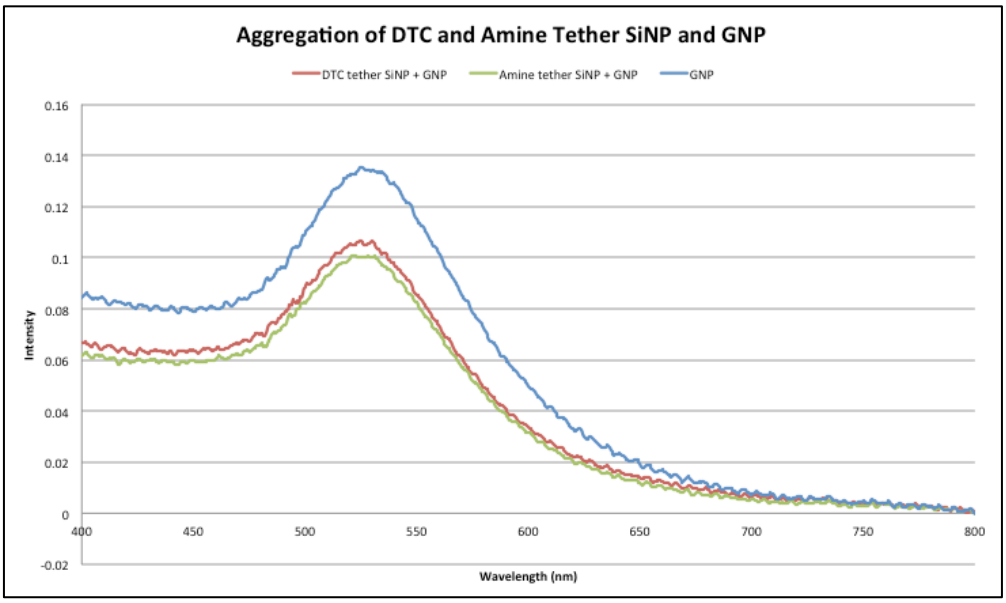

Figure 3.56. Absorbance spectra of long chain tether amine and DTC coated SiNP mixed with ether-capped GNP.

Both amine and DTC samples showed a decrease in the gold absorbance spectra but, interestingly, the amine sample showed a slightly greater decrease. This would suggest that the amine ligand bound to gold nanoparticles more readily than DTC. However, DTC has historically been shown to be a better binding unit than amines.[17b, 19] Thus, it is more likely that this preparation failed to produce the DTC ligand effectively giving rise to similar aggregations of both samples as no appreciable amount of dithiocarbamate was ever present on the surface of the SiNP. We can identify the issues arising with the production of DTC given the ninhydrin assay confirmed the presence of amines before the silica particles were carried on. Possible DTC issues being investigated include the concentration of base and the ability to remove excess reagents prior to gold aggregation versus reacting the gold *in situ*.

Long chain TEG-derived ligands can be efficiently synthesized and attached to the surface of silica nanoparticles bearing terminal amine groups. These groups can then be theoretically converted to DTC moieties in order to produce a strong gold binding group, but this has yet to be accomplished in our lab.

3.4 Chapter summary

This chapter described our efforts to functionalize the surface of dye-doped silica with amines, thiols, dithiocarbamate (DTC), and a synthetic long-chain ligands and gold nanoparticles with citrate and ether cappings to promote hetero-aggregation[1] in order to achieve metal enhanced fluorescence. These capping agents were chosen based on their ability to form strong interactions with gold nanoparticles while minimizing silica-silica aggregation. The use of piranha solution was also investigated for efficacy of pre-cleaning the surface of the silica nanoparticles. The efficacy of these experiments was determined by ninhydrin amine assay, zeta potential analysis, UV/visible absorption studies of gold nanoparticle solutions, and TEM imaging. A desirable ligand would be identified by its ability to preferential form silica-gold heteroaggregates as evidenced by TEM and absorption spectroscopy while minimizing any silica destruction or homoaggregation. The use of amines, thiols, dithiocarbamate (DTC), and synthetic long-chain ligands will promote desirable silica-gold aggregation to produce metal enhanced fluorescence of dye-doped silica nanoparticles in solution.

Piranha cleaning was studied for it efficacy in preparing dye-doped silica nanoparticles for surface functionalization with small molecule siloxanes. Our aim was to determine if the benefit of creating a more reactive silica surface, and thus produce a better functionalized particle, outweighed the risk of destroying the nanospheres

outright. TEM imaging indicated that even brief exposure to piranha solution resulted in the destruction of the silica framework and thus this technique would not be useful in the coating of silica nanoparticles (Figure 3.14).

We investigated the effect of coating the silica surface with amines in order to promote aggregation between dye-doped silica nanoparticles and gold nanospheres. The most common method for installing amines onto silica substrates is the acid catalyzed hydrolysis of (3-aminopropyl)triethoxysilane (APTES). No significant changes in the morphology of the silica post APTES coating in glacial acetic acid (Figure 3.17) and amines were confirmed to be present on the surface of the silica by ninhydrin assay (Figure 3.18). However, amine ligands do not consistently produce similar aggregates when mixed with citrate-capped gold (Figure 3.19). We speculate that the amine interactions are complicated by subtle changes in pH when introduced to citrate capped-gold nanoparticles. For this reason we investigated the use of thiols in the solution. Amine ligands are easily installed and verified on silica nanoparticles but do not consistently produce similar SiNP-GNP aggregates.

We investigated thiol coatings of dye-doped silica nanoparticles in order to reproducibly aggregate gold nanoparticles. Thiol coating was accomplished by acid catalyzed condensation of (3-mercaptopropyl)trimethoxysilane (MPTMS) onto the surface of silica nanoparticles by the same procedure APTES was used during amine coating. Thiol coated particles were shown to be stabilized compared to un-coated silica nanoparticles by zeta potential analysis (Figure 3.21) and, similar to amine coating, did not show any sign of silica degradation (Figure 3.24). However, a large amount of SiNP homoaggregation was observed in initial mixtures of thiol-coated SiNP and CTAB-

coated gold nanorods (Figure 3.23). Thiol coating is a possibly productive pathway towards achieving dye-doped silica- gold nanoparticle aggregates as it does to appear to be as sensitive to environmental changes as amine coatings but struggles from issues of homo-aggregation.

Dithiocarbamate (DTC) ligands were applied to dye-doped silica nanoparticles to provide a strong binding interaction with gold, similar to amines, while simultaneous decreasing the amount of silica-silica aggregation, often seen with thiols, due to electrostatic surface charge repulsion (Figure 3.25). No useful aggregation was produced by a short chain DTC ligand coated on the surface of dye-doped silica nanoparticles when mixed with ether-capped gold nanoparticles possibly due to the inability of the two nanoparticles to get within close proximity of each other due to the long ether-capping agent on gold (Figure 3.26). Thus, we studied the effects of attaching a longer chain DTC ligand to silica to overcome distance restrictions of the shorter ligands.

We investigated applying a synthetic long chain tetraethylene glycol (TEG) siloxane derivative with superficial gold binding moieties in order to achieve improved aggregation with ether-capped gold nanoparticles through ligand interdigitation (Figure 3.27). The long tether was synthetically accessible (Figures 3.28 and 3.29) and was confirmed to successfully add amine groups to the surface of the silica via ninhydrin assay before being converted to DTC (Figure 3.30). Both the amine and DTC samples showed a decrease in the gold absorbance spectra but the amine sample showed a slightly greater decrease, which likely indicated a poor conversion to DTC. Possible issues hindering the development of DTC include the concentration of base used and

the presence of excess reagents remaining in the flask upon mixing gold. Long chain TEG-derived ligands can be efficiently synthesized and attached to the surface of silica nanoparticles bearing terminal amine groups before, theoretically, being converted to DTC moieties in order to form a more robust binding unit on the surface of dye-doped silica nanoparticles.

The use of amines, thiols, dithiocarbamate (DTC), and synthetic long-chain ligands will promote desirable silica-gold aggregation to produce metal enhanced fluorescence of dye-doped silica nanoparticles in solution while simultaneously decreasing the amount of silica homoaggregation. Our initial investigations show that altering the surface functionality of dye-doped silica nanoparticles greatly impacts the degree of aggregation, which gives rise to different arrangements within gold nanosphere and nanorod binding for application to metal enhanced fluorescence and plasmon mediated waveguide systems.

3.5 Experimental

3.5.1 Piranha cleaning silica nanoparticles[22] !!Caution: Piranha solution reacts violently when in contact with organic matter!!

Piranha solution was prepared by mixing hydrogen peroxide (H_2O_2) (300 µL, 30%) with concentrated sulfuric acid (H_2SO_4) (700 µL) in a new 10 mL cylindrical vial (*Caution: addition of H_2SO_4 causes H_2O_2 to boil if added quickly*). The piranha solution was allowed to cool for several minutes before addition to aqueous suspension of silica nanoparticles. SiNP (1 mL, ~1 mg/mL) were concentrated in water (100 µL) by centrifuging for 10 min at 15,000 rpm and removing the majority of the aqueous supernatant. Piranha solution (100 µL) was then added to the concentrated aqueous

suspension of SiNP (100 μL) and mixed via micropipette for 5 sec in a 1.5 mL snap-top centrifuge tube before the mixture was diluted to 1.5 mL with de-ionized water (17.8 MΩ). The particles were then immediately centrifuged for 10 min at 15,000 rpm and the piranha solution was removed and slowly neutralized with a concentrated sodium bicarbonate solution. The particles were similarly washed twice more with water (1.5 mL each) and additionally three times with ethanol (1.5 mL, 95%). The particles were finally re-suspended in water before TEM imaging.

3.5.2 Amine Coating procedure[11]

A typical procedure would involve suspending dye-doped silica nanoparticles (~1-20 mg/mL) into ethanol (1 mL, 95%) in a snap-top centrifuge tube (1.5 mL capacity) before adding glacial acetic acid (20 μL). The centrifuge tube was inverted several times by hand before (3-aminopropyl)triethoxy silane (20 μL) was added. The centrifuge tube was then rotary inverted overnight in the dark at room temperature. Amine-coated silica nanoparticles were cleaned by centrifuging for 10 min at 15,000 rpm before the supernatant was removed and the particles were re-suspended in ethanol (1.5 mL). This process was repeated for a total of three washes with ethanol and three additional washes with water (each 1.5 mL additions). The particles can then finally be re-suspended in water or ethanol (generally 1 mL).

3.5.3 Ninhydrin amine assay[23]

Ninhydrin amine assays were performed on silica thin-layer chromatography plates. The plates were spotted with suspensions of amine coated silica nanoparticles with capillary tubes. Spots were allowed dry before ninhydrin solution (10 % w/w in ethanol) was thoroughly applied via mist bottles. Excess ninhydrin solution was blotted off with

a paper towel before the TLC plates were placed in a drying oven (~100 °C) for 15 min. Blue-purple spots developed in the presence of amine. Figure 3.18 shows a control sample of concentrated free amine samples vs those bound to silica nanoparticles.

3.5.4 Thiol coating procedure[11]

A typical procedure would involve suspending dye-doped silica nanoparticles (~1-20 mg/mL) into ethanol (1 mL, 95%) in a snap-top centrifuge tube (1.5 mL capacity) before adding glacial acetic acid (20 μL). The centrifuge tube was inverted several times by hand before (3-mercaptopropyl)trimethoxy silane (20 μL) was added. The centrifuge tube was then rotary inverted overnight in the dark at room temperature. Thiol-coated silica nanoparticles were cleaned by centrifuging for 10 min at 15,000 rpm before the supernatant was removed and the particles were re-suspended in ethanol (1.5 mL). This process was repeated for a total of three washes with ethanol and three additional washes with water (each 1.5 mL additions). The particles can then finally be re-suspended in water or ethanol (1 mL).

3.5.5 Lipoic acid siloxane preparation[8a]

α-lipoic acid (206.3 mg, 1.0 mmol) was added to a 10 mL flame-dried, pear-shaped flask containing 1-Ethyl-3-(3-dimethylaminopropyl)carbodiimide (EDC) (465.77 mg, 3.0 mmol), 4-dimethylaminopyridine (DMAP) (24.43 mg, 0.2 mmol), and a magnetic stir bar in dry chloroform (5 mL). The reaction vessel was purged of with an atmosphere of nitrogen and stirred at room temperature. After 10 min of stirring (3-aminopropyl)triethoxysilane (APTES) (210.0 μL, 0.9 mmol) was added and the solution continued to stir for 12 h at room temperature to produce a highly coagulated light-green gel. Thin layer chromatography (1:1, petroleum ether : ethylacetate) did not

indicate any APTES remained in the gel. The highly gelled product was not soluble in NMR solvents.

3.5.6 Conversion of amine coating into dithiocarbamate (DTC)[19]

A general procedure proceeded by adding an ethanolic suspension of amine-coated silica nanoparticles (1.0 mL, 1-5 mg/ mL) to a 1.5 mL snap-top centrifuge vial before the pH was adjusted to >9 by addition of potassium hydroxide (KOH) (1M, ~4 drops). The centrifuge tube was inverted several times by hand before carbon disulfide (CS_2) (100 mM in 95% ethanol) was added. The formation of dithiocarbamate (DTC) ligands was allowed to proceed for 2 h before reacting aliquots of the solution (without further purification) with ether capped gold nanoparticles. Attempts to remove excess reagents via centrifugation/ sonication have not yet proved successful but may be possible.

3.5.7 Synthesis of TEG DTC tether

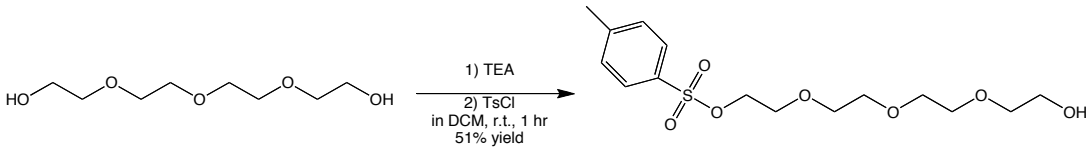

Mono-tosyl TEG:[15c] Tetraethylene glycol (TEG) (20 g, 0.1 mol) and triethylamine (TEA) (17.8 mL, 0.05 mol) were mixed together in a dichloromethane (DCM) (80 mL) in a 200 mL round bottom flask equipped with a magnetic stir bar. The solution was stirred for approximately one minute at room temperature to ensure both species had properly dissolved before the addition of tosyl chloride (TsCl) (1.9 g, 10 mmol) dissolved in DCM (20 mL). The reaction was stirred at room temperature for 1 h before work up. Organic material was extracted from saturated sodium bicarbonate solution (~20 mL) with DCM (10 mL, 3X). The collected organic portion was washed once with

brine solution (~20 mL) before the organic portion (DCM) was collected and dried over anhydrous sodium sulfate (Na_2SO_4). The solvent was removed under reduced pressure to yield a light yellow oil. The product was purified by flash silica column chromatography (2% methanol in DCM) (R_f= 0.2) to give a pure monotosylated TEG (4.6 g, 51% yield based on tosyl chloride). ^{1}H NMR (300 MHz, $CDCl_3$): δ 7.80 (d, 2H, *J* = 8 Hz), 7.34 (d, 2H, *J* = 8 Hz), 4.16 (t, 2H, *J* = 10 Hz, 5 Hz), 3.66 (m, 14H) 2.44 (s, 3H).

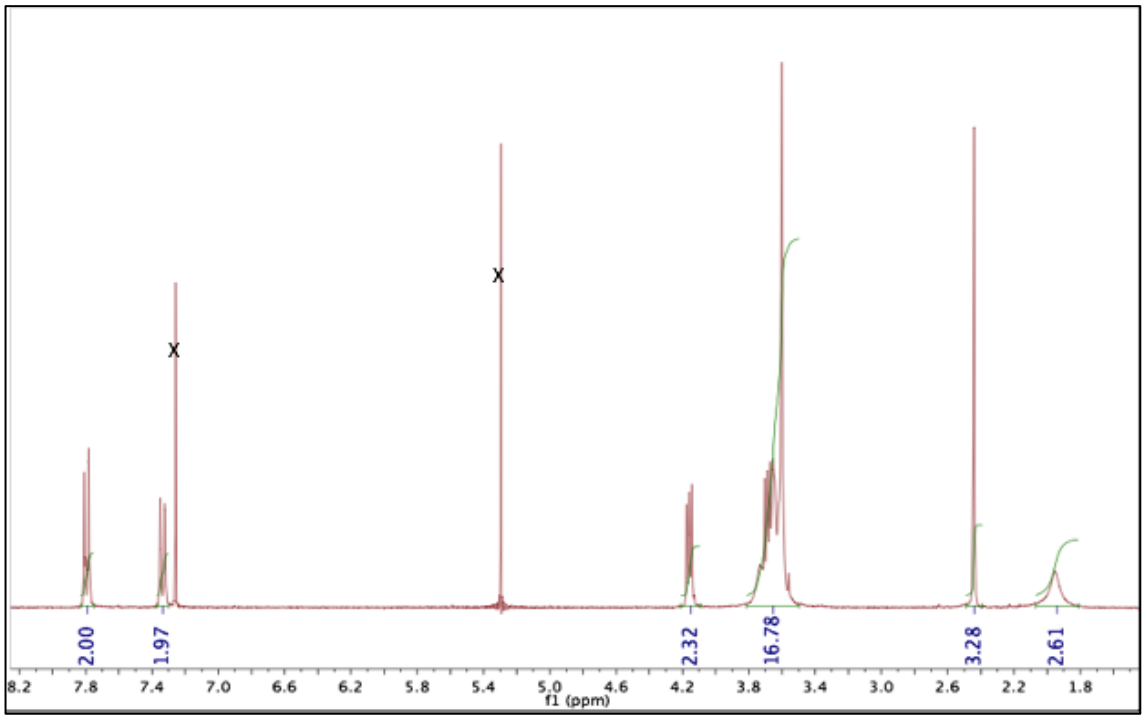

Figure 57. ^{1}H NMR of monotosyl TEG. (300 MHz)

Azide TEG:[24] Monotosyl TEG (4.6 g, 0.013 mol, from previous step) was dissolved in anhydrous dimethylformamide (DMF) (50 mL) in a 100 mL round bottom flask containing a magnetic stir bar. After one minute of stirring at room temperature sodium azide (NaN_3) (4.29 g, 0.066 mol) was added before the reaction flask was heated to 60 ºC under nitrogen atmosphere. After 5 h the DMF was removed *in vacuo* before aqueous workup. Organic material was extracted from saturated sodium bicarbonate solution (~20 mL) with DCM 3X (10 mL). The collected organic portion was washed once with brine solution (~20 mL) before the organic portion (DCM) was collected and dried over anhydrous sodium sulfate (Na_2SO_4). The solvent was removed under reduced pressure to yield the pure azide TEG as a light-yellow oil (1.8 g, 63%). ^{1}H NMR (300 MHz, $CDCl_3$): δ 3.67 (m, 14H), 3.39 (t, 2H, J = 10 Hz, 5 Hz), 2.22 (s, 1H).

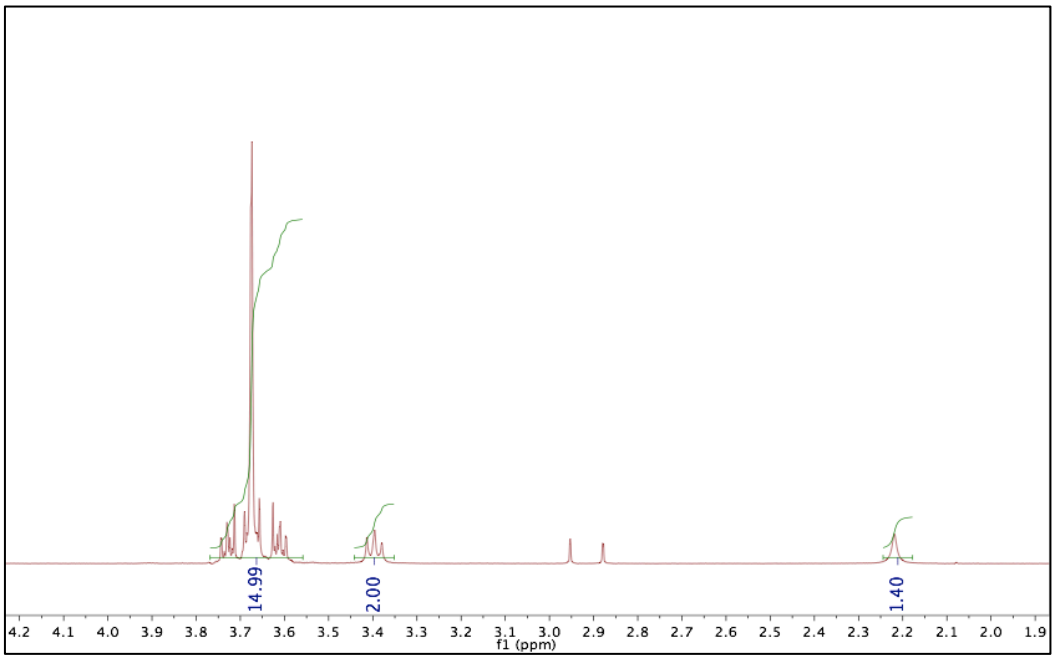

Figure 58. ^{1}H NMR of azide TEG (300 MHz).

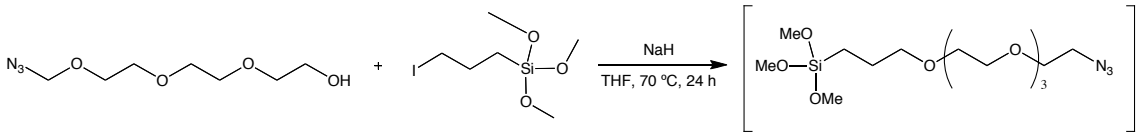

Azide TEG siloxane attachment and silica coating:[25] Sodium hydride (NaH) (2 mg, 0.045 mmol, 60% in mineral oil) was cleaned in a flame dried 50 mL round bottom flask by washing with petroleum ether (2 mL) three times under nitrogen atmosphere to remove excess mineral oil. Azide TEG (10 mg, 0.045 mmol, from previous step) was dissolved in anhydrous tetrahydrofuran (THF) (18 mL) and added to the flask containing cleaned NaH with a magnetic stir bar. The reaction was stirred for 5 min at room temperature before (3-iodopropyl)trimethoxysilane (IPTMS) (0.18 mL, 0.9 mmol) was added. The reaction was then heated to 70 °C for 24 h under nitrogen atmosphere. THF was removed *in vacuo* to yield a dark green oil that was not silica or air stable. The material was carried on without further purification or analysis. Silica nanoparticle attachment was attempted by mixing SiNP (1 mL, ~1 mg/mL, 150 nm diameter) with glacial acetic acid (20 μL) and gently inverting before adding azide TEG siloxane (20 μL) in a 1.5 mL snap-top centrifuge tube. The tube was rotary inverted over night at room temperature before being cleaned by centrifugation/ sonication. Azide TEG-coated silica nanoparticles were cleaned by centrifuging for 10 min at 15,000 rpm before the supernatant was removed and the particles were re-suspended in ethanol (1.5 mL). This process was repeated three times before finally resuspending in ethanol (1.0 mL, 95%).

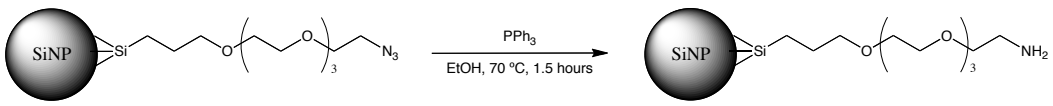

Conversion of azide TEG to amine TEG via Stuadinger reaction:[26] Azide TEG-coated SiNP (1 mL, ~1 mg/mL in 95% EtOH) was added to a 10 mL round bottom flask containing triphenylphosphine (TPP) (25 mg, 0.09 mmol) dissolved in ethanol (4 mL, 95%) and a magnetic stir bar. The round bottom flask was attached to an air condenser and refluxed (~70 ºC) under nitrogen atmosphere for 1.5 h. Ethanol was removed *in vacuo* before two drops of HCl (1M) and toluene (250 μL) were added to yield the free amine. The particles were then cleaned via centrifugation for 10 min at 15,000 rpm before the supernatant was removed and the particles were re-suspended in ethanol (1.5 mL). This process was repeated three times before finally resuspending in ethanol (1.0 mL, 95%). Ninhydrin assay (dissucssed above) confirmed the presence of free amine in the particles by the development of a blue-purple TLC spot. TEG amine-amine coated particles were then studied as is and with DTC conversion (discussed above).

3.6 References

1. Islam, A. M.; Chowdhry, B. Z.; Snowden, M. J., Heteroaggregation in colloidal dispersions. *Adv. Colloid Interface Sci.* **1995,** *62*, 109-136.

2. Kelly, L. E.; Coronado, E.; Zhao, L. L.; Schatz, G. C., The Optical Properties of Metal Nanoparticles: The Influence of Size, Shape, and Dielectric Environment. *J. Phys. Chem. B* **2003,** *107*, 668-677.

3. Lakowicz, J. R., Radiative Decay Engineering 5: Metal-Enhanced Fluorescence and Plasmon Emission. *Anal. Biochem.* **2005,** *337*, 171-194.

4. (a) Dhumale, V. A.; Gangwar, R. K.; Datar, S. S.; Sharma, R. B., Reversible Aggregation Control of Polyvinylpyrrolidone Capped Gold Nanoparticles as a Function of pH. *Mater. Express* **2012,** *2* (4), 311-318; (b) Westcott, S. L.; Oldenburg, S. J.; Lee, R. T.; Halas, N. J., Formatin of Adsorption of Clusters of Gold Nanoparticles onto Functionalized Silica Nanoparticle Surfaces. *Langmuir* **1998,** *14*, 5396-5401; (c) Gunawardana, K. B. Study of Metal-Enhanced Fluorescence of Dye Doped Silica Nanoparticles. University of Oklahoma, Norman, 2012.

5. Xie, W.; Walkenfort, B.; Schlucker, S., Label-Free SERS Monitoring of Chemical Reactions Catalyzed by Small Gold Nanoparticles Using 3D Plasmonic Superstructures. *J. Am. Chem. Soc.* **2013,** *135* (5), 1657-1660.

6. (a) Pan, S.; Wang, Z.; Rothberg, L. J., Enhancment of Adsorbed Dye Monolayer Fluorescence by a Silver Nanoparticle Overlayer. *J. Phys. Chem. B* **2006,** *110*, 17383-17387; (b) Ismali, H.; Geng, D.; Sun, A. X.; Kantzas, T. T.; Workentin, M. S., Light-Actived Covalent Formation of Gold Nanoparticle-Graphene and Gold Nanopartcile-Glass Composites *Langmuir* **2011,** *27*, 13261-13268.

7. Dobbs, D. A.; Bergman, R. G.; Theopold, K., H, Piranha Solution Explosion. *Chem. Eng. News* 1990, p 2.

8. (a) Henderson, L. C.; Altimari, J. M.; Dyson, G.; Servinis, L.; Niranjan, B.; Risbridger, G. P., A Comparative Assessment of alpha-lipoic acid N-phenylamides as Non-Steriodal Androgen Receptor Antagonists Both On and Off Gold Nanoparticles. *Bioorg. Chem.* **2012,** *40*, 1-5; (b) Yong, K.-T.; Sahoo, Y.; Swihart, M. T.; Prasad, P. N., Synthesis and plasmonic properties of silver and gold nanoshells on polystyrene cores of different size and of gold–silver core–shell nanostructures. *Colloids and Surfaces A: Physicochem. Eng. Aspects* **2006,** *290*, 89-105.

9. Weiser, H. B., *Inorganic Colloid Chemistry*. Wiley: New York, NY, 1933; Vol. 1.

10. Burda, C.; Chen, X.; Narayanan, R.; El-Sayed, M. A., Chemistry and Properties of Nanocrystals of Different Shapes. *Chem. Rev.* **2005,** *105*, 1025-1102.

11. Wang, L.; Tan, W., Multicolor FRET Silica Nanoparticles by Single Wavelength Excitation. *Nano Lett.* **2006,** *6* (1), 84-88.

12. Hanaor, D.; Michelazzi, M.; Leonelli, C.; Sorrell, C. C., The effects of carboxylic acids on the aqueous dispersion and electrophoretic deposition of ZrO2. *J. Eur. Ceramics Soc.* **2012,** *32*, 235-244.

13. Malvern Zeta potential using laser Doppler electrophoresis (LDE). http://www.malvern.com/LabEng/technology/zeta_potential/zeta_potential_LDE.htm.

14. Greenwood, R.; Kendall, K., Selection of Suitable Dispersants for Aqueous Suspensions of Zirconia and Titania Powders using Acoustophoresis. *J. Eur. Ceramics Soc.* **1999,** *19*, 479-488.

15. (a) Harding, V. J.; MacLean, R., The ninhydrin reaciton with amines and amides. *J. Bio. Chem* **1916,** (2), 337-350; (b) Pereira, C.; Silva, J.; Pereira, A. M.; Araujo, J. P.; Blanco, G.; Pintado, J. M.; Freire, C., [VO(acac)2] hybrid catalyst: from complex immobilization onto silica nanoparticles to catalytic application in the epoxidation of geraniol. *Catal. Sci. Technol.* **2011,** *1*, 784-793; (c) van Ameije, J.; Liskamp, R. M. J., Synthesis of novel trivalent amino acid glycoconjugates based of the cyclotriveratrylene ('CTV') scaffold. *Org. Biomol. Chem.* **2003,** *1*, 2661-2669.

16. Friedman, M.; Sigel, C. W., A Kinetic Study of the Ninhydrin Reaction. *Biochem* **1966,** *5* (2), 478-485.

17. (a) Aslan, K.; Perez-Luna, V. H., Surface Modification of Colloidal Gold by Chemisorption of Alkanethiols in the Prescence of a Nonionic Surfactant. *Langmuir* **2002,** *18*, 6059-6065; (b) Park, M.-H.; Ofir, Y.; Samanta, B.; Arumugam, P.; Miranda, O. R.; Rotello, V. M., Nanoparticle Immobilization on Surfaces via Activatable Heterobifunctional Dithiocarbamate Bond Formation. *Adv. Mater.* **2008,** *20*, 4185-4188.

18. Whitesides, G. M.; Laibinis, P. E., Wet Chemical Approaches to the Characterization of Organic Surfaces: Self-Assembled Monolayers, Wetting, and the Physical-Organic Chemistry of the Solid-Liquid Interface *Langmuir* **1990,** *6* (1), 87-97.

19. Zhao, Y.; Perez-Segarra, W.; Shi, Q.; Wei, A., Dithiocarbamate Assembly on Gold. *J. Am. Chem. Soc.* **2005,** *127*, 7328-7329.

20. Huff, T. B.; Hansen, M. N.; Zhao, Y.; Cheng, J.-X.; Wei, A., Controlling the Cellular Uptake of Gold Nanorods. *Langmuir* **2007,** *23*, 1596-1599.

21. Singh, A.; Dahanayaka, D.; Biswas, A.; Bumm, L. A.; Hlaterman, R. L., Molecularly Ordered Decanethiolate Self-Assembled Monolayers on Au(111) from in situ Cleaved Decanethioacetate: An NMR and STM Study of the Efficacy of Reagents for Thioacetate Cleavage. *Langmuir* **2010,** *26* (16), 13221-13226.

22. Gupta, R. K.; Srinivasan, M. P.; Dharmarajan, R., Synthesis of short chain thiol capped gold nanoparticles, their stabilization and immobilization on silicone surface. *Colloids and Surfaces A: Physicochem. Eng. Aspects* **2011,** *390*, 149-156.

23. Hoefnagels, H. F.; Wu, D.; de With, G.; Ming, W., Biomimetic Superhydrophobic and Highly Oleophobic Cotton Textiles. *Langmuir* **2007,** *23*, 13158-13163.

24. Shirude, P. S.; Kumar, V. A.; Ganesh, K. N., BisPNA Targeting to DNA: Effect of Neutral Loop on DNA Duplex Strand Invasion by *aep*PNA-N7G/*aep*PNA-C Substituted Peptide Nucleic Acids. *Eur. J. Org. Chem.* **2005**, 5207-5215.

25. Zamadar, M.; Ghosh, G.; Mahendran, A.; Minnis, M.; Kruft, B. I.; Ghogare, A.; Aebisher, D.; Greer, A., Photosensitizer Drug Delivery via an Optical Fiber. *J. Am. Chem. Soc.* **2011,** *133*, 7882-7891.

26. Vugts, D. J.; Vervoort, A.; Walsum, M. S.-v.; Visser, G. W. M.; Robillard, M. S.; Versteegen, R. M.; Vulders, R. C. M.; Hercheid, J. D. M.; van Dogen, G. A. M. S., Synthesis of Phosphine and Antibody-Azide Probes for in Vivo Staudinger Ligation in Pretargeted Imaging and Therapy Approach. *Bioconjugate Chem.* **2011,** *22*, 2072-2081.

Chapter IV: Aggregation of dye-doped silica nanoparticles and gold nanospheres to produce metal-enhanced fluorescence in solution

4.1 Chapter Overview

This chapter describes the need for and our efforts to produce metal-enhanced fluorescence (MEF)[1] in solution by aggregating dye-doped silica nanoparticles with gold nanospheres. Plasmonics, the study of exciting surface electrons of metal nanostructures, has recently enjoyed a surge of interest due its potentially transformative effects on fluorescent, medicinal, and materials chemistry.[2] Currently, the most effective application of MEF is on solid substrates[3] to produce surface enhanced Raman spectroscopy (SERS), which produces dramatic enhancements of fluorescent brightness of molecules near the surface of a rough metal.[4] Producing metal-enhanced fluorescent in solution would allow similar dramatic increases in fluorescent signal without requiring a solid phase substrate. The solution based approach would provide a path to new and sensitive biosensors[5] and potential applications to light harvesting systems.[6] This chapter describes our efforts to reproducibly produce metal-enhanced fluorescence in solution by aggregating dye-doped silica nanopartciles with gold nanospheres.

4.2 Introduction

Metal-enhanced fluorescence has been intensely studied over the last decade, after being reported by Geddes and Lakowicz in 2002, as a method for greatly increasing the fluorescent brightness of a fluorophore when brought near the surface of

a metal nanostructure.[1] This phenomenon is thought to occur by two processes: increased excitation of the fluorophore and additional rapid emission pathways.[3] Figure 4.1 displays how placing a fluorophore near the surface of a metal results in the increased excitation events due to electromagnetic radiation cross-section increase near the metal.[7] The increased concentration of incident light provides increased fluorophore excitation similar to increasing the power of the incident light.[8]

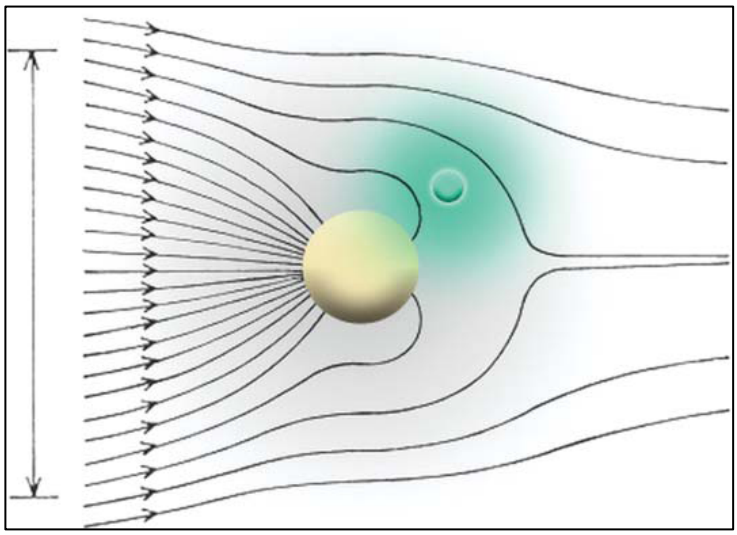

Figure 4.59. A metal nanostructure (light-yellow sphere) interacting with local incident light (black lines) near an organic fluorophore (green sphere). (Image from Lakowicz et al)[7]

Bringing a fluorophore near a metal nanoparticle surface provides additional emission pathways leading to a greater turnover of excitation/ emission events due to a decrease in the fluorophore fluorescent lifetime.[1] Figure 4.2 displays a Jabloski diagram depicting the increased excitation pathways that are afforded to a fluorophore near the surface of a metal. The increase in excitation energy is one important method for producing metal-enhanced fluorescence.

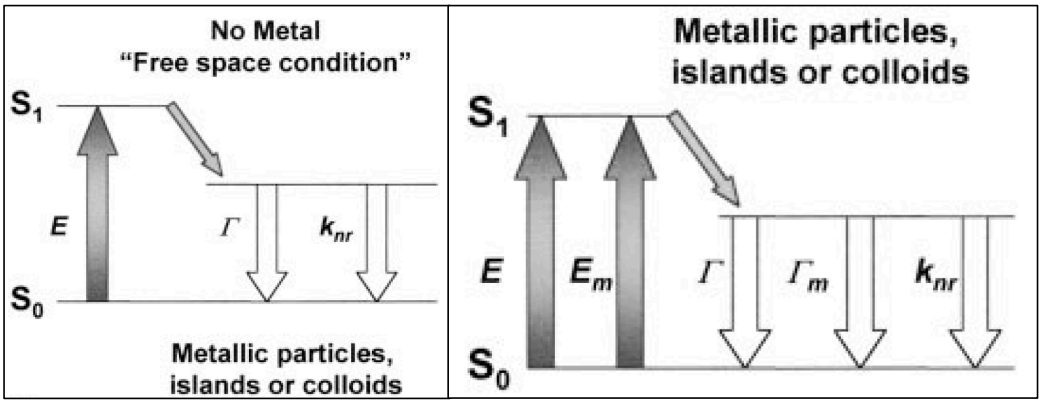

Figure 4.60. Jabloski diagram of the excitation/emission process of (left) a fluorophore unbound to a metal nanostructure (free-space condition) and, (right) a fluorophore near the surface of a metal nanostructure. (image from Geddes et al)[1]

The increase in the number of radiative pathways, by the introduction of the emission for interaction with the metal (Γ_m), decreases the fluorescent lifetime of the dye. Equation (1) represents the fluorescent lifetime (τ) of a free dye:[7]

$$\tau = \frac{1}{\Gamma + k_{nr}} \qquad (1)$$

Where Γ is the radiative decay rate and k_{nr} is the non-radiative rate. The lifetime of a dye near the surface of a metal nanoparticle is given by (2).[7]

$$\tau = \frac{1}{\Gamma + \Gamma_m + k_{nr}} \qquad (2)$$

Increasing the overall radiative decay rate by placing a fluorophore near the surface of a metal decreases the amount of time the fluorophore spends in the excited state. Thus, the number of excitation events in a given time is greater for a fluorophore when appropriately placed from the surface of a metal. However, metal-enhanced

fluorescence is highly dependent on distance, as placing the fluorophore too close to the metal results in fluorescent quenching while being too far away results in no interaction at all.[3] Figure 4.3 depicts the quenching effects of close proximity and optimal conditions of 0.5-200 nm distance between the fluorophore and metal surface.

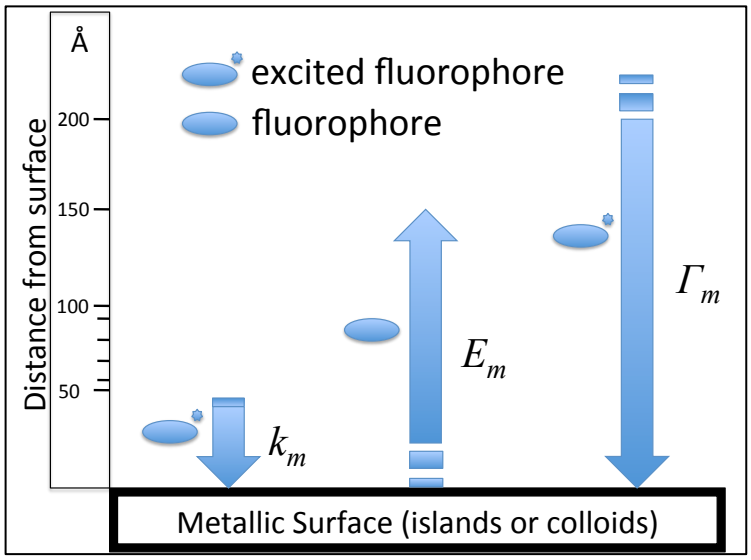

Figure 4.61. Schematic of distance dependence between a dye and metal surface on quenching (k_m), excitation (E_m), and emission (Γ_m). (Image adapted from Geddes et al)[1]

Since proximity to the dye is important to enhancing the fluorescent brightness, we investigated synthesizing dye-doped silica nanoparticles with desired barriers (5-20 nm)[1] upon aggregation with gold nanoparticles. This would allow beneficial excitation and emission events to take place while minimizing the amount of quenching that occurs via oscillation dampening when the fluorophore is too close to the surface of the metal.[9] Furthermore, doping fluorophores into silica nanoparticles also allows for multiple gold nanospheres to aggregate around a single sphere, which leads to fluorescent brightness increases due to increased gold scattering.

Increasing scattering by aggregated gold nanospheres increases the overall brightness enhancement of our metal-enhanced fluorescence system. Scattering refers to the elastic reflection of incident light, as compared to other pathways where the light may be absorbed by the plasmon resulting in energy dissipation via heat loss.[7] Schatz et al have theoretically shown that the scattering portion of gold nanospheres increases upon aggregation.[10] Figure 4.4 displays the calculated scattering portion of the gold nanospheres. Increasing scattered light increase overall fluorescent brightness as excitation energy is transferred from the excited dye to the plasmon of the gold nanoparticle before it is either emitted via scattering or absorbed via other non-radiative pathways.[11]

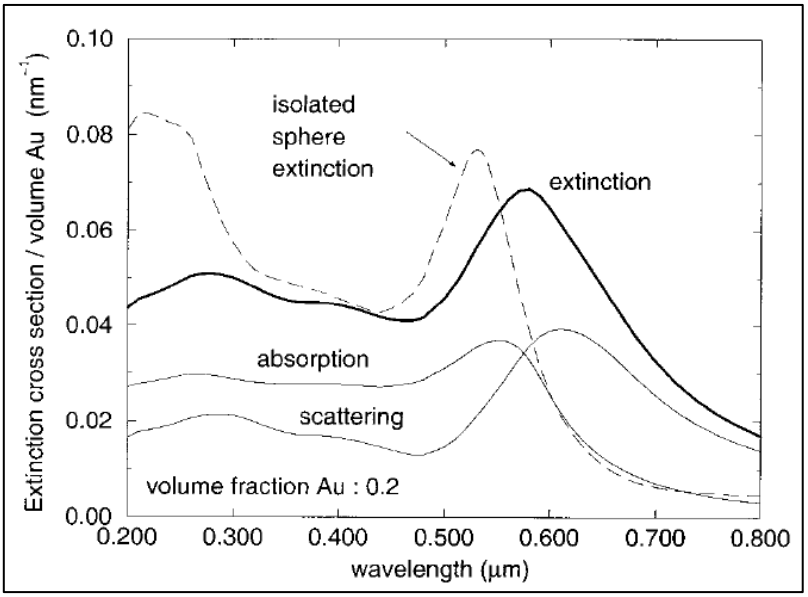

Figure 4.62. Extinction spectrum of isolated and aggregated gold nanospheres with calculated scattering component.[10]

This increase in scattering is important as the rate of emission from energy transfer between the dye and gold is dependent on the metal scattering component.[12] The total

emission intensity of a fluorophore-plasmon (plasmophore) complex is given by equation (3).

$$I_T = I_F + I_P = k\varepsilon_F Q_0(1 - E) + k\varepsilon_F Q_S \qquad (3)$$

Here, I_F is the fluorescence emission intensity, I_P is the plasmon emission intensity, ε_F is the dye extinction, Q_0 is the quantum yield of the dye, and Q_s is the scattering quantum yield. E, the energy transfer efficiency between the fluorophore and the metal, is given by equation (4).

$$E = \frac{k_T}{\Gamma + k_{nr} + k_T} \qquad (4)$$

The energy transfer rate between the dye and metal is given by k_T, Γ is the radiative decay rate, and k_{nr} is the nonradiative decay rate. Thus, as the energy transfer efficiency between the dye and metal improves E begins to approach 1. As this occurs the overall emission intensity is dominated by the scattering ability of the gold shown in equation (5).[12]

$$I_T = k\varepsilon_F Q_S \qquad (5)$$

Therefore, aggregating multiple gold nanospheres around a single dye-doped silica nanoparticle increases GNP scattering, which becomes the dominate source of emission for systems like SiNP-GNP aggregates that display a high efficiency energy transfer rates.

Metal-enhanced systems have been extensively studied on solid phase substrates where the metal-fluorophore distance can be easily controlled.[3-4, 7, 13] Lakowicz et al

previously demonstrated a five-fold enhancement of N,N[1]-(dipropyl)-tetramethylindocarbocyanine (Cy3) when placed near silver island films (SIFs) (Figure 4.5), as the polymer places the fluorophores within the previously discussed optimal range to increase excitations while diminishing fluorescent quenching.[3]

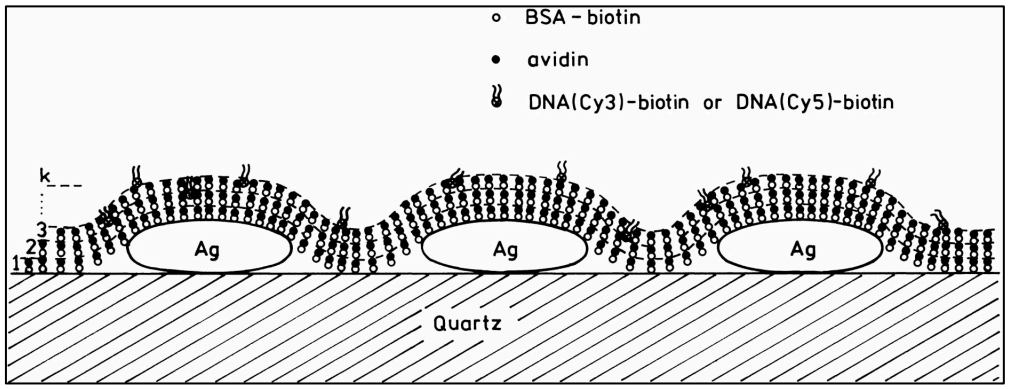

Figure 4.63. Schematic of Cy3-bound polymer in multiple layers on top of a silver island film. (Image from Lakowicz et al)[3]

Each additional polymer monolayer added to the silver island films increased the overall fluorophore metal distance.[3] Figure 4.6 displays the effect seen on the emission of the fluorophore-doped polymers as they were continuously added.

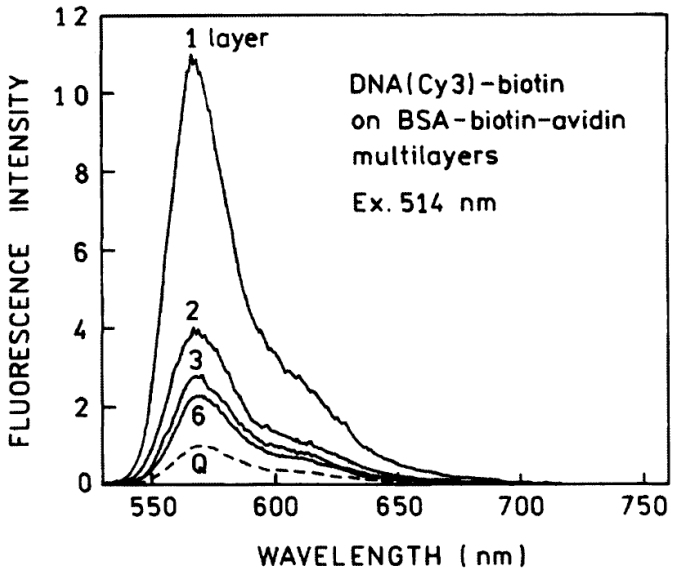

Figure 4.64. Emission spectra of Cy3-doped biotin polymer layered (1,2,3, and 6) on a quartz (Q) slide covered with a silver island film. (Image from Lakowicz et al)[3]

The silver island films offer control over the degree of metal aggregation, through deposition of the silver islands on glass, as well as the distance of the dye and metal surface, which is controlled by the number of monolayers that were grown on top of the islands. The greatest enhancement was seen for a single biotin monolayer where the fluorophores are roughly 1 nm away from the surface. Increasing the number of layers showed a marked drop in fluorescent brightness due to increasing the distance between the surface of the silver and fluorophores, which does not allow increasing emission pathways and thus cycles through excitation/emission at a slower rate.[3] The silver island film system provides excellent insight to underlying factors of MEF but it is limited to solid silver substrates. Moving into solution with gold substrates allows for greater utility in chemical sensing[14] as well as potentially dramatically higher brightness increases, as the stronger plasmonic field of the gold nanoparticles theoretically can

much more efficiently produce the increased excitation and faster cycling phenomena that lead to increased fluorescent brightness.[15]

Aggregation of dye-doped silica nanoparticles has shown a 200-fold enhancement previously by Kalani Gunawardana in our group.[8] Rhodamine B was doped into silica nanoparticles by the Stöber method (chapter II) and coated in propyl dithiocarbamate (DTC) ligands (chapter III) before being mixed with ether-capped gold to produce well-aggregated silica-gold clusters. Figure 4.7 shows TEM images of the SiNP and GNP aggregates after 2 and 20 days. The DTC functionalized surface of the silica nanoparticles clearly increases the amount of SiNP-GNP aggregates over time as seen by several free gold particles in the left image (lone dark black dots) compared to very few on the right image (clusters of grey and black dots are SiNP-GNP aggregates).

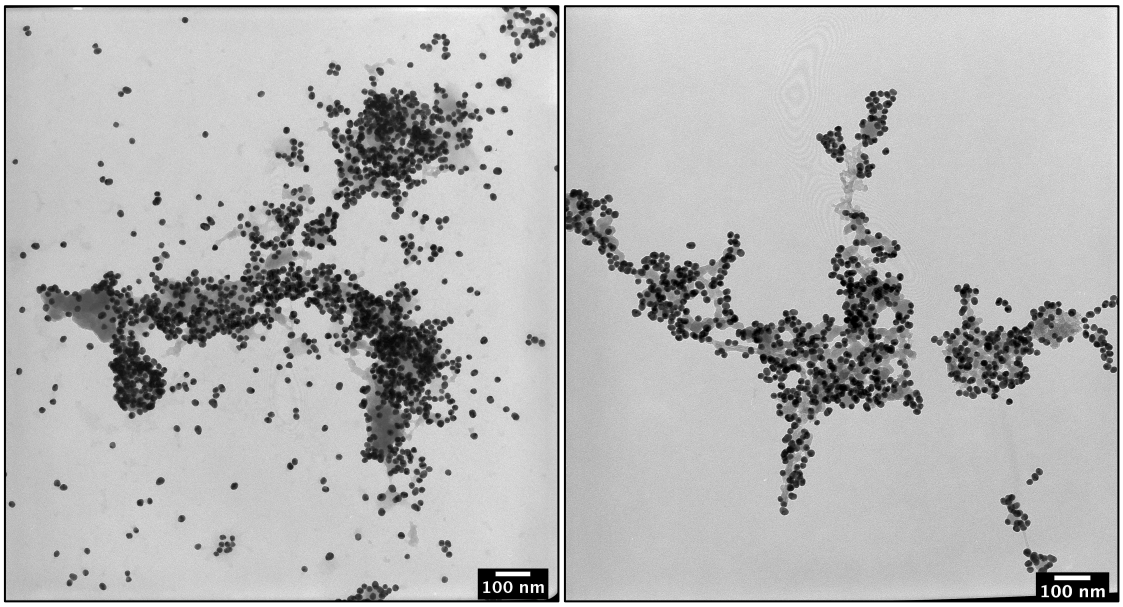

Figure 4.7. Gold nanoparticles (dark black) and DTC coated silica nanoparticles (grey) (left) 2 days after mixing (right) 20 days after mixing. (Image from Gunawardana, Green, and Halterman).

The increase in dye-doped silica and gold aggregates clearly seen in the TEM images above were accompanied by significant brightness enhancements of greater than 200 fold (Figure 4.8).

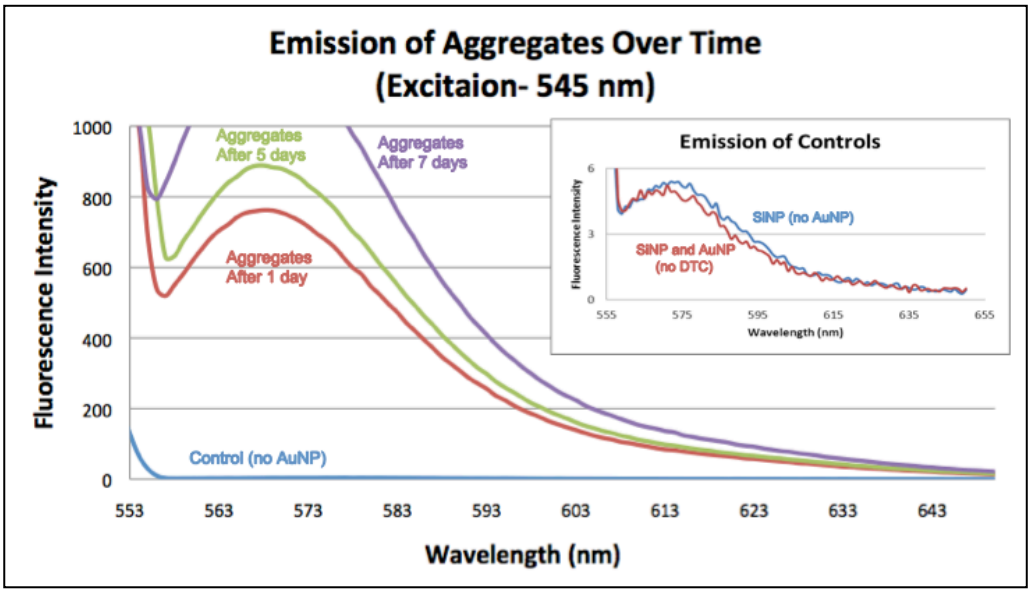

Figure 4.8. Time study of emission spectra for RhB doped silica particles in the presence of gold nanospheres (Image from Gunawardana, Green, and Halterman).

No enhancement was seen in emission or aggregation by TEM. As a control, gold nanospheres were mixed with dye-doped silica nanoparticles that had not been functionalized with DTC (insert of Figure 4.8). These results support the model of DTC mediated aggregation and aggregation induced metal-enhanced fluorescence by increase of plasmon scattering and thus faster cycling of the excitation/emission pathway.[3, 8, 10] The early work from Gunawardana, Green, Halterman and provides an excellent proof-of-concept but suffers from issues reproducibility of aggregation of particles. That solution phase assembly was sensitive to changes in aggregation, which more than likely arose from the inconsistency of silica nanoparticles produced in the Stöber

preparation. To overcome that problem, the current work focused on investigating the effects of more uniform layered silica nanoparticles with various gold binding ligands.

We anticipated that metal-enhanced fluorescence could be achieved by aggregating functionalized dye-doped silica nanoparticles and gold nanospheres in solution. Doping fluorophores into silica nanoparticles provides the necessary distance between the dye and the surface of the metal[3] while binding multiple gold nanospheres around a single silica particle increases the excitation volume[1] and the gold scattering efficiency[10], which leads to greater fluorescence brightness enhancements.[7] Previous systems on solid substrates[3] and in solution[8] have shown great promise but lack reproducibly high brightness enhancements. Further investigation of the interaction between dye-doped silica nanoparticles and gold nanospheres will provide a path to consistent and dramatic fluorescent brightness enhancements in solution for applications to bio-sensing[14] and potentially to light harvesting systems.[6]

4.3 Results and Discussion

Metal-enhanced fluorescence (MEF) was studied in solution by attempting to measure the lifetime of previously enhanced systems, varying the concentration of dye within the layer silica nanoparticles, varying the relative concentrations of silica and gold species in solution, and increasing the overall distance between the dye and gold by producing large diameter (150 nm) silica nanoparticles. These variations would allow for an optimized dye-gold distance to be established en route to solution phase metal-enhanced fluorescence. The effect of varying the surface coating was also measured and is the topic of chapter III. Photophysical changes were investigated with fluoremetry, excitation spectroscopy, and photoluminescent (PL) lifetime spectroscopy,

while aggregation measurements were performed using transmission electron microscopy (TEM) and gold UV/visible absorbance spectroscopy. By correlating these measurements, we aimed to investigate the gold and fluorophore photophysical changes that could be supported by morphological electron imaging studies. Our aim is to create a robust and reproducible metal-enhanced fluorescent system by aggregating surface functionalized dye-doped silica nanoparticles with gold nanospheres.

4.3.1 Photoluminescent (PL) lifetime measurements

Dramatic emission increases seen previously in our lab (Figure 4.8) likely benefitted from a significant increase in cycling of the excitation/emission processes given the large (200-fold) enhancements produced.[8] Increased cycling of the excitation/emission processes would require decreasing the fluorescence lifetime, τ_0, so that the amount of time dye molecules occupy the excited state is decreased.[1] Thus, we investigated the relative PL lifetimes of free rhodamine B and dye-doped rhodamine B in our MEF system (Figure 4.8). These measurements were made possible through collaboration with Drs. Gregory Salamo and Dorel Guzun at the University of Arkansas Institute for Nanoscience and Engineering. Figure 4.9 shows the time-resolved absorption difference from a pump-probe experiment for free rhodamine B in solution measured from a femptosecond pulse laser with a sampling oscilloscope detector (details of measurements are in experimental section A.B.C).

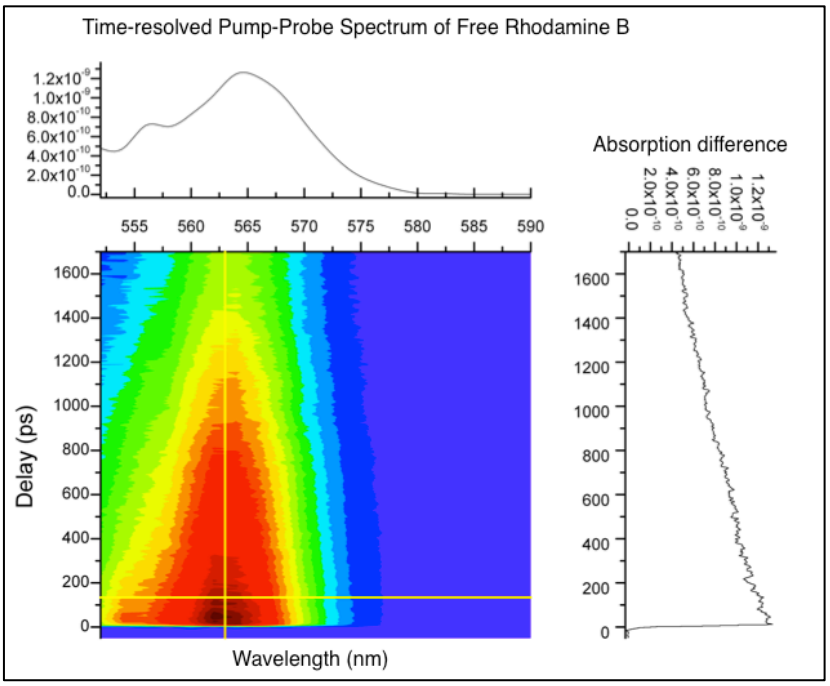

Figure 4.9. Time-resolved pump-probe absorption difference spectrum for free rhodamine B in solution. Excitation decay graph shown on the right. (Image from collaborator Dr. Dorel Guzun, University of Arkansas).

Free rhodamine B displayed a very slow decay of the excited state to produce a very long undetermined lifetime. The fluorescent lifetime of rhodamine B has previously been reported to be ~6 nanoseconds.[16] The experimental lifetime, calculated from the spectrum shown above, is shown in equations 6 and 7.

$$I = I_0 e^{kt} \qquad (6)$$

$$k = \frac{\ln\left(\frac{I}{I_0}\right)}{t}$$

$$k = \frac{\ln\left(\frac{1.3\times10^{-9}}{4.5\times10^{-10}}\right)}{1.7\ nanoseconds} = 0.624$$

$$\tau = \frac{1}{k} = \frac{1}{0.624} = 1.6\ nanoseconds$$

The significant discrepancy between the previously reported lifetime and the experimental lifetime found here may possibly be due to the use of water in our setup compared to ethanol of the literature value, as changes in the dielectric constant of the solvent are known to cause changes in excitation lifetime.[16] However, only changes in the lifetime of rhodamine B between free rhodamine and dye in our MEF system matter absolutely. Figure 4.10 shows a very noisy pump-probe absorption spectrum of rhodamine B-doped silica nanoparticles from the MEF system shown in Figure 5.8.

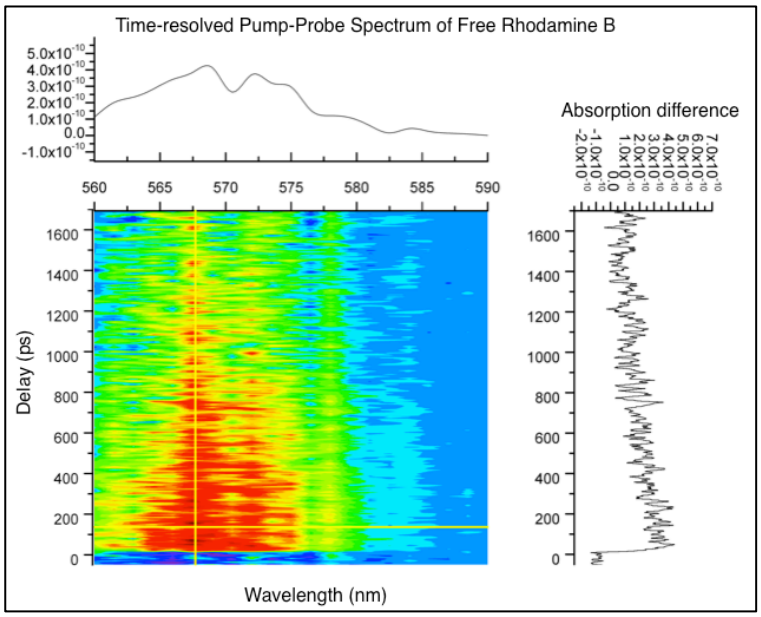

Figure 4.10. Time-resolved pump-probe absorption spectrum for metal-enhanced rhodamine B-doped silica nanoparticles. Excitation decay graph shown on the right. (Image from collaborator Dr. Dorel Guzun, University of Arkansas).

A decrease in PL lifetime would have been marked by a more rapid decrease in fluorescent signal over time. Unfortunately, the low concentration of our sample

produced too much noise to establish a substantial decay curve in Figure 4.10. Furthermore, the small fraction of rapidly cycling aggregates would be masked by the slow decay of un-aggregated dye in the noise. Our inability to reproduce this level of enhancement did not allow for additional sample to be produced and thus no additional measurements were taken. However, our initial PL lifetime study has provided, given a higher concentration, a path towards verifying the hypothesis of increasing fluorescent brightness by decreasing the PL lifetime and thus cycling through excitation/emission events at a faster rate. Layered silica nanoparticles, discussed in chapter II, were investigated as an alternative to the inconsistency of enhancement results given by the Stöber preparation and highlighted the need for much more homogeneous samples of purely SiNP-GNP aggregates.

4.3.2 Investigating the doping concentration effect of core-doped silica nanoparticles when mixed with gold nanospheres

We investigated the effects of different concentrations of rhodamine B core-doped silica nanoparticles during aggregation with gold nanospheres in order to produce metal-enhanced fluorescence. Core-doped silica nanoparticles were constructed by growing the silica seed cores in aqueous solutions of free rhodamine B followed by a silica-capping with an additional layer of silica to ensure no dye leaching occurred (Figure 4.11).

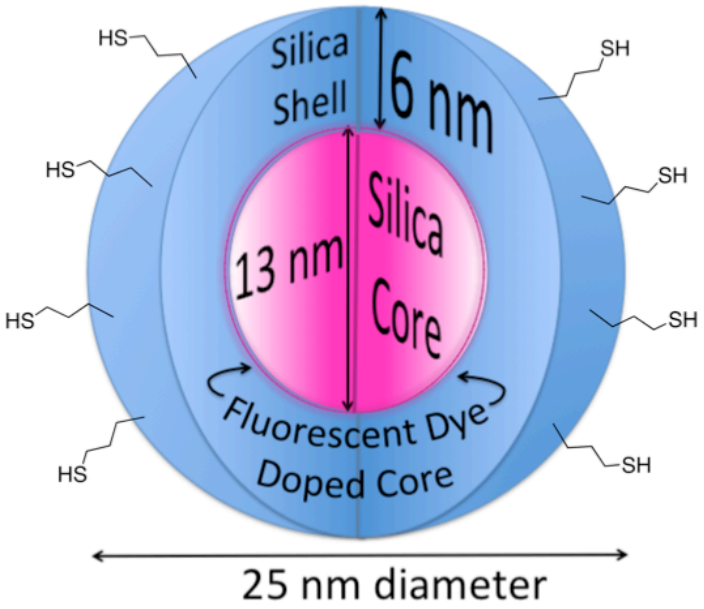

Figure 4.11. Cartoon schematic of 25 nm diameter rhodamine B core-doped silica nanoparticles coated with thiol ligands.

Two different concentrations of rhodamine B, 0.69 mM and 0.069 mM, were doped into 13 nm diameter silica cores before growing a 6 nm shell onto the surface. The core-doped silica nanoparticles were then coated in thiol ligands before mixing with gold nanoparticles. Cores that were doped with a ten-fold dilution of RhB were mixed with ten-fold as many silica particles in order to maintain a fluorescent signal (experimental section 4.5.4). Figure 4.12 shows the absorbance spectra of RhB core-doped thiol coated silica nanoparticles (Figure 4.11) mixed with gold nanoparticles on the first day.

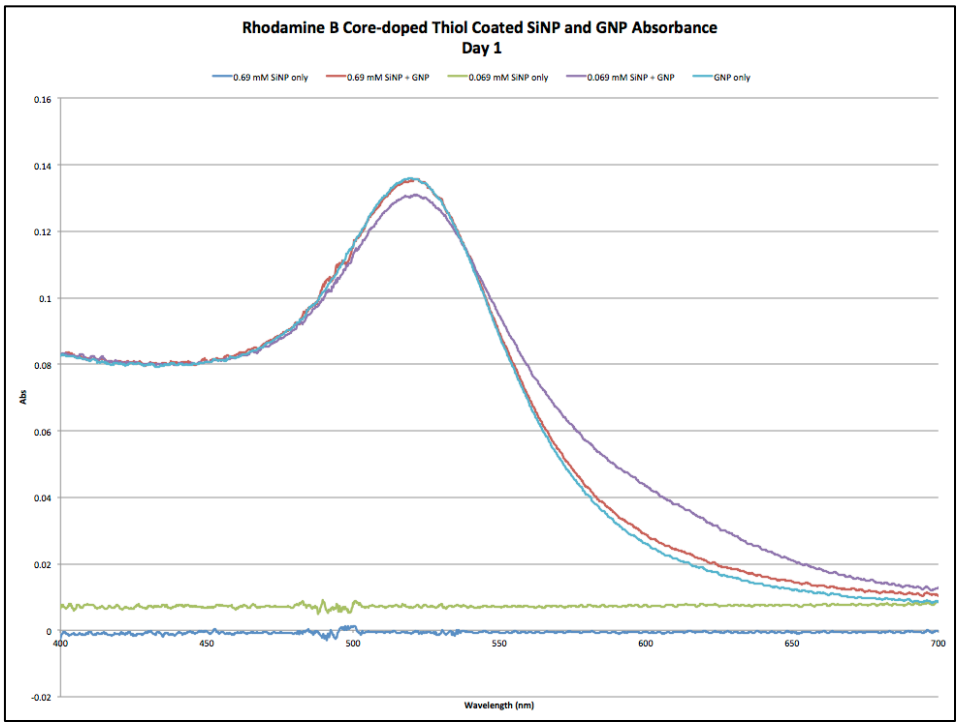

Figure 4.12. Rhodamine B core-doped thiol coated SiNP and GNP absorbance spectra at day 1.

These absorbance traces contain such small amounts of silica that the spectra are dominated by the gold absorbance curves. Thus, the 'SiNP only' samples are featureless in this spectrum due to masking by the overwhelming higher concentration of GNP, but will be taken into consideration with the emission spectra *vida infra*.

The larger amount of silica nanoparticles from sample '0.069 mM SiNP + GNP' (purple line Figure 4.12) has a clear effect of increasing the gold aggregation over the other samples. In these spectra of SiNP and GNP mixtures dominated by GNP abosrption, a slight shoulder, recorded at ~600 nm for aggregate GNP, can be seen in the '0.69 mM SiNP + GNP' (red line) over the control of 'GNP only' but not to the extent of the lower concentration sample. Not surprisingly, the increased concentration of SiNPs mixed

with GNPs continued to show a much more rapid aggregation, which was displayed by a decrease in the GNP absorbance signal at day 2 (Figure 4.13).

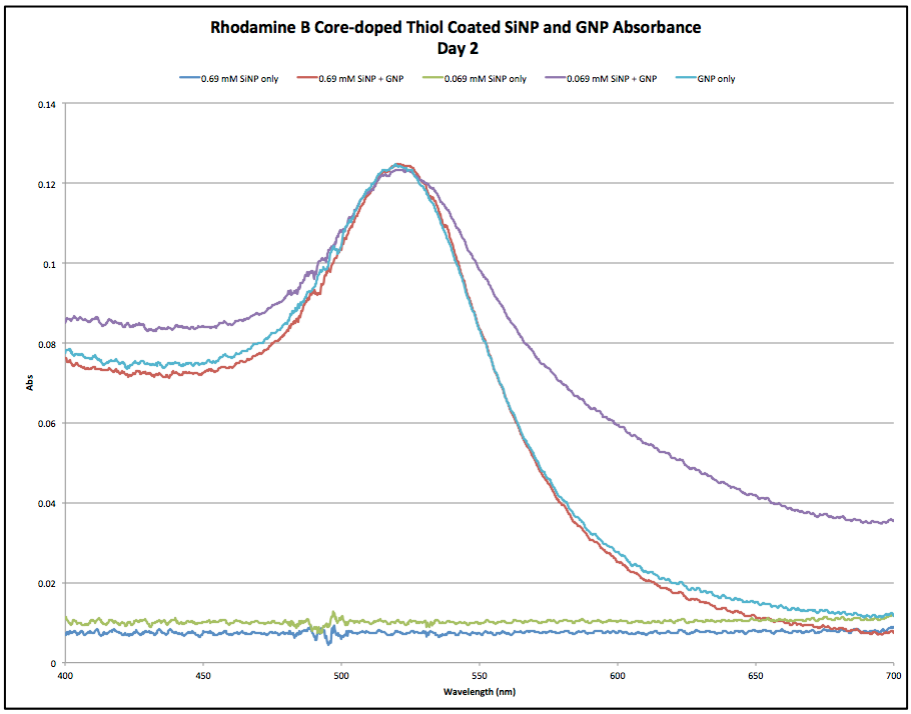

Figure 4.65. Rhodamine B core-doped thiol coated SiNP and GNP absorbance spectra at day 2.

The sample containing ten times the amount of less concentrated RhB-doped SiNP displayed a significant red-shifted shoulder after 2 days, while the other samples did not show any spectral shifts. These results indicate that the '0.069 mM' sample showed significant aggregation while the other did not. While comparing relative absorbance intensities within a given experiment is likely meaningful, comparison across multiple days should be done with caution as the incident bulb and detector conditions can produce different relative absorbance intensities. This large increase in GNP aggregation led to the eventual total loss of signal after day 5, as consistent with the previously observed higher rate of aggregation. (Figure 4.14).

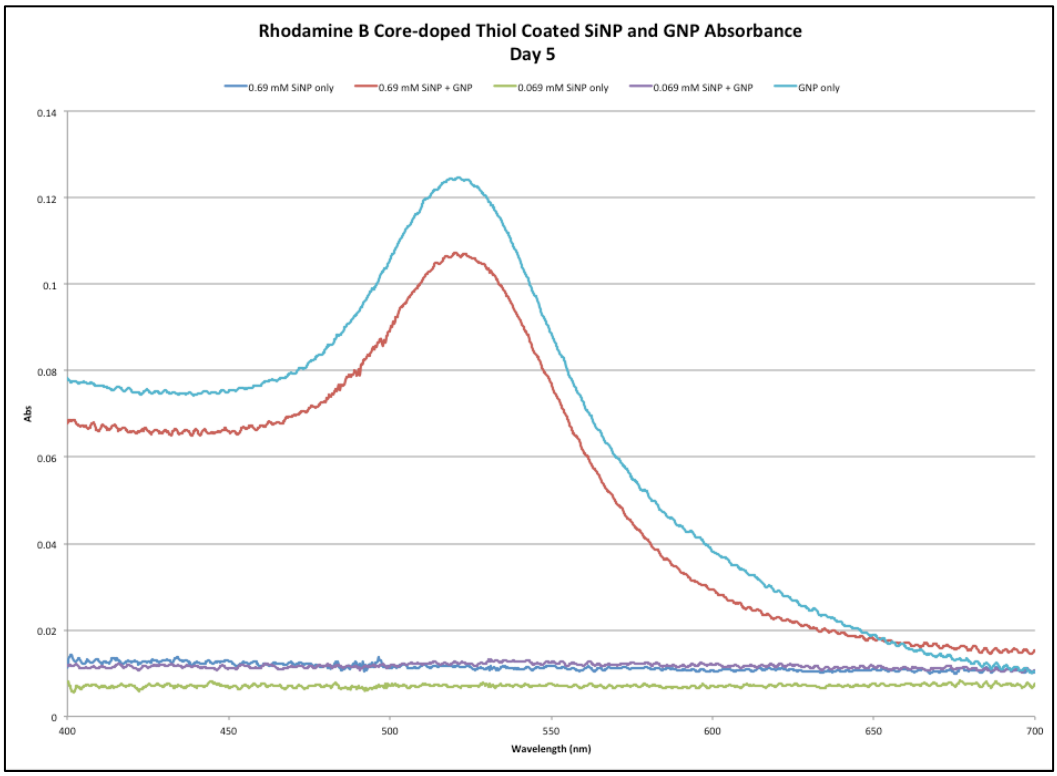

Figure 4.14. Rhodamine B core-doped thiol coated SiNP and GNP absorbance spectra at day 5.

The GNP control and '0.69 mM SiNP + GNP' sample (red line) were the only prominent absorbance features present after five days. Interestingly, the GNP control, which has no SiNP present, showed more signs of aggregation after 5 days than the sample containing silica, which suggests that dilution of the GNPs alone may cause aggregation.

Absorbance spectra, monitored over the course of five days, indicate that more GNP aggregation occurred in the sample containing a larger concentration of lesser-doped SiNP based on the large shift and eventual loss of GNP signal in this sample.

The fluorescence spectra showed an overall decrease for in fluorescent brightness when dye-doped silica nanoparticles were mixed with gold nanoparticles. This indicates that the gold is quenching fluorescence through either far-field (absorbing light emitted from the dye) or near-field (quenching of the excited state through oscillation dampening). Figure 4.15 shows the emission spectra, excited at the λ_{max} of 545 as indicated by the absorbance spectra of controls (not shown), of these samples after the first day. Interestingly, the higher concentration of lesser-doped SiNP '0.69 mM' samples showed a slight red-shift λ_{max} at ~574 nm from ~567 nm of the '0.069 mM' samples.

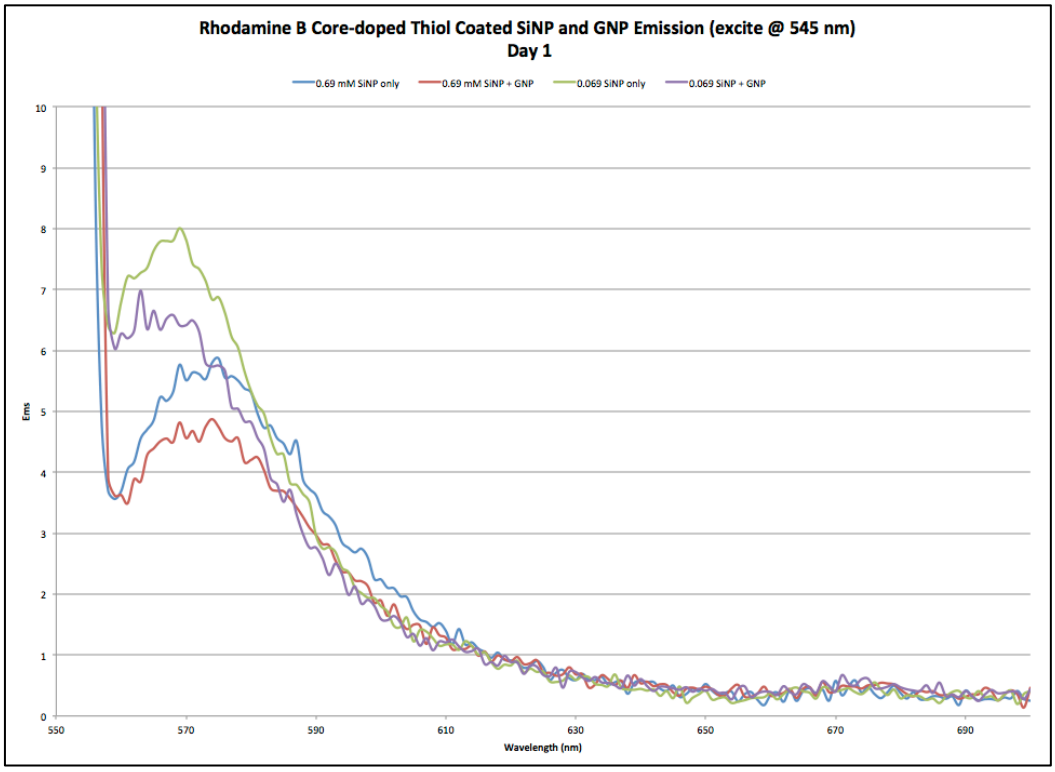

Figure 4.15. Rhodamine B core-doped thiol coated SiNP and GNP emisison spectra at day 1 (excited at 545 nm, slit width = 5 nm).

Both the concentrations of core-doped SiNP mixed with GNP showed lower emission than the control samples of SiNP only. The lowered emission intensities indicate that quenching, far-field or near-field, is taking place within these samples. The relative red-shift of the '0.69 mM' SiNPs indicate that the more concentrated SiNPs formed fluorophore dimers, which is known to cause red-shifts in concentrated samples.[17] The relative concentrations of dye within the silica nanoparticles did not appear to effect the interaction with gold, as both the '0.69 mM' and '0.069 mM' sample showed a decrease in fluorescent brightness from GNP absorption (near or far-field). Furthermore, the increase concentration of dye within the '0.69 mM' sample was displayed a relative red-shift in the emission spectra (Figure 4.15).

The emission spectra of rhodmaine B core-doped thiol coated SiNP and GNP showed a significant drop, ~1.5 arb. units, in the higher concentrated '0.069 mM' samples after five days, while the other samples showed little change (~0.5 arb. units) (Figure 4.16). This indicates that the continued aggregation of the '0.069 mM' sample, seen in the previous absorbance spectrum Figure 4.14, continued to lower the fluorescent brightness most likely through removal of sample via sedimentation of large aggregates.

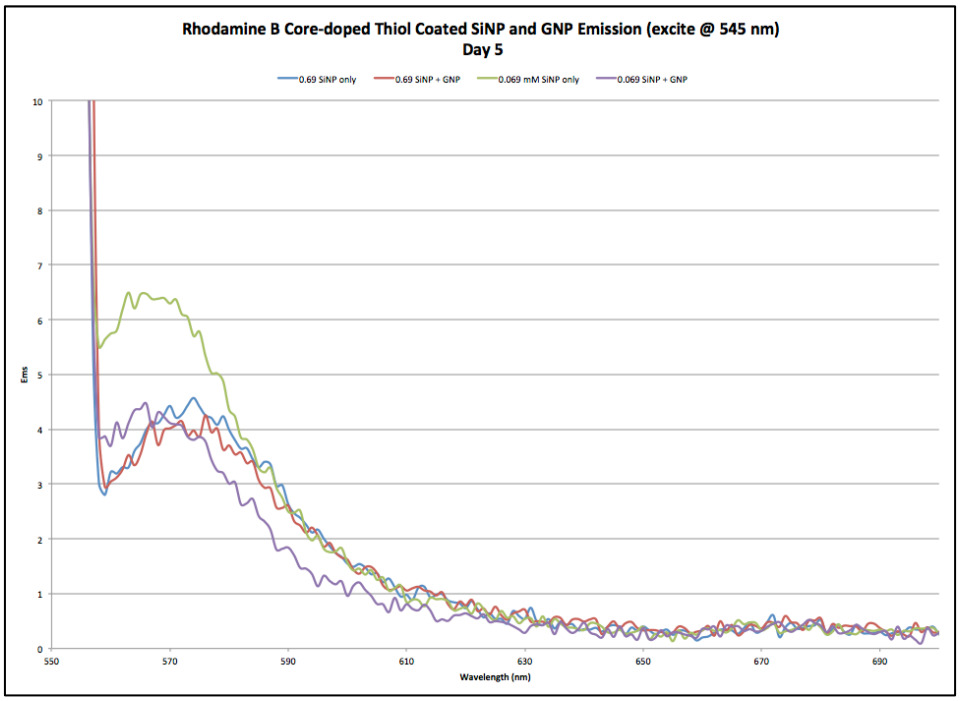

Figure 4.16. Rhodamine B core-doped thiol coated SiNP and GNP emission spectra at day 5 (excited at 545 nm, slit width = 5 nm).

The relatively low drop in emission intensity of the (0.069 mM SiNP + GNP) sample after five days indicates that a significant amount of gold-gold aggregation is occurring, as the formation of these aggregates would not effect the emission intensity of SiNP, when compared to the complete loss of GNP absorbance signal in the same time (Figure 4.14). The other spectra do not show any significant increases or decreases during the course of five days, which suggests that no significant aggregation has occurred to decrease the amount of emitting species in solution. Excitation spectra were also taken for this study that showed a similar drop in signal for only sample '0.069 mM SiNP + GNP'. Inferring GNP aggregation from absorbance spectra and dye-doped SiNP changes from emission spectra is merely speculative of the physical interaction of the two nanoparticle species. Thus, TEM imaging was done performed after five days to

establish the physical binding that gave rise the spectra shown above. Figure 4.17 shows TEM images of the less concentrated greater-doped SiNP (0.69 mM SiNP + GNP). These images of '0.69 mM SiNP + GNP' after 5 days show very little silica is present with a high amount of free GNP.

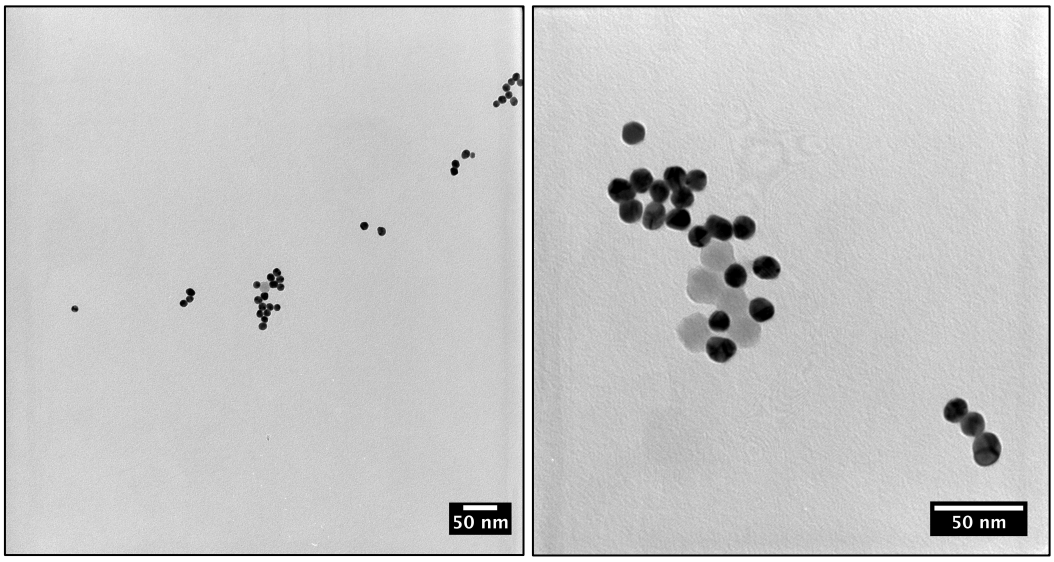

Figure 4.17. TEM images (63 kX and 200 kX magnification) of sample '0.69 mM SiNP + GNP' after 5 days. Darker spots are GNP and lighter grey are SiNP.

While some SiNP-GNP interaction is shown, there is no significant heteroaggregation when compared to sample '0.069 mM SiNP + GNP' after 5 days (Figure 4.18). TEMs of '0.069 mM SiNP + GNP' show a significantly higher concentration of SiNP and with it a greater concentration of SiNP-GNP aggregation.

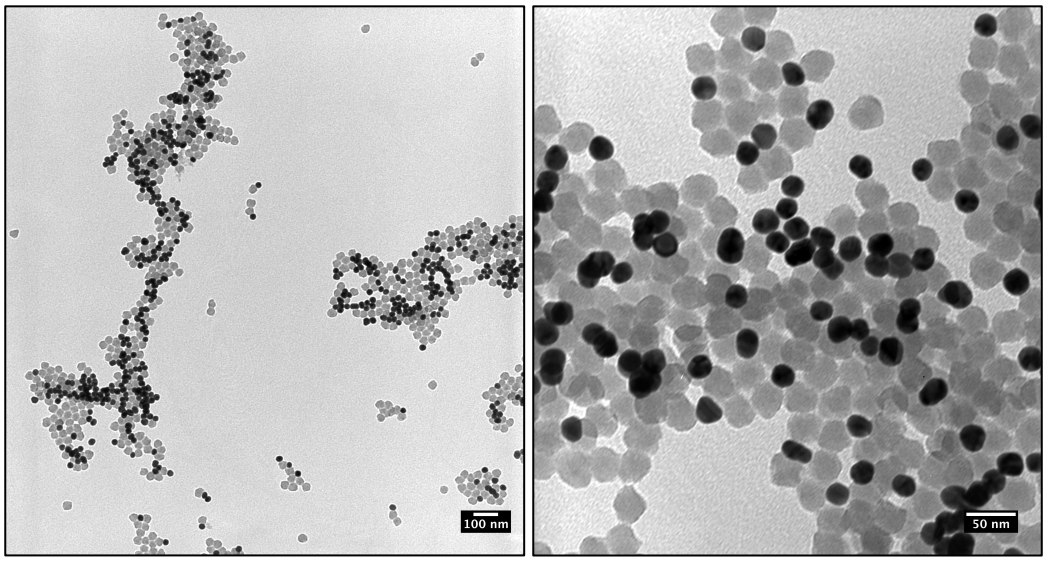

Figure 4.18. TEM images (50 kX and 200 kX magnification) of sample '0.069 mM SiNP + GNP' after 5 days. Darker spots are GNP and lighter grey are SiNP.

These images support that higher concentrations of silica produce larger amounts of aggregation when mixed with GNP. Here, no free GNP is visible, which accounts for the loss of absorbance intensity seen in Figure 4.14, that would result from no free gold nanoparticles available to absorb light in solution. However, these images do not confirm the hypothesis of fluorescence loss due to sedimentation of dye-doped silica nanoparticles, as it is difficult to quantitatively evaluate TEM images due to the increased magnification of random sample areas between highly concentrated samples (Figure 4.18) and those with very low concentrations (Figure 4.17).

Varying the concentration of the rhodamine B within core-doped thiol functionalized SiNP requires adding increased amounts of less-concentrated silica to GNP mixtures in order to maintain a viable fluorescent signal. Unfortunately, this dye concentration variation experiment does not allow for the direct comparison of

aggregates, as the silica concentration is clearly a factor in controlling aggregation. However, the more-concentrated '0.69 mM' core-doped SiNP are slightly red-shifted to SiNPs with a higher concentration. It remains to be seen if this shift plays a significant role in the enhancement of fluorescence by GNP aggregation, as would be expected if larger emission changes were seen with more concentrated dye samples.

4.3.3 Investigation of relative concentration effect between layered dye-doped silica nanoparticles and gold nanospheres

We investigated vary the relative concentration of core-doped silica nanoparticles and gold nanoparticles in order to identify the influence over aggregation. Whitney Costello performed aggregate formation, characterization, and data formatting during her undergraduate research thesis work with Drs. Lloyd Bumm and Ronald Halterman in the Halterman lab. Larger core-doped silica nanoparticles were prepared according to previous results that suggested a larger spacer might be necessary to produce MEF.[18]

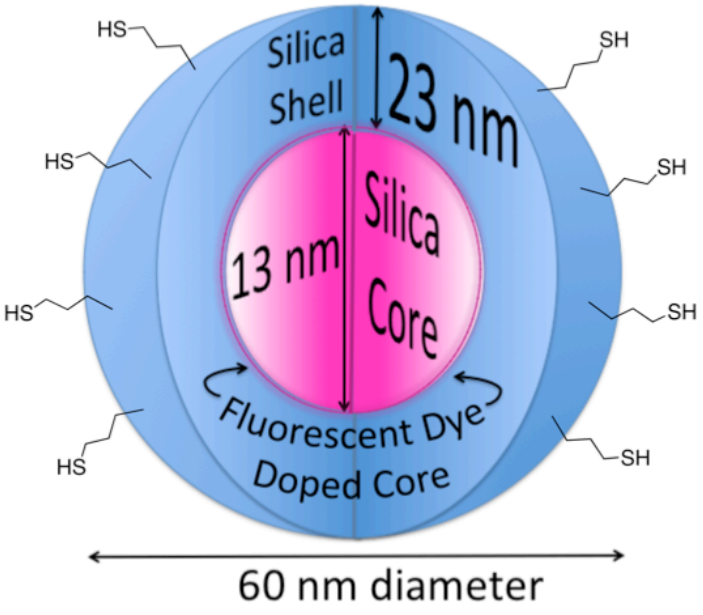

Figure 4.19. Cartoon schematic of 60 nm diameter rhodamine B core-doped silica nanoparticles coated with thiol ligands. (Image from this work).

Figure 4.19 above shows the core-doped silica nanoparticles, surface functionalized with thiol groups, used in the following experiment. The particles are identical to those described in section **4.3.2**, by biphasic hydrolysis of TEOS catalyzed by arginine in the aqueous phase, except they have are larger outer silica coating. The particles were similarly characterized by TEM imaging *vida infra*. Here, we mixed increasing amounts of large diameter, thiol coated, RhB-core doped SiNPs with citrate capped in aqueous solutions. Figure 4.20 shows the absorption data upon initial mixing.

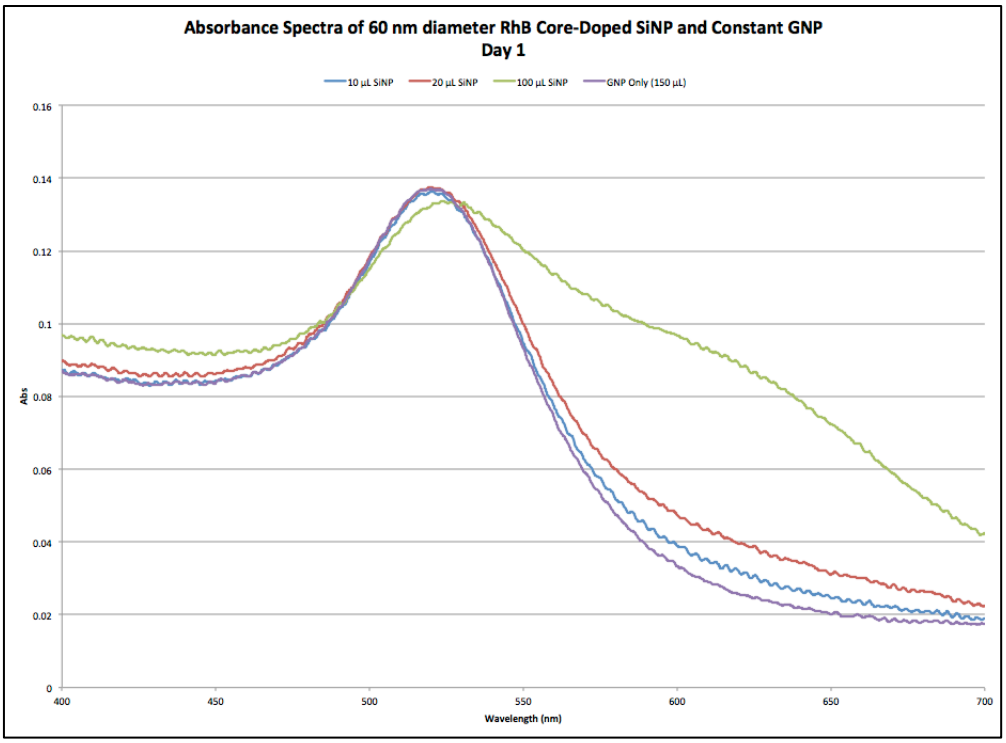

Figure 4.20. Absorbance spectra of 60 nm diameter RhB core-doped SiNP and constant GNP (150 µL) on day 1.

These data support the hypothesis that functionalized silica nanoparticles play a role in the aggregation of GNP in solution based on the large shoulder present around 600 nm, which indicates GNP aggregation. The emission spectra were then analyzed for potential increases or decreases in fluorescent brightness signal (Figure 4.21).

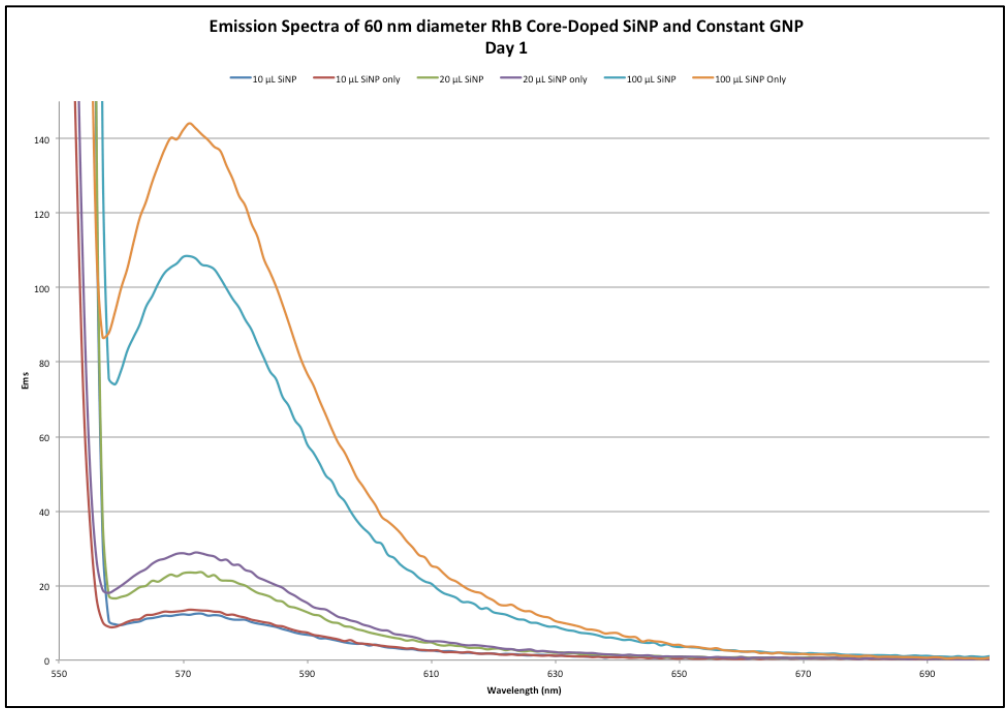

Figure 4.21. Emission spectra of 60 nm diameter RhB core-doped SiNP and constant GNP (150 µL) Day 1 (excited at 545 nm, slit width = 5 nm).

There is a significant drop in emission from samples without gold present to those with gold after the first day. This initial drop is reasonably expected as the gold nanoparticles absorb strongly in the excitation region leading to a decrease in the excitation of light emitted. This can be roughly calculated by determining the percent transmittance, and thus the percent light filtered by equation 7.

$$\%T = 10^{-A} \times 100 \qquad (7)$$

The λ_{max} is 571 nanometers for the samples '100 μL SiNP' and '100 μL SiNP only' meaning that this value should be investigated for absorbance by excess gold in the corresponding absorption spectrum 4.20. The corresponding absorbance intensity at this wavelength was 0.136 on day one. Thus the transmittance of the sample is given by:

$$\%T = 10^{-0.136} \times 100 = 73.1\%$$

Therefore, the amount of light filtered by the sample is 26.9%. Thus, we should expect to see at least a 26.9% drop in fluorescent brightness from this sample. The difference in emission intensity of the samples '100 μL SiNP' and '100 μL SiNP only' is 36 (from an original signal intensity of 144) representing a 25% drop in fluorescent brightness. This analysis neglects the entire inner-filtration effect method[8] but provides a reasonable picture of filtered light. A similar analysis can be performed to account for the overall drop in intensity seen in the excitation spectra (Figure 4.22).

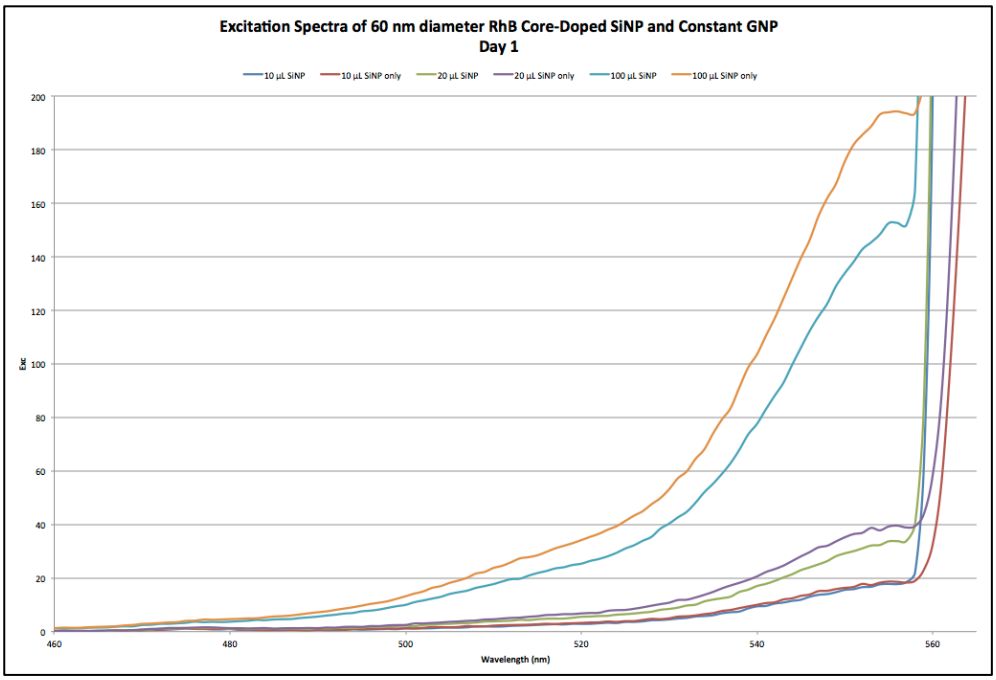

Figure 4.22. Excitation spectra of 60 nm diameter RhB core-doped SiNP and constant GNP (150 µL) Day 1 (monitor emission at 570 nm, slit width = 5 nm).

There is a clear connection between the amount of SiNP added to GNP and the overall decrease experience within the sample. It is interesting to note that almost no change is see in both the emission (Figure 4.21) and the excitation (Figure EXC 4.22) after day one for the '10 µL SiNP' samples. The absorbance spectra (Figure 4.20) indicate a similar 25% drop should be expected but the emission signal only decreased by 5% for these samples. It is not immediately clear what causes this phenomenon but it is commonly observed over many preparations. The photo filtration effects, the absorbance of both incident and emitted light by excess gold in solution (described above), are then augmented as the samples are monitored over several days (Figure 4.23).

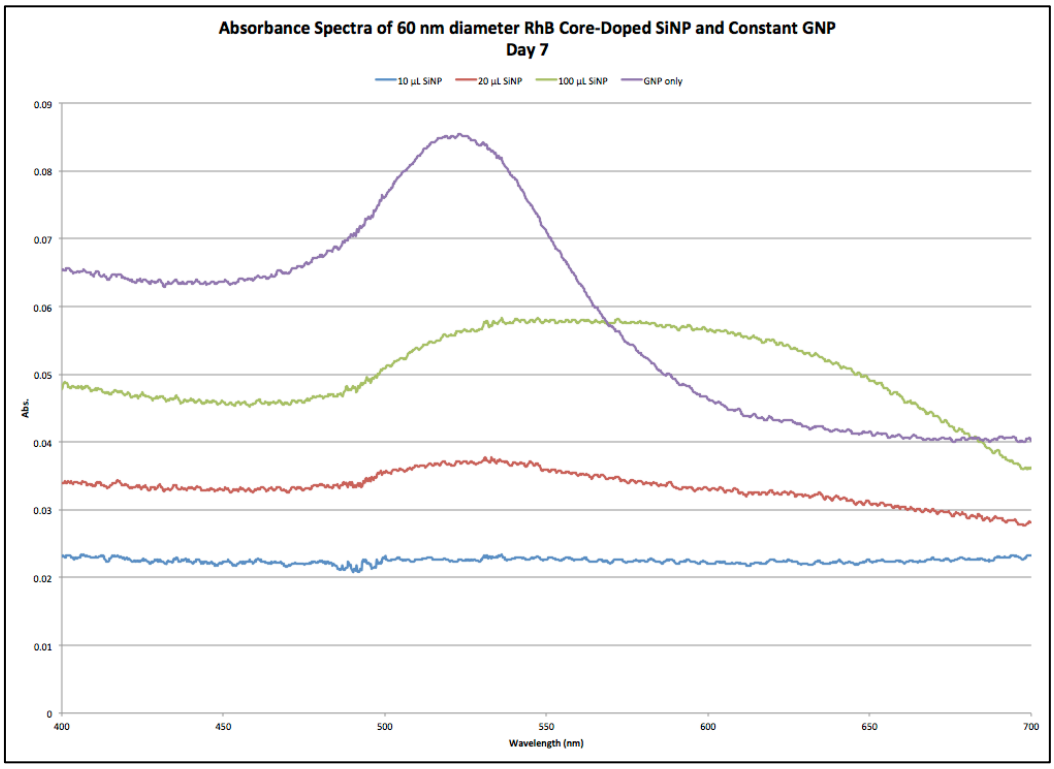

Figure 4.23. Absorbance spectra of 60 nm diameter RhB core-doped SiNP and constant GNP (150 µL) Day 7.

The absorption spectra showed a significant amount of gold aggregation activity after day 7, especially in the sample '100 µL SiNP' as indicated by the very large feature that has developed between 500-700 nanometers, indicating a significant amount of GNP aggregation. It is noteworthy that the sample bearing the lowest concentration of SiNP (10 µL) showed no gold absorption after 7 days, although this is likely to contamination and was not frequently observed in other samples. The emission spectra for these samples after 7 days is shown in Figure 4.24. Changes in the emission spectra are not explained by photo filtration analysis after day 7 for samples '20 µL' and '10 µL'. The sample containing 100 µL of SiNP continued to show a predicted decrease

(12.5%), while the ’20 µL’ sample did not decrease at all (predicted 5% loss) and the ’10 µL’ sample decreased more (predicted 13% loss, actual 38%).

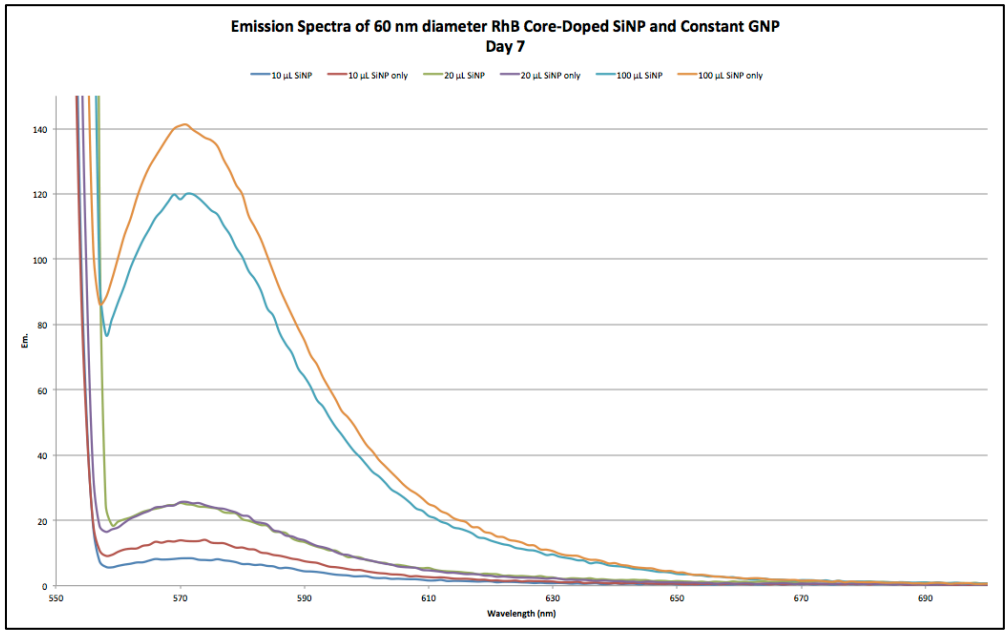

Figure 4.24. Emission spectra of 60 nm diameter RhB core-doped SiNP and constant GNP (150 µL) Day 7 (excited at 545 nm, slit width = 5 nm).

Thus, the absorbance spectra (Figure 4.23) do not account for the relative changes in the emission spectra (Figure 4.24). The excitation spectra are helpful, in that we see changes in absorption of light from the perspective of emission which means we can monitor changes specifically in the fluorophore even in the presence of excess gold, for investigating the source of these fluctuations in emission from the view of the fluorophores (Figure 4.24).

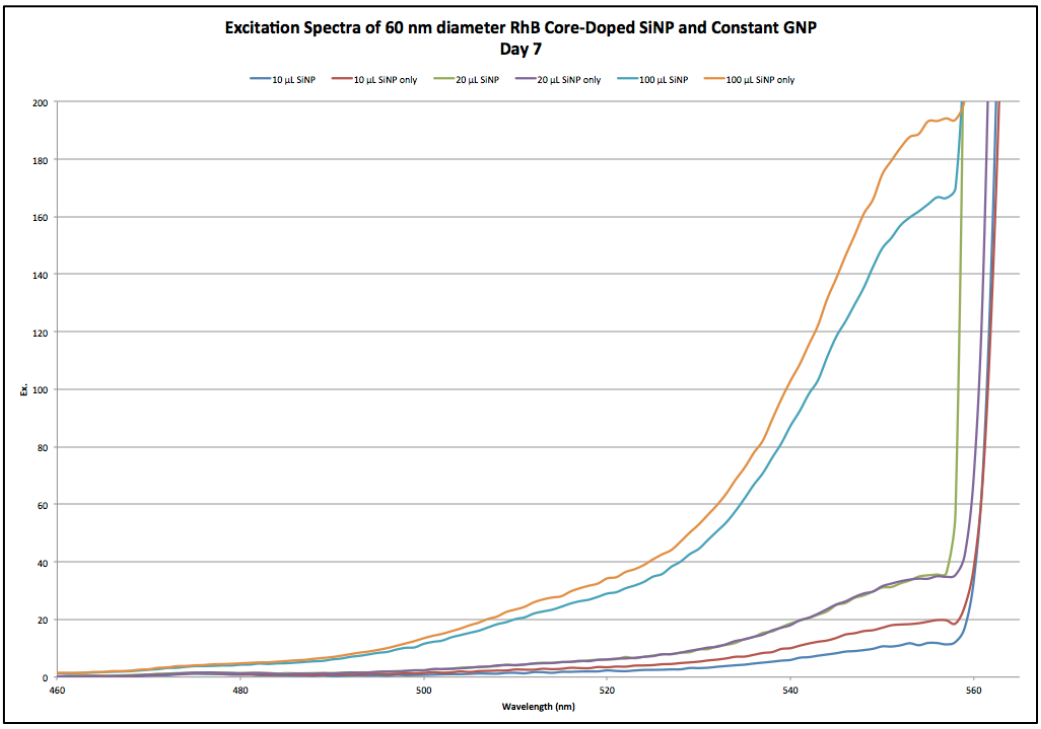

Figure 4.25. Excitation spectra of 60 nm diameter RhB core-doped SiNP and constant GNP (150 µL) Day 1 (monitor emission at 570 nm, slit width = 5 nm).

The excitation spectra indicate a proportional relationship between the excitation and emission of fluorophores in this system. Decreases seen in the '100 µL sample' emission (Figure 4.24) (12.5%) match a decrease in excitation (Figure 4.25) (13.9%). Furthermore, no significant shift in the excitation λ_{max} = 555 nm was observed between day 1 (Figure EXC 4.22) and day 7 (Figure EXC 4.25). Thus, there is no immediate photophysical explanation for the observed spectral shifts. TEM imaging is then useful for investigating the role of aggregation in possibly removing material from free in solution by precipitating in large clusters. A large zoom out TEM image for the '10 µL SiNP' sample from day 7 (Figures ABS, EMS, EXC DAY 7) is shown below. Figure 4.26 shows the presence of large aggregates of silica nanoparticles with no un-aggregated gold present.

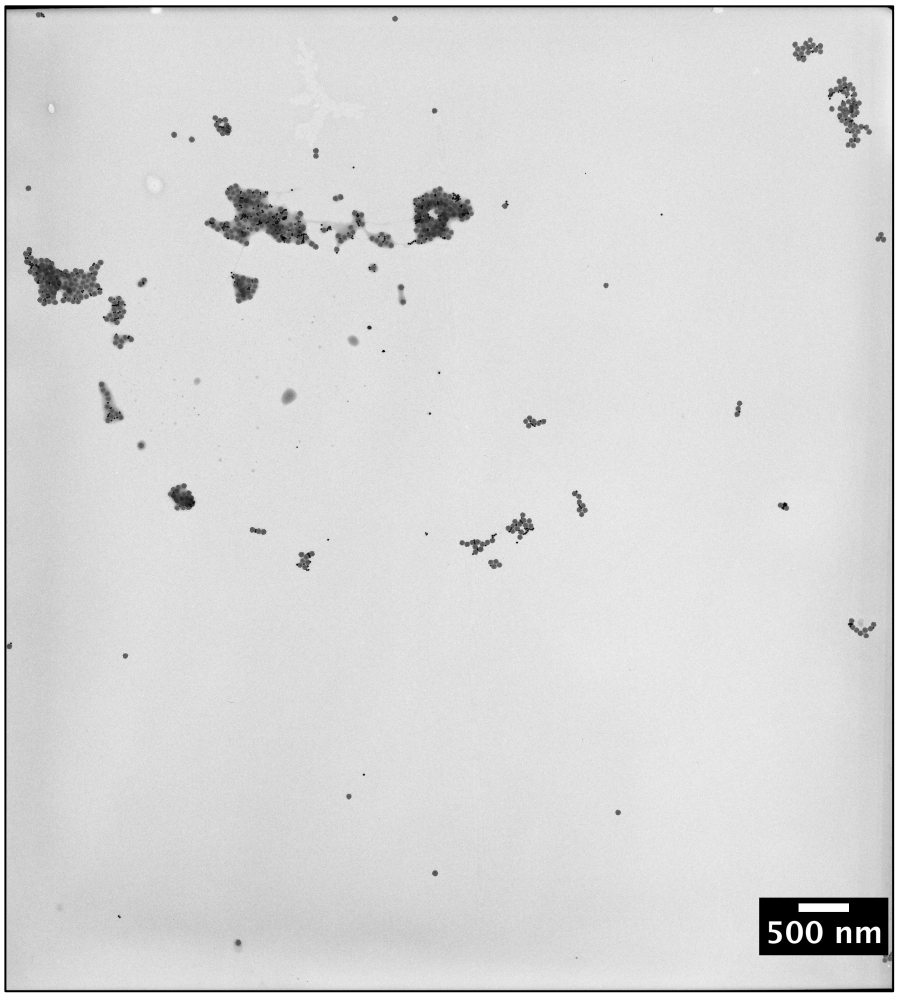

Figure 4.26. Low magnification TEM image of the ’10 µL SiNP’ sample from Figures 4.23-4.25 after 7 days.

Magnified TEM images display a clearer picture of the interaction of gold and silica nanoparticles (Figure 4.27). The magnified TEM image shown in Figure X shows well-formed SiNP (60 nm average diameter) with closely associated gold nanoparticles. No free gold was observed in this sample, which supports the overall loss of absorbance signal due to the formation of large aggregates.

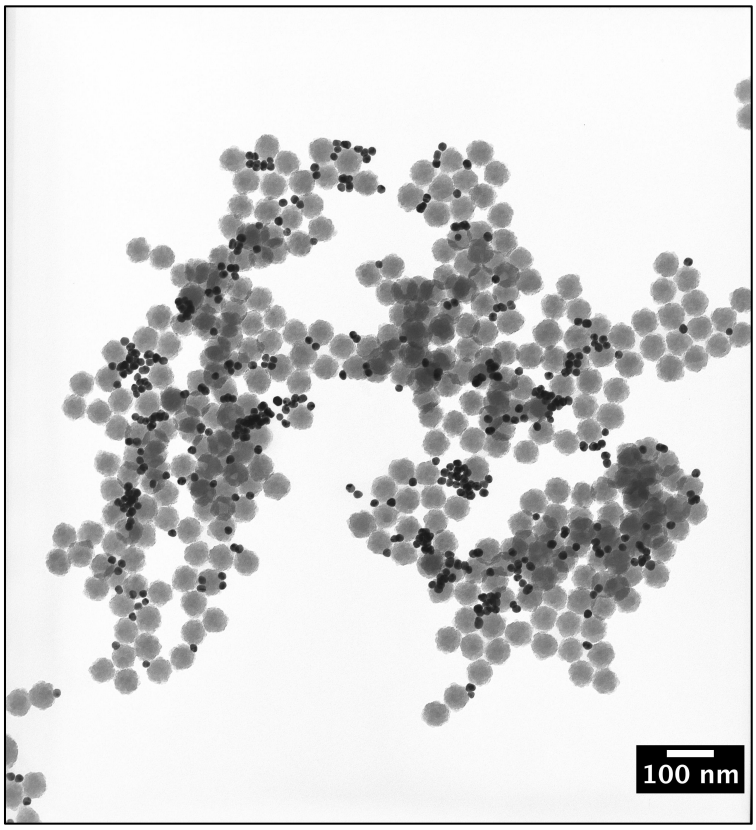

Figure 4.27. Magnified TEM image of the ’10 μL SiNP’ sample from Figures X,Y,Z after 7 days.

These images closely resemble those obtained for the samples with a much higher relative concentration of silica nanoparticles (Figure 4.28). Significantly fewer large aggregates were seen in the sample with ‘100 μL SiNP’ (Figure 4.28) than the sample with ’10 μL SiNP’ (Figure 4.27).

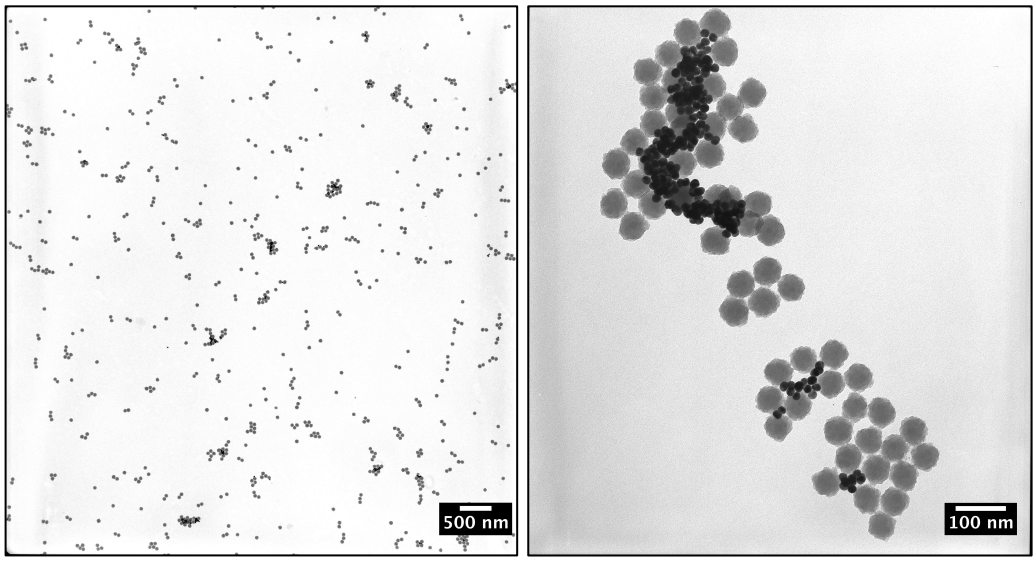

Figure 4.28. Lower magnification (left) and higher magnification (right) TEM images for the '100 μL SiNP' sample after 7 days (from Figures X,Y,Z).

The higher magnification image shows gold aggregation with no free GNP visible. Figure 4.28 supports the increase of gold aggregation while not removing any particles from solution in large aggregates. However, it is clear between Figures 4.26-28 that these preparations still suffer from inconsistent aggregation motifs.

Increasing the concentration of thiol coated dye-doped silica nanoparticles relative to gold nanoparticles in solution increases the rate of SiNP-GNP aggregation. This experiment, and others, was found to be routinely inconsistent for with samples at very low concentrations of silica or gold. No emission brightness enhancements were observed upon aggregation of the dye-doped silica and gold nanoparticles. Relative decreases between samples that contained SiNP and GNP and those that contained only SiNP suggest that large aggregate formation is removing particles from solution or the distance between the dye and gold nanoparticle surface is too small. Inconsistencies

between large aggregate formation and fluorescence decreases led us to believe the distance dependence played a larger role. For this reason we investigated aggregating larger dye-doped silica nanoparticles with gold nanoparticles.

4.3.4 Investigation of distance dependence between dye-doped silica and gold nanoparticles on emission intensity

We investigated larger diameter (150 nm) rhodamine-B core-doped silica nanoparticles as a means of increasing the distance between the dyes and the surface of the metal in order to achieve metal-enhanced fluorescence. The larger silica nanoparticles were prepared by growing an additional silica layer around previously prepared core-doped particles before functionalizing the surface with amines (Figure 4.29).

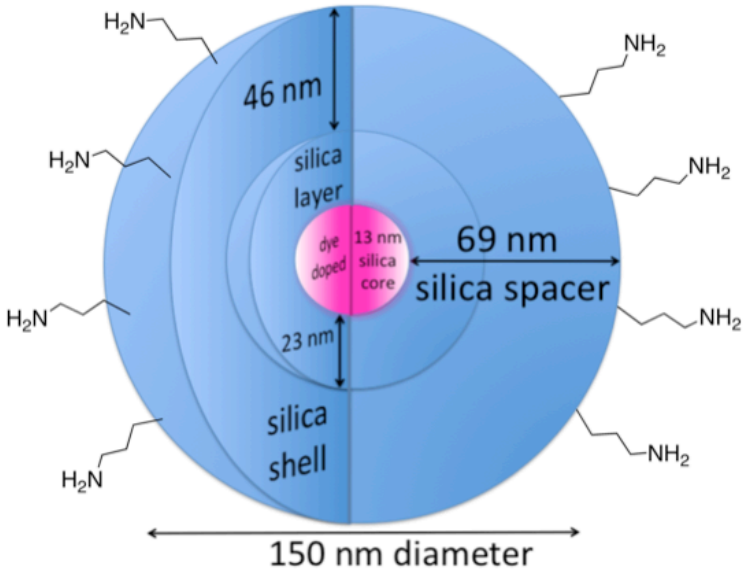

Figure 4.29. Cartoon schematic of large diameter rhodamine B core-doped layered silica nanoparticles surface functionalized with amines.

Growing an additional 46 nanometer thick shell onto the surface of the previously prepared 60 nanometer diameter core-doped silica nanoparticles (Figure 4.19) created a 69 nanometer silica barrier between the dye and the surface of the silica and resulted in an average diameter of 150 nanometers (Figure 4.29), as characterized by TEM imaging.

The amine functionalized large diameter silica nanoparticles were then mixed with citrate capped gold nanoparticles to investigate the effect of increasing the silica shell on the degree of aggregation and changes in the emission brightness of rhodamine B. Figure 4.30 shows the absorbance spectra of one sample followed over the course of several days.

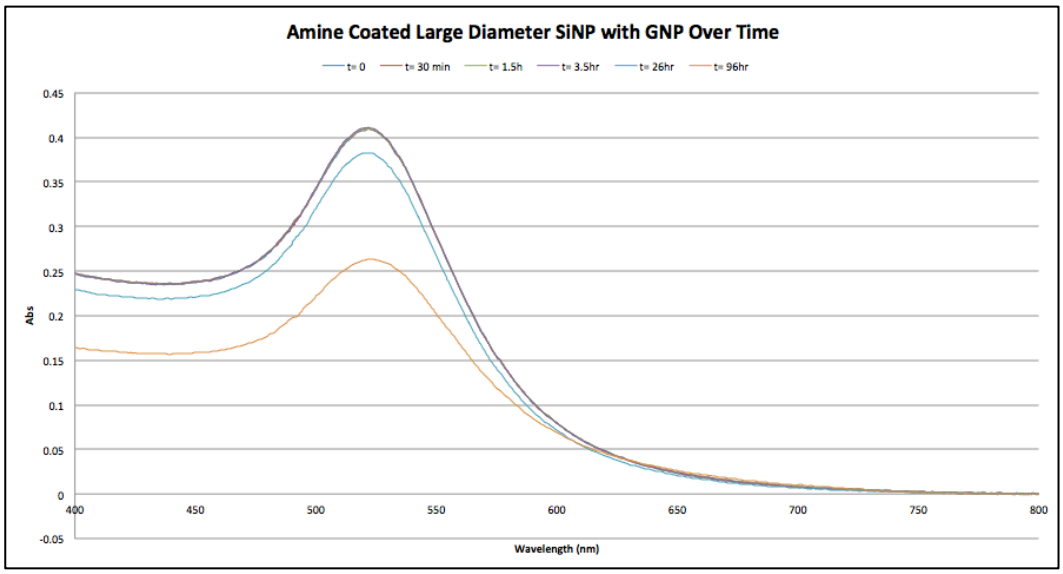

Figure 4.30. Absorbance spectra of large diameter silica nanoparticles mixed with citrate capped gold nanoparticles over the course of several days.

The significant drop in gold plasmon absorption, λ_{max} = 525 nm, is indicative of gold aggregation but the lack of a development of a shoulder, expected to appear > 600 nm,

suggests that primarily gold-gold sedimentation is occurring. Note that, once again, the absorbance spectra are dominated by GNP absorbance due to very low concentrations of rhodamine B-doped SiNPs present in solution. These samples showed decreases in emission intensity (not shown) similar to previous experiments. However, TEM imaging revealed the formation of aggregates consisting of a few silica nanoparticles that were well-covered with gold nanoparticles. The absorbance and emission spectra do not account for the small concentration of desired heteroaggregates formed in this sample (Figure 4.31).

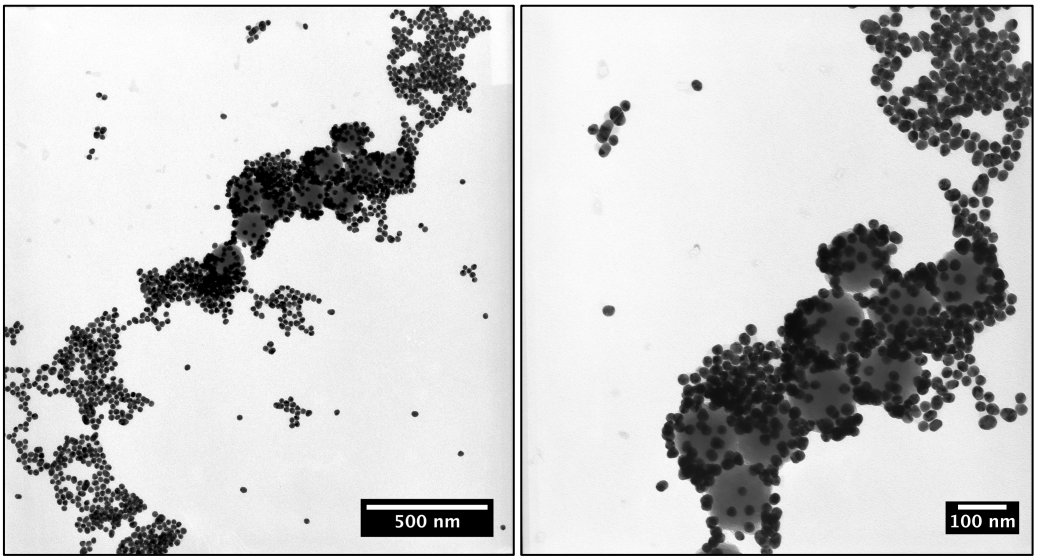

Figure 4.31. TEM images of large diameter amine coated silica nanoparticles aggregated with citrate capped gold nanoparticles in aqueous solutions.

The TEM images above indicated that useful silica-gold aggregation is occurring and that there is a large excess of free gold present in solution. A large excess of gold is expected, as samples were prepared with great GNP excess to promote SiNP-GNP aggregation. We then attempted to separate the aggregates from excess gold by

carefully centrifuging out the larger silica-gold complexes while leaving free gold in solution (Figure 4.32).

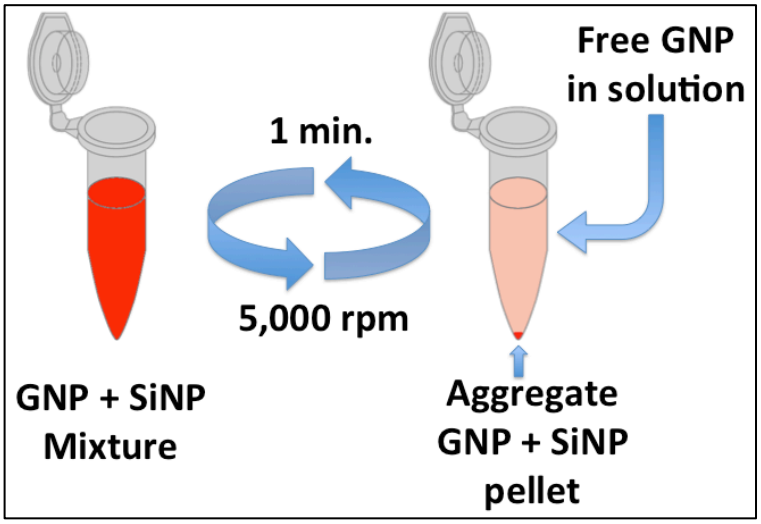

Figure 4.32. Cartoon schematic of centrifuging only larger SiNP-GNP aggregates into a pellet, while leaving free gold in solution. (centrifuge tube clipart from antidopingresearch.com)

SiNP-GNP aggregates sediment more rapidly over the lighter SiNP or GNP isolated species and can thus be crudely separated under mild centrifuge conditions. Rotating at 5,000 rpms for one minute afforded coarse separation between aggregated SiNP-GNP from free GNP in solution. This separation technique does not completely isolate aggregates from free particles in after one centrifuge cycle, thus the process was repeated several times while monitoring the contents of both the supernatant and sediment by UV/vis absorption and emission spectroscopy as well as TEM imaging. The absorption spectra for supernatant and sediment aliquots of the SiNP-GNP aggregate mixture are shown below.

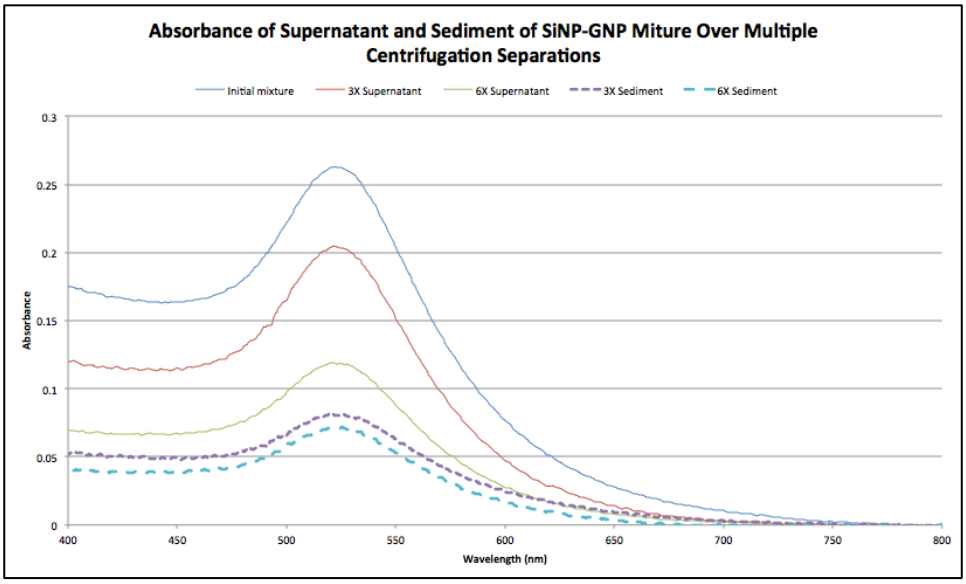

Figure 4.33. Absorbance spectra of supernatant and sediment samples after multiple centrifugation separation cycles (solid lines indicate supernatant, dotted lines are sediment).

Figure 4.33 shows a gradual decrease in the gold plasmon absorption band in the supernatant from 3 to 6 centrifugation cycles for the supernatant. GNP absorption of the sediment sample fell much faster in comparison to the supernatant sample (0.182 compared to 0.062 relative intensity drop). Furthermore, the GNP intensity drop between the 3X and 6X sediment extractions was relatively small (0.01 arb. unit). A decrease in GNP absorption indicates that the amount of gold present after three centrifugation cycles is similar to that in samples after six centrifugation cycles. There is a slight shoulder present in the 3X sediment sample that is not detected in the 6X sample when the absorbance spectra are magnified, indicating GNP aggregates are relatively increasing in concentration compared to free GNP in solution (Figure 4.34).

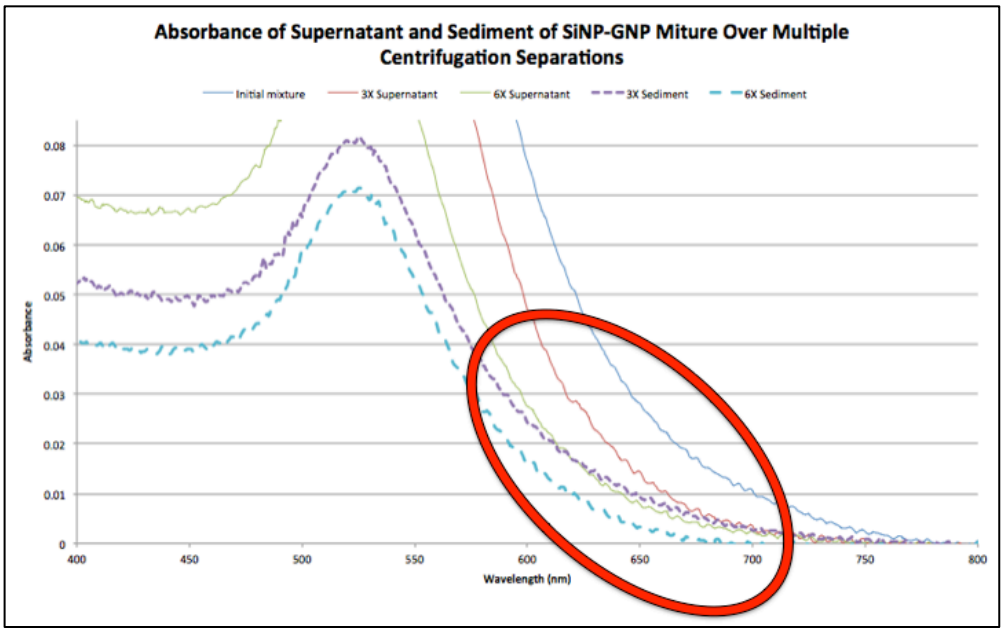

Figure 4.34. Magnified absorbance spectra highlighting the slight development of a shoulder in the '3X sediment' sample (purple line) between 550-700 nm.

Development of shoulder between 550-700 nm indicates that SiNP-GNP aggregation is occurring in solution. It is interesting to note that the shoulder does not appear to be present in the 6X sediment sample. The lack of the gold absorbance shoulder may be due to an increase in free gold that is found in the sediment layer after extra centrifugation separation cycles. The free gold absorption could then re-mask the aggregated gold signal that was most likely already present in the original sample but was too low in concentration to be detected. The gradual decrease seen in the supernatant GNP absorbance measurements supports this claim (Figure 4.33).

The emission spectra for large diameter rhodamine-B doped amine coated SiNP-GNP aggregates were compared to samples containing only SiNPs that were subjected to similar multiple centrifugation cycles (Figure 4.35). The SiNP-GNP sediment sample

after 3 centrifugation/ sonication cycles showed the highest emission brightness of both the aggregate and control samples. The overall increase between the control and aggregate samples should not be directly compared, as more dye-doped SiNP should be expected in the sample aggregated to GNP, as the aggregates are denser than SiNP alone.

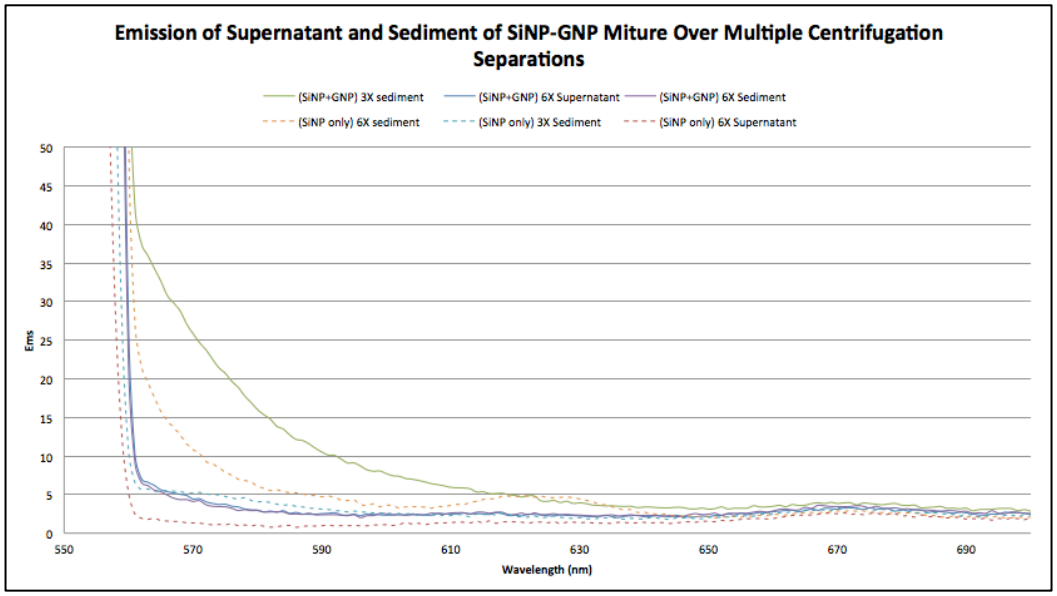

Figure 4.35. Emission spectra of SiNP-GNP aggregate (solid lines) and SiNP only control (dotted lines) samples from supernatant and sediment solutions after multiple centrifugation/ sonication cycles.

The 3X sediment emission band is greater than the 6X sample. A greater emission of the 3X sample is counter to the expectation that the SiNP signal should continue to increase as more SiNP material is collected over more centrifugation cycles (a trend shown in the control sample Figure ABOVE EMS). One possible explanation for the decrease seen from the 3X to 6X sediment samples (solid green line to solid purple line Figure ABOVE) may be due to increased gold in solution causing photo

filtering of both the excitation and emission intensities. However, the decrease in the gold absorption of the 6X sample does not support this claim (Figure 4.33). TEM images were taken to identify the nature of the significantly higher 3X sedimentation sample (Figure 4.36) to determine the relative species, aggregates or free particles, present in solution.

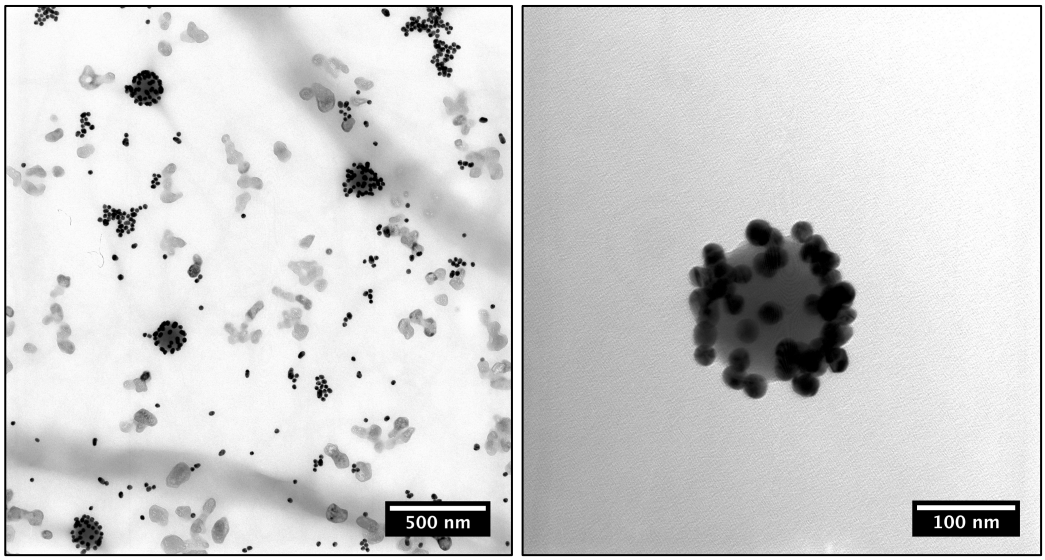

Figure 4.36. TEM images of SiNP-GNP aggregates from '3X sediment' sample in (Figure 4.35).

While there is a significant amount of unknown decomposition in the 3X sediment sample, several desirable aggregates are visible wherein many gold nanospheres are aggregated around a single dye-doped silica nanoparticle. It is clear from these images that the SiNP and GNP are bound to one another instead of a loose association from drying on a TEM grid. The atomic compositional analysis of the SiNP-GNP aggregates was performed by Dr. Preston Larson at the Samuel Roberts Noble Electron

Microscopy Laboratory at the University of Oklahoma to determine the nature of the excess light grey material visible in Figure 4.36 (Figure 4.37).

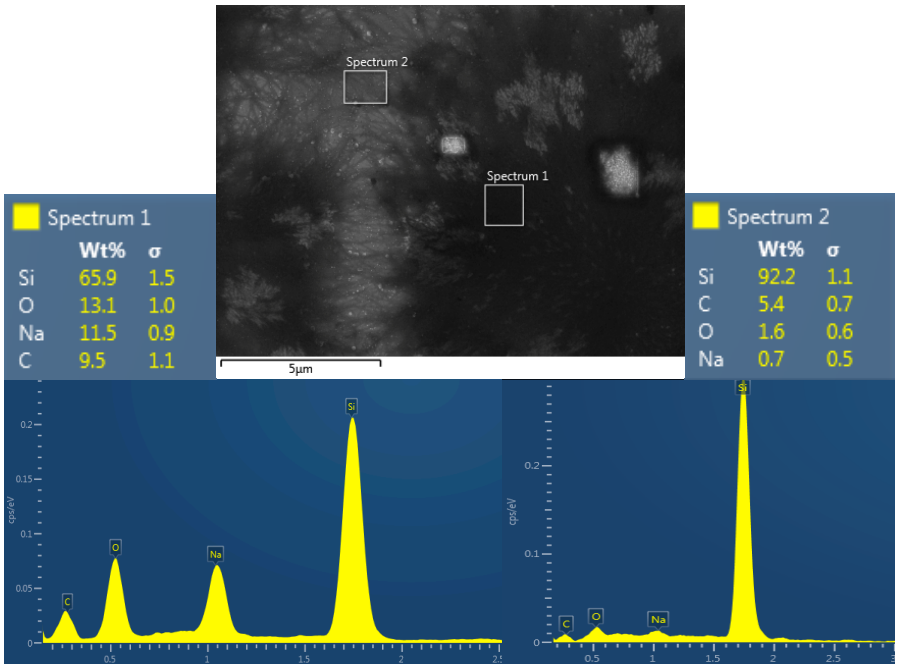

Figure 4.37. Energy Dispersive X-ray Spectroscopy (EDS) spectra of SiNP-GNP aggregate solution on a polished silicon wafer.

Energy Dispersive X-ray Spectroscopy (EDS) shows the unknown material seen in the previous TEM images (Figure 4.36) and highlighted as the dark black material on 'spectrum 1' (Figure 4.37) to be comprised of primarily oxygen, carbon, and sodium (silicon shows in such high amounts because the sample was loaded onto a silicon wafer). The EDS technique identifies the atomic composition of surface material by measuring emitted X-rays from atomic shell transitions via interaction with the initial electron beam. The emitted X-rays have unique energy signatures of the parent element that caused the emission.[19]

The EDS spectrum of 'sample 1' (Figure 4.37) indicates that the unknown material is composed of oxygen (13.1%), sodium (11.5%), and carbon (9.5%), which may possibly be trisodiumcitrate ($Na_3C_6H_5O_7$). Given that hydrogen X-ray emission is not registered by the EDS detector we can assume the molecular weight percent of each atom to be ($Na_3C_6O_7$): oxygen (44%), sodium (26%), carbon (28%). Excluding the background silicon wafer signal gives the following experimental percentages: oxygen (38%), sodium (33%), carbon (27%). Given the lack of uniformity to the sampling error it is reasonable to assume the relatively small inconsistency between the predicted and actual values are within range to identify the unknown substance as citrate.

Scanning electron microscopy (SEM) images were also taken to further analyze the SiNP-GNP aggregate samples (Figure 4.38).

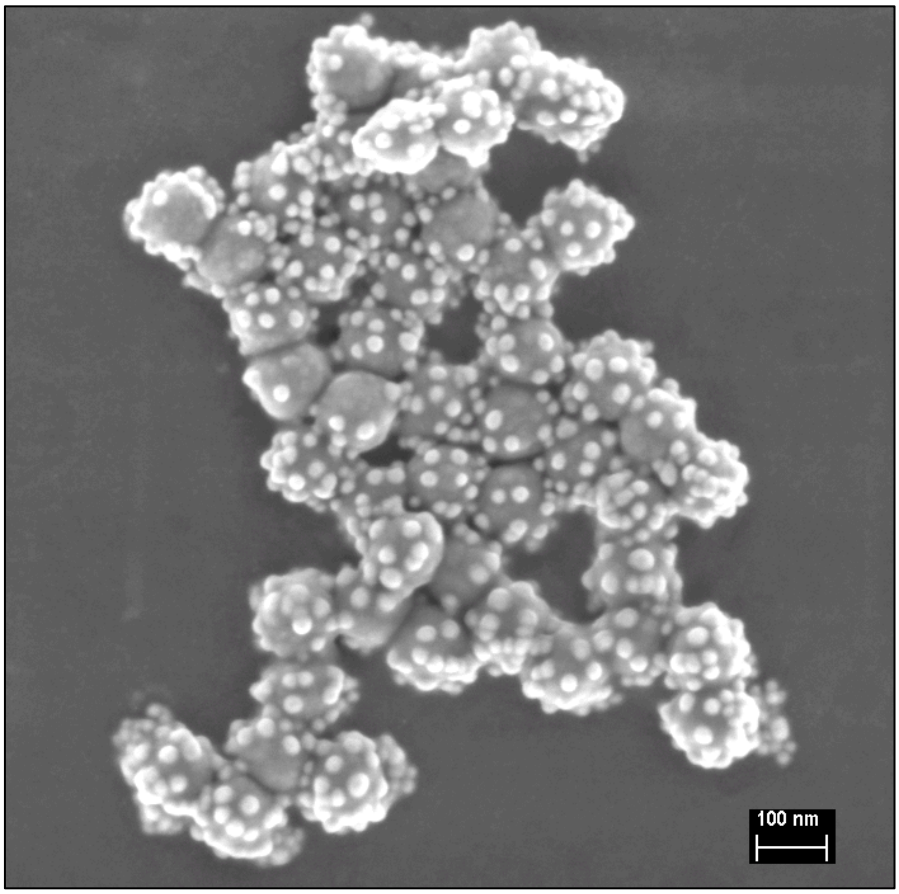

Figure 4.38. HRSEM image of SiNP-GNP aggregate cluster. (Image taken by Dr. Preston Larson).

SEM imaging confirms selective SiNP-GNP binding to produce a significant amount of desired aggregation. It is important to note that these samples are very dilute and thus these clusters were spread very far apart. However, all of the identifiable silica was bound to gold nanospheres and the amount of GNP-GNP homoaggregation was minimal. Energy selective backscattering, a technique dependent on scattering material's composition, was then imaged to confirm that Figure 4.38 consisted of two different species (Figure 4.39). The ESB images clearly show two different species aggregated together. Materials that efficiently scatter electrons, such as gold, are

displayed by brighter signals as higher amounts of energy are reflected from these surfaces. Materials that do not scatter electrons as efficiently, such as silica, appear darker as less energy is reflected from these surfaces.

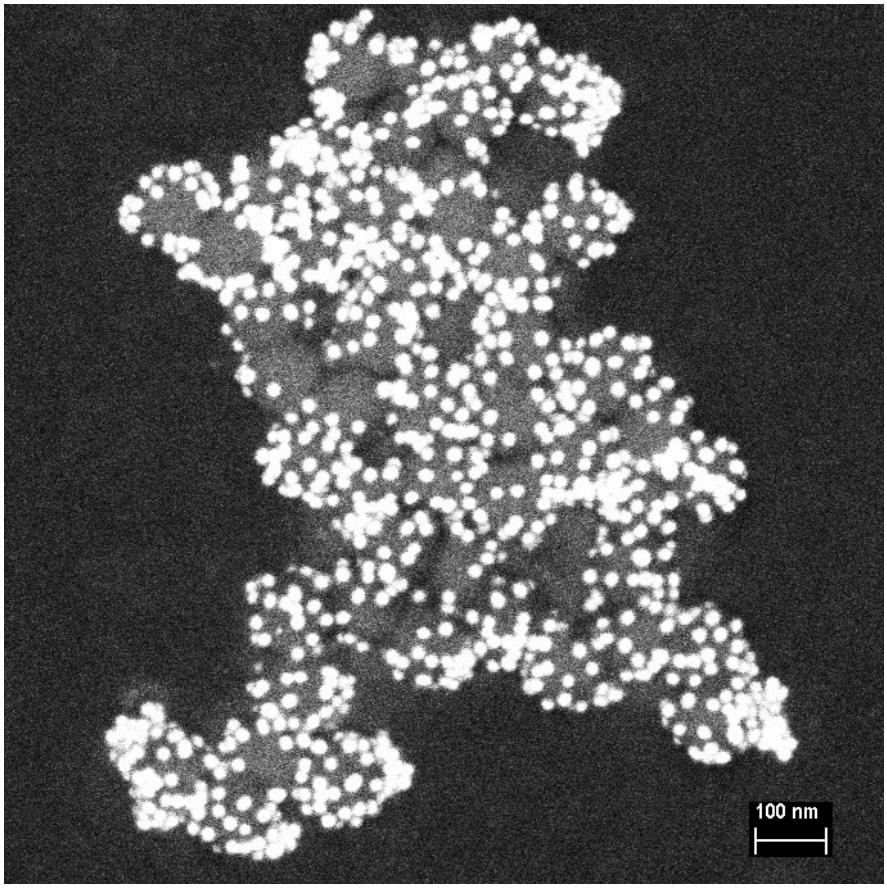

Figure 4.39. Energy selective backscattering (ESB) SEM image of SiNP-GNP cluster in Figure 4.38. (Image taken by Dr. Preston Larson).

Thus, Figure 4.39 shows gold nanoparticles in bright white spots surrounding silica nanoparticles, which are represented by the darker grey spots. The sample was imaged from to different angles in order to verify the gold nanoparticles were indeed completely aggregated around the surface of the silica nanoparticles (Figure 4.40).

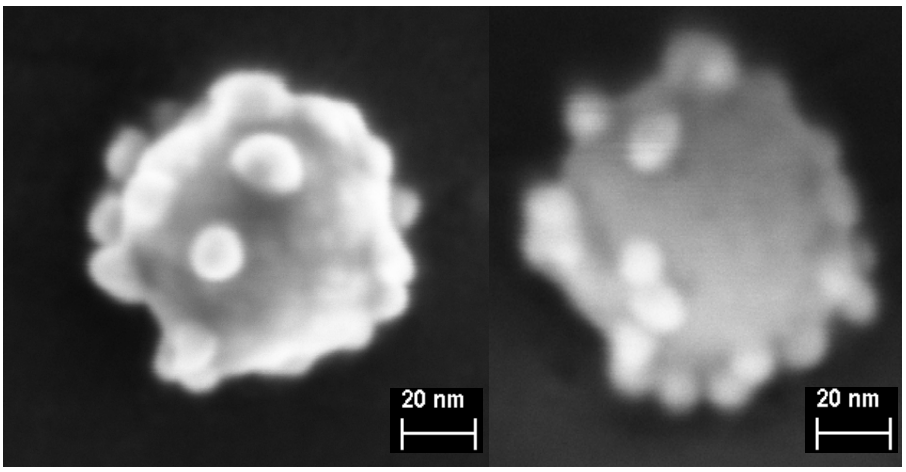

Figure 4.40. SEM 45 º angle tilt series of the same SiNP-GNP aggregate. (Images taken by Dr. Preston Larson)

The tilt series confirms the complete coverage of silica nanoparticles in gold nanoparticles by gaining a more three-dimensional view of the aggregates from two separate angles.

There is strong evidence to suggest that larger diameter silica nanoparticles increase the amount of SiNP-GNP aggregation when excess gold is added to the system. Excess gold in the system can be selectively removed via centrifugation separation, which has clear consequences to the absorbance and emission spectra. However, EDS spectroscopy indicates that this process appears to liberate large amounts of sodium citrate that were introduced from the GNP preparation. SEM and TEM imaging confirm that strongly and completely bound SiNP-GNP aggregates were formed and are stable during electron bombardment during imaging (compared to sodium citrate which is beam sensitive, white squares Figure 4.37). This investigation strongly supports our efforts to build a robust in solution metal enhanced fluorescence system but still needs

to be refined in order to show consistent enhancement. Perhaps the use of gradient centrifugation would allow for a more clean separation of silica and gold aggregates.

4.4 Chapter Summary

This chapter described the need for and our efforts to produce metal-enhanced fluorescence (MEF)[1] in solution by aggregating dye-doped silica nanoparticles with gold nanospheres. Our group previously showed that a similar system produced significant enhancements (200-fold) but struggled from inconsistent enhancement (Figure 4.7).[8] We then investigated well-ordered layered dye-doped silica nanoparticles (chapter II) in order to establish a robust method for reproducing fluorescent brightness enhancement. Metal-enhanced fluorescence (MEF) was studying in solution by attempting to measure the lifetime of previously enhanced systems, varying the concentration of dye within the layer silica nanoparticles, varying the relative concentrations of silica and gold species in solution, and increasing the overall distance between the dye and gold by producing large diameter (150 nm) silica nanoparticles.

Dramatic emission increases seen previously in our lab (Figure 4.8) necessarily must have benefitted from a significant increase in cycling of the excitation/emission process given the large (200-fold) enhancements produced.[8] Measurements, made possible through collaboration with Drs. Gregory Salamo and Dorel Guzun at the University of Arkansas Institute for Nanoscience and Engineering, determined that very low concentrations of dye used for these experiments require very sensitive detection limits (Figure 4.10). These measurements showed lower PL liftimes than literature value for rhodamine B (calculated 1.6 nanoseconds, reported 6 nanoseconds).[16] However, these values may differ due to the use of water instead of ethanol for lifetime

determination. We were not able to determine the lifetime of the enhanced sample but we did gain insight to the use of time-resolved ultra-fast laser spectroscopy as a technique for investigation future systems.

We investigated the effects of different concentrations of rhodamine B core-doped silica nanoparticles during aggregation with gold nanospheres in order to produce metal-enhanced fluorescence (Figure 4.11). Cores that were doped with a ten-fold dilution of RhB were mixed with ten-fold as many silica particles in order to maintain a fluorescent signal, which caused a significant increase in the rate of GNP aggregation as indicated by the absorption spectra (Figures 4.12 and 4.13). These aggregates did not show emission brightness increases but did show a slight blue shift in λ_{max} (567 nm from 574 nm), which is indicative of a lower concentration of sample (Figure 4.15). TEM images confirmed that increased aggregation occurred in samples that contained larger amounts of SiNP (Figure 4.18). Increasing the amount of lesser-doped silica nanoparticles drives the aggregation of SiNP and GNP forward but it is unclear if there is a direct consequence of having less dye present in the silica nanoparticles at this time. This led us to investigate the difference in concentration of particles that were equally dye-doped.

We investigated vary the relative concentration of core-doped silica nanoparticles and gold nanoparticles in order to identify the influence over aggregation. Larger core-doped silica nanoparticles were prepared according to previous results that suggested a larger spacer might be necessary to produce MEF (Figure 4.19).[18] The absorbance spectra showed an increase in gold aggregation with respect to increased SiNP in solution by the increasingly present shoulder appearing greater than 600 nm

(Figure 4.20), but the emission spectra displayed lowered emission (Figure 4.21). Inner filtration effects were thought to be the cause of the observed lowering of emission brightness. However, the samples observed to change (increasing and decreasing) not according to inner filtration effects after 7 days (Figures 4.23-25). TEM images suggested that large aggregate sedimentation may play a role in the loss of emission signal (Figures 4.26-28). Increasing the concentration of thiol coated dye-doped silica nanoparticles relative to gold nanoparticles in solution increases the rate of SiNP-GNP aggregation. Inconsistencies between large aggregate formation and fluorescence decreases led us to believe the distance dependence played a larger role.

We investigated larger diameter (150 nm) rhodamine-B core-doped silica nanoparticles as a means of increasing the distance between the dyes and the surface of the metal in order to achieve metal-enhanced fluorescence (Figure 4.29). Decreases in the absorbance spectra suggested that primarily gold-gold aggregation was occurring (Figure 4.30), but TEM imaging confirmed a significant amount of SiNP-GNP aggregation with a large excess of gold present (Figure 4.31). SiNP-GNP aggregates fell out as sediment more rapidly over the lighter SiNP or GNP isolated species and thus were crudely separated under mild centrifuge conditions (Figure 4.32). The supernatant and sediment samples were then measured to determine the effect of removing excess gold (Figures 4.33). Relative decrease in absorbance and increases in emission suggest that removing excess gold from the system increases the overall brightness of the sample (Figure 4.35). TEM and SEM images clearly showed well-formed aggregates of multiple gold nanoparticles about a few silica nanoparticles (Figures 4.36). Extra unknown material present in TEM samples (Figure 4.36) was determined to be sodium

citrate by EDS measurements (Figure 4.37). SEM imaging confirmed that gold was bound three-dimensionally about the silica surface (Figures 4.38-40). This investigation strongly supports our efforts to build a robust in solution metal enhanced fluorescence system but still needs to be refined in order to show consistent enhancement.

This chapter described our efforts to reproducibly produce metal-enhanced fluorescence in solution by aggregating dye-doped silica nanoparticles with gold nanospheres. The experiments outlined here lay the groundwork to produce high quality SiNP-GNP heteroagggregates for future studies that will optimize the exciting fluorescent enhancement potential of our MEF in solution system. Photophysical measurements provided insight into the various parameters (concentration, size, surface coating) that affect the rate and nature of aggregates formed in solution. Control of the aggregation process is vital for the development of a reproducible solution phase metal-enhanced fluorescence system.

4.5 Experimental

4.5.1 Preparation of gold nanoparticles (GNP)[20]

All glassware was washed with aqua-regia (HNO_3:HCl, 1:3) and milipore water (17.8 MΩ) before use. Gold (III) chloride trihydrate ($HAuCl_4 \cdot 3H_2O$) and trisodium citrate ($Na_3C_6H_5O_7$) were purchased from Sigma-Aldrich and used without any further purification.

An aqueous solution of gold (III) chloride trihydrate (1.75 mL, 0.01 M) was added to water (17.8 MΩ, 48.75) in a 250 mL Erlenmeyer flask along with a magnetic stir bar. The solution was brought to a boil before an aqueous solution of trisodium citrate (1 mL,

34 mM) was added. The solution gradually turned a dark blue color before becoming the dark red color associated with a complete formation of GNP (approximately 5 min after boiling). The solution was diluted, with water, back to 50 mL to account for any volume lost during boiling.

4.5.2 Measurement of photoluminescent (PL) Lifetime

PL lifetime measurements were carried out by Dr. Dorel Guzun in the lab of Dr. Greg Salamo at the University of Arkansas Institute for Nanoscience and Engineering. The measurements were performed by a spectrally-resolved pump probe measurement technique. The pump-probe technique works by exciting a sample with an ultra fast femtosecond laser pulse (the pump), which is followed by a second pulse (the probe), which feeds to a monochromator and a detector (Figure 4.41).

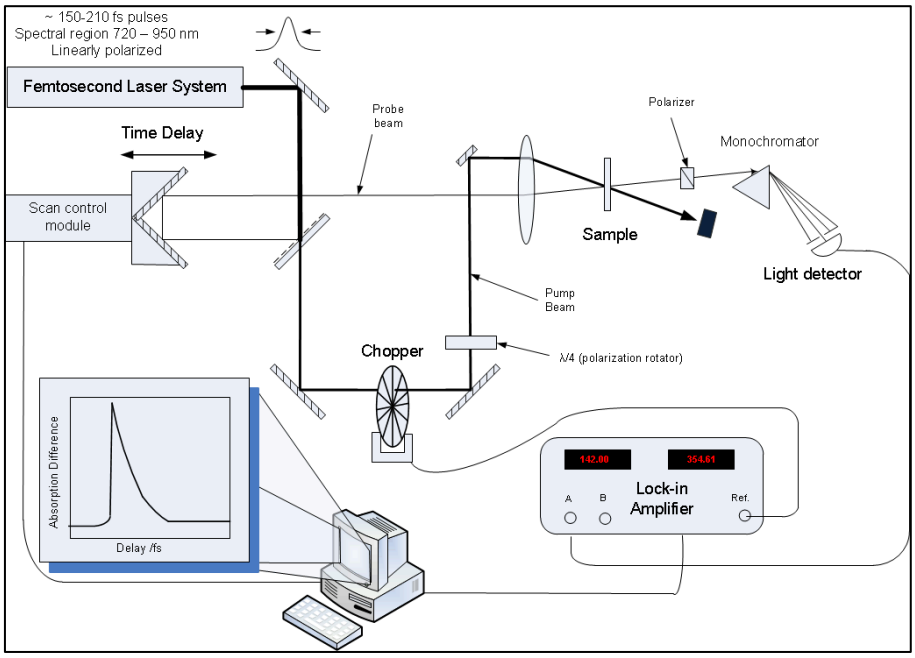

Figure 4.41. Schematic of the pump-probe setup. (Image from Dr. Dorel Guzun).

Delaying the probe pulse provides time-resolved absorption data about the sample. The probe pulse passes through the sample with the highest transmittance (lowest absorption) immediately following the pump pulse, thus giving the highest intensity signal. As the delay is increased the amount of probe light absorbed by the sample increases and thus the signal decreases. This process produces the 'decay graphs' seen in the right hand corner of the pump-probe spectra (Figures 4.9 and 4.10).

4.5.3 Synthesis of core-doped silica nanoparticles

Core-doped SiNP preparation: Rhodamine B (RhB) (3.34 mg, 0.0069 mmol) was dissolved in milipore water (10 mL, 17.8 MΩ) to produce a '0.69 mM stock RhB' solution. A 1 mL aliquot of 'stock RhB' was diluted into milipore water (10 mL, 17.8 MΩ) to produce a '0.069 mM dilute RhB' solution. L-arginine (9.1 mg, 0.052 mmol) was dissolved in 'stock RhB' and 'dilute RhB' aliquots (6.9 mL) in respective clean 20 mL scintillation vial with a small magnetic stir bars. From here both samples were treated under identical conditions. Cyclohexane (0.45 mL) was then added to form a biphasic (aqueous/organic) system that was heated in an oil bath to 60 °C. Tetraethylorthosilicate (TESO) (0.55 mL, 2.5 mmol) was added carefully to the top organic layer before the vial was tightly re-capped and placed back in the oil bath. The mixture was slowly stirred, attempting to minimize disturbance of the top organic layer. The vial was heated at 60 °C for 24 h before the small diameter (13 nm) silica nanoparticles were removed from the aqueous layer.

Silica shell re-growth: A 20 mL scintillation vial was charged with layered RhB-doped core SiNP (1 mL, 16 nm diameter), water (3.6 mL), and a magnetic stir bar. Then, cyclohexane (0.5 mL) was added to create a top organic layer. The vial was heated to

~60 °C before TEOS (0.352 mL) was added carefully to the top layer. The vial was then tightly capped and slowly stirred, to minimize perturbation of the top layer as much as possible, at 60 °C overnight. This resulted in a cloudy pink solution.

Dialysis: The entire aqueous portion of the SiNP preparation, post shell growth, was added to a 5-6 inch strip of cellulose dialysis tubing (MWCO 12-14 kDA, Spectrum Labs) after it had been soaked in water for 15 min and sealed from on end with a dialysis clamp. Any excess air was removed from the dialysis tubing before a second clamp was added to the top, leaving roughly 20% of negative space, a section of tubing that is deflated, in the bag to allow for water influx. A small strip of Styrofoam was then added to the top clamp in order to float the dialysis tube. This assembly was then placed in a 4 L beaker filled with 2 L of milipore water and a magnetic stir bar. The water was replaced after an initial 4 hours and again after 12 hrs to ensure there was never a significant concentration of dye in the dialysis water. The clamp was removed and the freshly cleaned particles were diluted with water to 10 mL in a volumetric flask to account for variations in the amount of water that entered the membrane in each preparation. TEM confirmed the resulting clean particles had an average diameter of ~25 nm.

Thiol coating: Aqueous aliquots (1 mL) of both cleaned core-doped SiNP from above (0.69 mM and 0.069 mM) were respectively added to snap-top centrifuge tubes (1.5 mL capacity) before adding glacial acetic acid (20 μL). The centrifuge tube was inverted several times by hand before (3-mercaptopropyl)trimethoxy silane (20 μL) was added. The centrifuge tube was then rotary inverted overnight in the dark at room temperature

before being cleaned by dialysis as previously described. The samples were finally re-suspended in milipore water (10 mL, 17.8 MΩ).

4.5.4 Investigating the doping concentration effect of core-doped silica nanoparticles when mixed with gold nanospheres

Rhodamine B core-doped thiol coated silica nanoparticles, described above, were mixed with gold nanoparticles (average 13 nm diameter) in aqueous solutions by rotary inversion over the course of several days. Samples were periodically taken off stirring to be measured for absorbance, emission, and excitation changes. The samples contained the following components:

Sample ID	NG2-247 added (Thiol coated SiNP)	GNP added	Water added (μL)
A control (0.69 mM)	1 μL	0 μL	999 μL
A (0.69 mM)	1 μL	150 μL	849 μL
B control (0.069 mM)	20 μL	0 μL	980 μL
B (0.069 mM)	20 μL	150 μL	830 μL
GNP control	0 μL	150 μL	850 μL

Table 4.1. Amounts of various concentration dye-doped silica and GNP nanoparitcles.

4.5.5 Investigation of relative concentration effect between layered dye-doped silica nanoparticles and gold nanospheres

Core-doped silica nanoparticles were prepared as previously described in section **4.5.3** with rhodamine B (2.10 g, 0.004 mmol). Additional silica shell growth was accomplished by the following procedure:

Silica shell re-growth: A 20 mL scintillation vial was charged with RhB-doped core SiNP (1 mL, 13 nm diameter), water (3.6 mL), and a magnetic stir bar. To this, L-arginine (1.07 mg) was added. Then, cyclohexane (0.5 mL) was added to create a top organic layer. The vial was heated to ~60 °C before TEOS (0.4 mL) was added carefully to the top layer. The vial was then tightly capped and slowly stirred, to minimize perturbation of the top layer as much as possible, at 60 °C for 30 h. This resulted in a partially cloudy pink solution. The suspension was cleaned via centrifugation three times, spinning at 15,000 rpm for 10 minutes, replacing the supernatant with milipore water (1.5 mL, 17.8 MΩ) each time. TEM confirmed the resulting clean particles had an average diameter of 60 nm. The cleaned SiNPs were then thiol coated as described in **4.5.3**.

4.5.6 Investigating of varying concentration of core-doped thiol coated silica nanoparticles when mixed with gold nanospheres

Silica nanoparticles (60 nm average diameter, from section **4.5.5**) were mixed with citrate capped gold nanoparticles (13 nm, from section **4.5.1**) were mixed in aqueous solutions according to the following table:

Sample	**SiNP (µL) (NG2-263)**	**GNP (µL)**	**H_2O (µL)**

A1	10	150	840
C1	10	0	990
A2	20	150	830
C2	20	0	980
A3	100	150	750
C3	100	0	900
GNP control	0	150	850

Table 4.2. Volumes of SiNP added during titration of GNP

4.5.7 Preparation of large diameter (150 nm) rhodamine B core-doped silica nanoparticles

A 20 mL scintillation vial was charged with RhB-doped core SiNP prepared in section **4.5.5** (1 mL, 60 nm diameter), water (3.6 mL), and a magnetic stir bar. To this, L-arginine (1.0 mg) was added. Then, cyclohexane (0.7 mL) was added to create a top organic layer. The vial was heated to ~60 °C before TEOS (0.5 mL) was added carefully to the top layer. The vial was then tightly capped and slowly stirred, to minimize perturbation of the top layer as much as possible, at 60 °C for 48 hours. This resulted in a partially cloudy pink solution. The suspension was cleaned via centrifugation three times, spinning at 15,000 rpm for 5 min, replacing the supernatant with milipore water (1.5 mL, 17.8 MΩ) each time. The particles were finally suspended in milipore water (10 mL, 17.8 MΩ). TEM confirmed the resulting clean particles had an average diameter of 150 nm. The cleaned SiNPs were then amine coated as described in chapter 2.

4.5.8 Investigation of large diameter (150 nm) rhodamine B-doped silica nanoparticles mixed with citrate-capped gold nanoparticles

Amine-coated SiNP (from section **4.5.7**) (from stock 10 mL) and GNP (section **4.5.1**) were mixed in aqueous solutions according to the following:

Sample	SiNP	GNP	H_2O
SiNP+GNP	20 μL	500 μL	490 μL
SiNP only	20 μL	0 μL	980 μL

Table 4.3. Volumes of large diameter SiNP added to GNP.

Samples were kept in plastic capped sealed cuvettes at rest in the dark when not being measured over the course of several days.

4.5.9 Centrifugation separation of free GNP and SiNP-GNP aggregates

Samples from section **4.5.8** were separated by centrifugation in a Tomy MTX-150 high-speed micro refrigerated centrifuge. The samples were spun for 1 minute at 5,000 rpms. This value was determined from experimenting with standard gold and silica samples. The supernatant was removed after centrifugation with a micropipette (900 μL) to ensure sample consistency. All supernatants were combined for the 3X and 6X wash respectively. The sediment portions were re-suspended in the remaining 100 μL via sonication. The sediment fractions were also combined during the 3X and 6X collections.

4.5.10 TEM, SEM, and EDS parameters and sample preparation

Transmission electron microscopy (TEM) imaging was performed on a Zeiss 10A Conventional microscope operating at 80 kV from a tungsten filament source at the

University of Oklahoma Samuel Roberts Noble Electron Microscopy Laboratory. Samples were prepared by drop coating 4 μL of sample onto a 300 mesh formvar coated copper TEM grid (Ted Pella Corp.) and allowing to air dry.

Scanning electron microscopy (SEM) imaging was performed on a Zeiss NEON High Resolution SEM microscope operating between 0.1-30 kV from Gemini lens Schottky emitter at the University of Oklahoma Samuel Roberts Noble Electron Microscopy Laboratory. Samples were prepared by drop coating on polished silicon <100> wafers or directly from the previously prepared formvar copper-coated TEM grids.

Energy dispersive X-ray Spectroscopy (EDS) was performed on a Zeiss NEON High Resolution SEM microscope operating between 0.1-30 kV from Gemini lens Schottky emitter outfitted with an Oxford EDSD (energy and angle selective BSE) detector at the University of Oklahoma Samuel Roberts Noble Electron Microscopy Laboratory. Samples were drop coated on to polished silicon <100> wafers.

4.6 References

1. Geddes, C. D.; Lakowicz, J. R., Metal-Enhanced Fluorescence. *J. Fluor.* **2002,** *12* (2), 121-130.

2. (a) Halas, N. J., Plasmonics: An Emerging Field Fostered by Nano Letters. *Nano lett.* **2012,** *10*, 3816-3822; (b) Hartland, G. V.; Schatz, G., Virtual Issue: Plasmon Resonanced- A Physical Chemistry Perspective. *J. Phys. Chem. C* **2011,** *115*, 15121-15123.

3. Lakowicz, J. R.; Geddes, C. D.; Gryczynski, I.; Malicka, J.; Gryczynski, Z.; Aslan, K.; Lukomska, J.; Matveeva, E.; Zhang, J.; Badugu, R.; Huang, J., Advances in Surface-Enhanced Fluorescence *J. Fluor.* **2004,** *14* (4), 425-441.

4. (a) Jackson, J. B.; Halas, N. J., Surface-enhanced Raman scattering on tunable plasmonic nanoparticle substrates. *PNAS* **2004,** *101* (52), 17930-17935; (b) Moula, G.; Aroca, R. F., Plasmon-Enhanced Resonance Raman Scattering and Fluorescence in Langmuir-Blodgett Monolayers. *Anal. Chem.* **2011,** *83*, 284-288.

5. Dragan, A. I.; Golberg, K.; Elbaz, A.; Marks, R.; Zhang, Y.; Geddes, C. D., Two-color, 30 second microwave-accelerated Metal-Enhanced Fluorescence DNA assays: A new Rapid Catch and Signal (RCS) technology. *J. Immunol. Methods* **2011,** *366*, 1-7.

6. Deceglie, M. G.; Ferry, V. E.; Alivisatos, P. A.; Atwater, H. A., Design of Nanostructured Solar Cells Using Coupled Optical and Electrical Modeling. *Nano lett.* **2012,** *12*, 2894-2900.

7. Lakowicz, J. R.; Ray, K.; Chowdhury, M.; Szmacinski, H.; Fu, Y.; Zhang, J.; Nowaczyk, K., Plasmon-controlled Fluorescence: A New Paradigm in Fluorescence Spectroscopy. *Analyst* **2008,** *133*, 1308-1346.

8. Gunawardana, K. B. Study of Metal-Enhanced Fluorescence of Dye Doped Silica Nanoparticles. University of Oklahoma, Norman, 2012.

9. Jones, M. R.; Osberg, K. D.; Macfarlane, R. J.; Langille, M. R.; Mirkin, C. A., Templated Techniques for the Synthesis and Assembly of Plasmonic Nanostructures. *Chem. Rev.* **2011,** *111*, 3736-3827.

10. Lazarides, A. A.; Schatz, G. C., DNA-Linked Metal Nanosphere Materials: Structural Basis for the Optical Properties. *J. Phys. Chem. B* **2000,** *104*, 460-467.

11. Kelly, L. E.; Coronado, E.; Zhao, L. L.; Schatz, G. C., The Optical Properties of Metal Nanoparticles: The Influence of Size, Shape, and Dielectric Environment. *J. Phys. Chem. B* **2003,** *107*, 668-677.

12. Lakowicz, J. R., Radiative Decay Engineering 5: Metal-Enhanced Fluorescence and Plasmon Emission. *Anal. Biochem.* **2005,** *337*, 171-194.

13. Folmar, M.; Shtoyko, T.; Fudala, R.; Akopova, I.; Gryczynski, Z.; Raut, S.; Gryczynski, I., Metal enhanced fluorescence of Me-ADOTA-Cl dye by silver triangle nanoprisms on a gold film. *Chem. Phys. Lett.* **2012,** *531*, 126-131.

14. Bardhan, R.; Grady, N. K.; Cole, J. R.; Joshi, A.; Halas, N. J., Fluorescence Enhancement by Au Nanostrcutures: Nanoshells and Nanorods. *ACS Nano* **2009,** *3* (3), 744-752.

15. Mohamed, M. B.; Volkov, V.; Link, S.; El-Sayed, M. A., The 'lightning' gold nanorods: fluorescence enhancement of over a million compared to the gold metal. *Chem. Phys. Lett.* **2000,** *317*, 517-523.

16. Strickler, S. J.; Berg, R. A., Relationship between Absorption Intensity and Fluorescence Lifetime of Molecules. *J. Chem. Phys.* **1962,** *37* (4), 814-822.

17. Halterman, R. L.; Moore, J. L.; Yip, W. T., Cucurbit[7]uril Disrupts Aggregate Formation Between Rhodamine B Dyes Covalently Attached to Glass Substrates. *J. Fluoresc.* **2011,** *21*, 1467-1478.

18. Liu, J.; Li, A.; Tang, J.; Wang, R.; Kong, N.; Davis, T. P., Thermoresponsive Silver/polymer Nanohybrids with Switchable Metal Enhanced Fluorescence. *Chem. Commun.* **2012,** *48*, 4680-4682.

19. Goldstein, J., *Scanning electron microscopy and x-ray microanalysis*. Springer: London, 2003; Vol. 3rd.

20. Frens, G., Controlled Nucleation for the Regulation of the Particle Size in Monodisperse Gold Suspensions. *Nature Phys. Sci.* **1973,** *241* (105), 20-22

Chapter V: Development of a plasmonic waveguide by aggregation of gold nanorods with dye-doped silica nanoparticles

5.1 Chapter Overview

This chapter describes the need for and our efforts to employ gold nanorods as nanowaveguides[1] in order to establish radiationless plasmon resonance mediated energy transfer over a long range by aggregating fluorophore-doped silica nanoparticles at the end caps of the rods. This interaction is expected to mimic the well established phenomenon of Förster resonance energy transfer (FRET)[2] in that energy is passed from the donor fluorophore to the acceptor fluorophore via a radiationless transfer to and from the gold plasmon. Gold nanorods are desirable substrates due to their tunable size (aspect ratio) and photophysical properties. Further, recent evidence suggests that the favorable end-cap attachment is achievable via preferential displacement of surfactant at the caps due to unique crystal structure found in these regions.[3] The variables that must be addressed to investigate the possibility of gold nanorod waveguides are: the absorption and emission profiles of dyes and the plasmon absorption of the gold nanorods, the concentration of each particle, the dye-metal distance (established by the shell thickness of the silica), and the ability to control assembly. This chapter describes our efforts to establish radiationless energy transfer between hetero dye-doped silica nanoparticles via gold nanorod plasmon mediated FRET by aggregating the fluorophores preferentially at the end-caps of the nanorods.

5.2 Introduction

Recent advances in the synthesis of well-formed, monodisperse gold nanorods have opened the door to exploring their unique optical[4] and morphological[5] properties for applications as phototherapeutic agents, in biological imaging, and in metal enhanced fluorescence systems.[6] Gold nanorods are synthetically fine-tuned as they develop an increasingly red-shifted longitudinal plasmonic resonance absorption band as the aspect ratio increases due to increased amounts of silver nitrate added during growth (Figure 5.1).[7]

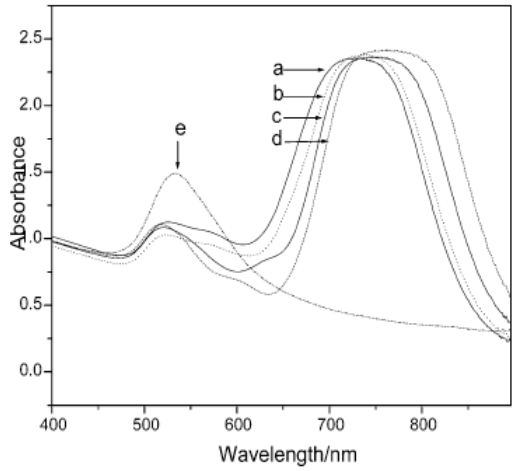

Figure 5.1. Gold nanorods of increasing larger (a<d) aspect ratio are shown to extend their absorption into the NIR (image from Sau et al).[7]

Furthermore, gold nanorods have been shown to be amenable to post production modifications, such as selectively replacing the CTAB coated ends with small thiol ligands, which allow for higher order structures to be established.[8] The unique morphological and photophysical properties combined with control of synthesis and

postproduction modifications make gold nanorods an attractive substrate to address long-range FRET assemblies.

Our aim is to establish gold nanorods as plasmonic waveguides in long distance FRET-like systems to allow for the radiationless transfer of energy between two dye-doped silica nanoparticles. Previous theoretical[9] and experimental[10] work has shown that near field coupling of rod shaped metal nanostructures are capable of guiding electromagnetic energy that is below the diffraction limit of light. This process occurs via the close plasmon coupling of adjacent nanostructures.[11] Our work looks to expand on the radiationless energy transfer by exchanging addition metal nanostructures with fluorophores. Here, a donor dye-dope silica nanoparticle non-radiatively propagates a signal across a gold nanorod, via a near-field interaction, to an acceptor dye-doped silica nanoparticle on the opposite end of the rod (Figure 5.2).

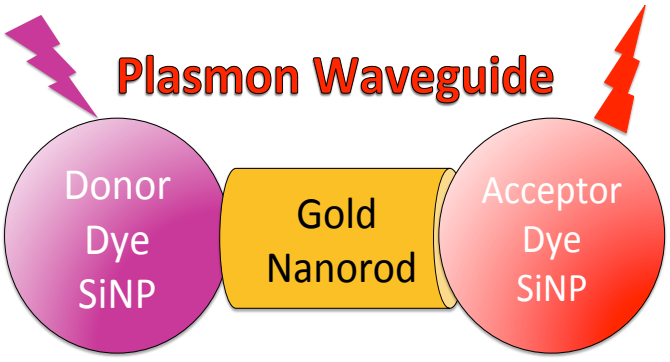

Figure 5.2. Cartoon schematic of a dye-doped silica nanoparticle and gold nanorod waveguide assembly. (this work)

We hypothesize that long range FRET-like energy transfer is possible between two dye-doped silica nanoparticles by employing gold nanorods as plasmonic waveguides.

Nanorods are an especially attractive target given the fine-tune control over their morphological, and thus photophysical, control via the seed mediated growth process.[12]

The plasmonic properties of gold nanostructures are highly dependent on their size, shape, and coating.[13] A gold nanorod absorbance spectrum is dominated by the longitudinal plasmon resonance, which is dependent on the aspect ratio and controlled synthetically by the amount silver nitrate added to the surfactant micelle template. Nanorods are prepared by seed mediated growth in the presence of a capping agent. The anisotropic rods were prepared by quickly reducing chloroauric acid (IV) to produce a large amount of small gold clusters that act as nucleation sites. Once the large metallic gold concentration decreases, the reduction continues to proceed slowly with gold ions preferring to add to the nucleation sites.[14] The shape, size, and dispersity of the growing nanospheres is then influenced by the capping agent as summarized below.[12]

Capping agents bind on a continuum from loosely bound trisodium citrate (which produces spheres with 13 nm diameters) to restrictively bound to cetyltrimethylammonium bromide (CTAB) with silver nitrate; the latter complex produces gold nanorods. In general, tightly binding capping agents produce smaller nanoparticles as the steric hindrance of the surfactant slows the addition of monomer gold to the nucleation site.[14] The gold nanorod synthesis utilizes this slow growth process by increasing the ratio of silver nitrate to CTAB in solution. These two species purportedly form a firm layer of silver bromide around the tubular CTAB micelle greatly increasing its rigidity and promoting elongation of the rods.[5] (Figure 5.3)

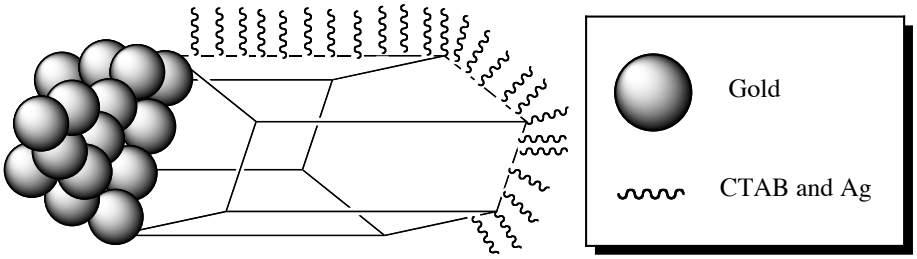

Figure 5.3. Nanorod formation via a tubular micelle formation using CTAB and silver nitrate (image from this work).

Both of these morphologies have been synthesized reproducibly and with high-quality in our lab (Figure 5.4).

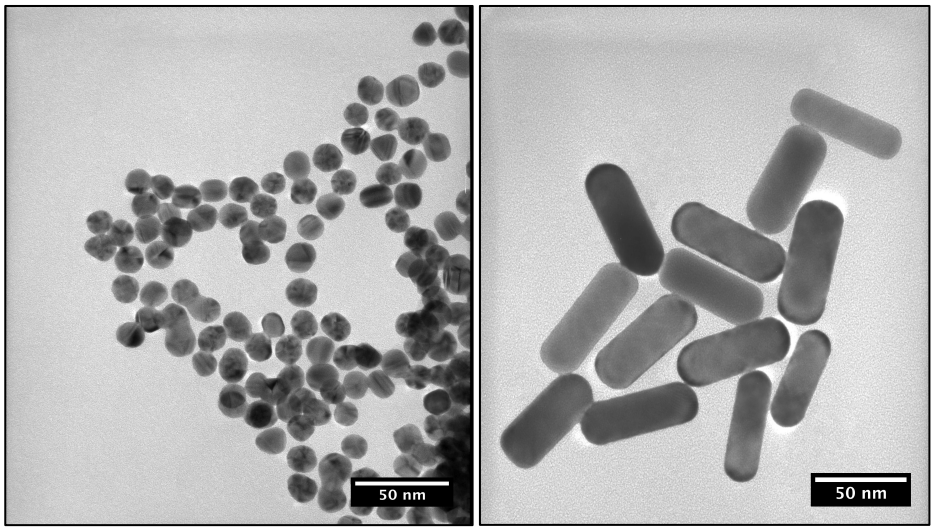

Figure 5.4. TEM micrographs of (left) gold nanospheres and (right) nanorods. (images from this work).

Aggregating dye-doped silica nanoparticles at the longitudinal ends of the silica nanoparticles is essential for tapping into the appropriate plasmonic mode for waveguide formation (Figure 5.2). Fortunately, the unique crystal structure and thus the resulting surfactant packing enables a pathway for end-cap aggregation. Murphy et al

provide a detailed description of the crystallographic facets of gold nanorods along with an excellent discussion of the factors that assist this formation.[5] The surfactant CTAB closely packs along the entire surface of the gold nanorods in order to prevent gold-gold aggregation from occurring. The end caps consist of five triangular facets of {111} while the lateral sides consist of a mixture of {100} and {110} faces (Figure 5.5). The net result is that CTAB cannot pack as closely on the slopped sides of the {111} faces resulting in a greater dissociation of surfactant at these facets.[8]

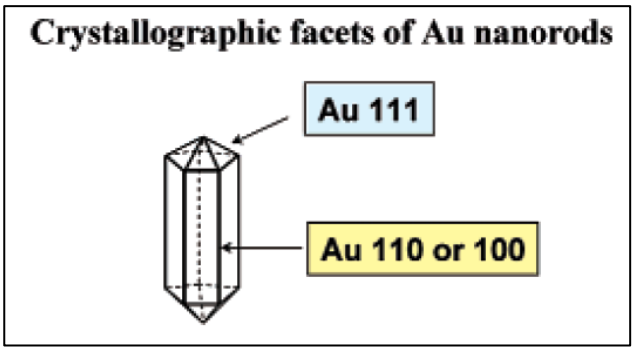

Figure 5.5. Crystallographic facets of gold nanorods (image from Joseph et al).[8]

Multiple research groups have been able to selectively form 'end on' aggregates by replacing CTAB with various moieties (e.g. mercaptocarboxylic acids) at predominately the ends of gold nanorods (Figures 5.6).[3, 15]

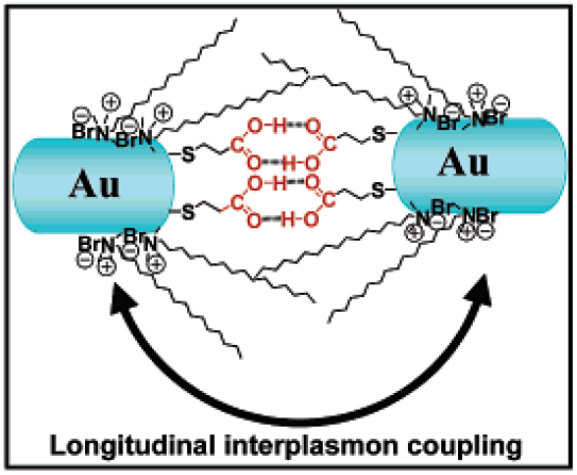

Figure 5.6. Schematic of nanorod end-cap aggregation through carboxylic acid H-bonding thiol ligands. (image from Thomas et al)[3]

These ligands were verified by TEM imaging to produce preferential end-cap aggregation of gold nanorods (Figure 5.7).

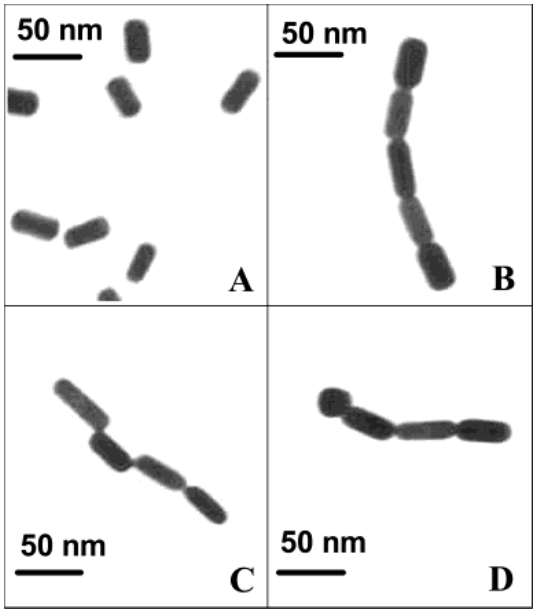

Figure 5.7. TEM images of rods longitudinally aggregated in a) the absence and b-d) prescence of 3-mercaptopropionic acid (MPA) (image from Thomas et al).[3]

Dye-doped silica nanoparticles must be associated at the end-caps of gold nanorods as the longitudinal plasmon resonates along this axis. The electric field surrounding a gold nanorod is most intense at the ends of the longitudinal axis but it quickly dissipates into the surrounding medium (Figure 5.8).[16]

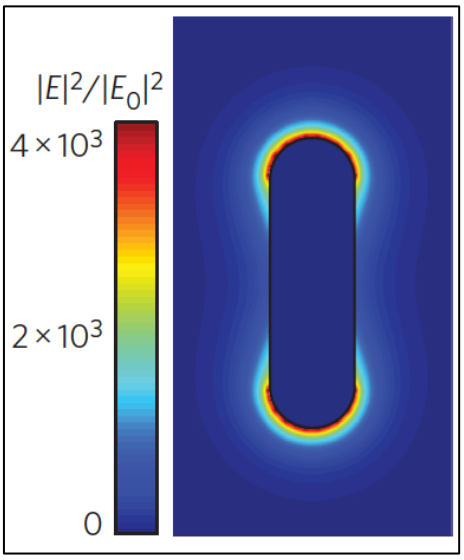

Figure 5.8. Calculation in the discrete dipole approximation of the electric field intensity around a gold nanorod, evaluated on resonance with its longitudinal SPR. (image from Zijlstra et al)[16]

A waveguide is established when coupled particles interact within a wavelength of light (so called 'near field') so that gold plasmon resonance and dipole of the fluorophore physically overlap, causing the oscillating electric field about gold to carry the energy released from an excited dye.[10] Thus, in order to employ gold nanorods as waveguides dye-doped silica nanoparticles must be tightly bound preferentially to the end-caps of gold nanorods.

Gold nanorods are attractive synthetic targets as their morphological and

photophysical properties can be fine-tuned as well as unique post-production modification opportunities. Our hypothesis is that by binding dye-doped silica nanoparticles to the end-caps of appropriately sized gold nanorods long-range FRET-like radiationless energy transfer can be induced via the longitudinal surface plasmon resonance of the rod acting as a nanowaveguide.

5.3 Results and Discussion

Gold plasmonic waveguides were pursued by synthesizing high-quality gold nanorods, investigating potential end-cap aggregation moieties on silica nanoparticles, varying the relative concentrations of silica and gold used in the aggregates, and varying the spectral overlap of the absorbance of the longitudinal plasmon with the absorbance and emission of the interacting fluorophores.

Gold nanorods were prepared by a variety of previously established and studied by UV-Vis absorption and TEM imaging before being aggregated with dye-doped silica nanoparticles. Once a robust method for producing uniform rods in solution was established we investigated the effect of varying spectral features of the dyes and gold as well as the concentration of each species. These studies show promise for a proof-of-concept for the development of gold nanorod waveguides and are on going.

5.3.1 Synthesis and Spectroscopy of Gold Nanorods

Gold nanorods were prepared following established methods.[17] There are several procedures for growing gold nanorods but the seed mediated approach was taken based on it success and relative ease. However, the growth of the nanorods depends heavily on the parameters of the preparation such as temperature and small amounts of contaminent. Even the presence or absence of stirring has been shown to have an

effect.[18] Figures 5.9 and 5.10 show examples of two experiments that were run under similar silver nitrate conditions in the Halterman lab but produced very different absorbance spectra. In the first, CTAB precipitated out of solution slightly due to a change in the room temperature. This caused a breakdown in the tubular micelle and the rods took increasingly larger amount of silver nitrate to form properly. Note the longitudinal plasmon resonance mode (> 600 nm) comes to dominate the transverse mode (545 nm) as increasing amounts of silver nitrate re-enforce the surfactant template, causing the aspect ratio of the nanorods to increase. Spheroidal samples R1 and R4 show predominately transverse modes and would not be acceptable for waveguide experiments as they lack the obligatory longitudinal mode.

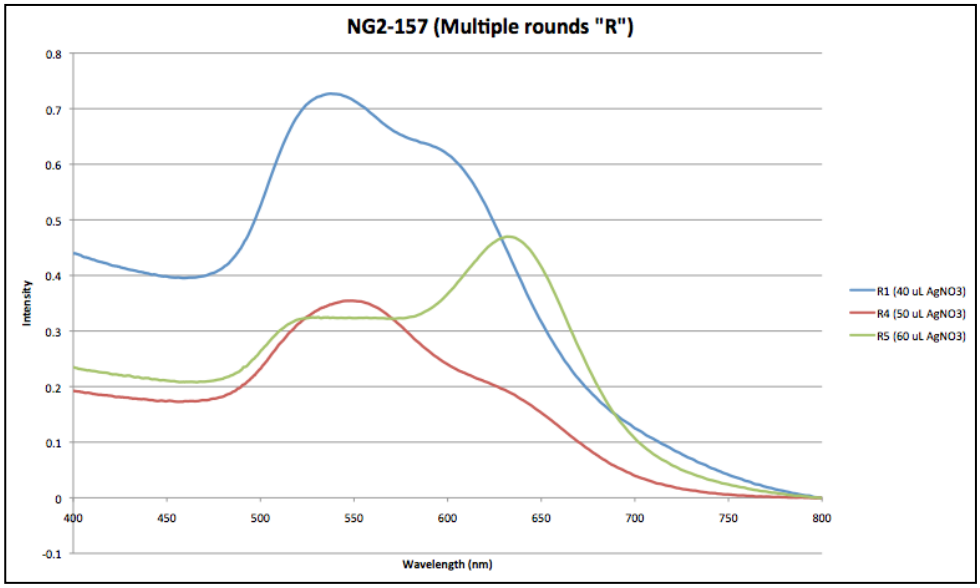

Figure 5.9. Absorbance spectra of gold nanorods grown in a CTAB deficient environment.

Figure 5.10 shows gold nanorods grown in a proper surfactant environment. Here, even a small amount of silver nitrate (40 μL) produces the desired longitudinal plasmon

dominated spectrum centered over 700 nm. Increasing the amount of silver nitrate from 40 to 90 µL continually grows longer nanorods while maintaining the same diameter (increasing aspect ratio) as expected. The aspect ratio varies from ~2.7 when 40 µL of silver nitrate was added to ~3.8 in the 90 µL sample.

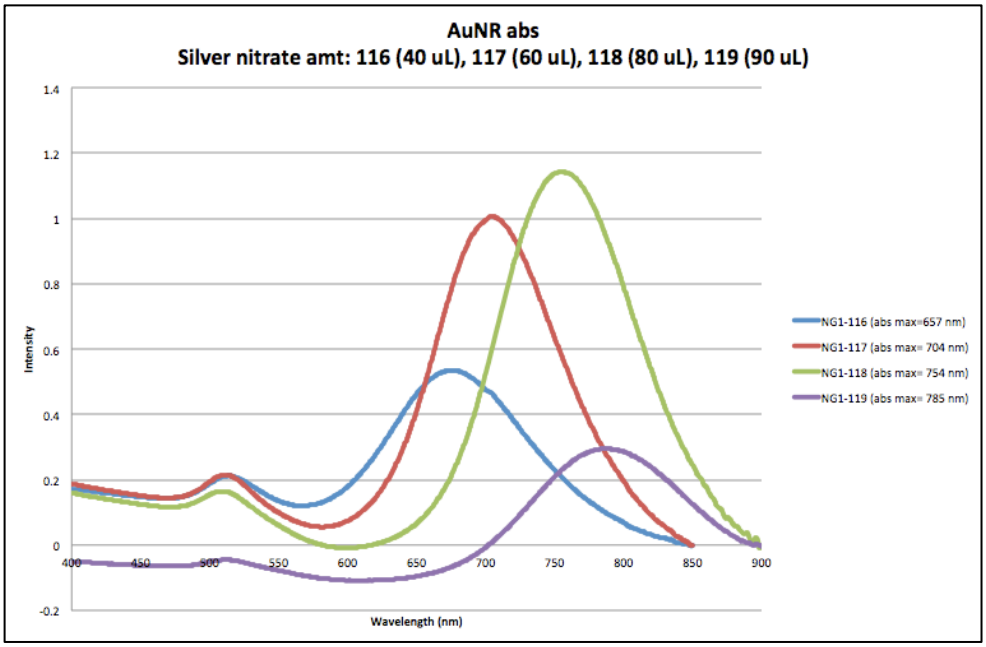

Figure 5.10. Absorbance spectra of gold nanorods grown under ideal surfactant conditions.

Gold nanorod growth can be easily monitored qualitatively by monitoring the gradual blue-purple color development as the seeds begin to form rods with aspect ratios higher than ~1.2. The rod growth continues to quickly develop, pushing the longitudinal plasmon further towards the near IR (NIR), giving the rods a pale peach color at higher aspect ratios like 3.8 (Figure 5.11).

Figure 5.11. (left) Reaction vials of gold nanorod preparation: Seed solution (brown) 40-90 µL of silver nitrate added (respectively); (right) GNR 40-90 µL (respectively) with excess CTAB (white crystals seen left) removed via centrifugation.

Colorimetric and spectroscopic details provide quick qualitative measures of successful nanorod growth but TEM imaging provides the best possible measure of aspect ratio and quality of rod formation. Figures 5.12 and 5.13 show a clear increase of aspect ratio from 2.7 (40 µL silver nitrate added) to 3.8 (90 µL silver nitrate added). This excellent control over aspect ratio allows the longitudinal band to be finely tuned to optimize gold nanorods as plasmonic waveguides.

Figure 5.12. TEM image of gold nanorods with average AR of 2.7 (see Figure 5.10 for absorption spectrum).

Figure 5.13. TEM image of gold nanorods with average AR of 3.8 (see Figure 5.10 for absorption spectrum).

The purity of reagents also has been found to have a profound impact on the development of gold nanorods even once a proper CTAB surfactant concentration is established. Iodide ions in the PPM can ruin a GNR prep by increasing the amount of isotropic morphologies in the mixture.[19] This led to the need for elevated amounts of silver nitrate required to produce small aspect ratio gold nanorods as the CTAB used in these preparations was 98% grade. Silver nitrate is thought to exchange with the bromide on the ammonium head group of CTAB and that AgBr is the actual anisotropic promoting species.[18] Small amounts of iodide ions lead to an inconsistent use of silver nitrate in replicate preparations of similar aspect ratio nanorods.

Preparing gold nanorods by the seed mediated growth method allowed for a fine-tuned control over the size and uniformity of the sample. Slight variations in the procedure were capable of hindering the process but can these obstacles could be overcome by carefully monitoring each additive. The ability to form well-shaped and uniform gold nanorods then allowed for the study of exchanging end surfactant molecules with dye-doped silica nanoparticles.

5.3.2 Investigation of End-Cap Aggregation of Gold Nanorods and Dye-Doped Silica Nanoparticles

In order to address preferential nanorods end-cap binding we investigated the role of dye-doped silica nanoparticles surface functionalization had on desired aggregation to establish a longitudinal waveguide orientation. Amine and thiol capping agents were investigated for their efficacy in aggregating with CTAB coated gold nanorods in aqueous suspensions. Thomas et al showed adding mercaptopropionic acid (MPA) to a mixture of GNR they would preferentially align end to end via self

assembly through hydrogen bonding of the acids.[3] Rubpy-doped SiNP were functionalized with aminopropyltriethoxysilane (APTES) and mercaptopropyltrimethylsiloxane (MPTMS) before mixing with gold nanorods in water.

Rubpy-doped SiNP were taken from a reverse emulsion silica nanoparticle preparation (discussed in chapter II) and independently coated with amine and thiol ligands. The resulting colloids were washed several times with water in order to remove excess reagents before being mixed with gold. Figure 5.14 shows a larger drop in the absorbance of free gold nanorods over 7 days for amine coated particles compared to those coated in thiol. The loss of transverse and longitudinal plasmon bands in the amine SiNP + GNR 7 day spectrum is indicative of little-to-no prescence of gold particles left intact. This is not desirable as a controlled, end-cap preferential, binding is desired to promote waveguide formation. GNRs mixed with thiol-coated particles maintained a small distribution of nanorod absorbance after 7 days (orange line) indicating that significant, but not complete, aggregation has occurred. This is still not the desired degree of aggregation but is closer to optimal binding than the amine coated particles.

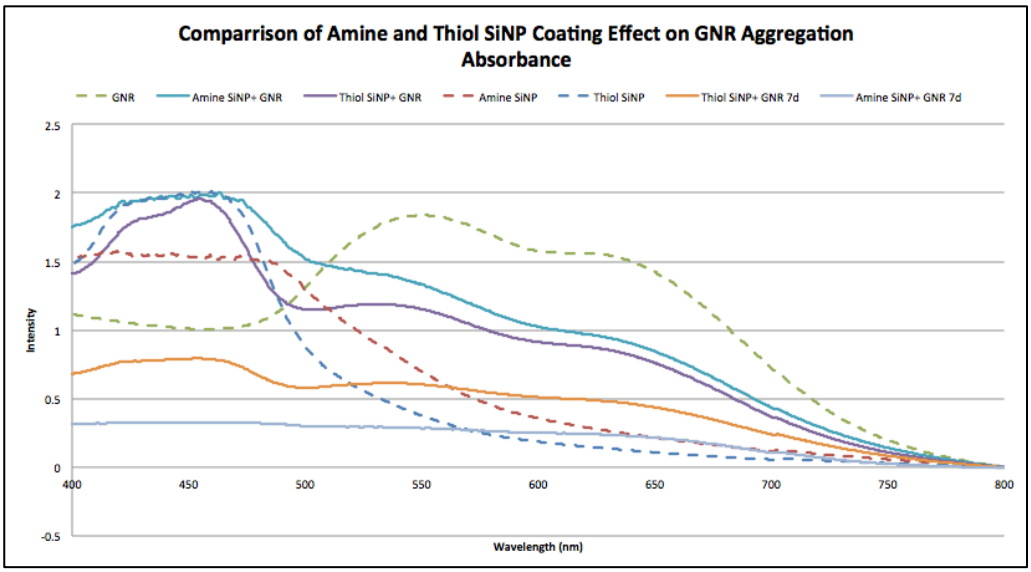

Figure 5.664. Absorption spectra of gold nanorods mixed with amine and thiol coated dye-doped silica nanoparticles.

The emission spectra of the amine and thiol SiNP-GNP aggregate systems are shown in Figure 5.15. Emission spectra of dye-doped silica nanoparticles are useful not only for monitoring the photophysical outcomes of aggregation but also of determining a relative concentration of the particles. It is interesting to note that there are relatively more thiol coated nanoparticles than amine used in each preparation based on the relative emission (these variations are common as the centrifugation/ sonication cleaning process involves some loss during multiple solution changes) even though the amine clearly aggregated with gold more rapidly and completely based on absorbance shifts.

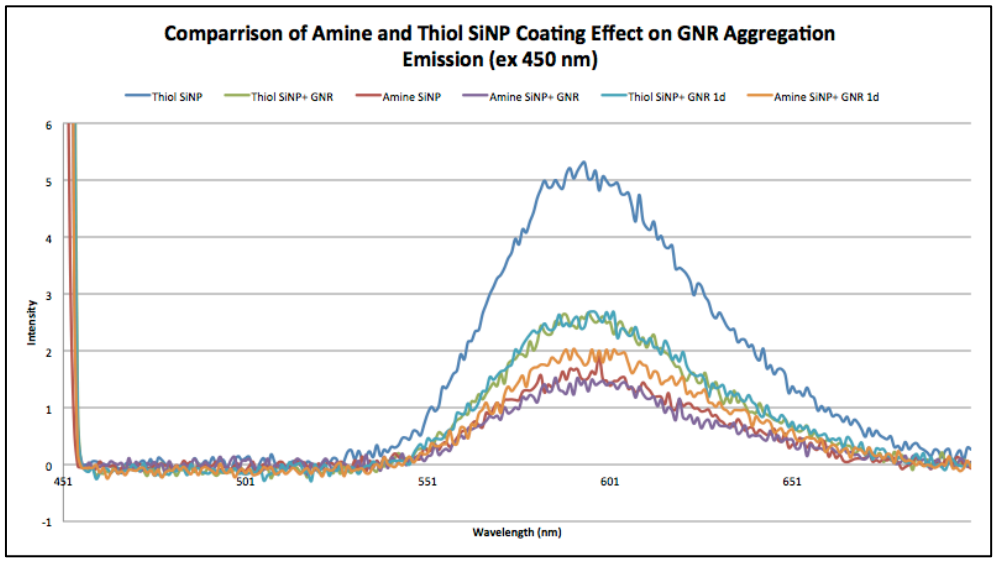

Figure 5.15. Emission spectra of gold nanorods with amine and thiol coated silica nanoparticles.

We did observe an aggregation dependence on silica functionality but these results do not support emission brightness increases via metal enhanced fluorescence. Note that the fluorescence initially drops in both samples due to dilution of the samples upon addition of the nanorods. The dilution factor was accounted for when determining whether or not enhancement occurred by preparing similarly diluted standards for comparrison. Furthermore, these spectra are the net sum of constructive near and destructive far-field interactions with the longitudinal plasmon. Gold nanorods strongly absorb in the same region of emission the Rubpy-doped silica nanoparticles (Figure 5.14). Thus, emitted light from unbound particles may not escape the cuvette due to absorption from gold nanorods that are farther away than the constructive MEF distance (~10-100 nm) commonly reffered to as ‘inner-filtration effects’.

While the emission spectra are not particularly telling, the absorption spectra can be used to measure the quality of the aggregation. Silica nanoparticles with greater gold

association constants reduce the characteristic absorption profile of the gold nanorods faster than those that don't bind as well. For example Figure 5.14 shows a clear drop in both the transverse (λ_{max} = 550 nm) and longitudinal (λ_{max} = 650 nm) plasmon resonance modes (green dotted line) at 7 days following the addition of amine coated silica nanoparticles (light-blue line). However, the thiol coated particles maintain broad peaks related to absorption of the Rubpy-doped silica nanoparticles as well as the longitudinal and transverse plasmon of the gold nanorods after seven days (Figure 5.14). These results suggest that thiol coating may perhaps be a more efficient weak binding source that may be tunable, via controlling silica nanoparticle concentration *vida infra*, as a method for aggregating SiNP only at the more readily dissociated CTAB end-cap regions of the GNRs while the amines more aggressively bind at both the ends and the lateral faces non-selectively. Unfortunately, these samples were taken before our group began running TEM measurements so this conclusion is based on a number of spectral experiments similar to the experiment shown in Figure 5.14 and 5.15. Investigating the absorbance spectra for a selective drop in longitudinal plasmon in a sample with a low concentration of thiol coated silica nanoparticles in comparison to gold nanorods would further examine this conclusion.

Our goal is to use silica nanoparticle surface functionality to bind silica nanoparticles to the end-caps of gold nanorods. Amine and thiol silica nanoparticle coatings provide additional means for fine-tuning their aggregation with gold nanorods. The ideal ligand will bind tightly to gold following the dissociation of CTAB but has a low enough affinity to only associate at the end caps of the nanorods where the surfactant dissociation is highest. Thus, we hypothesize that maintaining a relatively

small concentration of SiNP in the presence of a large concentration of GNR will lead to selectively binding at the more easily accessible end-caps only as we press towards a hetero-SiNP gold nanorod aggregate.

5.3.3 Investigation of Relative Concentration Effects of Gold Nanorods and Dye-doped Silica Nanoparticles

In order to examine the effect of silica nanoparticle functionalization on end-cap gold nanorod aggregation we studied the effect of changing the concentration of silica and gold in solution to determine the driving force behind the previously observed non-selective aggregation (Figure 15.14). Aggregation of two silica nanoparticles for every one gold nanorod provides the optimal relative concentration for just end-cap binding without aggregation along the transverse face (Figure 5.2). Inner filtration effects may also be investigated by varying the amount of SiNP and GNR while monitoring the change in fluorophore emission. Presumably a larger concentration of gold nanorods will decrease the emission intensity relative to those samples with less gold. We hypothesize that selective end-cap binding can be monitored by comparing the change in absorbance intensity of the transverse and longitudinal peaks of the gold nanorod while fluorophore emission data will support a decreased emission signal due to inner filtration effects.

In order to get preliminary data on our ability to preferentially bind SiNP to the end caps of GNR the two species (gold nanorods AR ~2.7, and thiol coated silica nanospheres 40 nm diameter) were combined in aqueous solutions and monitored by UV-vis and fluorescence spectroscopy. Ten samples were created (five experimental and 5 control) with increasing concentration of thiol-coated Rubpy-doped silica

nanoparticles (Rubpy@SiNP-SH) while the amount of gold was held constant in each sample. The longitudinal and transvers plasmon resonance absorptions (625 and 525 nm respectively) were monitored for relative decreases indicating physical overlap of the fluorophore dipole with the specific mode of the nanorod's electric field. Figure 5.16 shows the absorption of each sample in the titration. Interestingly, the addition of silica particles virtually destroys the GNR absorption after the first addition. The transverse and longitudinal plasmon resonances are visible only after larger amounts of SiNP are added. This is counter to previous results (Figure 5.14) where the GNR absorbance proportionally decreased with increasing amounts of silica. The reason for this is not immediately clear but it is noteworthy that several of these samples (Figures 15.17-21) showed fluorescent enhancement of the Rubpy-doped silica nanoparticles. Thus, a possible explanation for the increase seen in the gold band absorption upon increased dye-doped silica is the coupling of the fluorophore dipole and plasmon resonance increased the overall absorption of the complexed 'plasmophore' species.[4] Increasing the thiol coated Rubpy-doped silica nanoparticles then increases the number of aggregates in solution and thus the number of pathways for absorbing light into the plasmophore. Further TEM studies would be needed to support this argument.

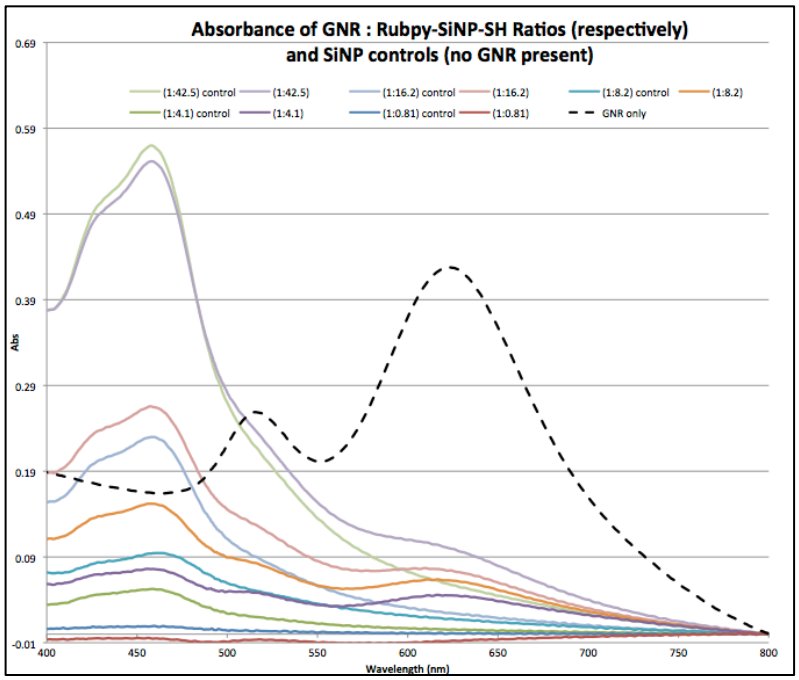

Figure 5.16. Absorption spectra of varying concentrations of dye-doped silica nanoparticles in the presence of constant concentration of gold.

The emission spectra showed a small amount of fluorescent enhancement for each sample. Figure 5.17 shows a clear increase from the control sample that had no GNR present. The increase in emission intensity supports a successful coupling of the silica nanoparticles to the nanorods.

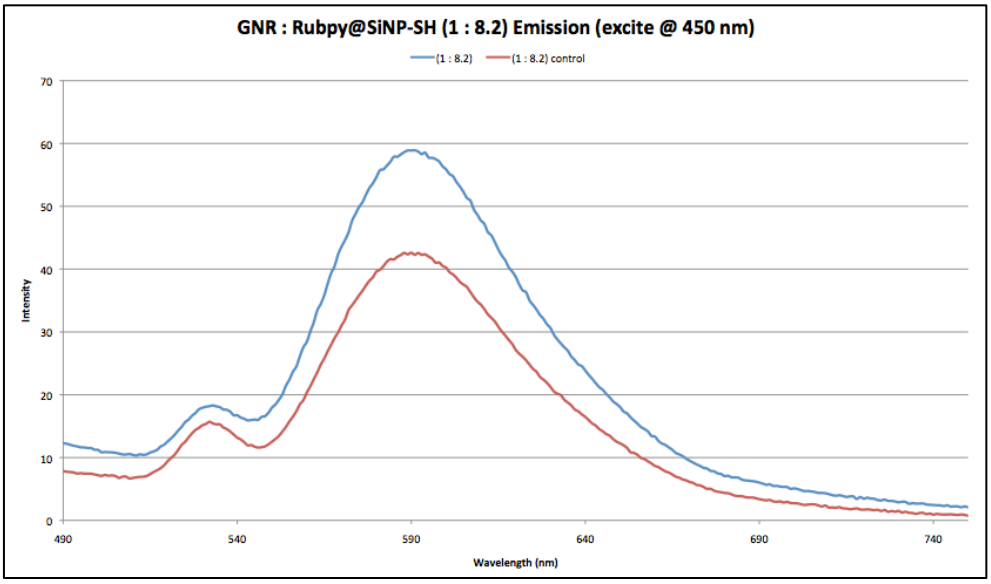

Figure 15.17. Emission spectrum of gold nanorod/ Rubpy-doped silica nanoparticle (1:8.2) aggregation.

The largest fluorescent enhancement was seen when the gold nanorods were at a ratio of 1:8.2 with Rubpy-doped silica (Figure 15.17). This followed a general trend of increasing enhancement as the amount of silica increased. However, as the silica concentrations grew in large excess of the gold nanorods (1:16.2) the enhancement began to decrease (Figure 15.18).

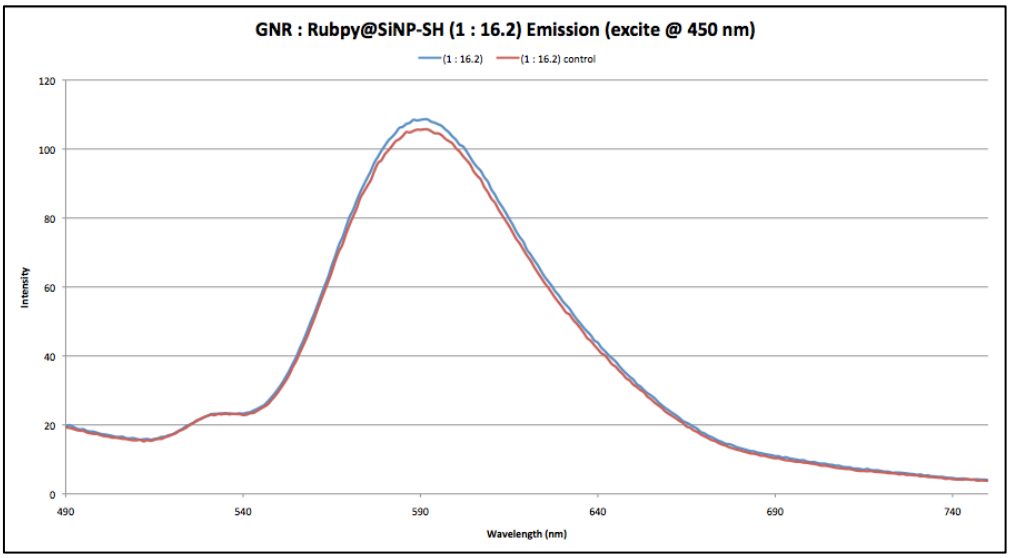

Figure 15.18. Emission spectrum of gold nanorod/ Rubpy-doped silica nanoparticle (1:16.2) aggregation.

As the concentration of silica grew even larger (1:42.5) an overall decrease was observed in the emission intensity (Figure 15.19). This data suggests that there is an upper limit to the amount of silica that can efficiently bind to gold nanorods to establish a beneficial dipole plasmon interaction, which is displayed in this case as metal enhanced fluorescence. It is also important to note the variation in the two emission bands of Rubpy as the concentration of silica changes. The emission band at 530 nm is often dominant over the band at 590 nm at low concentrations but it is not clear at this moment what causes the variations in these bands or if the gold nanorods have any effect on their relative heights.

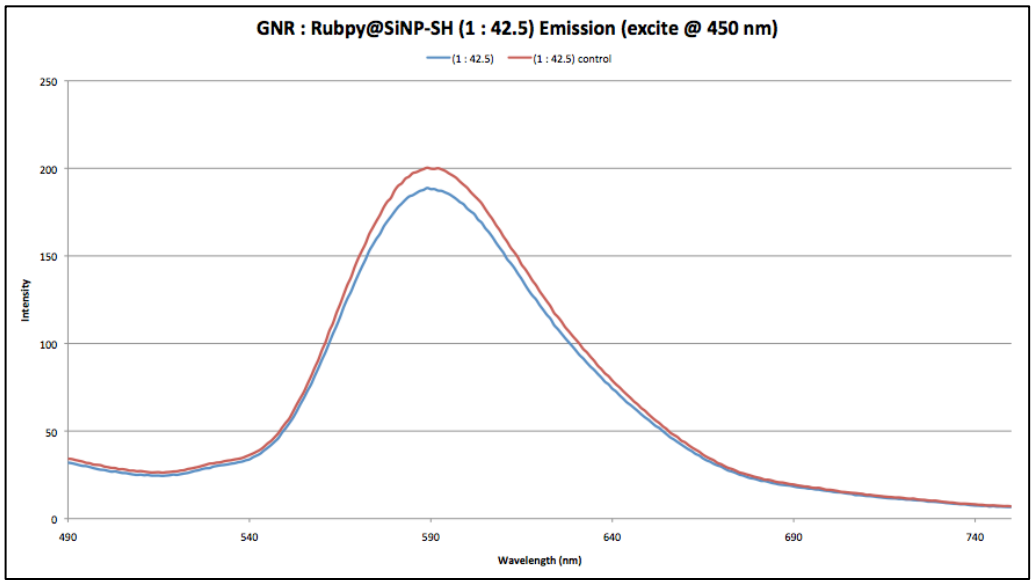

Figure 15.19. Emission spectrum of gold nanorod/ Rubpy-doped silica nanoparticle (1:42.5) aggregation.

A summary of the difference in emission and absorption intensities of the silica nanoparticle titration are shown in Figure 15.20. The x-axis units are in reference to the equivalents of Rubpy@SiNP-SH) added to one equivalent of GNR. The fluorescent peaks refer to the second λ_{max} (~590 nm) (see Figures 15.17-19). This analysis is useful because we can directly compare the changes in gold aggregation, via the absorbance spectra, to the changes in the fluorophore, via changes in the emission spectra. We would expect that as more silica binds to gold nanorods that the emission should increase while the GNR absorbance decreases. Instead, the change in the gold absorption appears to be tracking proportionally with the increase in fluorescence (Figure 15.20, samples 4.1-16.2). This supports the model that the gold and fluorophore act as a single *plasmophore* complex instead of independent particles.

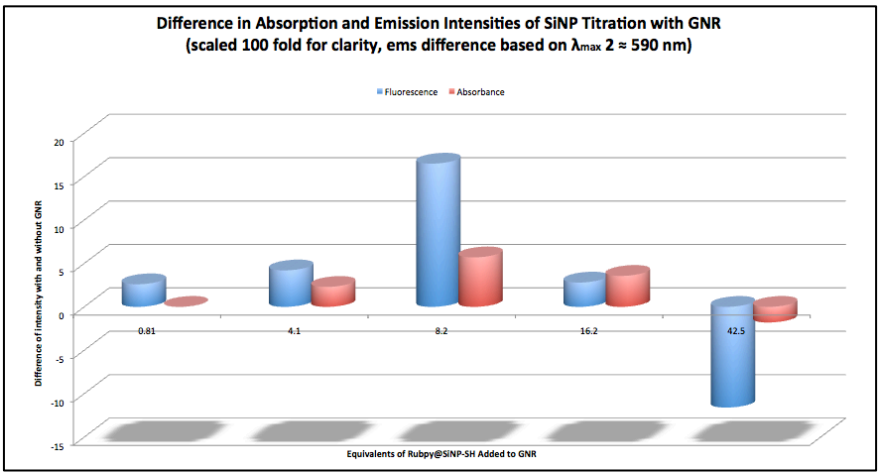

Figure 15.670. Comparison of changes in emission and absorption intensities as increasing amounts of thiol coated Rubpy-doped silica nanoparticles are mixed with gold nanorods.

TEM analysis later showed that the 1:8.2 sample was not as close to this ratio as previously predicted by calculations but did possibly display desired end-cap aggregation in some images (Figure 15.21). It is difficult to quantitatively predict the amounts of material in a given sample (concentration calculations are shown in the experimental and methods section). However, it is also important to note that TEM images were produced by drop coating sample onto formvar coated grids. It is likely that gold and silica material do not interact with the substrate identically, which may skew the proportions of each material on the grid. Further studies are needed to confirm the relationship between concentration of silica nanoparticles and gold nanorods.

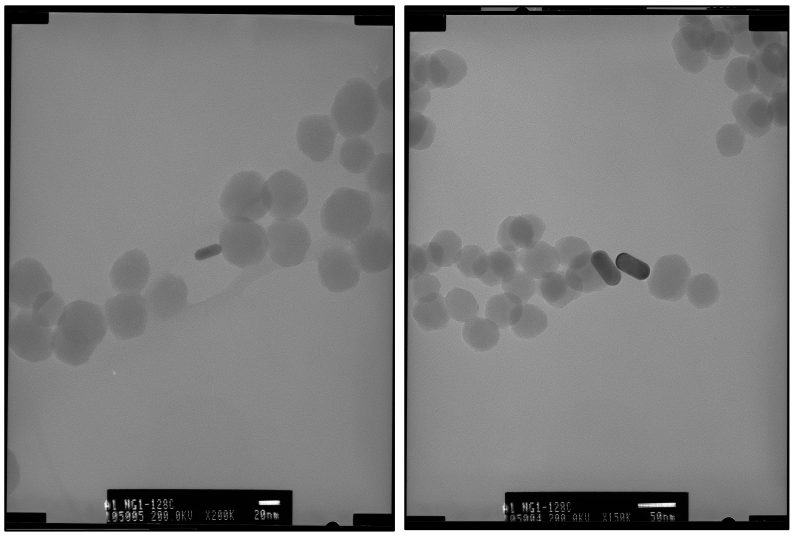

Figure 15.21. TEM images of GNR : Rubpy-doped silica nanoparticles (1:8.2) (from Figure 15.17).

We investigated increasing Rubpy-doped silica nanoparticles relative to gold nanorods in order to study the optimal concentrations for selective longitudinal aggregation. The degree of aggregation was measured by monitoring absorbance and emission spectra. We found that increasing the amount of silica to 16.2 equivalents of gold nanorods produced enhancement, but a decrease in emission intensity was seen beyond this (Figure 15.20). We can only conclude that concentration does play an important role in the aggregation, and thus the plasmonic interaction, of gold nanorods and dye-dope silica nanoparticles. Further studies showing a clear trend between decreasing absorbance, supported by TEM imaging, and increasing emission of the dye are needed to determine the ideal concentration of silica nanoparticles and that this effect will certainly be a factor in hetero-dye systems.

5.3.4 Investigation of Spectral Overlap of Dye-doped Silica Nanoparticles and Gold Nanorods – Rubpy and Cy3

In order to demonstrate a plasmon mediated FRET system we attempted to mix FRET donor-doped SiNP (Rubpy) with FRET acceptor-doped SiNP (Cy3) in the presence of gold nanorods. The goal was to determine, by monitoring a decrease in donor emission with a coinciding increase in acceptor emission, if gold nanorods would serve as an acceptable energy transfer agents between two different dye-doped silica nanoparticles.

Spectral overlap between the relative absorbance and emission profiles of the fluorophores and gold nanorods is key to establishing a long range FRET-like interaction. Individual fluorophores must be separately investigated as spectral features are inherent to specific dyes while the SiNP/GNP association constant and the relative concentrations can be fine-tuned synthetically. These experiments have only begun to be explored by our group and their study is ongoing as they represent one of the most important areas of the project.

In order to establish a plasmon mediated energy transfer system we first examined the aggregation of gold nanorods and thiol functionalized FRET-paired donor (tris(bipyridine)ruthenium(II) chloride) (Rubpy) and acceptor (1,1′-diethyl-2,2′-carbocyanine iodide**)** (Cy3) dye-doped silica nanoparticles in order to form desired end-cap aggregation (Figure 5.2). We hypothesize that titrating GNR in increasing amounts will slowly change the landscape of the fluorescence spectrum by decreasing the Rubpy emission (λ_{max}= 590 nm) while simultaneously increasing the Cy3 emission (λ_{max}= 620 nm) until the Cy3 signal will come to dominate the spectrum (see Figure 15.22).

The emission band of Rubpy (λ_{max}= 590 nm) and the absorption of Cy3 at (λ_{max}= 560 nm) and (λ_{max}= 610 nm) provide good overlap for energy to be transferred from an excited Rubpy to a ground state Cy3 (FRET) (Figure 15.22). Several issues to address regarding the measurements being used to investigate waveguide utility include the emission strength of each dye. The concentration of Cy-doped silica nanoparticles had to be increased ten-fold with respect to Rubpy-doped SiNP in order to produce similar intensities of emission. Figure 15.24 shows essentially only the emission spectra of Rubpy when only 5 μL of GNR have been added at an intensity of 16. The same sample shows an emission intensity of 14 for a ten-fold increased concentration of Cy3 when excited at 560 nm (Figure 15.25). Furthermore, the Stoke's shift of Rubpy is very large (150 nm) while Cy3 is relatively small (10 nm). Thus, it may be difficult to resolve if directly exciting Cy3 at 610 nm plays a role in the emerging signal as this incident light neccesarily overlaps with the Cy3 emission wavelength at 620 nm at large slit widths (Figure 15.22).

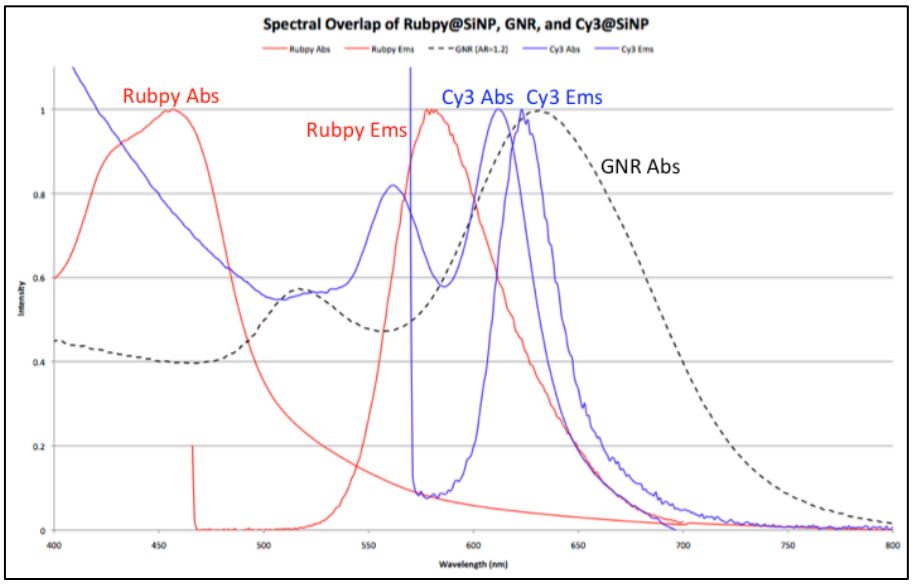

Figure 15.22. Normalized spectral overlap of Rubpy and Cy3 doped silica nanoparticles along with the absorbance of gold nanorods.

An ideal FRET experiment would involve matching a donor dye that has significant emission overlap with the absorption of an acceptor dye so that, upon excitation of the donor dye, energy is non-radiatively transferred to the acceptor dye.[20] The FRET efficiency would be monitored by a decreasing donor emission signal with a simultaneous increase in the acceptor emission. Initial investigations of FRET-like nanorods mediated energy transfer were performed with a 1:1 mixture of Rubpy and Cy3. It would be ideal to monitor the decrease in Rubpy fluorescence as the Cy3 fluorescence is increasing to confirm FRET is indeed occurring but this may not be possible if the Cy3 peak is dwarfed by the emission of Rubpy. Thus, an alternative GNR titration was setup using a using a 1:10 (Rubpy:Cy3) concentration to allow for the possibility of the Cy3 peak overtake the strongly emitting Rubpy fluorescent signal and gold nanorods were then added in separate increasing amounts.

Figure 5.23 shows the absorbance spectra for each titration of gold nanorods. The first 5 µL addition shows only a small longitudinal plasmon peak from the gold and absorption from Cy3 at ~615 nm with a significant Rubpy absorption at 450 nm. Increasing to 100 µL shows a spectrum dominated by gold transverse (530 nm) and longitudinal (620 nm) plasmon absorption indicating that the bulk of light absorbed in the system is into the gold. It is interesting to note that the 200 µL sample is red-shifter approximately 5 nm and shows a lower plasmon absorption than the 100 µL sample. This may be due to the formation of a slight shoulder that develops ~660 in concentrations above 100 µL. The development of a absorbance shoulder typically indicates aggregation has occurred as the plasmons couple between gold molecules (chapter III) but we are not able to conclude this without TEM measurements.

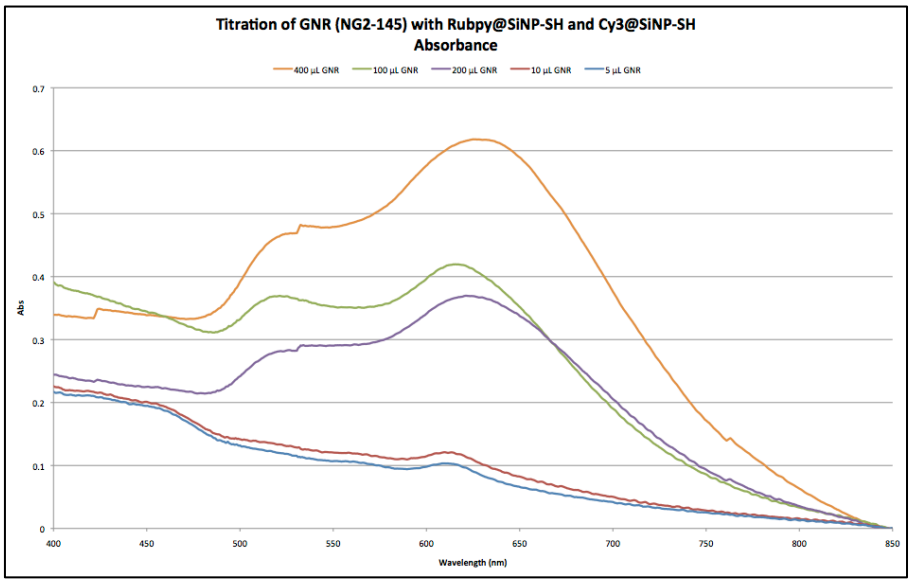

Figure 15.23. Absorbance spectra of Rubpy-doped SiNP, Cy3-doped SiNP, and GNR

Figure 15.24 shows the emission of Rubpy-doped SiNP, Cy3-doped SiNP, and GNR (AR~2.7) that have been excited at 450 nm. No energy transfer was observed in

this study as the decreasing emission of Rubpy-doped SiNP was not replaced by an increase in Cy3-doped silica nanoparticles. It is possible that energy is indeed being transferred between the two species but that the Cy3 emission is being re-absorbed, via far-field absorption (see gold nanorod absorption overlap with Cy3 emission in Figure 15.22). Re-absoprtion could be confirmed by monitoring the emission of Cy3 upon direct excitation at 560 nm.

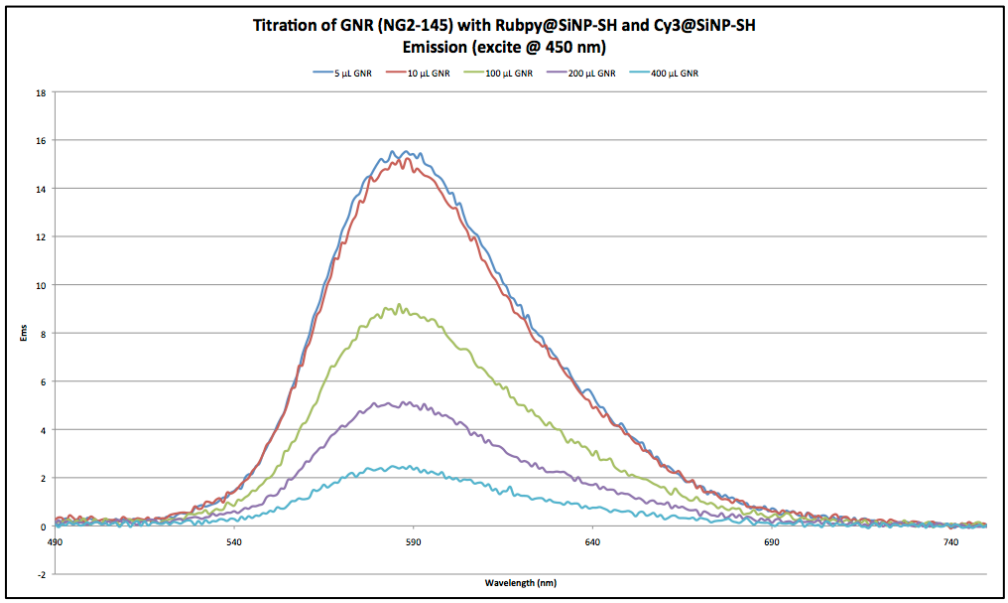

Figure 15.24. Emission spectra of Rubpy-doped SiNP, Cy3-doped SiNP, and GNR (AR~2.7). Excited at 450 nm.

Figure 15.25 confirms a decrease in Cy3 emission (620 nm) upon direct excitation at 560 nm. This supports the theory of Cy3 re-absorption but does not indicate if energy transfer is occurring. The excitation spectra were then investigated to determine the amount of light Rubpy-doped SiNP and Cy3-doped SiNP absorbed to produce emission at 620 nm.

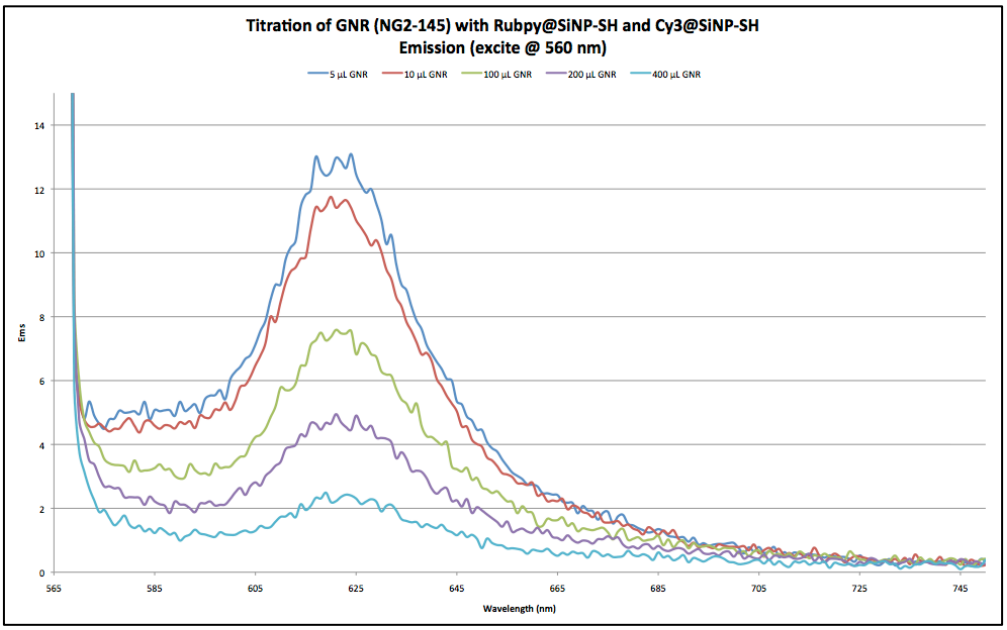

Figure 15.25. Emission spectra of Rubpy-doped SiNP, Cy3-doped SiNP, and GNR (AR~2.7). Excited at 560 nm.

The excitation spectra for the mixtures of Rubpy-doped SiNP, Cy3-doped SiNP, and GNR are shown in Figure 15.26. Excitation spectra are significant because they account for which spectral regions, and thus fluorophores, are responsible for emitted light. We would expect to see a slightly lower excitation peak for Rubpy-doped SiNP (450 nm) than Cy3-doped silica nanoparticles (560 nm) if there is no energy transfer between the two fluorophores as Rubpy emits less intensely than Cy3 at 620 nm (Figure 15.22). Rubpy-doped silica nanoparticles display a lower excitation profile than Cy3-doped silica nanoparticles, which indicates that no energy transfer is occurring.

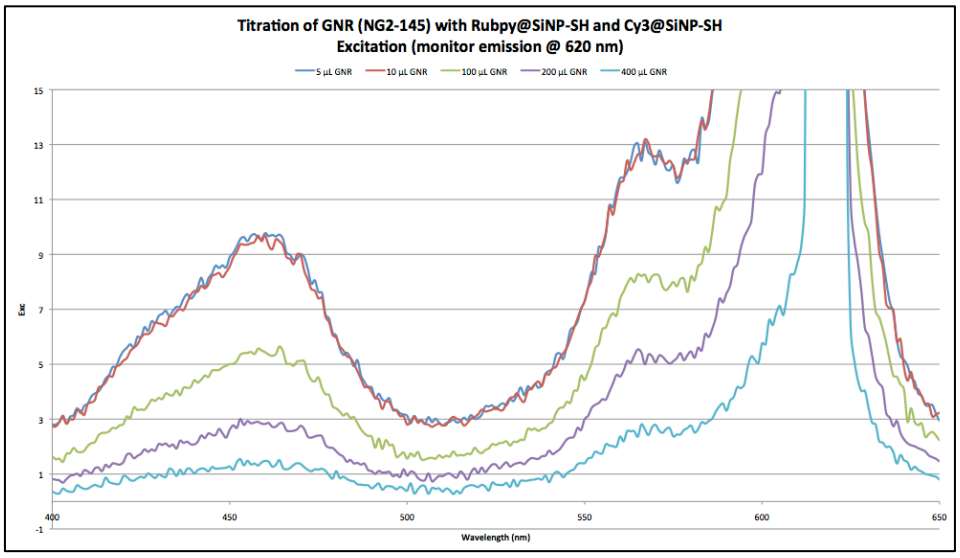

Figure 15.26. Excitation spectra of Rubpy-doped SiNP, Cy3-doped SiNP, and GNR (AR~2.7). Emission monitored at 620 nm.

We measured the gold nanorod mediated energy transfer between Rubpy-doped and Cy3-doped silica nanoparticles. A succesful energy transfer experiment would have yielded increasing emission of the acceptor dye (Cy3, 620 nm) with a simultaneous decrease in donor emission (Rubpy, 590 nm). These spectra do not indicate energy transfer between the two dye species but they do provide insight to the re-absorption of emitted light from Rubpy and Cy3 by the gold nanorods. The nanorods long tail into the red clearly has an effect to decrease the emission via far-field inter system absorption at 620 nm which may mask any increased Cy3 emission (Figure 15.22). There is no immediate method for determining if the gold is quenching the fluorescence in the near-field or absorbing far from this study. Further studies are needed to explore different dyes and a range of longitudinal plasmon absorptions. It would be preferable to have a red-shifted acceptor (>700 nm) fluorophore absorption to minimize any far-field effects.

Furthermore, a greater Stoke's shift (> 10 nm), similar to Rubpy (150 nm), in the acceptor would provide a more dramatic demonstration energy transfer.

Initial attempts to produce plasmon mediated FRET-like energy transfer show that much work is still needed in this area. However, these spectral overlap investigations lay the groundwork for more advanced experiments as the Halterman lab's precision of synthesis, modification, and aggregation increases. The potential of long-range radiationless energy transfer by aggregating dye-doped silica nanoparticles with gold nanorods is an exciting frontier in the area nanophotonics and materials chemistry and is an area of ongoing research in our lab.

5.4 Chapter Summary

This chapter described the need for and our efforts to employ gold nanorods as nanowaveguides[1] in order to establish radiationless plasmon resonance mediated energy transfer over a long range by aggregating fluorophore-doped silica nanoparticles at the end-caps of the rods.

Gold nanorods were prepared by a previously established seed-mediated growth method[12] and studied by UV-Vis absorption and TEM imaging before being aggregated with dye-doped silica nanoparticles. The growth of the nanorods allows fine-tuned control over the size and shape of the rods by varying the amount of silver nitrate in the growth solution. However, this process is sensitive to changes in conditions such as CTAB concentration and the presence of iodide ions from impure surfactants, which can lead to inconsistent preparations (Figures 15.27 and 15.28). High quality gold nanorods can be grown in the seed-mediated growth preparation by carefully

monitoring the conditions mentioned above. The well-formed nanorods can then be employed in end-cap aggregation studies with dye-doped silica nanospheres.

In order to address preferential nanorods end-cap binding we investigated the role of dye-doped silica nanoparticles surface functionalization had on desired aggregation to establish a longitudinal waveguide orientation. Amine and thiol capping agents were investigated for their efficacy in aggregating with CTAB coated gold nanorods in aqueous suspensions. The amine coated particles bound more readily to the gold surface compared to the thiol coated silica (Figure 5.14). The ideal ligand will bind tightly to gold following the dissociation of CTAB but has a low enough affinity to only associate at the end caps of the nanorods where the surfactant dissociation is highest. Thus, thiol coatings were further investigated to determine if they would act as viable ligands for end-cap binding by varying the concentration of thiol-coated silica in the aggregate system.

In order to examine the effect of silica nanoparticle functionalization on end-cap gold nanorod aggregation we studied the effect of changing the concentration of silica and gold in solution to determine the driving force behind the previously observed non-selective aggregation (Figure 15.14). We hypothesized that selective end-cap binding could be monitored by comparing the change in absorbance intensity of the transverse and longitudinal peaks of the gold nanorod while fluorophore emission data would support a decreased emission signal due to inner filtration effects. We found that increasing the amount of silica to 16.2 equivalents of gold nanorods produced enhancement, but a decrease in emission intensity was seen beyond this (Figure 15.20). We can only conclude that concentration does play an important role in the aggregation,

and thus the plasmonic interaction, of gold nanorods and dye-dope silica nanoparticles and that this effect will certainly be a factor in hetero-dye systems.

We attempted to mix FRET donor-doped SiNP (Rubpy) with FRET acceptor-doped SiNP (Cy3) in the presence of gold nanorods in order to demonstrate a plasmon mediated FRET system (Figure 15.22). The goal was to determine, by monitoring a decrease in donor emission with a coinciding increase in acceptor emission, if gold nanorods would serve as an acceptable energy transfer agents between two different dye-doped silica nanoparticles. Our system apparently failed to transfer energy through a gold nanorod (Figure 15.24) but we did see evidence of potential plasmonic influence by a decrease in the over emission intensity of the fluorophores (Figures 15.24 and 15.25). Furthermore, Rubpy-doped silica nanoparticles displayed a lower excitation profile than Cy3-doped silica nanoparticles, which indicated that no energy transfer was occurring (Figure 15.26). We concluded that energy transfer may still be occurring in the system but that re-absorption by the gold nanorods or heavy overlap of the Rubpy emission (both at 620 nm) may be masking any additional fluorescence of Cy3 (Figure 15.22). The potential of long-range radiationless energy transfer by end-cap aggregation of dye-doped silica nanoparticles with gold nanorods is an exciting frontier in the area nanophotonics and materials chemistry and is an area of ongoing research in our lab.

Final Conclusions and Future Directions

Incorporating fluorophores into silica nanoparticles provides a scaffold for aggregation with gold nanomaterials in order to overlap the plasmon resonance with the fluorophores to produce metal-enhanced fluorescence and plasmonic waveguides. The quality of the enhancement is highly dependent on the distance

between the surface of the metal and the dye. Thus, the layered dye-doped silica nanoparticle preparation is well suited to place the metal within a discrete location of the silica matrix. The layered preparation also prepares uniformly small diameter particles, which are ideal for coupling multiple gold nanospheres together to increase scattering and thus increase the fluorescent brightness of the system.

Gold aggregation was promoted by functionalizing the surface of silica nanoparticles. The surface coatings ideally should promote gold-silica aggregation while minimizing silica-silica aggregation. Dithiocarbamate ligands should ideally fit this model but are difficult to produce and analyze. Thiol and amine ligands, the latter assayable by ninhydrin solution, were shown to be easily installed and produce silica-gold aggregation.

Multiple gold nanoparticles were bound around a single layered dye-doped silica nanoparticle functionalized with amines to produce desirable heteroaggregates. The aggregation was shown to increase with increasing concentration and size of the silica nanoparticles but no clear trend in enhancement was shown.

Future directions of this work involve incorporating the architecturally unique silica materials discussed in chapter II into investigations of MEF principles of spectral overlap, distance and concentration dependence of gold nanoparticle aggregates. Furthermore, the silica particles can be employed to study the possibility of plasmon mediated waveguides as discussed in this chapter.

5.5 Experimental and Methods

5.6.1 Seed mediated gold nanorod synthesis.[12]

An aqueous solution of cetyltrimethylammonium bromide (CTAB) (5 mL, 0.20 M) and chloroauric acid ($HAuCl_4$) (5 mL, 0.5 mM) were added mixed together in a new 20 mL scintillation vial containing a magnetic stir bar (1 cm) producing a bright yellow translucent mixture. Once the CTAB and $HAuCl_4$ were homogeneously mixed, ice-cold sodium borohydride ($NaBH_4$) (0.60 mL, 0.01 M) was added, all at once, under vigorous stirring, causing the solution to become a light peach color. This "seed solution" continued to stir for 2 minutes before being set aside.

The "growth solution" was then prepared. CTAB (9.5 mL, 0.1 M) was added to silver nitrate ($AgNO_3$) (40 μL, 0.01 M) while stirring. $HAuCl_4$ (0.5 mL, 0.01 M) was then added followed by ascorbic acid (55 μL, 0.1 M) causing the bright yellow solution to become clear. The growth solution was then allowed to sit, undisturbed, for 1 hour.

Finally, the nanorods were prepared by adding 12 μL of the seed solution to the growth solution. The clear mixture was gently mixed by hand before being left undisturbed for approx 12 hr. The solution slowly developed in color from light blue to dark blue, to reddish purple (depending on the amount of $AgNO_3$ added) as the particles grew in aspect ratio (AR). TEM confirmed the particles were well monodisperse and free of defects with an average AR of 2.7. The solutions color offers an easy qualitative analysis of how well formed the nanorods are or are not (Figures 15.26 and 15.27).

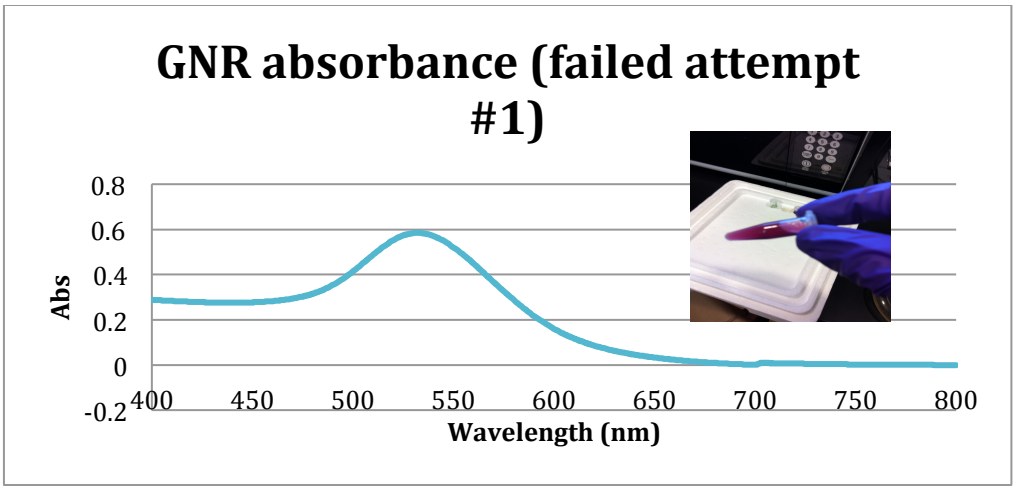

Figure 15.27. Image and spectra of failed GNR preparation suspended in CTAB/water.

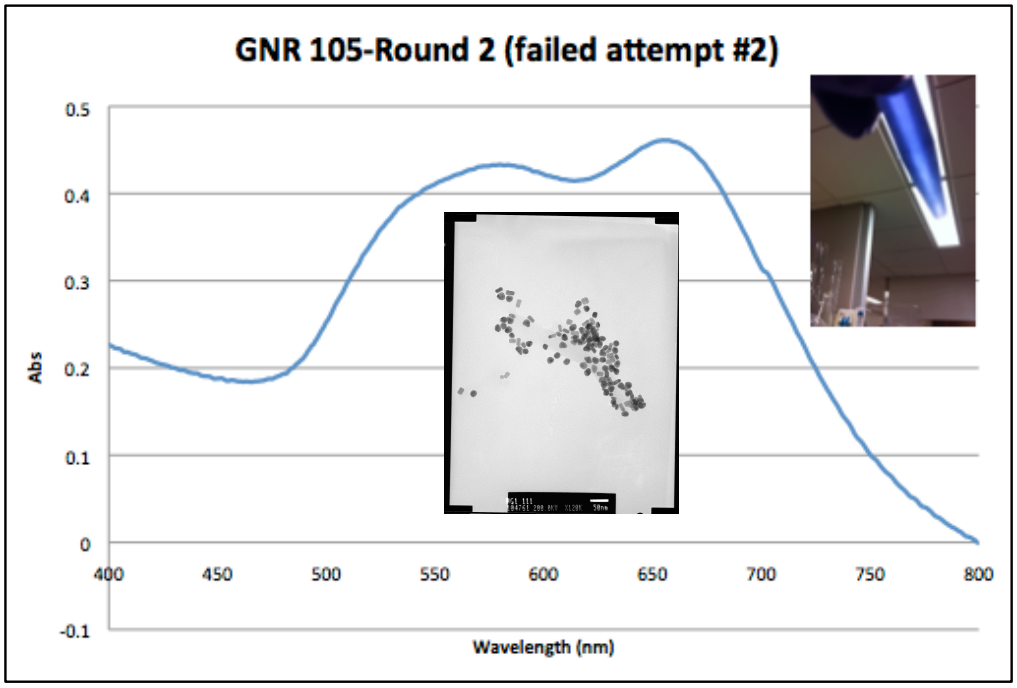

Figure 15.28. Image and spectra of failed GNR preparation suspended in CTAB/water.

5.5.2 Preparation of amine and thiol coated silica nanoparticles.

Reverse emulsion prepared SiNP (1.5 mL aliquot of stock) (from NG1-104) (see chapter II for discussion of silica formation and chapter III for coating protocols) were centrifuged at 15,000 rpm for 10 min to form a pellet. The supernatant was then

removed and the clean particles were re-suspended in water (1 mL, 17.8 MΩ) in a 1.5 mL pop-cap centrifuge tube. Next, glacial acetic acid (20 μL) was added and gently mixed before mercaptopropyltrimethyl siloxane (MPTMS) (20 μL) was added. The same procedure was separately used to prepare amine-coated particles by exchanging MPTMS with 3-aminopropyltriethoxysilane (APTES) (20 μL). The SiNPs were then rotary inverted over night at room temperature. Each sample was separately washed by the centrifugation/ sonication re-suspension process described above by 1X ethanol (1.5 mL, absolute) 2X with water (1.5 mL, 17.8 MΩ). The solutions were finally suspended in water (1 ml, 17.8 MΩ).

5.5.3 Aggregation of amine and thiol coated silica nanoparticles with gold nanorods.

Functionalized particles (0.5 mL, described above) were added to an aqueous solution of gold CTAB coated gold nanorods (0.5 mL, AR~ 2.7). The solutions were kept stirring at room temperature in 1.5 mL pop-cap centrifuge tubes for several days while measuring absorbance changes.

5.5.4 Relative concentration effects of dye-doped silica nanoparticles and gold nanorods.

Each solution was diluted ten-fold. Equivalents were calculated based on dry weights and assumed yields from starting materials. Table 5.1 below describes the contents of each sample and the respective control.

Sample	GNR added (2 nM)	GNR : SiNP	SiNP added(34 nM)
A	100 μL	1 : 0.81	4.77 μL
B	100 μL	1 : 4.1	23.89 μL

C	100 µL	1: 8.2	47.7 µL
D	100 µL	1 : 16.2	95.5 µL
E	100 µL	1 : 42.5	250 µL

Sample	Variable (water addn)	Control (water addn)
A	0.895 mL	0.995 mL
B	0.876 mL	0.976 mL
C	0.852 mL	0.952 mL
D	0.804 mL	0.904 mL
E	0.650 mL	0.750 mL

Table 5.1. Volumes of GNR and SiNP added in concentration dependent study.

5.5.5 Calculation of gold nanorods concentration.

Gold nanorods concentration was determined by assuming 100% conversion of chloroauric acid forming an ideal cylinder. Therefore, the area is given by equation 1:

$$V = \pi r^2 h \qquad (1)$$

A nanorod with an aspect ratio (AR) of 2.7 has a diameter of 13.5 nm and a length of 36.45 nm.

$$V = \pi(6.75\ nm)^2 47.5\ nm = 5{,}217\ nm^3$$

Gold crystals are face centered cubic (fcc) structures with a unit cell density of 0.068 nm^3.

$$\frac{5{,}217\ nm^3}{0.068\ nm^3} = 76{,}726.5\ {unit\ cells}/{nanorod}$$

Given the fcc orientation, there are four gold atoms per unit cell of a nanorod.

$$76{,}726.5\ {}^{unit\ cells}/_{nanorod} \times 4\ {}^{atoms}/_{unit\ cell} = 306{,}906\ {}^{atoms}/_{nanorod}$$

0.005 mmols of $HAuCl_4$ (0.5 mL of 0.01 M) was added to the *growth solution*, assuming a cylindrical shape neglects the rounded end-caps which are composed of gold nanospheres from the *seed solution*, giving:

$$\frac{6.02\times10^{23}\ {}^{atoms}/_{mol}}{5\times10^{-6}\ mols\ Au} = 3.01\times10^{18}\ Au\ atoms\ in\ growth\ solution$$

Assuming 100% conversion of gold atoms to nanorod formation gives:

$$\frac{3.01\times10^{18}\ atoms}{306{,}906\ {}^{atoms}/_{nanorod}} = 9.8\times10^{12}\ nanorods\ in\ stock\ solution$$

The total volume of the stock solution is 10.135 mL.

$$\frac{9.8\times10^{12}\ nanorods}{6.02\times10^{23}\ {}^{nanorods}/_{mol}} = 1.63\times10^{-11}\ mols\ of\ nanorods$$

$$\frac{1.63\times10^{-11}\ mols}{0.010135\ L} = 2\times10^{-9}\ M = 2\ nM\ solution\ of\ nanorods$$

5.5.6 Calculation of silica nanoparticles.

The number of silica nanoparticles were determined by measuring the dry weight before being suspended into an aqueous solution. The volume of a sphere is given by eq. 2.

$$V = \frac{4}{3}\pi r^3 \qquad (2)$$

The given spheres are approximately 60 nm in diameter, so:

$$V = \frac{4}{3}\pi 30^2 = 37{,}699.9\ nm^3$$

$$37{,}699.9\ nm^3 \times \left(\frac{1\ cm}{10^7 nm}\right)^3 = 3.77\times10^{-17}\ cm^3$$

Given the density of SiO_2 is 2.648 g/cm^3 than each silica sphere has a mass of:

$$3.77\times10^{-17}\ cm^3 \times 2.648\ {}^{g}/_{cm^3} = 9.9\times10^{-17}\ {}^{g}/_{SiNP}$$

The dried weight of SiNPs was approximately 2 mg.

$$\frac{0.002\ g\ SiNP}{9.9\times10^{-17}\ {}^{g}/_{SiNP}} = 2.02\times10^{13}\ SiNPs$$

The particles were re-suspended in 1 mL of water giving a concentration of:

$$\frac{2.02\times10^{13}\ SiNPs}{6.02\times10^{23}\ {}^{SiNPs}/_{mol}} = 3.3\times10^{-11}\ mols\ of\ SiNP$$

$$\frac{3.3\times10^{-11}\ mols\ of\ SiNP}{0.001\ L} = 3.4\times10^{-8}\ M = 34\ nM$$

5.5.7 Investigation of Spectral Overlap of Dye-doped Silica Nanoparticles and Gold Nanorods – Rubpy and Cy3 Initial FRET study.

Dye-doped silica nanoparticles were prepared using the reverse microemulsion method (discussed in chapter 2). Rubpy and Cy3 SiNPs were then washed 2X with ethanol (1.5 mL, 95%) and 1X with water (1.5 mL, 17.8 MΩ) before being re-suspended in water (1 mL, 17.8 MΩ). These aqueous stock concentrations were used directly in the gold nanorod titration. An aqueous solution of CTAB coated gold nanorods (AR~2.7) was prepared by the seed mediate growth method (see top of experimental section). The

samples were mixed together with water additions to provide the same dilution for each sample (1 mL total volume). Table 5.2 details the contents of each sample.

Sample id	AuNR added	Water added
A	5 µL	445 µL
B	10 µL	440 µL
C	100 µL	350 µL
D	200 µL	250 µL
E	400 µL	50 µL

Each sample contained:

5 µL Rubpy

500 µL Cy3

Table 5.2. Relative volumes of GNR added a constant mixture of Rubpy and Cy3 doped SiNP.

5.6 References

1. Maier, S. A.; Kik, P. G.; Atwater, H. A.; Meltzer, S.; Harel, E.; Koel, B. E.; Requicha, A. A. G., Local Detection of Electromagnetic Energy Transport Below the Diffraction Limit In Metal Nanoparticle Plasmon Waveguides. *Nature Mater.* **2003,** *2* (4), 229-232.

2. Wang, L.; Tan, W., Multicolor FRET Silica Nanoparticles by Single Wavelength Excitation. *Nano Lett.* **2006,** *6* (1), 84-88.

3. Thomas, G. K.; Barazzouk, S.; Ipe, B. I.; Joseph, S. S.; Kamat, P. V., Uniaxial Plasmon Coupling Through Longitudinal Self-Assembly of Gold Nanorods. *J. Phys. Chem. B* **2004,** *108*, 13066-13068.

4. Lakowicz, J. R.; Ray, K.; Chowdhury, M.; Szmacinski, H.; Fu, Y.; Zhang, J.; Nowaczyk, K., Plasmon-controlled Fluorescence: A New Paradigm in Fluorescence Spectroscopy. *Analyst* **2008,** *133*, 1308-1346.

5. Murphy, C. J.; Thompson, L. B.; Alkilany, A. M.; Sisco, P. N.; Boulos, S. P.; Sivapalan, S. T.; Yang, J. A.; Chernak, D. J.; Huang, J., The Many Faces of Gold Nanorods. *J. Phys. Chem. Lett.* **2010,** *1*, 2867-2875.

6. (a) Lazarides, A. A.; Schatz, G. C., DNA-Linked Metal Nanosphere Materials: Structural Basis for the Optical Properties. *J. Phys. Chem. B* **2000,** *104*, 460-467; (b) Jain, P. K.; Huang, X.; El-Sayed, I. E.; El-Sayed, M. A., Nobel Metals on the Nanoscale: Optical and Photothermal Properties and Same Applications in Imaging, Sensing, Biology, and Medicine. *Acc. Chem. Res.* **2008,** *41* (12), 1578-1586; (c) Zhang, J.; Fu, Y.; Chowdhury, M.; Lakowicz, J. R., Metal-Enhanced Single-Molecule Fluorescence on Silver Particle Monomer and Dimer: Coupling Effect between Metal Particles. *Nano lett.* **2007,** *7* (1), 2101-2107.

7. Sau, T. K.; Murphy, C. J., Seeded High Yield Synthesis of Short Au Nanords in Aqueous Solution. *Langmuir* **2004,** *20*, 6414-6420.

8. Joseph, S. S. T.; Ipe, B. I.; Pramod, P.; Thomas, G. K., Gold Nanorods to Nanochains: Mechanistic Investigations on Their Longitudinal Assembly Using alpha,omega-Alkanedithiols and Interplasmon Coupling. *J. Phys. Chem. B* **2006,** *110*, 150-157.

9. Barthas, J.; Colas des Francs, G.; Bouhelier, A.; Weeber, J.-C.; Dereux, A., Purcell factor for a point-like dipolar emitter coupled to a two-dimensional plasmonic waveguide. *Phys. Rev. B* **2011,** *84*, 073403.

10. Maier, S. A.; Kik, P. G.; Atwater, H. A.; Meltzer, S.; Harel, E.; Koel, B. E.; Requicha, A. A. G., Local Detection of Electromagnetic Energy Transport Below the Diffraction Limit in Metal Nanoparticle Plasmon Waveguides. *Nature Mater.* **2003,** *2*, 229-233.

11. Brongersma, M. L.; Hartman, J. W.; Atwater, H. A., Electromagnetic energy transfer and switching in nanoparticle chain arrays below the diffraction limit. *Phys. Rev. B* **2000,** *62* (24), 356-359.

12. Jana, N. R.; Gearheart, L.; Murphy, C. J., Seed-Mediated Growth Approach for Shape-Controlled Synthesis of Spheroidal and Rod-like Gold Nanoparticles Using a Surfactant Template. *Adv. Mater.* **2001,** *13* (18), 1389-1393.

13. Kelly, L. E.; Coronado, E.; Zhao, L. L.; Schatz, G. C., The Optical Properties of Metal Nanoparticles: The Influence of Size, Shape, and Dielectric Environment. *J. Phys. Chem. B* **2003,** *107*, 668-677.

14. Burda, C.; Chen, X.; Narayanan, R.; El-Sayed, M. A., Chemistry and Properties of Nanocrystals of Different Shapes. *Chem. Rev.* **2005,** *105*, 1025-1102.

15. Caswell, K. K.; Wilson, J. N.; Bunz, U. H. F.; Murphy, C. J., Preferential End-to-End Assembly of Gold Nanorods by Biotin-Steptavidin Connectors. *J. Am. Chem. Soc.* **2003,** *125*, 13914-13915.

16. Zijlstra, P.; Paulo, P. M. R.; Orrit, M., Optical detection of single non-absorbing molecules using the surface plasmon resonance of a gold nanorod. *Nature Nanotech.* **2012,** *379-382*.

17. Kioobakht, B.; El-Sayed, M. A., Preparation of Growth Mechanism of Gold Nanorods (NRs) Using Seed-Mediated Growth Method. *Chem. Mater.* **2003,** *15*, 1957-1962.

18. Garcia, M. A.; Bouzas, V.; Carmona, N., Influence of stirring in the synthesis of gold nanorods. *Mat. Chem. Phys.* **2011,** *127*, 446-450.

19. Grzelczak, M.; Sanchez-Iglesias, A.; Rodriguez-Gonzalez, B.; Alvarez-Puebla, R.; Perez-Juste, J.; Liz-Marzan, L. M., Influence of Iodide Ions on the Growth of Gold Nanorods: Tuning Tip Curvature and Surface Plasmon Resonance. *Adv. Funct. Mater.* **2008,** *18*, 3780-3786.

20. Lakowicz, J. R., *Principles of Fluorescent Spectroscopy*. 2nd ed.; Springer: **1999**; p 725.